

Cation Exchange Poly(arylene ether sulfone) Copolymers for Capacitive Deionisation Applications

*A thesis for the Degree of Doctor of Philosophy in the Department of
Chemical Engineering at Monash University*

by

Benjamin Matthew Asquith

BEng (Hons), BA

September 2014

Under the Copyright Act 1968, this thesis must be used only under the normal conditions of scholarly fair dealing. In particular no results or conclusions should be extracted from it, nor should it be copied or closely paraphrased in whole or in part without the written consent of the author. Proper written acknowledgement should be made for any assistance obtained from this thesis.

I certify that I have made all reasonable efforts to secure copyright permissions for third-party content included in this thesis and have not knowingly added copyright content to my work without the owner's permission.

Table of Contents

Abstract	vii
Publications.....	ix
Acknowledgements.....	x
Declaration	xi
Abbreviations	xii
Nomenclature.....	xiv

Chapter One: Cation Exchange Polymers for Capacitive Deionisation Applications 1-1

1.1 Desalination: A Means to Meet the Water Demand	1-2
1.2 Research Gaps and Project Aims	1-3
1.3 Thesis Outline.....	1-4
1.4 References.....	1-4

Chapter Two: State-of-the-Art Membranes and Carbon Materials for Capacitive Deionisation ... 2-1

2.1 Capacitive Deionisation as a Novel Method of Desalination.....	2-2
2.1.1 Historical Overview and Theoretical Concepts	2-2
2.1.2 Applications of CDI.....	2-3
2.2 Carbon Materials for CDI Electrodes.....	2-4
2.2.1 Carbon Aerogels	2-4
2.2.2 Carbon Nanotubes.....	2-5
2.2.3 Graphene.....	2-6
2.2.4 Activated Carbon	2-7
2.2.4.1 Activated Carbon Modification	2-7
2.2.4.2 Conductive Fillers.....	2-9
2.2.4.3 Polymeric Binders	2-9
2.2.4.4 Activated Carbon Porosity.....	2-11
2.2.5 Conclusions on Materials for CDI.....	2-12
2.3 Membrane Capacitive Deionisation.....	2-13
2.3.1 Ion-Exchange Membranes for Membrane Capacitive Deionisation.....	2-14
2.3.2 Commercial Cation Exchange Membranes.....	2-14
2.3.3 Alternative Approaches to Commercial Membranes	2-17
2.4 Poly(arylene ether sulfone) Cation Exchange Membranes	2-19
2.4.1 Poly(arylene ether sulfone) Sulfonation.....	2-19
2.4.1.1 Pre-sulfonation.....	2-21
2.4.1.2 Post-sulfonation	2-22
2.4.1.3 Side-chain Sulfonation	2-23

2.4.2 Poly(arylene ether sulfone) Copolymers	2-27
2.5 Summary	2-29
2.6 Publications.....	2-30
2.7 References	2-30

Chapter Three: Side-chain Sulfonated Random and Multiblock Copolymer Cation Exchange

Membranes for Membrane Capacitive Deionisation	3-1
3.1 Overview	3-2
3.2 Relevant Theory	3-2
3.2.1 Ion-Exchange Capacity	3-2
3.2.2 Water Uptake.....	3-3
3.2.3 Conductivity	3-3
3.2.4 Selectivity and Transport Number	3-4
3.3 Experimental	3-5
3.3.1 Materials	3-5
3.3.2 Random Copolymer Synthesis	3-6
3.3.3 Multiblock Copolymer Synthesis.....	3-6
3.3.4 Copolymer Sulfonation.....	3-7
3.3.5 Polymer Characterisation	3-7
3.3.6 Membrane Preparation.....	3-8
3.3.7 Membrane Characterisation	3-8
3.3.7.1 Contact Angle.....	3-8
3.3.7.2 Ion-Exchange Capacity	3-8
3.3.7.3 Water Uptake.....	3-9
3.3.7.4 Conductivity	3-9
3.3.7.5 Transport Number.....	3-9
3.4 Results and Discussion	3-10
3.4.1 ¹ H NMR Analysis	3-10
3.4.1.1 ¹ H NMR of Random Copolymers Prior to Sulfonation	3-10
3.4.1.2 Sulfonated Random Copolymers ¹ H NMR.....	3-13
3.4.1.3 Multiblock Copolymer ¹ H NMR.....	3-15
3.4.2 FTIR Analysis	3-16
3.4.3 Ion Exchange Capacity and Water Uptake	3-19
3.4.4 Contact Angle	3-23
3.4.5 Conductivity	3-25
3.4.6 Transport Number and Selectivity	3-26
3.5 Conclusions	3-27
3.6 Publications.....	3-28
3.7 References	3-29

Chapter Four: Double Layer Formation in Activated Carbon Electrodes.....	4-1
4.1 Overview	4-2
4.2 Relevant Theory	4-2
4.2.1 Specific Surface Area and Pore Size Distribution	4-2
4.2.2 The Electrical Double Layer	4-4
4.2.3 Cyclic Voltammetry to Measure the Electrical Double Layer	4-5
4.2.4 Electrochemical Impedance Spectroscopy and Equivalent Circuits	4-6
4.2.4.1 Transmission Line Model.....	4-6
4.2.4.2 Equivalent Circuits.....	4-8
4.3 Experimental	4-9
4.3.1 Materials	4-9
4.3.2 Fabrication of Carbon Electrodes	4-9
4.3.3 Carbon & Graphite Specific Surface Area and Pore Size Distribution	4-9
4.3.4 Electrode Characterisation	4-10
4.3.4.1 SEM and Contact Angle.....	4-10
4.3.4.2 Electrochemical Characterisation	4-10
4.4 Results and Discussion	4-11
4.4.1 Activated Carbon and Graphite Specific Surface Area and Pore Size Distribution	4-11
4.4.2 Electrode Preparation Optimisation	4-13
4.4.3 Electrode Morphology and Contact Angle	4-14
4.4.4 Cyclic Voltammetry	4-17
4.4.5 Electrochemical Impedance Spectroscopy.....	4-21
4.4.5.1 Capacitance from Electrochemical Impedance Spectroscopy	4-22
4.4.5.2 Diffusive Resistance	4-23
4.4.5.3 Equivalent Circuits.....	4-25
4.4.6 Resistance to Electrical Double Layer Formation	4-27
4.5 Conclusions	4-31
4.6 References	4-32

Chapter Five: Activated Carbon Electrodes with Poly(arylene ether sulfone) Copolymer

Coatings	5-1
5.1 Overview	5-2
5.2 Experimental	5-2
5.2.1 Materials	5-2
5.2.2 Electrode Preparation.....	5-2
5.2.3 Electrode Characterisation	5-4
5.2.3.1 Physical Electrode Characterisation	5-4
5.2.3.2 Electrochemical Characterisation	5-4
5.3 Results and Discussion	5-5

5.3.1 Electrode Morphology	5-5
5.3.1.1 Polymer Coatings.....	5-5
5.3.1.2 Hydro and Thermal Stability	5-7
5.3.1.3 FTIR Analysis	5-7
5.3.2 Cyclic Voltammetry	5-7
5.3.2.1 Uncoated Electrodes	5-8
5.3.2.2 Coated Electrodes	5-9
5.3.3 Electrochemical Impedance Spectroscopy.....	5-15
5.3.3.1 Capacitance from Electrochemical Impedance Spectroscopy	5-15
5.3.3.2 Polymer Resistance and Conductivity	5-17
5.3.3.3 Charging Resistance	5-18
5.4 Conclusions	5-19
5.5 Publications.....	5-20
5.6 References	5-20

Chapter Six: Poly(arylene ether sulfone) Copolymers as Binders for Activated Carbon

Electrodes.....	6-1
6.1 Overview	6-2
6.2 Experimental	6-3
6.2.1 Materials	6-3
6.2.2 Carbon Electrode preparation	6-3
6.2.3 Binder Properties	6-3
6.2.4 Electrode Properties.....	6-3
6.3 Results and Discussion	6-4
6.3.1 Mechanical Properties of Binder Materials	6-4
6.3.1.1 Water Uptake and Contact Angle.....	6-4
6.3.1.2 Molecular Weight and Thermogravimetric Analysis	6-5
6.3.1.3 Polymer Tensile Strength	6-6
6.3.2 Physical Properties of Carbon Electrodes with Copolymer Binders.....	6-7
6.3.2.1 Electrode Thickness.....	6-7
6.3.2.2 Electrode Contact Angle	6-8
6.3.2.3 Effect of Binder Type and Electrode Composition on Physical Structure.....	6-10
6.3.3 Electrode Electrochemical Characterisation.....	6-13
6.3.3.1 Comparison of Binder Type Using Cyclic Voltammetry	6-13
6.3.3.2 Electrochemical Impedance Spectroscopy.....	6-15
6.4 Conclusions	6-17
6.5 References	6-18

Chapter Seven: Conclusions and Future Work	7-1
7.1 Thesis Conclusions	7-2
7.2 Recommendations for Future Work	7-4
7.2.1 Improved Membrane Conductivity Testing	7-4
7.2.2 Variation in Carbon Material	7-5
7.2.3 Optimised Polymer Coating Thickness	7-5
7.2.4 Hydrophilic Polymer Optimisation	7-5
7.2.5 Testing of Electrodes in a CDI Cell	7-5
7.2.6 Anion Exchange Coatings	7-6
 Appendices.....	 8-1
Appendix A1 - Ion Exchange Capacity Calculations	8-2
Appendix A2 - Calculation of BET Surface Area for a Microporous Material	8-3
Appendix A3 - Carbon Electrode Preparation	8-6
Appendix A4 - Stress Versus Strain Curves for Swollen Membranes	8-7
Appendix A5 - Published Papers	8-8

Abstract

In this thesis, cation exchange poly(arylene ether sulfone) copolymers for capacitive deionisation applications were studied, with the focus of enhancing the performance of activated carbon electrodes. Activated carbon has been studied extensively as an electrode material for capacitive deionisation, but faces a number of significant drawbacks, including the requirement of a polymeric binder, unfavourable pore distribution and low conductivity.

Poly(arylene ether sulfone) random and multiblock copolymers were synthesised from 2,5-diphenylhydroquinone and diphenylsulfone monomers. The 2,5-diphenylhydroquinone monomer was found to impart conductivity and ion exchange properties, while the diphenylsulfone increased the stability of the polymers when cast as membranes. Sulfonation of pendant phenyl rings using post-sulfonation resulted in a high degree of sulfonation. The synthesis of copolymers with different monomer ratios was used to examine the effects of side-chain sulfonation, monomer ratio and copolymer structure on fundamental membrane properties for capacitive deionisation. Membranes prepared from poly(arylene ether sulfone) random and multiblock copolymers were found to have favourable properties, especially ion-exchange capacity, water uptake and transport number. Importantly, their conductivities were found to be similar to commercially available membranes used for capacitive deionisation.

The use of activated carbon as an electrode material and the effects of graphite as a conductive filler were examined. The graphite content, while not greatly affecting electrode wettability, was found to greatly vary electrochemical performance. Samples with too low a graphite content were observed to have poor conductivity and low mesoporous and microporous capacitance. Increased graphite content resulted in only modest capacitance increases, highlighting the need for both an appropriate conductive filler and a carbon material with a favourable pore size distribution. Through electrochemical impedance spectroscopy and equivalent circuit modelling, slow double layer formation in these electrodes was found to be caused by poor wettability and large resistance to electrolyte diffusion.

When cation exchange copolymers were applied as coatings to activated carbon electrodes, the additional resistance was found to not significantly hinder the rate of double layer formation. Cyclic voltammetry revealed that a greater micropore capacitance could be achieved over a wide range of potentials due to the selective transport properties of polymers. The penetration of polymer into the

carbon substrate during casting was also observed to improve electrode capacitance and kinetics. Electrochemical impedance spectroscopy results identified that both conductivity and water uptake are important properties that affect charging resistance and capacitance, and that optimal polymer design for membrane capacitive deionisation applications will require a high ion-exchange capacity without compromising polymer mechanical stability.

To further improve the properties of activated carbon electrodes, random copolymers were used as novel binder materials. With a high enough concentration, good adhesion of particles comparable to commonly used hydrophobic binders was achieved. The wettability of the electrodes was greatly increased, however electrode capacitance was reduced due to polymer swelling and a loss of particle conductivity. Nonetheless, electrochemical impedance spectroscopy revealed lower charging resistances compared to electrodes prepared with hydrophobic binders, suggesting there is potential to improve the performance of activated carbon electrodes with optimised hydrophilic binders.

Publications

Book

Ladewig, B.P. and Asquith, B.M., *Desalination Concentrate Management*, Springer, Heidelberg, 2012

Book Chapters

Ladewig, B.P., Asquith, B.M. and Meier-Haack, J., Key Materials for Low-Temperature Fuel Cells: An Introduction, in B. Ladewig, S. Jiang, Y. Yan & M. Lu (eds.), *Materials for Low-Temperature Fuel Cells*, Wiley-VCH, Weinheim, 2014.

Ladewig, B.P., Asquith, B.M. and Meier-Haack, J., Membranes for Direct Methanol Fuel Cells, in B. Ladewig, S. Jiang, Y. Yan & M. Lu (eds.), *Materials for Low-Temperature Fuel Cells*, Wiley-VCH, Weinheim, 2014.

Conference Presentations

Asquith, B.M., An Introduction to Membrane Capacitive Deionisation, in: *1st Annual Monash University Chemical Engineering Conference*, Monash University, Clayton Campus, 2012.

Asquith, B.M., Ladewig, B.P. and Meier-Haack, J., Preparation and Characterisation of Side-Chain Sulfonated Copolymer Cation Exchange Membranes, in: *3rd Early Career Researchers Membrane Symposium*, University of Queensland, St. Lucia Campus, Brisbane, 2012.

Asquith, B.M., Ladewig, B.P. and Meier-Haack, J., Preparation and Characterisation of Side-Chain Sulfonated Random Copolymer Cation Exchange Membranes, in: *2nd Annual Monash University Chemical Engineering Conference*, Monash University, Clayton Campus, 2012.

Journal Articles

Asquith, B.M., Meier-Haack, J., Vogel, C., Butwilowski, W. and Ladewig, B.P., Side-chain sulfonated copolymer cation exchange membranes for electro-driven desalination applications, *Desalination*, 324 (2013) 93-98.

Asquith, B.M., Meier-Haack, J. and Ladewig, B.P., Cation exchange copolymer enhanced electrosorption, *Desalination*, 345 (2014) 94-100.

Acknowledgements

Of all the pages in this thesis, perhaps this is the most significant. Without the support and contributions of the following people and many others not listed, this work would not exist, nor would it be as important to me.

I would like to thank my supervisor Bradley Ladewig, whose advice has shaped this thesis and whose guidance has shaped me both professionally and personally. I am grateful for his support in applying for funding, the opportunity to travel locally, interstate and overseas to pursue my studies, providing an enjoyable office environment, and the bottomless cups of coffee from the group's coffee machine. I would also like to thank the members of my research group, Ben, Bec, Con, Adam, Richelle, Stefan, Jack and Brad, who in addition to their practical help have provided me with lasting friendships and memories.

I would like to acknowledge the Department of Chemical Engineering, including all academic, technical and office staff, for making me feel at home at Monash throughout the duration of both my undergraduate and postgraduate studies, and for preparing me to become an engineer. I would especially like to acknowledge Kim Phu for her tireless work and willingness to go above and beyond the call of duty to assist me with my research.

I would like to acknowledge the financial support I received from the Australian Postgraduate Award (APA), from the National Centre for Excellence in Desalination Australia (NCEDA) for their generous PhD Supplementary Scholarship, and from both the German Academic Exchange Service (DAAD) and Monash University for providing funding for six months of study in Dresden, Germany.

I am thankful for the research opportunities provided to me at the Leibniz-Institut für Polymerforschung Dresden. The advice and ideas provided by Jochen Meier-Haack, Claus Vogel, Christian Langner, Kornelia Schlenstedt, Ute Leuteritz and Wladimir Butwilowski became the driving force for much of my work, and their friendships made my time there not only productive but also most memorable.

Finally, I would like to thank my friends and family who have supported me over the last 22 years of study. Most of all I must acknowledge the support of my brothers Jimmy and Mike, and my parents Mary and Peter. I am very grateful to have such a loving family and owe many of my accomplishments to you.

Declaration

I hereby declare that this thesis contains no material that has been accepted for the award of any degree or diploma at an university or other institution, and that to the best of my knowledge, contains no material previously published or written by another person except where due reference is made in the text of the thesis.

Benjamin Asquith

September 2014

Abbreviations

AC	Alternating current
ATR-FTIR	Attenuated total reflectance Fourier transform infrared spectroscopy
BET	Brunauer-Emmett-Teller
bis-TMS-DHDPHS	4,4'-dihydroxydiphenyl sulfone bis-trimethylsilylether
bis-TMS-DPhHQ	2,5-diphenylhydroquinone bis-trimethylsilylether
BPPO	Bromomethylated poly(2,6-dimethyl-1,4-phenylene oxide)
CDI	Capacitive deionisation
CNT	Carbon nanotube
CPE	Constant phase element
CV	Cyclic voltammetry
DFDPhS	Difluorodiphenyl sulfone
DFT	Density functional theory
DHDPHS	Dihydroxydiphenyl sulfone
DMAc	<i>N,N</i> -Dimethylacetamide
DPhHQ	Diphenylhydroquinone
DS	Degree of sulfonation
EDL	Electrical double layer
EDX	Energy-dispersive X-ray spectroscopy
EIS	Electrochemical impedance spectroscopy
FTIR	Fourier transform infrared spectroscopy
GA	Glutaric acid
GPC	Gel permeation chromatography
IEC	Ion-exchange capacity
MB	Multiblock copolymer
MCDI	Membrane capacitive deionisation
MED	Multiple effect distillation
MSF	Multi-stage flash distillation
NMP	<i>N</i> -Methyl-2-pyrrolidone
NMR	Nuclear magnetic resonance
oligo-DP-PES	Oligomer prepared from bis-TMS-DPhHQ and DFDPhS
oligo-PES	Oligomer prepared from bis-TMS-DHDPHS and DFDPhS

PES	Poly(ether sulfone)
PTFE	Poly(tetrafluoroethylene)
PVA	Poly(vinyl alcohol)
PVDF	Poly(vinylidene fluoride)
PZC	Point of zero charge
RCP	Random copolymer
SEM	Scanning electron microscope
sPES	Sulfonated poly(ether sulfone)
TDS	Total dissolved solids
TGA	Thermogravimetric analysis

Nomenclature

a	Activity	α	Dimensionless parameter denoting CPE behaviour
A	Area	λ	Hydration number
c	Concentration	ν	Sweep rate
C	Capacitance, specific capacitance	σ	Conductivity
C_{DL}	Double layer capacitance	ψ	Selectivity
E	Potential	ω	Angular frequency
F	Faraday constant	Ω	Ohm
i	Current	$^{\circ}$	Degrees
J	Molar flux		
L	Length		
m	Mass		
n	Mole		
P	Pressure		
P_0	Saturation pressure		
q	Charge		
Q	Constant phase element		
Q	Gas quantity adsorbed		
R	Gas constant		
R	Resistance		
R_i	Interface resistance		
R_s	Solution resistance		
t	Time		
t_+	Transport number		
T	Temperature		
v	Volume		
W	Warburg impedance		
Y_0	Constant phase element capacitance		
z	Valence		
z	Pore penetration depth		
Z	Impedance		
Z'	Real impedance		
Z''	Imaginary impedance		

Chapter One

Cation Exchange Polymers for Capacitive Deionisation Applications

1.1 Desalination: A Means to Meet the Water Demand

As global population and living standards increase so too does the demand for fresh water, while its availability continues to decrease. In response to this demand, water conservation strategies and new sources of water are continually being explored. Additionally, research is being focused on ways to supplement existing water supplies, with a large focus on the desalination of water to produce potable water from otherwise non-drinkable sources.

Although desalination has existed in various forms for many centuries, the field has rapidly developed over the last half century. Of the many desalination technologies available, the most commonly used are multi-stage flash distillation (MSF), multiple effect distillation (MED) and reverse osmosis [1]. MSF and MED are thermal desalination processes that consume large amounts of thermal energy to extract fresh water from salt water [2]. Reverse osmosis is the most widely used form of desalination, and is generally the most economical, however this process requires significant pretreatment and produces a significant amount of concentrate [3]. The basic principle of these thermal and filtration processes is to extract fresh water from a salt water feed, producing a purified stream of water while concentrating the feed stream. This is done through the application of either thermal or mechanical energy and is usually most efficient for large scale seawater desalination. On the other hand, electro-driven desalination processes such as electrodialysis and capacitive deionisation (CDI) take advantage of the charged nature of the salt particles. By applying electrical energy across a stream of water, salt ions can be removed from the water efficiently desalinating brackish water without the need for expending large amounts of thermal or mechanical energy.

Capacitive deionisation (CDI) is a developing desalination technology that can be used for the highly efficient desalination of brackish water, the production of ultra pure water, water softening and the removal of other charged impurities from water streams [4-6]. It is an electrosorption process that relies on the formation of an electrical double layer (EDL) on a porous, polarisable electrode. The build up of charge in the electrode creates a similar build up of oppositely charged ions from an electrolyte solution at the electrode-solution at the interface, thereby removing salt ions from solution. As a desalination process that works most effectively for low salinity water, the development of CDI will help improve the options available for the desalination of inland brackish water in both Australia and around the world.

1.2 Research Gaps and Project Aims

As a novel desalting technology, CDI is part of a priority research theme by the National Centre of Excellence in Desalination Australia (NCEDA) due to a number of benefits, including [6]:

- The potential to provide cheap water in remote areas
- A high process efficiency
- Reduced energy costs compared to reverse osmosis
- An improving commercial viability
- A reduced stream of concentrated waste

CDI technology faces several difficulties before it can become competitive with current desalination methods. These challenges include low ion retention at the electrodes, the high cost of electrodes and membranes, and the relatively poor performance of commercial membranes. As such, there is scope to develop novel polymers for use in CDI processes to improve electrode performance, reduce costs and increase the efficiency of CDI.

In recent years numerous state-of-the-art cation exchange polymers have been developed as pressure-driven desalination membranes and/or proton exchange membranes for use in fuel cells. However, little work has been done in preparing and characterising these materials for electro-driven desalination techniques, and in particular CDI. The aim of this study is to examine the effects of cation exchange copolymers on activated carbon electrodes, with the goal of producing electrodes with enhanced transport properties for use in CDI. Specifically, the project aims to:

- Synthesise and characterise sulfonated poly(arylene ether sulfone) copolymer membranes, with the aim of developing ion-exchange membranes with high permselectivity and low electrical resistance specifically for use in membrane capacitive deionisation.
- Understand the performance of activated carbon electrodes and the impacts of conductive graphite on electrode wettability, conductivity and capacitance.
- Prepare and characterise electrodes coated with cation exchange polymers with enhanced transport properties to better facilitate the adsorption/desorption of ions in CDI.

- Gain an understanding of the effects of fundamental ion-exchange membrane properties on the MCDI process, including ion-exchange capacity (IEC), water uptake, transport number and conductivity.
- Prepare and characterise electrodes using cation exchange copolymers as a binder material to improve the electrode capacitance and reduce resistance without the need for a polymer coating layer.

1.3 Thesis Outline

Each chapter of this chapter focuses on a different aspect of electrodes for CDI. Chapter two provides a comprehensive review of state-of-the-art carbon materials and polymers for CDI applications. Chapter three focuses on the synthesis and characterisation of polymers and membranes with potential for use in MCDI, while chapter four examines the use of activated carbon as a material for electrode preparation. Chapter five combines the work of the two proceeding chapters through the application of thin polymer coatings on activated carbon electrodes, analogous to placing an ion-exchange membrane directly against the carbon electrode. Chapter six studies the potential for hydrophilic polymers to be applied as binder materials instead of commonly used hydrophobic polymers, and chapter seven draws together the conclusions of the project and makes recommendations for further studies.

1.4 References

- [1] Khawaji, A., Kutubkhanah, I., and Wie, J., Advances in seawater desalination technologies, *Desalination*, 221 (2008) 47-69.
- [2] Mezher, T., Fath, H., Abbas, Z., and Khaled, A., Techno-economic assessment and environmental impacts of desalination technologies, *Desalination*, 266 (2011) 263-273.
- [3] Broséus, R., Cigana, J., Barbeau, B., Daines-Martinez, C., and Suty, H., Removal of total dissolved solids, nitrates and ammonium ions from drinking water using charge-barrier capacitive deionisation, *Desalination*, 249 (2009) 217-223.
- [4] Farmer, J. C., Method and Apparatus for Capacitive Deionization, Electrochemical Purification, and Regeneration of Electrodes, US Patent 5,425,858, June 20 1995.
- [5] Anderson, M. A., Cudero, A. L., and Palma, J., Capacitive deionization as an electrochemical means of saving energy and delivering clean water. Comparison to present desalination practices: Will it compete?, *Electrochimica Acta*, 55 (2010) 3845-3856.
- [6] National Centre of Excellence in Desalination Australia, Australian Desalination Research Roadmap, 2012.

Chapter Two

State-of-the-Art Membranes and Carbon Materials for Capacitive Deionisation

2.1 Capacitive Deionisation as a Novel Method of Desalination

2.1.1 Historical Overview and Theoretical Concepts

As described in chapter one, CDI is a developing desalination technology that can be used for the highly efficient desalination of low salinity water. It is an electrosorption process that relies on the formation of an EDL on a porous, polarisable electrode. When a potential is applied across two porous electrodes, there is a build up of charge in the carbon electrode. As water passes between these electrodes, the charge is balanced by the ionic charge of dissolved components being removed from the solution, that is to say anions and cations are adsorbed onto the electrode surface. Once the electrodes become saturated with ions, the electrical potential is removed and ions are released back into solution, creating a concentrated waste stream. A simplified representation of CDI adsorption and desorption cycles is shown in Figure 2.1. The high efficiency of CDI for brackish water desalination is a result of the direct removal of ions from the water, compared with the removal of fresh water from a more concentrated feed solution in thermal or pressure driven desalination processes (such as MSF or reverse osmosis).

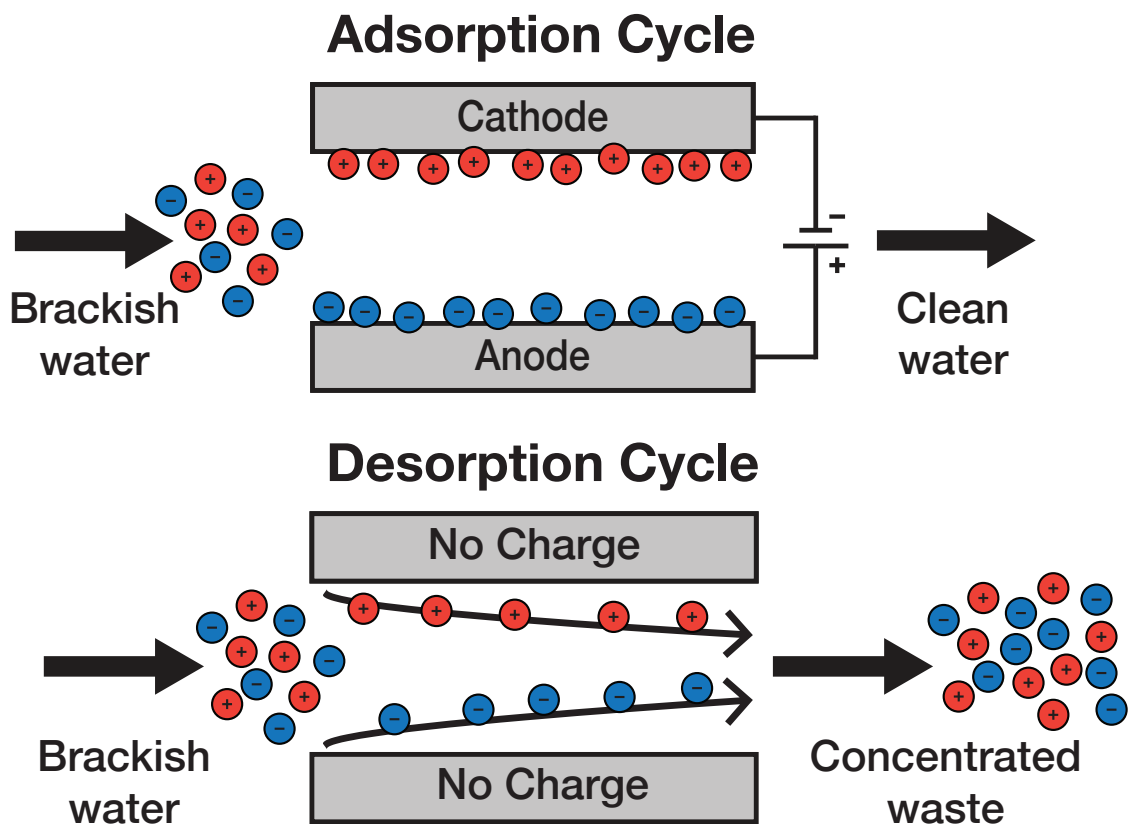


Figure 2.1 - Schematic representation of the CDI process.

The concept of electrosorption for the desalination of saline water was first considered by Blair and Murphy [1], which relied on the adsorption of ions onto porous carbon. The theory for this process was later established by Murphy and Caudle [2], Johnson et al. [3] and Johnson and Newman [4]. Throughout the 1970s and early 1980s a number of studies further examined EDL theory for CDI and the development of adsorption and desorption cycles [5-7]. This early work was unsuccessful in producing an efficient method for deionising water, largely due to highly resistive electrodes and inefficient current collectors. However, it had been shown that electrosorption could become a low-cost desalination solution if suitable electrode materials with large enough surface areas were developed. Since the 1990s there has been a renewed interest in CDI, with recent research focused on the development of more efficient materials and increasing their electrosorption capacity. This began with carbon aerogels [8-15] and has subsequently branched out into activated carbon [16-24], carbon nanotubes (CNTs) [25-29] and graphene [30-36]. In spite of this research, the poor performance of electrodes is still considered to be one of the major obstacles that must be overcome to develop CDI into a commercial technology [37].

2.1.2 Applications of CDI

The selection of a particular desalination technology depends on several factors, including the concentration and composition of the feedwater, available energy sources, and options available for concentrate management and/or disposal. It is important to note that the concentration of the source water is highly variable, and this can be the defining factor in selecting technology. Reverse osmosis is most often used for seawater desalination, which typically has total dissolved solid (TDS) levels of 33,000 – 37,000 mg/L. Brackish water however has a much more variable concentration, and depending on location TDS concentration can range from several hundred to several thousand mg/L [38]. The process of selectively removing salt ions becomes more efficient when low concentrations are used, and as such CDI is most efficient at low salinities, typically less than 10,000 mg/L [39, 40]. Studies have shown that at low salinity, CDI consumes three times less energy than reverse osmosis, largely due to the high pressure requirements of reverse osmosis [41].

CDI is typically operated with low cell voltages in the range of 1.2-1.5 V, and has the potential to be coupled directly with renewable energy sources such as wind or solar power. Along with low volume streams of concentrated waste, CDI is potentially useful in regional areas that have poor access to fresh

water [42]. Other applications for CDI include water polishing for processes where ultrapure water is required, such as in the manufacturing of semiconductors [43].

2.2 Carbon Materials for CDI Electrodes

Research into CDI electrodes is largely focused on the development of materials that have a high sorption capacity. To achieve this, materials need to have a high specific surface area, good electrical conductivity to improve energy efficiency, and possess a favourable pore arrangement that both maximises sorption capacity and allows for easy pore access [44]. Electrodes must have favourable regeneration properties to allow for the removal of adsorbed ions back into a waste stream. Furthermore, in addition to an electrode's chemical and physical properties, the cost of manufacturing must be kept low to help CDI compete with both developed and emerging desalination technologies.

Due to its high specific surface area, good electronic conductivity and chemical and electrochemical stability, carbon is typically used as an electrode material. Commonly used types of carbon include activated carbon, activated carbon cloth, carbon aerogels, CNTs, graphene and other composites of these materials. The following section will briefly describe carbon materials used for CDI, before focusing on activated carbon, the material selected for this study.

2.2.1 Carbon Aerogels

Carbon aerogels are highly crosslinked, solid networks of covalently bonded carbon particles [45]. They are highly conductive, with typical surface areas of 400 - 1000 m²/g and a pore size distribution of <50 nm [12, 14, 46]. A renewed interest in electrosorption desalination in the 1990's saw a number of studies on carbon aerogels by Farmer, Tran and coworkers at the Lawrence Livermore National Laboratory [8-10, 12]. This work saw the development of an electrosorption process that used multiple carbon aerogel electrodes polarized with a direct current power supply to remove ions from water. However, due to the microporous nature and unfavorable pore size distribution of carbon aerogel, much of its large surface area is unavailable for ion adsorption. Furthermore, its use is limited by its complex fabrication process [47]. More recent studies have shown carbon aerogels to have specific capacitances up to 220 F/g [48], nonetheless pilot scale testing indicates that further work is required to improve sorption capacity before these materials become economically viable for the desalination of brackish water [49].

2.2.2 Carbon Nanotubes

Due to their unique one-dimensional structure, CNTs possess excellent thermal, electrical and mechanical properties [50-52]. For CDI, their major advantages are a high surface area to volume ratio [53], a favourable pore size distribution, and an ordered structure which allows easier pore access for adsorbing/desorbing ions [44]. Furthermore, their higher conductivity allows for a faster adsorption of ions and a faster electrode regeneration time [44].

A number of studies have shown the modification of CNTs can significantly enhance CDI performance. Zhang et al. [26] showed that modification to ensure that the nanotube tip is open increases the available surface area for adsorption. Increased hydrophilicity and lower zeta potential of CNTs has been achieved by both Yang et al. [27], who directly grafted both positively and negatively charged ion-selective functional groups onto the surface of CNTs (see Figure 2.2), and Zhan et al. [29] who grafted chitosan onto the surface of CNTs. In both of these instances, the modifications increased the electrosorption capacity of the CNT electrodes. Improved electrosorption performance has also been observed for CNT composite electrodes with polyaniline [54], carbon nanofibres [47, 55-60] and activated carbon [61, 62].

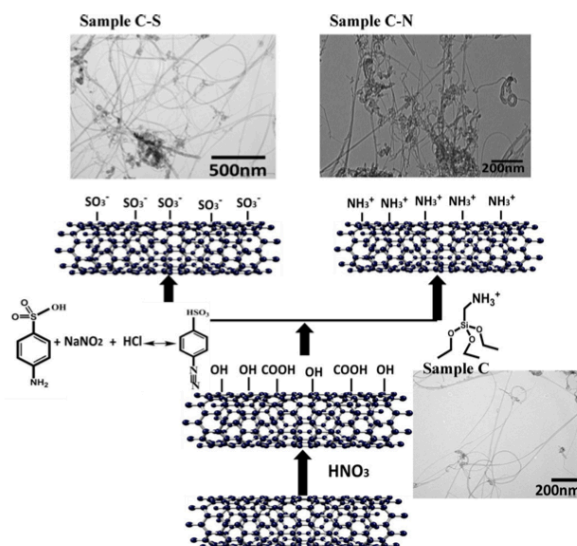


Figure 2.2 - Synthesis scheme of the sulfonation and amination of CNTs by Yang et al. [27] (reprinted with permission from Elsevier).

Despite the performance advantages of CNTs, there are a number of drawbacks with their use, including the requirement for a polymeric binder that can hinder performance. Electrophoretic deposition as a method of carbon nanotube electrode fabrication, as studied by Nie et al. [63, 64], was found to negate the requirement of a polymer binder and produce electrodes with similar desalination capabilities to other

carbon materials. In spite of this, the potential risks to human health continues to be a major drawback of the use of CNTs [53].

2.2.3 Graphene

Graphene consists of layers of two-dimensional sheets of sp^2 -bonded carbon atoms, and has excellent properties for CDI applications including high specific surface area, electrical conductivity and mechanical strength. Its exciting potential as an electrode material has seen several recent studies by Zou and coworkers [30-32]. Graphene nanoflakes have been shown to have a high electrosorption capacitance due to their shape and arrangement, allowing pores to be more accessible to adsorbing ions compared with activated carbon. Although the specific surface area of graphene nanoflakes can be reduced by the presence of graphitized carbon remaining from the graphite precursor, this may also serve to increase the conductivity of the graphene, which promotes a better adsorption efficiency. In another study, graphene nanosheets prepared using a novel three step reduction of graphene oxide were found to have a mean pore size of 3.3 nm, a specific capacitance of up to 149.58 F/g and yielded a specific electrosorption capacity of 8.6 mg/g [33].

Within the last 12 months significant improvements in the performance of graphene materials for CDI have been made. Yan et al. [34] have shown that polyaniline/graphene composites increase the capacitance and regeneration rate of electrodes compared with graphene only electrodes, a result of the polyaniline acting as conductive linkers between the graphene sheets. El-Deen et al. [35] synthesised graphene wrapped MnO_2 -nanostructures in a one pot reaction involving graphite oxidation and reduction, in addition to MnO_2 synthesis. The excellent electrosorptive properties of electrodes prepared with this material (a specific capacitance of 292 F/g and a salt removal efficiency of approximately 93%) were complemented by the simplicity and low cost of fabrication. Finally, Li et al. [36] prepared sulfonated reduced graphene oxide on carbon fibre cloth, whereby the graphene oxide nanosheets encapsulated the carbon fibres and formed a cylindrical-shell microstructure. Charge efficiency was double that of unmodified carbon fibre cloth, a result of decreased internal resistance and potentially the functionalised graphene oxide layer acting a charge barrier, restricting anion movement (analogous to using a cation exchange membrane, see section 2.3).

Graphite oxide is used as a precursor for many graphene-based materials, and now offers the potential for economical large-scale production of graphene-based materials [65]. Despite the potential of graphite as a material for CDI, it is thought that improvements in preparation methods, electrosorption potential and cost of manufacturing are needed to produce and use graphene on a large scale [65].

2.2.4 Activated Carbon

Activated carbon is an attractive material for electrosorption due to its relatively low cost and large specific surface area, typically in the order of 1000 - 2000 m²/g. Due to these benefits, numerous studies have focused on its use for CDI, both as activated carbon powder and activated carbon cloth [16-24]. Unfortunately the potential for activated carbon to adsorb salt ions from solution is hindered by its microporous nature, low conductivity, and high electrical and mass transfer resistances [47]. Furthermore, it typically exhibits a randomly arranged pore network that may hinder ion movement and thus sorption [44]. As such, research efforts to improve its electrosorption capacity and efficiency are ongoing, with techniques such as surface modification, the incorporation of fixed charges into the carbon, and the use of ion-exchange membranes. The following section outlines these improvements in activated carbon and highlights several areas that still need further study.

2.2.4.1 Activated Carbon Modification

The modification of the activated carbon surface has been shown to improve electrosorption efficiency by reducing physical adsorption. By neutralising polar surface charges, ions are less like to adsorb onto the electrode and subsequently be held there during the desorption cycle [66]. Studies have shown that enhanced performance can be achieved through chemical surface modification of activated carbons with titanium [66, 67], titanium dioxide nanoparticles [17], potassium hydroxide and nitric acid [20, 68], zinc oxide nanorods [69], and thermal treatment [23].

Both Seo and Park [70] and Zou et al. [17] have loaded an activated carbon surface with titanium dioxide nanoparticles. Although this decreased the specific surface area of the material, it was found that surface modification reduced physical adsorption and was able to increase the total specific capacitance of the activated carbon (see Figure 2.3). Activated carbon has also shown enhanced performance in CDI testing when treated with H₂ at 400 °C [23]. This was shown to increase the number of oxygenated groups on the surface, which helps to improve the wettability of the activated carbon. Myint and Dutta [69] achieved

the modification of activated carbon cloth with zinc oxide nanorods, which was found to double the adsorption efficiency compared to unmodified electrodes.

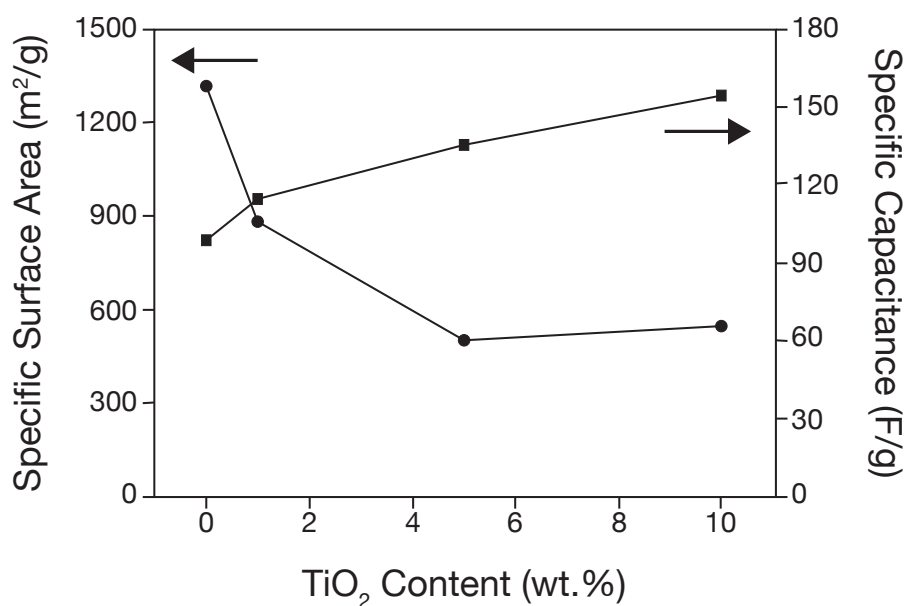


Figure 2.3 - Reduction in surface area and increase in specific capacitance of activated carbon with increasing TiO₂ content. Adapted from [70].

Treatment with potassium hydroxide was seen to particularly increase the hydroxyl groups on electrode surface, while nitric acid treatment saw notable increases in hydroxyl, carboxyl and carbonyl groups present on the electrode surface [68]. When tested for electrosorption performance, the hydroxyl groups of the potassium hydroxide treated electrodes were seen to promote ion exchange reactions due to their hydrophilicity, improving salt removal efficiency. Electrodes treated with nitric acid underwent faradaic reactions when a potential was applied, which caused a loss of current build up at the electrodes, somewhat offsetting the increased hydrophilicity from the hydroxyl and carboxyl groups. In a more recent study on electrosorption using activated carbon, Hou et al. [20] pretreated activated carbon electrodes with 1M potassium hydroxide for 24 h, again increasing the hydrophilicity of the electrodes. This was shown through cyclic voltammetry (CV) experiments, where a greater specific capacitance was observed over a lower number of cycles compared with untreated electrodes, as presented in Figure 2.4.

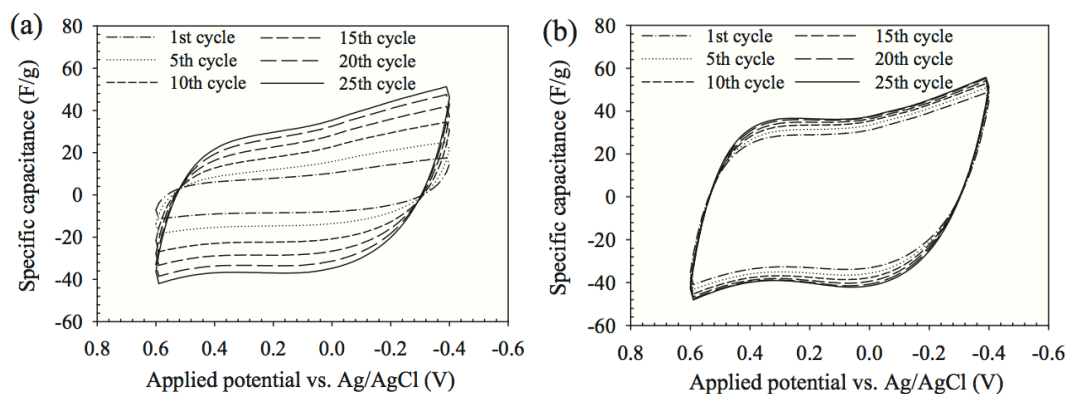


Figure 2.4 - Cyclic voltammograms of (a) activated carbon electrodes and (b) activated carbon electrodes treated with potassium hydroxide, as shown by Hou et al. [20] (reprinted with permission from Elsevier).

2.2.4.2 Conductive Fillers

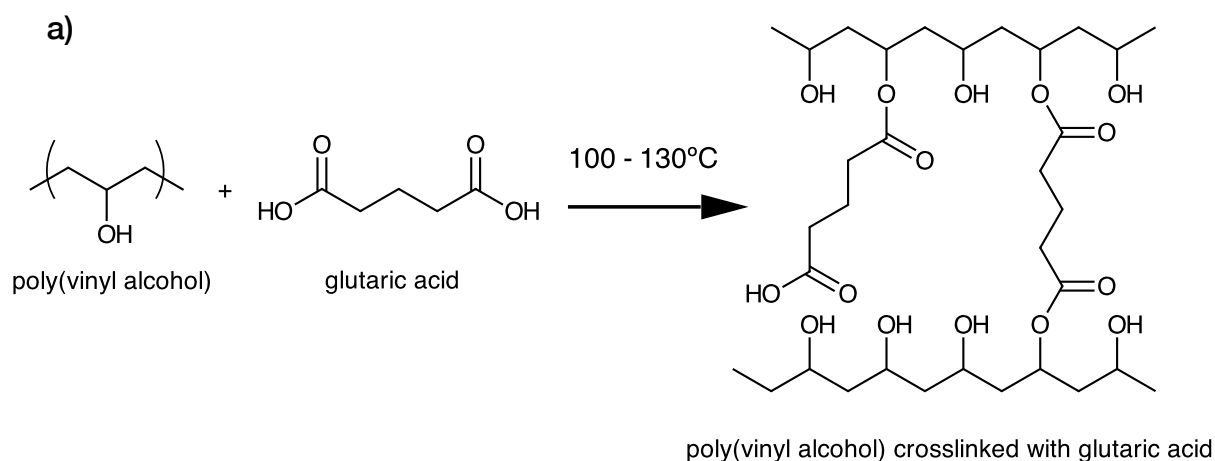
There are a number of factors that contribute to the electrical resistance of activated carbon electrodes: intra-particle resistance, contact resistance between particles, and the actual current carrying path. For each pore, the resistance becomes a function of its position, the packing of the carbon particles, and the resistance of the carbon material [71-73]. To improve the conductivity of a carbon coating, small quantities of conductive fillers such as graphite or carbon black can be added to the electrodes.

In their study on the influence of conductive additives for activated carbon electrodes, Pandolfo et al. [71] have shown that the incorporation of a conductive additive significantly improves the performance of activated carbon. It was discovered that although graphite typically has a lower intrinsic resistance than carbon black, practically this is only achieved at high compaction pressures. This phenomenon is due to the two-dimensional conductivity of graphite, which requires the edges of the graphite particles to be in contact. At low packing pressures, carbon black is likely to make better contact with the activated carbon particles [71, 74, 75]. It was also shown that graphite is not as effective as carbon black in filling voids between the carbon particles and creating effective contact to improve electrical conductivity. Particle orientation to create good edge contact is therefore important when using graphite. This has been shown practically in CDI experiments by Nadakatti et al. [24], who observed that replacing 10% of the activated carbon with mesoporous conductive carbon black can produce up to a three fold increase in capacitance.

2.2.4.3 Polymeric Binders

A further difficulty associated with the use of activated carbon is the requirement for a polymeric binder to hold the carbon particles together. Typically hydrophobic polymers such as poly(tetrafluoroethylene)

(PTFE) or poly(vinylidene fluoride) (PVDF) are used to bind activated carbon powder, however they can hinder ion access to the pores and reduce the wettability of an electrode, reducing adsorption capacity [22]. Binders may be also susceptible to chemical attack and yield electrodes with poor electrical conductivity, and while increasing the binder content increases mechanical strength, it also reduces electrode capacitance and adsorption efficiency [20, 45].



b)

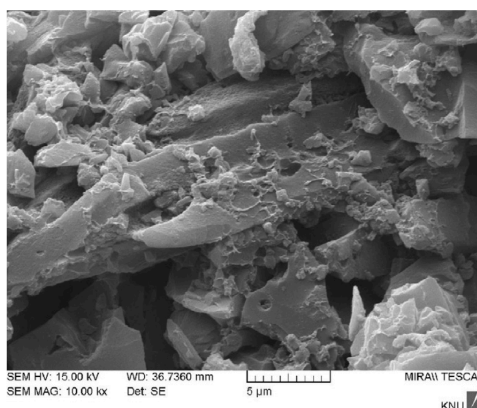


Figure 2.5 - a) Reaction scheme of poly(vinyl alcohol) crosslinked with glutaric acid and b) an SEM image of electrodes with poly(vinyl alcohol)/glutaric acid binder as shown by Park et al. [22] (reprinted with permission from Elsevier).

An alternative method to improve electrode performance is to increase hydrophilicity using fixed charges in the binder. Using this approach, Park et al. [22] fabricated activated carbon electrodes with a poly(vinyl alcohol) (PVA) binder crosslinked with glutaric acid (GA). As PVA is a water-soluble polymer, crosslinking with GA was used to prevent PVA dissolution, as shown in Figure 2.5. Greater degrees of crosslinking were seen to reduce the swelling of the PVA polymer and also resistance, and greater concentrations of GA improved electrode sorption capacity. Furthermore, unreacted carboxylic acid groups on the GA molecule gave the electrodes a negative surface potential, yielding cation-selective electrodes that could

be used as cathodes. This phenomenon was more pronounced with higher concentrations of GA, as a greater number of unreacted groups were present. When used in a CDI system, the adsorption efficiency of desalting a 200 mg/L NaCl solution was found to be 85%. In contrast, similar electrodes fabricated from activated carbon and PVDF as a binder, were found to have a CDI salt removal efficiency of only 78% for a 200 mg/L NaCl solution under optimised operating conditions [19]. Similar to the approach by Park et al. [22], enhanced CDI performance was shown by Lee et al. [18] through the incorporation of an ion exchange resin into an activated carbon powder electrode.

The incorporation of fixed charges has also been shown to work with CNTs. Nie et al. [64] prepared composite carbon nanotube-polyacrylic acid film electrodes using an electrophoretic deposition method, which showed enhanced desalination performance over carbon nanotube electrodes, and carbon nanotube electrodes combined with a cation exchange membrane. In this instance, the polyacrylic acid acts both as a binder to hold the CNTs and a cation exchange membrane (for the benefits of ion-exchange membranes in the CDI process, see section 2.3).

2.2.4.4 Activated Carbon Porosity

A major drawback of activated carbon is its microporosity. Although microporous materials (characterised by having predominate pore size <2 nm) will often yield a larger specific surface area, pores that are too small for salt ions to enter do not contribute to total electrosorption capacitance [76]. In their studies on activated carbons, graphene nanoflakes, ordered mesoporous carbons and CNTs, Zou and coworkers have observed enhanced CDI performance using carbon types with lower specific surface areas but a more favourable pore size distribution [32, 44, 77]. The same studies also highlighted the negative impact of the randomly arranged pore networks of activated carbon, which can hinder ion movement and thus the sorption of ions [44].

Microporous structures are also hindered by the electrical double-layer overlapping effect. This occurs when the pore size is approximately the same magnitude as the EDL, causing the EDLs inside each pore to overlap, greatly reducing electrosorption capacity. It has been shown by Yang et al. [14] that this effect occurs predominantly in the microporous range while only partially in the mesoporous range. Strong overlapping of EDLs results in a cut-off pore width, which is the smallest pore size that still contributes to electrosorption capacity [14]. The presence of ordered mesopores and control over micropore size and

pore size distribution has been shown to allow excellent electrosorption capacity in mesoporous carbons [78]. Peng et al. [79] synthesised mesoporous carbons with variable pore structures, and electrodes prepared from these materials were shown to have good hydrophilicity and good electrical stability. Further, the pore structure was shown to affect the adsorption of monovalent, divalent or trivalent ions, meaning these materials can be tailored to suit the feed water and the specific contaminants that require removal.

2.2.5 Conclusions on Materials for CDI

A brief summary of the advantages and disadvantages of carbon materials for CDI is shown in Table 2.1. While there are several drawbacks associated with the use of activated carbon, the above discussion has highlighted a number of areas where research has improved its performance, namely surface modification, conductive fillers and the incorporation of fixed charges into the binder. As a cheap alternative to other, more efficient materials such as CNTs and graphene, there is scope to investigate the potential enhancement of activated carbon as an electrode material for CDI.

Table 2.1 - Summary of the advantages and disadvantages of common carbon materials used for CDI electrodes.

Material	Advantages	Disadvantages
Carbon Aerogel	High conductivity Large specific surface area	Unfavourable pore size distribution Complex fabrication process Not yet commercially viable
Carbon Nanotubes	High conductivity High surface area to volume ratio Favourable pore size distribution and more ordered structure Can be modified to improve electrosorption performance Able to be used as a composite with other materials to enhance electrosorption	Generally requires the use of a polymeric binder Potential risks to human health
Graphene	Large specific surface area High conductivity Excellent electrosorption capacity	Preparation methods can be complex Large-scale production not yet cost effective
Activated Carbon	Large specific surface area Low cost Readily available Easy to manufacture	Requires the use of a polymeric binder when in the powder form Unfavourable pore size distribution Low conductivity Typically has lower salt removal capacity compared with other materials

This thesis focuses on the enhancement of activated carbon using state-of-the-art polymers as both membrane coatings and ion-exchange binders. Additionally, the use of graphite as a conductive filler is examined, including its effect on the capacitance and resistance of activated carbon electrodes. This also incorporates a study of physical adsorption and the poor wettability of activated carbon electrodes.

2.3 Membrane Capacitive Deionisation

In addition to the drawbacks of activated carbon, an inherent disadvantage of the CDI process is that during the adsorption of counterions (ions with the opposite charge to that of the electrode), a simultaneous desorption of co-ions (ions with the same charge as that of the electrode) occurs. Thus, for each electron passing through the external circuit, less than one salt molecule is adsorbed [4, 6, 80, 81]. To restrict this co-ion desorption during the adsorption cycle of a CDI process and improve energy efficiency, ion-exchange membranes may be placed in front of each electrode. This is known as membrane capacitive deionisation (MCDI), and was first introduced by Andelman and Walker in 2004 [82]. A simplified representation of an MCDI cell is shown in Figure 2.6. It has been shown to significantly increase salt adsorption and energy efficiency as more electrons in the external circuit are available for the adsorption of counterions [83-88]. Andelman [85] has shown that the addition of ion-exchange membranes barriers can increase the Coulombic efficiency of CDI processes beyond 90%.

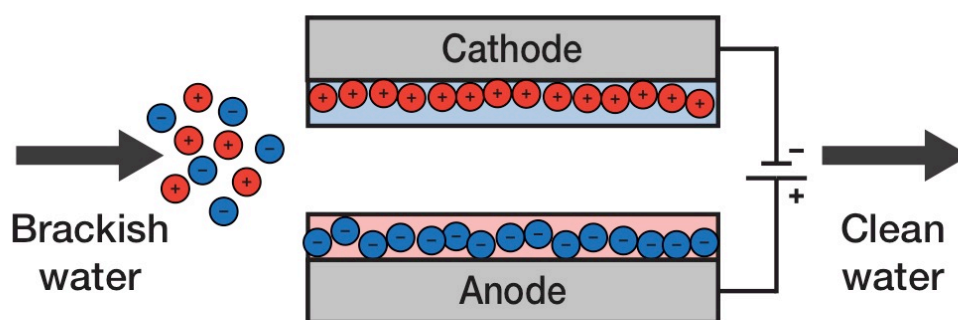


Figure 2.6 - Simplified diagram of an MCDI cell, showing cations passing through a cation exchange membrane (blue) and anions passing through an anion exchange membrane (red).

In addition to restricted co-ion movement during adsorption, a charge barrier permits the application of a reverse potential during the desorption phase, thereby allowing for a greater depletion of ions at the electrode during desorption and a greater adsorption capacity in following cycles [89]. In the absence of ion-exchange membranes if a reverse potential was applied, desorbed ions would be adsorbed by the opposing electrode rather than being removed in the waste stream. Furthermore, restricted co-ion

movement can prevent the precipitation of salts within the electrodes that may cause fouling in CDI cells [85]. With further developments, in the short term MCDI may be well suited for the treatment of brackish water, including the removal of components such as arsenic, nitrates and heavy metals. In the longer term, a reduction in costs may see the desalination of seawater using MCDI become possible [85].

2.3.1 Ion-Exchange Membranes for Membrane Capacitive Deionisation

Ion-exchange membranes have found uses in many processes, most notably for electrodialysis, chlor-alkali electrodialysis, recovery and purification of acids and bases and fuel cells applications. For electro-driven desalination processes such as electrodialysis and MCDI, enhanced process efficiency relies on the effective use of ion-exchange membranes to remove unwanted charged particles from the feed stream while restricting the movement of co-ions. For the development of cation exchange membranes for electro-driven desalination processes, the most important membrane properties are [90]:

- High permselectivity
- High IEC
- Low electrical resistance
- Mechanical and chemical stability

Unfortunately a trade-off exists between these properties; membranes that have a high IEC and low electrical resistance often have lower permselectivities and are less mechanically stable. In addition to these properties, the commercial success of any membrane will rely on membranes having a good long-term stability and a simple and cheap production method. There is therefore a need to select membranes with properties best suited to MCDI applications. Although there is a large volume of work on ion-exchange membranes for fuel cells and electrodialysis, presently there is little information in the literature examining the fundamental properties of ion-exchange membranes and their effects on CDI processes.

2.3.2 Commercial Cation Exchange Membranes

A number of commercial cation exchange membranes currently used for electro-driven processes such as electrodialysis and MCDI are outlined in Table 2.2. The membranes shown in the table highlight the balance of the properties described in section 2.3.1. Both Neosepta CM-1 [83] and Neosepta CMX [91-93] have been used in MCDI studies, and the variation in their properties shows the sacrifices in IEC,

resistance and thickness required to produce a membrane with greater mechanical stability. These membranes are manufactured by the Astom Corporation (Japan), and are poly(vinyl chloride) based membranes with styrene/divinylbenzene copolymers and fixed positive charges from sulfonic acid groups. They are designed for general concentration and desalination purposes due to their high permselectivity, low electrical resistance, and high mechanical, chemical and dimensional stability [94]. However, the membrane structure can be difficult to control during production with simultaneous copolymerisation and crosslinking processes, and membrane production costs are often quite high [95].

Of the other membranes described in Table 2.2, Ralex[®] type membranes are significantly thicker and have greater resistances, but are more mechanically stable. Similarly for the Selemion[®] membranes, additional mechanical strength is provided by the CMD membrane while sacrificing transport number (and permselectivity), resistance and thickness. Nafion 117 is a perfluorosulfonic acid/PTFE copolymer cation exchange membrane that is currently the most commonly used commercial membrane for polymer electrolyte fuel cells. Its properties are also shown in Table 2.2 due to its widespread commercial use for fuel cell applications and generally accepted status as a benchmark for ion-exchange membranes. In terms of use for MCDI, its high cost and environmental concerns due to the disposal of halogenated materials make it unsuitable for widespread use considering cheaper alternatives are available [96].

Table 2.2 - Properties of commercial membranes for electrodialysis and MCDI. Data from [94, 97-102].

Membrane	IEC (mmol/g)	Transport Number ^a	Permselectivity ^a (%)	Resistance ^b ($\Omega \cdot \text{cm}^2$)	Water Uptake (%)	Thickness (μm)	Uses	Properties
<i>Fumasep</i> [®] FKS	> 1	-	> 96	< 8	-	110 - 130 (wet)	Electrodialysis	High chemical stability
FKE	> 1	-	> 98	< 3	15	50 - 70 (dry)	Electrolysis	Excellent chemical and mechanical stability
<i>Neosepta</i> [®] CM-1	2.0 - 2.5	-	> 96	1.2 - 2.0	35 - 40	120 - 170	Electrodialysis	Low electrical resistance
CMX	1.5 - 1.8	-	> 96	3.0	25 - 30	140 - 200	General concentration and desalination	High mechanical strength
<i>Ralex</i> [®] CMH-PES	2.2	> 0.95	> 90	< 8	< 65	< 700 (wet)	Electrodialysis,	Resistance against aggressive chemicals and fouling components
CMH-PES HD	-	> 0.95	> 90	< 18	< 65	< 850 (wet)	Electrodialysis, electrodeionisation	High mechanical strength
CMH-PP	-	> 0.95	> 90	< 8	< 70	< 700 (wet)	Electrodialysis, electrodeionisation	Long-term stability in pH range 0–14
<i>Selemion</i> [®] CMV	2.01	> 0.96	> 92	3.0	20	130	Electrodialysis	Standard CEM
CMD	-	> 0.94	-	17	-	380	Electrodialysis	High mechanical strength
<i>DuPont</i> [®] Nafion 117	0.90	-	> 97*	1.5	16	200	Fuel cells	

^a Transport number and permselectivity measured using 0.5 and 0.1 M KCl solutions (*Nafion 117 permselectivity measured using 0.01 and 0.1 M NaCl solutions)

^b Resistance measured in 0.5 M NaCl

2.3.3 Alternative Approaches to Commercial Membranes

There are few examples in the literature of membranes fabricated specifically for CDI applications. Kwak et al. [84] synthesised novel cation exchange membranes from 4-styrenesulfonic acid sodium salt hydrate, methacrylic acid and methyl methacrylate. The copolymer synthesis can be seen in Figure 2.7. This copolymer was reacted with PVA to form ester links between polymer chains, and secondary crosslinking was achieved by reacting the polymer with glutaric dialdehyde. Greater degrees of crosslinking were found to decrease the IEC and conductivity, as the crosslinked polymer chains restricted the mobility of ions. Compared with state of the art membranes, membrane properties were quite poor, with ion exchange capacities only up to 0.99 meq/g. High levels of water uptake resulted in an optimal conductivity of 14 mS/cm, however the resulting ion transport number was 0.92, indicating relatively poor selectivity.

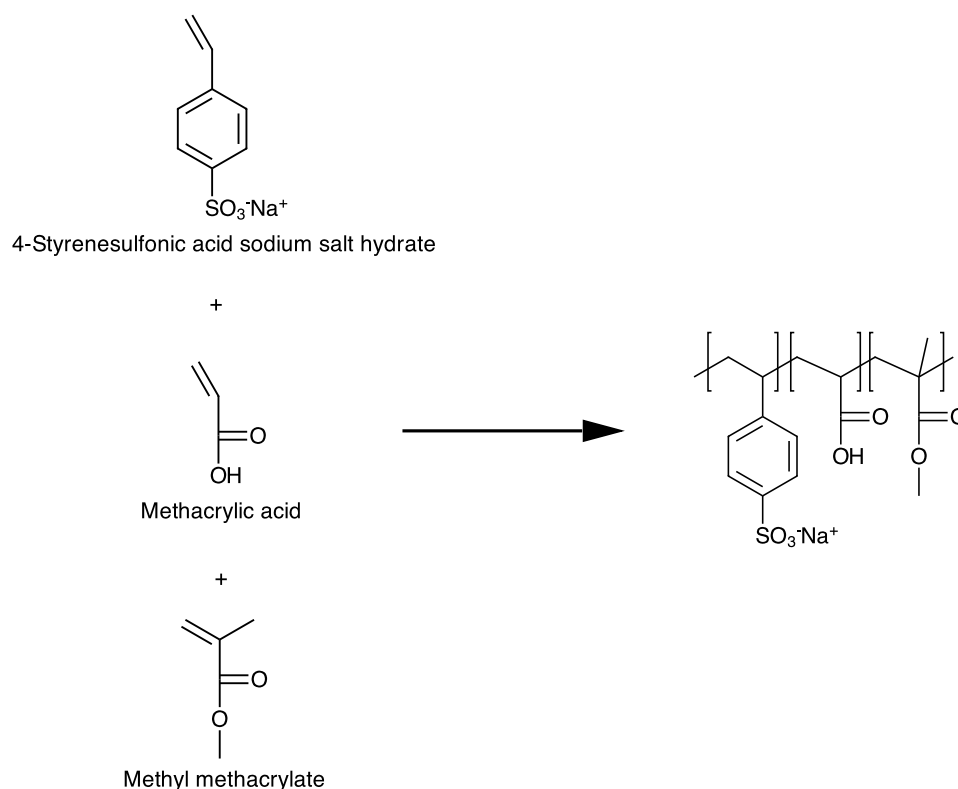


Figure 2.7 - Reaction mechanism for the copolymerisation of 4-styrenesulfonic acid sodium salt hydrate, methacrylic acid and methyl methacrylate.

Rhim et al. [101] synthesised a PVA cation exchange polymer crosslinked with sulfosuccinic acid for use in polymer electrolyte membrane fuel cells, which has subsequently been applied as a cation exchange polymer for use in MCDI [103]. The reaction scheme for the polymer is shown in Figure 2.8. The sulfosuccinic acid served as a crosslinker, preventing the water soluble PVA from dissolving in water. The

sulfonic acid group on the crosslinks introduced a fixed negative charge into the polymer matrix. High concentrations of sulfosuccinic acid therefore increased the IEC of the polymer, and up until a certain concentration increased the mechanical stability through crosslinking. However, it was observed that once the concentration of sulfosuccinic acid became too high, the hydrophilic effects of the sulfonic acid group outweighed the effects of crosslinking, resulting in an increase in water uptake, which reduced stability [101].

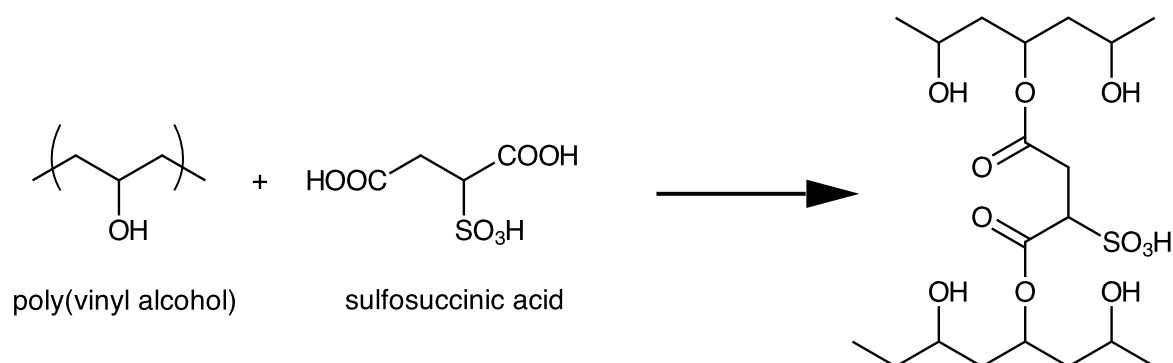


Figure 2.8 - Reaction mechanism of PVA and sulfosuccinic acid to form a crosslinked cation exchange polymer.

One problem with the use of commercial flat sheet membranes in CDI applications is the additional resistance caused between the membrane and the electrode [103]. The aforementioned PVA/sulfosuccinic acid polymer was used as a polymeric coating on activated carbon electrodes rather than being used as a flat sheet membrane by Kim et al. [103]. This technique yielded ion-exchange coatings with area specific resistances lower than those of commercial membranes. An alternative approach to reduce this resistance saw the spraying of carbon cloth electrodes with bromomethylated poly(2, 6-dimethyl-1, 4-phenylene oxide) (BPPO) solution, which was subsequently sulfonated with sulfuric acid to attach functional groups to the polymer [93]. An SEM image of the carbon cloth fibres pre- and post treatment is seen in Figure 2.9, whereby the coating forms a continuous ion-conducting surface on the carbon and interconnects individual carbon fibres. The electrodes were found to enhance CDI performance, however a reliable comparison to MCDI using a Neosepta CMX membrane was not achieved.

In light of the relatively few studies on membranes for MCDI, there is scope to prepare and characterise cation exchange membranes specifically for use in MCDI and to examine their effects on the CDI

process. The application of a coating technique to reduce resistance is of great importance, as it gives an inherent advantage over commercial and other flat-sheet membranes.

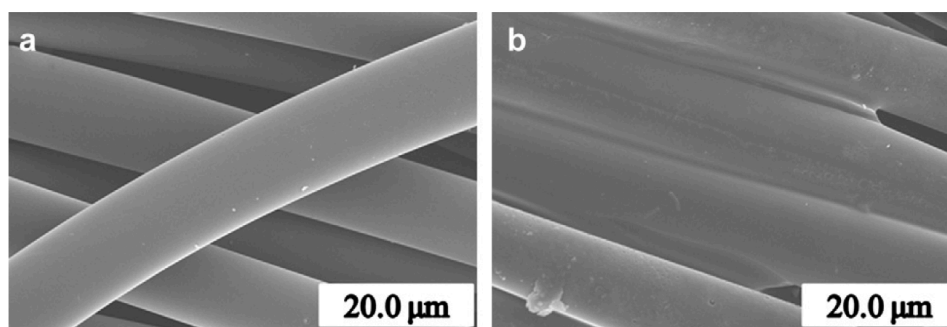


Figure 2.9 - SEM images of a) carbon cloth and b) carbon cloth coated with sulfonated BPPO solution. Reprinted from [93] with permission from Elsevier.

2.4 Poly(arylene ether sulfone) Cation Exchange Membranes

The driving force for the development of proton exchange membranes for fuel cells has been the high cost of commercial perfluorinated sulfonic acid membranes [104]. The production of more cost-effective membranes is seen as important step that can help drive the development of economically competitive and environmentally friendly separation technologies across a range of industries [96]. A number of recent advances in the development of cation exchange membranes have been made, in particular the development of new materials and fundamental research into membrane properties [105, 106]. A wider application of these new materials will be of benefit to numerous other processes, including MCDI.

Poly(arylene ether sulfone)s have a range of properties that make them suitable candidates for incorporation into cation exchange copolymer membranes. Their polymer backbone consists of phenyl rings bonded by ether or sulfone groups. They have excellent mechanical and thermal properties, and have high chemical stability due to the absence of readily oxidisable links along the polymer chain [107].

2.4.1 Poly(arylene ether sulfone) Sulfonation

To selectively allow the transport of cations through a dense polymer membrane, the poly(arylene ether sulfone) must be functionalised by introducing fixed negative charges to the polymer. The functionalisation process plays a large role in determining the properties of the polymer, in particular the electrical resistance and permselectivity [108]. Functionalisation creates hydrophilic regions that reduce mechanical and chemical stability, and so a trade-off between the stability and ion exchange properties

exists. Thus, the challenge is to modify the polymer without compromising its excellent mechanical properties.

Sulfonation is commonly used over other forms of functionalisation such as carboxylation or phosphonation, as the process is relatively simple and yields membranes with favourable ion transport properties [90]. As a strong acid, sulfonic acid also easily dissociates compared with weaker acids such as carboxylic acid [109]. Sulfonation is an electrophilic aromatic substitution reaction, where a hydrogen atom on an aromatic ring is substituted for an electrophile, i.e., the sulfonic acid group, SO_3H^+ . The mechanism for sulfonation of benzene is shown in Figure 2.10. Note that any substituents on the phenyl ring will affect its reactivity towards sulfonation; those that donate electrons to the ring increase reactivity, and those that withdraw electrons reduce reactivity. This can determine the choice of sulfonating agent, with options including chlorosulfonic acid, sulfuric acid and sulfur trioxide [104, 110].

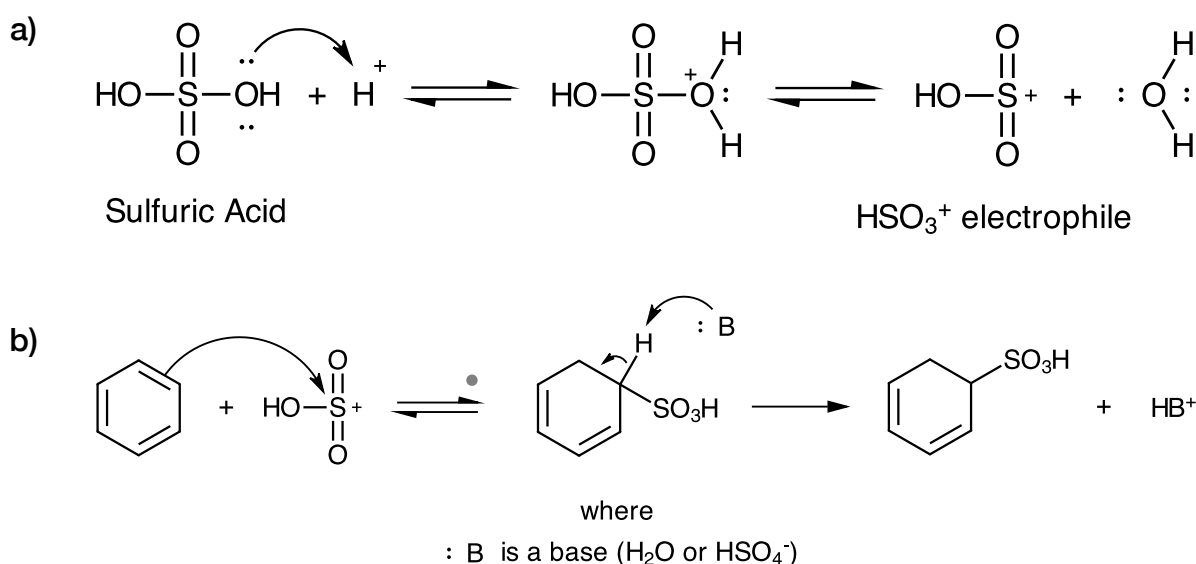


Figure 2.10 - Sulfonation of benzene via an electrophilic aromatic substitution reaction, where a) shows the formation of the electrophile SO_3H^+ from concentrated sulfuric acid and b) shows the sulfonation reaction mechanism.

Poly(arylene ether sulfone) sulfonation was first reported by Quentin [111], who used chlorosulfonic acid and sulfur trioxide as sulfonating agents. Further studies have examined the use of chlorosulfonic acid and trimethylsilyl chlorosulfonic acid as sulfonating agents for various poly(arylene ether sulfone)s [112-115]. It has been shown by Genova-Dimitrova et al. [113] that the use of trimethylsilyl chlorosulfonate can prevent undesirable chain scissions and branching which can occur when chlorosulfonic acid is used as the sulfonating reagent. In spite of these studies, sulfuric acid is widely used for sulfonation due to its low cost, availability and aggressiveness as a reagent.

2.4.1.1 Pre-sulfonation

Three methods exist for the sulfonation of polymers; the sulfonation of monomers which are subsequently polymerised (pre-sulfonation), the direct sulfonation of the polymer backbone post polymerisation (post-sulfonation), and the direct sulfonation of film-formed membranes [116]. Each of these methods affects the properties of the cation exchange membrane.

Pre-sulfonation generally allows for a greater control over the degree of sulfonation, molecular weight, ionic concentration and the chemical structure of the sulfonated polymer [117]. In their study on pre- and post-sulfonated poly(arylene ether sulfone)s, Kang et al. [110] demonstrated that pre-sulfonated polymers yielded IECs close to their maximum theoretical value, where for a disulfonated monomer, maximum theoretical IEC is calculated assuming two sulfonic groups are introduced per repeating unit. These polymers can be seen in Figure 2.11. For post-sulfonation, a large discrepancy between theoretical and experimental values was observed. This is due to the electrophilic substitution *ortho* to the ether link, which only allowed one sulfonate group per repeating unit, as shown in Figure 2.11 c). Direct monomer sulfonation on the other hand allowed electrophilic substitution *ortho* to each chlorine endgroup, allowing for two sulfonated groups per monomer as seen in Figure 2.11 a and b).

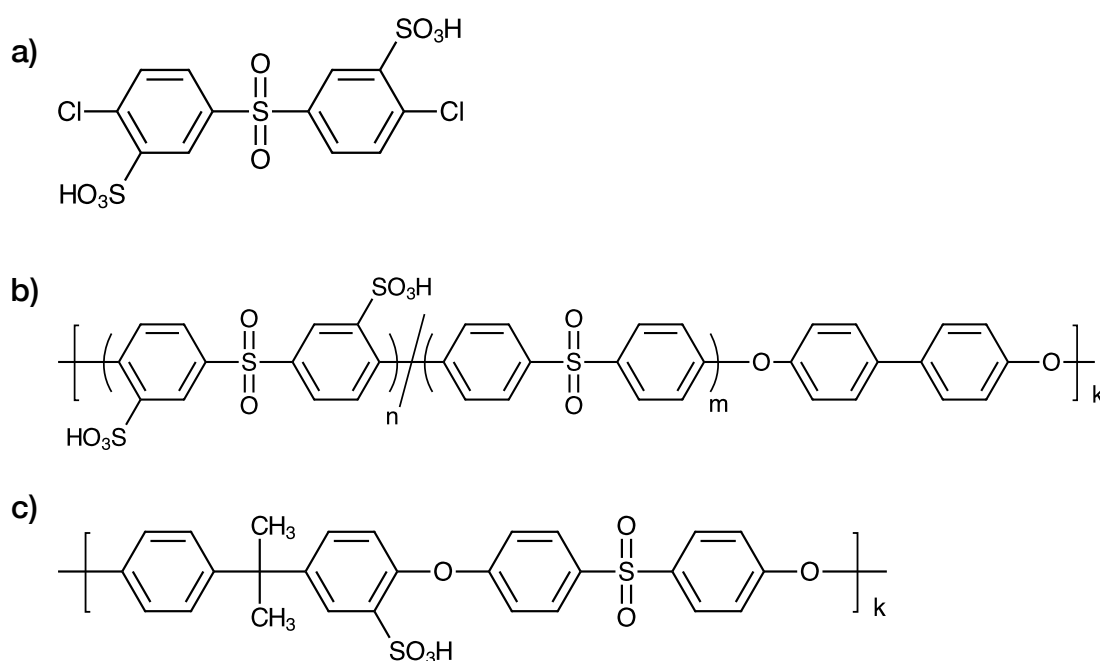


Figure 2.11 - a) Sulfonated precursor monomer, b) pre-sulfonated poly(arylene ether sulfone) and c) post-sulfonated poly(arylene ether sulfone), demonstrated by Kang et al. [110] .

2.4.1.2 Post-sulfonation

Although the direct modification of the polymer backbone is more difficult to control than pre-sulfonation, under defined conditions reproducible results are achievable [118]. This reproducibility, coupled with the simplicity and cost effectiveness of the process, has led to the widespread practice of post-sulfonation [96, 116, 118].

Post sulfonated poly(arylene ether sulfone) membranes have been widely studied for a range of applications, including fuel cells [119, 120], reverse osmosis and filtration membranes [121-124] and electrodialysis [124-128]. The post-sulfonation of poly(ether sulfone) (PES, a poly(arylene ether sulfone)), has been studied by a number of researchers [115, 119, 126]. The chemical structure of PES and sulfonated PES (sPES) can be seen in Figure 2.12. Nolte et al. [115] sulfonated the commercially available Victrex[®] polyethersulfone with sulfur trioxide. Greater degrees of PES sulfonation were seen to increase the glass transition temperatures (T_g) due to greater hydrogen bonding within the polymer matrix. The degree of sulfonation was approximately 90%, and polymers were measured to have an IEC of 3.0 meq/g, a permselectivity of 0.90 for membranes in aqueous KCl, and a water uptake of 74%. While the IEC and permselectivity is comparable to commercial cation exchange membranes (see Table 2.2), the high degree of swelling of the membrane resulted in a significant loss of mechanical stability. Swelling reductions were observed after crosslinking the membranes by reacting sulfonic acid groups activated with N-sulfonyl-imidazole with diamines. However due to the loss of fixed charges within the polymer matrix, this technique simultaneously reduced the permselectivity and conductivity.

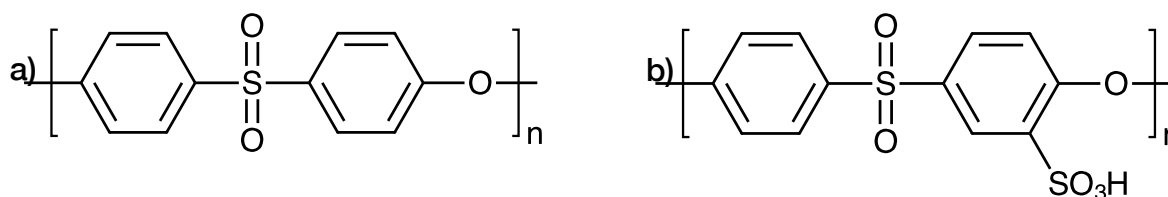


Figure 2.12 - Molecular structure of a) PES and b) sPES.

Dai et al. [119] prepared sPES membranes by sulfonating PES with chlorosulfonic acid, using concentrated sulfuric acid as a solvent. These membranes were found to have a percolation threshold at a degree of sulfonation of 39%. Above this value the water uptake drastically increased and mechanical stability was compromised. This was due to the observed microphase separation between hydrophobic and hydrophilic regions that exist in the sPES membranes. The hydrophilic clusters are due to regions of

aggregated sulfonic groups, and were seen to increase in size with degree of sulfonation. With a degree of sulfonation of 50%, ion rich channels rather than ionic clusters were observed, resulting in an undesirable, rapid change in polymer properties that compromised selectivity and mechanical stability.

Similar results have been demonstrated by Klagsom et al. [126], who also used chlorosulfonic acid for the sulfonation of PES rather than concentrated sulfuric acid. Here, the optimal degree of sulfonation was found to be 40% with an IEC of 1.44 meq/g, transport number of 0.925 and a conductivity of 0.0591 mS/cm. Higher IECs and conductivities similar to commercially available membranes were able to be obtained, however this was at the expense of both transport number and mechanical stability.

2.4.1.3 Side-chain Sulfonation

Due to the nature of the electrophilic substitution reaction, the post-sulfonation of poly(ether sulfone) occurs in the *ortho*-position to the ether linkage, as shown in Figure 2.13. Since the sulfonic acid group is positioned on the polymer backbone, this is known as main-chain sulfonation. When sulfonation of this nature occurs, the hydrophobic nature of the backbone is compromised which affects mechanical stability, and the sulfonic acid groups become less acidic [129, 130]. Generally, the mechanical stability for homogeneous sulfonated arylene main-chain polymers becomes compromised once the IEC exceeds 1.4-1.6 meq/g [131]. Acid groups on main chains also have poor ion clustering, reducing the effect of hydrophilic regions which are crucial for the transport of counterions through the polymer matrix [129].

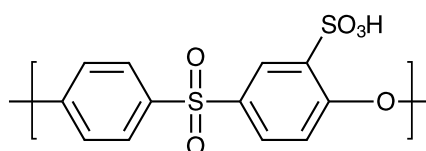


Figure 2.13 - An example of main chain sulfonation: a sulfonated poly(ether sulfone) with the sulfonated group in the *ortho*-position to the ether linkage.

To address this issue and to increase the practical maximum IEC and conductivity, numerous studies have investigated the introduction of sulfonated pendant phenyl side-chains along the polymer backbone. [132-138]. These studies have yielded polymers exhibiting enhanced chemical and mechanical properties. An example of side-chain sulfonation can be seen in Figure 2.14.

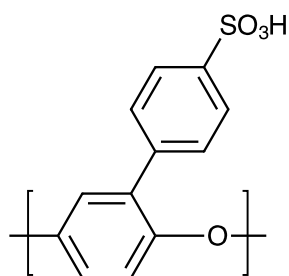


Figure 2.14 - An example of side-chain sulfonation: a pendant phenyl ring with the sulfonated group in the *para*-position

Jannasch et al. modified [132] polysulfone and polyphenylene sulfone with the addition of a pendant sulfonated phenyl group via ketone links. Lithiated sites on the polymer backbone were reacted with 2-sulfobenzoic acid cyclic anhydride. An example of this reaction scheme is shown in Figure 2.15. This synthesis route yielded no side-reactions resulting in crosslinking or other structural modifications. Membranes fabricated from this polymer yielded IECs of up to 1.5 meq/g, with water uptake in the protonated form no greater than 48%, providing good mechanical stability.

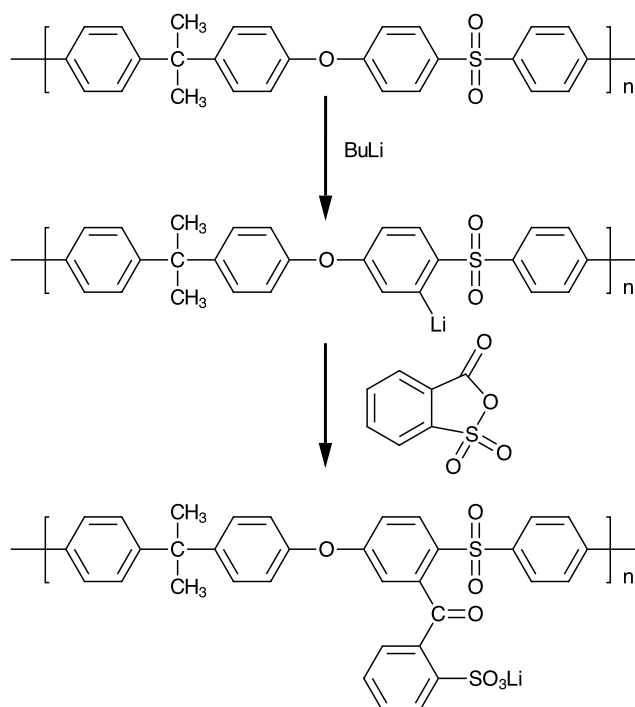


Figure 2.15 - Synthesis of sulfophenylated polysulfone via lithiation and reaction with 2-sulfobenzoic acid cyclic anhydride [132, 133]. Note that the sulfonation is on the side chain rather than the polymer backbone.

Liu et al. [134] investigated the sulfonation of poly(ether ether ketone)s containing a range of phenyl based side-chains. Presented in Figure 2.16, the polymers shown in a) and b) were found to have ion exchange capacities of 2.23 and 2.19 meq/g, respectively, while retaining good mechanical properties. Direct polymer sulfonation was used, and the pendant phenyl groups allowed for only a single sulfonation

site per repeat unit. Importantly, this control over the sulfonation would normally only be achievable through the copolymerisation of pre-sulfonated monomers.

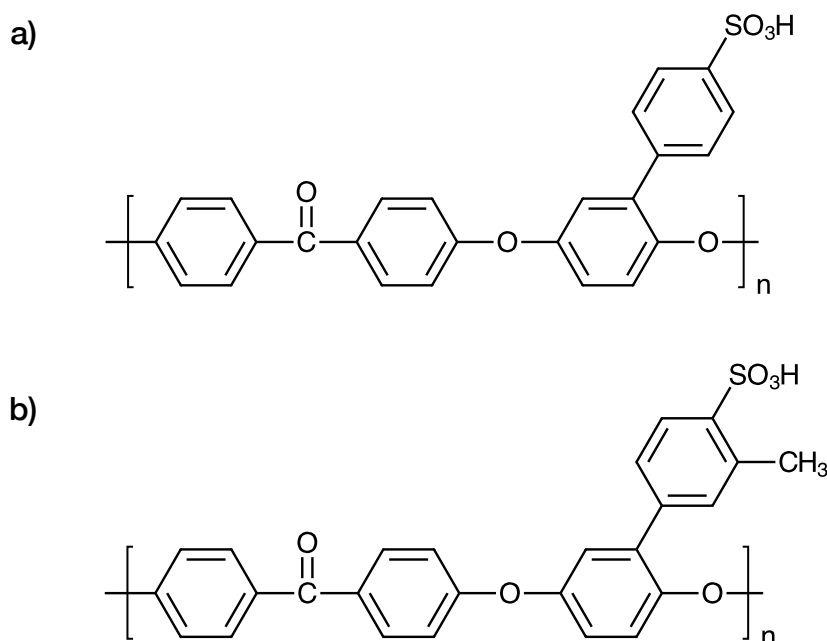


Figure 2.16 - Poly(ether ether ketone)s with a) sulfonated phenyl side-chain and b) sulfonated 3-methylphenyl side chain [134].

Similarly, Kim et al. [136] prepared poly(arylene ether)s with sulfonated groups in the *para* position of pendant phenyl rings. This produced a single sulfonated group per repeating unit, as shown in Figure 2.17, with sufficient sulfonation reaction time yielding polymers with a 100% degree of sulfonation. These membranes yielded high ion exchange capacities up to 2.71 meq/g and maintained high levels of mechanical stability.

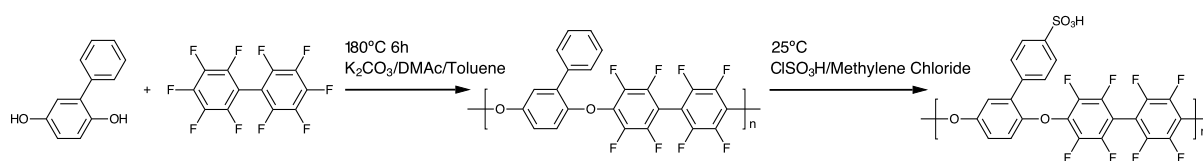


Figure 2.17 - Synthesis of sulfonated poly(arylene ether) copolymers containing a pendant sulfonic acid group [136].

Meier-Haack et al. [135] produced poly(arylene ether sulfone)s with IECs up to 1.5 mmol/g. The use of sulfuric acid as a sulfonating agent favoured sulfonation of the pendant phenyl ring, however as shown in Figure 2.18, main chain sulfonation was also observed. Furthermore, with the use of chlorosulfonic acid trimethylsilylester instead of sulfuric acid, as much as 75% of the main chain was sulfonated. The observed main chain sulfonation was due to the presence of the 4,4'-difluorodiphenyl sulfone monomer,

which increases the reactivity of the benzene ring towards electrophilic aromatic substitution. While the degree of sulfonation increased, the sulfonated main chain resulted in an undesirable loss of mechanical stability. In contrast, the sulfonated polymers prepared by Liu et al. [134] and Kim et al. [136] exhibited side-chain sulfonation only. This was a result of the greater electron withdrawing effects on the benzene ring of the precursor monomers in the polymer backbone (4,4'-difluorobenzophenone, decafluorobiphenyl and 2,6-difluorobenzonitrile), reducing the main chain's activity towards sulfonation.

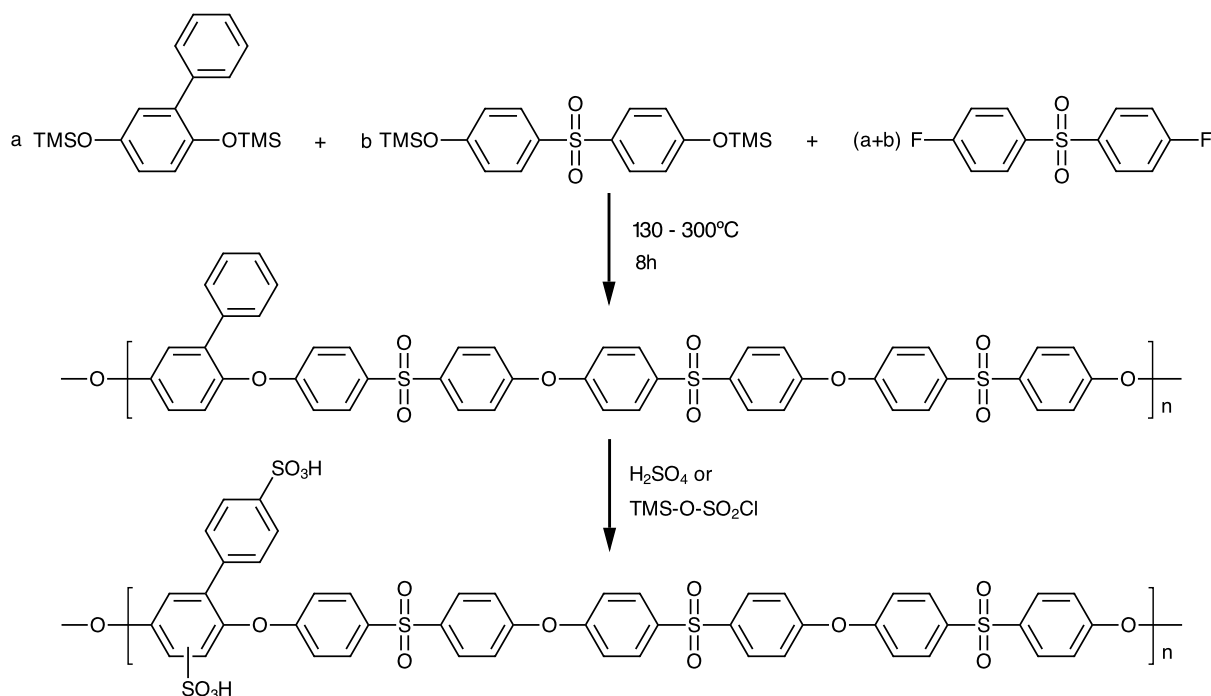


Figure 2.18 - Synthesis of sulfonated poly(arylene ether sulfone)s containing both a pendant sulfonic acid group and a main chain sulfonic acid group [135].

Both Liu et al. [137] and Vogel et al. [138] have recently introduced 2,5-diphenylhydroquinone into poly(arylene ether sulfone)s, which provided two pendant phenyl side-chains for sulfonation. The resulting polymers were found to have sulfonic acid groups on each pendant phenyl ring, allowing for two sulfonation sites per repeating unit, as shown in Figure 2.19. This approach increases the hydrophilicity of the polymer without compromising the main chain.

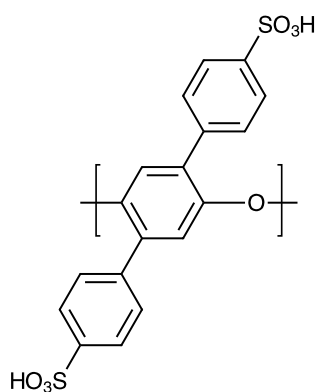


Figure 2.19 - Pendant phenyl rings with sulfonation in the *para*-position.

These advances in post-sulfonation techniques, particularly the introduction of sulfonated side-chains, have produced membranes with excellent properties that show good results when applied to fuel cells. However, similar side-chain sulfonated copolymers are yet to be studied for ion exchange desalination technologies. This study will examine the use of side-chain sulfonated poly(arylene ether sulfone)s synthesised using the 2,5 diphenylhydroquinone monomer, using the same polymers as those prepared by Vogel et al. [138].

2.4.2 Poly(arylene ether sulfone) Copolymers

In general, a high membrane water uptake increases conductivity at the expense of mechanical strength; conductivity therefore needs to be maximised while limiting water uptake. Crosslinking has been shown to be an effective method in increasing the stability of poly(arylene ether sulfone) membranes without greatly sacrificing conductivity [139]. This can also be achieved by segregating hydrophobic and hydrophilic regions of the polymer matrix through the synthesis of copolymers that combine both hydrophilic and hydrophobic monomers. By using suitable monomers, efficient ionic networks and mechanically stable backbones can be formed that increase membrane stability without compromising membrane performance.

Copolymers can be tailored to incorporate a blend of properties, and different configurations of copolymers exist. This study concerns itself with random and multiblock copolymers. Random or statistical copolymers have a statistical distribution of monomers along the polymer chain, while block copolymers exhibit an ordered structure, and are comprised of discrete polymer blocks that are bonded together to form longer polymer chains. Block copolymers are attractive materials for ion-exchange membranes, as the polymer architecture can easily be controlled, allowing for defined ionic and non-ionic

(or hydrophilic and hydrophobic) domains in the polymer chain. Studies have shown that compared with random copolymers, block copolymers with similar composition have a lower water uptake and are more mechanically robust without sacrificing IEC [138, 140-142].

The synthesis of disulfonated copolymers from 3,3'-disulfonated-4,4'-dichlorodiphenyl sulfone has been widely studied for use in fuel cells [104, 110, 143-146] and reverse osmosis processes [117, 147-150]. For use as reverse osmosis membranes, the chemical stability of these polymers provides a good tolerance to aqueous chlorine over a range of pH values. These membranes take advantage of the pre-sulfonation method, whereby the 4,4'-dichlorodiphenyl sulfone monomer is sulfonated via an electrophilic substitution reaction allowing two sulfonated groups per monomer, as described in section 2.4.1.1. The final copolymers benefit from easily reproducible levels of sulfonation, and controlled molecular weight, ionic concentrations morphology [117].

Ueda et al. [145] demonstrated the synthesis route of poly(arylene ether sulfone) random copolymers via an aromatic nucleophilic substitution reaction, shown in Figure 2.20. This is now the most common synthesis route to produce sulfonated poly(arylene ether sulfone)s [104]. This reaction controls the location of the sulfonic acid group, as well as the degree of sulfonation based on the feed ratio of the precursor monomers.

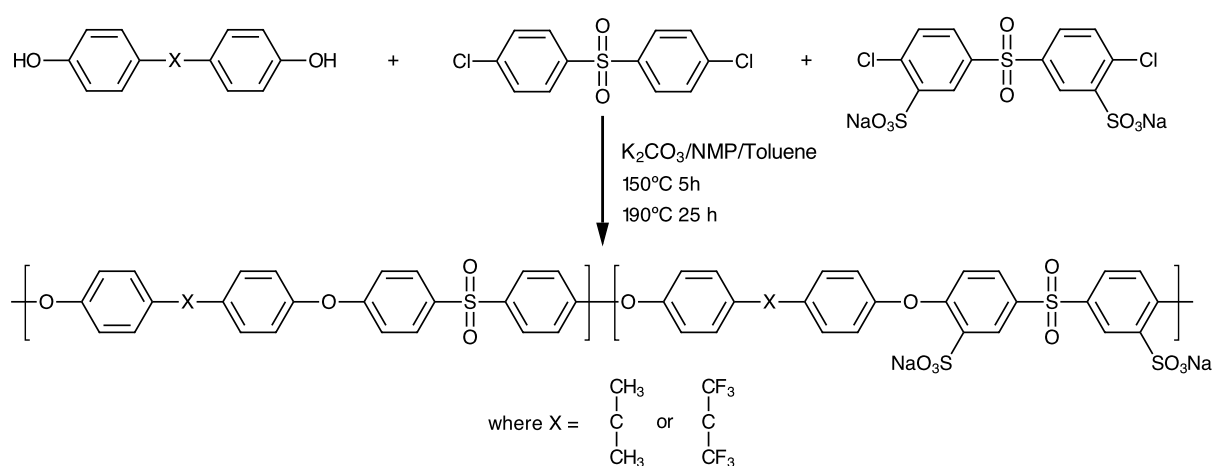


Figure 2.20 - Synthesis of a disulfonated poly(arylene ether sulfone) copolymer via an aromatic nucleophilic substitution reaction.

Studies on sulfonated poly(arylene ether sulfone)s have shown the importance on the microphase-separation between hydrophilic and hydrophobic domains and how this can effect membrane performance [143, 146]. Wang et al. [143] produced sulfonated poly(arylene ether sulfone) random

copolymers from 4,4'-dichlorodiphenylsulfone, 4,4'-biphenol and 3,3'-disulfonate-4,4'-dichlorodiphenylsulfone. It was found that phase separation occurs in polymers with a disulfonated monomer ratio up to approximately 50%. Above this ratio, hydrophilic domains became continuous, ionic rich phases rather than segregated ion domains, and the membranes become characterised by large water uptake and poor mechanical strength. This percolation threshold limits the practical maximum value of IEC and conductivity. As described in section 2.4.1.1, similar results were observed by Kang et al. [110] in their comparative study on pre and post sulfonated poly(ether sulfone)s.

2.5 Summary

Presently there are a large number of studies in the literature on the preparation of polymers and ion-exchange membranes for fuel cells and electrodialysis, however there are few studies that examine the fundamental properties of ion-exchange membranes and their effects on CDI processes. In particular, while a number of state of the art random and multiblock poly(ether sulfone) copolymers have been developed for pressure-driven desalination membranes [117, 147-150] and for fuel cell applications [138, 151], these materials have yet to be prepared and characterised for MCDI.

To address this gap in the literature, several state-of-the-art poly(arylene ether sulfone) polymers will be synthesised. For the scope of this thesis, despite the greater control of polymer properties that is achievable using the pre-sulfonation technique, the use of the post-sulfonation technique is justified by its simplicity and cost effectiveness. To compensate for the loss of control over polymer properties, random and multiblock copolymers of different compositions will be synthesised to balance the hydrophilic and hydrophobic properties required for an effective cation exchange membrane. The degree of sulfonation will be further controlled through the incorporation of the 2,5 diphenylhydroquinone monomer in the polymer backbone, which will allow for two sulfonation sites per repeating monomer and increase the hydrophilicity of the polymer without severely compromising the main chain and the polymers' hydrophobic properties.

Due to its economic benefits and ease of preparation, activated carbon will be used as the primary carbon material for electrosorption. This thesis will then focus on the enhancement of activated carbon using state-of-the-art polymers as both membrane coatings and ion-exchange binders. In addition, the properties of the activated carbon electrodes with graphite as a conductive filler will be examined. This

will include a study on the effect of graphite on electrode capacitance and resistance, as well as the physical adsorption and poor wettability of activated carbon electrodes.

2.6 Publications

In addition to this literature review, the following publications can be referred to for more information on the management of concentrated desalination waste, and on state-of-the-art polymers and ion-exchange membranes for fuel cells:

Book

Ladewig, B.P. and Asquith, B.M., *Desalination Concentrate Management*, Springer, Heidelberg, 2012

Book Chapters

Ladewig, B.P, Asquith, B.M. and Meier-Haack, J., Key Materials for Low-Temperature Fuel Cells: An Introduction, in B. Ladewig, S. Jiang, Y. Yan & M. Lu (eds.), *Materials for Low-Temperature Fuel Cells*, Wiley-VCH, Weinheim, 2014.

Ladewig, B.P, Asquith, B.M. and Meier-Haack, J., Membranes for Direct Methanol Fuel Cells, in B. Ladewig, S. Jiang, Y. Yan & M. Lu (eds.), *Materials for Low-Temperature Fuel Cells*, Wiley-VCH, Weinheim, 2014.

2.7 References

- [1] Blair, J. W. and Murphy, G. W., Electrochemical Demineralization of Water with Porous Electrodes of Large Surface Area, in *Saline Water Conversion*, American Chemical Society, 1960, pp. 206-223.
- [2] Murphy, G. W. and Caudle, D. D., Mathematical theory of electrochemical demineralization in flowing systems, *Electrochimica Acta*, 12 (1967) 1655-1664.
- [3] Johnson, A. M., Venolia, A. W., Wilbourne, R. G., and Newman, J., The Electrosorb Process for Desalting Water, United States Department of the Interior, 1970.
- [4] Johnson, A. M. and Newman, J., Desalting by Means of Porous Carbon Electrodes, *Journal of the Electrochemical Society*, 118 (1971) 510-517.
- [5] Oren, Y. and Soffer, A., Electrochemical Parametric Pumping, *Journal of the Electrochemical Society*, 125 (1978) 869-875.
- [6] Oren, Y. and Soffer, A., Water desalting by means of electrochemical parametric pumping. I. The equilibrium properties of a batch unit cell, *Journal of Applied Electrochemistry*, 13 (1983) 473-487.
- [7] Oren, Y. and Soffer, A., Water desalting by means of electrochemical parametric pumping. II. Separation properties of a multistage column, *Journal of Applied Electrochemistry*, 13 (1983) 489-505.
- [8] Farmer, J. C., Bahowick, S. M., Harrar, J. E., Fix, D. V., Martinelli, R. E., Vu, A. K., and Carroll, K. L., Electrosorption of Chromium Ions on Carbon Aerogel Electrodes as a Means of Remediating Ground Water, *Energy & Fuels*, 11 (1997) 337-347.

- [9] Farmer, J. C., Fix, D. V., Mack, G. V., Pekala, R. W., and Poco, J. F., Capacitive Deionization of NaCl and NaNO₃ Solutions with Carbon Aerogel Electrodes, *Journal of the Electrochemical Society*, 143 (1996) 159-169.
- [10] Farmer, J. C., Richardson, J. H., and Fix, D. V., Desalination with Carbon Aerogel Electrodes, Lawrence Livermore National Laboratory, 1996.
- [11] Gabelich, C. J., Tran, T. D., and Suffet, I. H., Electrosorption of Inorganic Salts from Aqueous Solution Using Carbon Aerogels, *Environmental Science and Technology*, 36 (2002) 3010-3019.
- [12] Pekala, R. W., Farmer, J. C., Alviso, C. T., Tran, T. D., Mayer, S. T., Miller, J. M., and Dunn, B., Carbon aerogels for electrochemical application, *Journal of Non-Crystalline Solids*, 225 (1998) 74-80.
- [13] Yang, K. L., Yiacoumi, S., and Tsouris, C., Electrosorption capacitance of nanostructured carbon aerogel obtained by cyclic voltammetry, *Journal of Electroanalytical Chemistry*, 540 (2003) 159-167.
- [14] Yang, K. L., Ying, T. Y., Yiacoumi, S., Tsouris, C., and Vittoratos, E. S., Electrosorption of Ions from Aqueous Solutions by Carbon Aerogel: An Electrical Double-Layer Model, *Langmuir*, 17 (2001) 1961-1969.
- [15] Ying, T. Y., Yang, K. L., Yiacoumi, S., and Tsouris, C., Electrosorption of ions from aqueous solutions by nanostructured carbon aerogel, *Journal of Colloid and Interface Science*, 250 (2002) 18-27.
- [16] Park, K.-K., Lee, J.-B., Park, P.-Y., Yoon, S.-W., Moon, J.-S., Eum, H.-M., and Lee, C.-W., Development of a carbon sheet electrode for electrosorption desalination, *Desalination*, 206 (2007) 86-91.
- [17] Zou, L., Morris, G., and Qi, D., Using activated carbon electrode in electrosorptive deionisation of brackish water, *Desalination*, 225 (2008) 329-340.
- [18] Lee, J., Park, K., Yoon, S., Park, P., Park, K., and Lee, C., Desalination performance of a carbon-based composite electrode, *Desalination*, 237 (2009) 155-161.
- [19] Choi, J. H., Fabrication of a carbon electrode using activated carbon powder and application to the capacitive deionization process, *Separation and Purification Technology*, 70 (2010) 362-366.
- [20] Hou, C.-H., Huang, J.-F., Lin, H.-R., and Wang, B.-Y., Preparation of activated carbon sheet electrode assisted electrosorption process, *Journal of the Taiwan Institute of Chemical Engineers*, 43 (2012) 473-479.
- [21] Wang, G., Pan, C., Wang, L., Dong, Q., Yu, C., Zhao, Z., and Qiu, J., Activated carbon nanofiber webs made by electrospinning for capacitive deionization, *Electrochimica Acta*, 69 (2012) 65-70.
- [22] Park, B.-H., Kim, Y.-J., Park, J.-S., and Choi, J., Capacitive deionization using a carbon electrode prepared with water-soluble poly(vinyl alcohol) binder, *Journal of Industrial and Engineering Chemistry*, 17 (2011) 717-722.
- [23] Villar, I., Roldan, S., Ruiz, V., Granda, M., Blanco, C., Menéndez, R., and Santamaría, R., Capacitive Deionization of NaCl Solutions with Modified Activated Carbon Electrodes, *Energy & Fuels*, 24 (2010) 3329-3333.
- [24] Nadakatti, S., Tendulkar, M., and Kadam, M., Use of mesoporous conductive carbon black to enhance performance of activated carbon electrodes in capacitive deionization technology, *Desalination*, 268 (2011) 182-188.
- [25] Dai, K., Shi, L., Fang, J., Zhang, D., and Yu, B., NaCl adsorption in multi-walled carbon nanotubes, *Materials Letters*, 59 (2005) 1989-1992.
- [26] Zhang, D., Shi, L., Fang, J., Dai, K., and Li, X., Preparation and desalination performance of multiwall carbon nanotubes, *Materials Chemistry and Physics*, 97 (2006) 415-419.

-
- [27] Yang, J., Zou, L., and Choudhury, N. R., Ion-selective carbon nanotube electrodes in capacitive deionisation, *Electrochimica Acta*, 98 (2012) 11-19.
 - [28] Yang, J., Zou, L., and Song, H., Preparing MnO₂/PSS/CNTs composite electrodes by layer-by-layer deposition of MnO₂ in the membrane capacitive deionisation, *Desalination*, 286 (2012) 108-114.
 - [29] Zhan, Y., Pan, L., Nie, C., Li, H., and Sun, Z., Carbon nanotube–chitosan composite electrodes for electrochemical removal of Cu(II) ions, *Journal of Alloys and Compounds*, 509 (2011) 5667-5671.
 - [30] Li, H., Zou, L., Pan, L., and Sun, Z., Using graphene nano-flakes as electrodes to remove ferric ions by capacitive deionization, *Separation and Purification Technology*, 75 (2010) 8-14.
 - [31] Li, H., Lu, T., Pan, L., Zhang, Y., and Sun, Z., Electrosorption behavior of graphene in NaCl solutions, *Journal of Materials Chemistry*, 19 (2009) 6773-6779.
 - [32] Li, H., Zou, L., Pan, L., and Sun, Z., Novel Graphene-Like Electrodes for Capacitive Deionization, *Environmental Science and Technology*, 44 (2010) 8692-8697.
 - [33] Jia, B. and Zou, L., Graphene nanosheets reduced by a multi-step process as high-performance electrode material for capacitive deionisation, *Carbon*, 50 (2012) 2315-2321.
 - [34] Yan, C., Kanaththage, Y. W., Short, R., Gibson, C. T., and Zou, L., Graphene/Polyaniline nanocomposite as electrode material for membrane capacitive deionization, *Desalination*, 344 (2014) 274-279.
 - [35] El-Deen, A. G., Barakat, N. A. M., and Kim, H. Y., Graphene wrapped MnO₂-nanostructures as effective and stable electrode materials for capacitive deionization desalination technology, *Desalination*, 344 (2014) 289-298.
 - [36] Li, H., Zaviska, F., Liang, S., Li, J., He, L., and Yang, H. Y., A high charge efficiency electrode by self-assembling sulphonated reduced graphene oxide onto carbon fibre: towards enhanced capacitive deionization, *Journal of Materials Chemistry A*, 2 (2014) 3484-3491.
 - [37] Oren, Y., Capacitive deionization (CDI) for desalination and water treatment — past, present and future (a review), *Desalination*, 228 (2008) 10-29.
 - [38] Ladewig, B. and Asquith, B., *Desalination Concentrate Management*, Springer, Heidelberg, 2012.
 - [39] Anderson, M. A., Cudero, A. L., and Palma, J., Capacitive deionization as an electrochemical means of saving energy and delivering clean water. Comparison to present desalination practices: Will it compete?, *Electrochimica Acta*, 55 (2010) 3845-3856.
 - [40] Porada, S., Zhao, R., van der Wal, A., Presser, V., and Biesheuvel, P. M., Review on the science and technology of water desalination by capacitive deionization, *Progress in Materials Science*, 58 (2013) 1388-1442.
 - [41] Christen, K., Desalination technology could clean up wastewater from coal-bed methane production, *Environmental Science and Technology*, 40 (2006) 639.
 - [42] Mossad, M., Zhang, W., and Zou, L., Using capacitive deionisation for inland brackish groundwater desalination in a remote location, *Desalination*, 308 (2012) 154-160.
 - [43] National Centre of Excellence in Desalination Australia, Australian Desalination Research Roadmap, 2012.
 - [44] Zou, L., Developing Nano-Structured Carbon Electrodes for Capacitive Brackish Water Desalination, in R. Y. Ning (Ed.) *Expanding Issues in Desalination*, InTech, 2011,
 - [45] Humplik, T., Lee, J., O'Hern, S. C., Fellman, B. A., Baig, M. A., Hassan, S. F., Atieh, M. A., Rahman, F., Laoui, T., Karnik, R., and Wang, E. N., Nanostructured materials for water desalination, *Nanotechnology*, 22 (2011) 292001.

- [46] Reynolds, G. A. M., Fung, A. W. P., Wang, Z. H., Dresselhaus, M. S., and Pekala, R. W., The effects of external conditions on the internal structure of carbon aerogels, *Journal of Non-Crystalline Solids*, 188 (1995) 27-33.
- [47] Wang, X. Z., Li, M. G., Chen, Y. W., Cheng, R. M., Huang, S. M., Pan, L. K., and Sun, Z., Electrosorption of ions from aqueous solutions with carbon nanotubes and nanofibers composite film electrodes, *Applied Physics Letters*, 89 (2006) 053127.
- [48] Jung, H.-H., Hwang, S.-W., Hyun, S.-H., Lee, K.-H., and Kim, G.-T., Capacitive deionization characteristics of nanostructured carbon aerogel electrodes synthesized via ambient drying, *Desalination*, 216 (2007) 377-385.
- [49] Xu, P., Drewes, J. E., Heil, D., and Wang, G., Treatment of brackish produced water using carbon aerogel-based capacitive deionization technology, *Water Research*, 42 (2008) 2605-2617.
- [50] Dresselhaus, M. S., Dresselhaus, G., and Saito, R., Physics of carbon nanotubes, *Carbon*, 33 (1995) 883-891.
- [51] Iijima, S., Helical microtubules of graphitic carbon, *Nature*, 354 (1991) 56-58.
- [52] Niyogi, S., Hamon, M. A., Hu, H., Zhao, B., Bhowmik, P., Sen, R., Itkis, M. E., and Haddon, R. C., Chemistry of Single-Walled Carbon Nanotubes, *Accounts of Chemical Research*, 35 (2002) 1105-1113.
- [53] Goh, P. S., Ismail, A. F., and Ng, B. C., Carbon nanotubes for desalination: Performance evaluation and current hurdles, *Desalination*, 308 (2013) 2-14.
- [54] Yan, C., Zou, L., and Short, R., Single-walled carbon nanotubes and polyaniline composites for capacitive deionization, *Desalination*, 290 (2012) 125-129.
- [55] Li, H., Gao, Y., Pan, L., Zhang, Y., Chen, Y., and Sun, Z., Electrosorptive desalination by carbon nanotubes and nanofibres electrodes and ion-exchange membranes, *Water Research*, 42 (2008) 4923-4928.
- [56] Gao, Y., Pan, L., Li, H., Zhang, Y., Zhang, Z., Chen, Y., and Sun, Z., Electrosorption behavior of cations with carbon nanotubes and carbon nanofibres composite film electrodes, *Thin Solid Films*, 517 (2009) 1616-1619.
- [57] Gao, Y., Pan, L., Zhang, Y., Chen, Y., and Sun, Z., Electrosorption of FeCl_3 solution with carbon nanotubes and nanofibres film electrodes grown on graphite substrates, *Surface Review and Letters*, 14 (2007) 1033-1037.
- [58] Pan, L., Wang, X., Gao, Y., Zhang, Y., Chen, Y., and Sun, Z., Electrosorption of anions with carbon nanotube and nanofibre composite film electrodes, *Desalination*, 244 (2009) 139-143.
- [59] Li, H., Pan, L., Zhang, Y., Zou, L., Sun, C., Zhan, Y., and Sun, Z., Kinetics and thermodynamics study for electrosorption of NaCl onto carbon nanotubes and carbon nanofibers electrodes, *Chemical Physics Letters*, 485 (2010) 161-166.
- [60] Liu, Y., Li, H., Nie, C., Pan, L., and Sun, Z., Carbon nanotube and carbon nanofiber composite films grown on different graphite substrate for capacitive deionization, *Desalination and Water Treatment*, 51 (2013) 3988-3994.
- [61] Dai, K., Shi, L., Zhang, D., and Fang, J., NaCl adsorption in multi-walled carbon nanotube/active carbon combination electrode, *Chemical Engineering Science*, 61 (2006) 428-433.
- [62] Zhang, D., Shi, L., Fang, J., and Dai, K., Removal of NaCl from saltwater solution using carbon nanotubes/activated carbon composite electrode, *Materials Letters*, 60 (2006) 360-363.
- [63] Nie, C., Pan, L., Li, H., Chen, T., Lu, T., and Sun, Z., Electrophoretic deposition of carbon nanotubes film electrodes for capacitive deionization, *Journal of Electroanalytical Chemistry*, 666 (2012) 85-88.

- [64] Nie, C., Pan, L., Liu, Y., Li, H., Chen, T., Lu, T., and Sun, Z., Electrophoretic deposition of carbon nanotubes–polyacrylic acid composite film electrode for capacitive deionization, *Electrochimica Acta*, 66 (2012) 106-109.
- [65] Zhu, Y., Murali, S., Cai, W., Li, X., Suk, J. W., Potts, J. R., and Ruoff, R. S., Graphene and Graphene Oxide: Synthesis, Properties, and Applications, *Advanced Materials*, 22 (2010) 3906-3924.
- [66] Ryoo, M.-W., Kim, J.-H., and Seo, G., Role of titania incorporated on activated carbon cloth for capacitive deionization of NaCl solution, *Journal of Colloid and Interface Science*, 264 (2003) 414-419.
- [67] Ryoo, M.-W. and Seo, G., Improvement in capacitive deionization function of activated carbon cloth by titania modification, *Water Research*, 37 (2003) 1527-1534.
- [68] Ahn, H.-J., Lee, J.-H., Jeong, Y., Lee, J.-H., Chi, C.-S., and Oh, H.-J., Nanostructured carbon cloth electrode for desalination from aqueous solutions, *Materials Science and Engineering: A*, 449-451 (2007) 841-845.
- [69] Myint, M. T. Z. and Dutta, J., Fabrication of zinc oxide nanorods modified activated carbon cloth electrode for desalination of brackish water using capacitive deionization approach, *Desalination*, 305 (2012) 24-30.
- [70] Seo, M.-K. and Park, S.-J., Effect of nanosize titanium oxide on electrochemical characteristics of activated carbon electrodes, *Current Applied Physics*, 10 (2010) 391-394.
- [71] Pandolfo, A. G., Wilson, G. J., Huynh, T. D., and Hollenkamp, A. F., The Influence of Conductive Additives and Inter-Particle Voids in Carbon EDLC Electrodes, *Fuel Cells*, 10 (2010) 856-864.
- [72] Rose, M. F., in *Proc. 33 Int. Power Sources Symp.*, Pennington, NJ, 1988.
- [73] Biniak, S. and Swiatkowski, A., in M. Pakula and L. R. Radovic (Eds.) *Chemistry and Physics of Carbon*, Marcek Dekker, New York, 2001,
- [74] Liu, X.-m., Zhang, R., Zhan, L., Long, D.-h., Qiao, W.-m., Yang, J.-h., and Ling, L.-c., Impedance of carbon aerogel/activated carbon composites as electrodes of electrochemical capacitors in aprotic electrolyte, *New Carbon Materials*, 22 (2007) 153-158.
- [75] Hess, W. H. and Herd, C. R., in J. B. Donet, R. C. Bansal, and M. J. Wang (Eds.) *Carbon Black: Science and Technology*, Marcel Dekker, New York, 1993, pp. 89.
- [76] Qu, D. and Shi, H., Studies of activated carbons used in double-layer capacitors, *Journal of Power Sources*, 74 (1998) 99-107.
- [77] Li, L., Zou, L., Song, H., and Morris, G., Ordered mesoporous carbons synthesized by a modified sol-gel process for electrosorptive removal of sodium chloride, *Carbon*, 47 (2009) 775-781.
- [78] Zou, L., Li, L., Song, H., and Morris, G., Using mesoporous carbon electrodes for brackish water desalination, *Water Research*, 42 (2008) 2340-2348.
- [79] Peng, Z., Zhang, D., Shi, L., Yan, T., Yuan, S., Li, H., Gao, R., and Fang, J., Comparative Electroadsorption Study of Mesoporous Carbon Electrodes with Various Pore Structures, *The Journal of Physical Chemistry C*, 115 (2011) 17068-17076.
- [80] Bazant, M. Z., Thornton, K., and Ajdari, A., Diffuse-charge dynamics in electrochemical systems, *Physical Review E*, 70 (2004) 021506.
- [81] Biesheuvel, P. M., Thermodynamic cycle analysis for capacitive deionization, *Journal of Colloid and Interface Science*, 332 (2009) 258-264.
- [82] Andelman, M. D. and Walker, G. S., Charge barrier flow-through capacitor, *US Patent 6,709,560*, March 23 2004.

- [83] Lee, J., Park, K., Eum, H., and Lee, C., Desalination of a thermal power plant wastewater by membrane capacitive deionization, *Desalination*, 196 (2006) 125-134.
- [84] Kwak, N.-S., Koo, J. S., Hwang, T. S., and Choi, E. M., Synthesis and electrical properties of NaSS–MAA–MMA cation exchange membranes for membrane capacitive deionization (MCDI), *Desalination*, 285 (2012) 138-146.
- [85] Andelman, M., Flow Through Capacitor basics, *Separation and Purification Technology*, 80 (2011) 262-269.
- [86] Li, H. and Zou, L., Ion-exchange membrane capacitive deionization: A new strategy for brackish water desalination, *Desalination*, 275 (2011) 62-66.
- [87] Zhao, R., Biesheuvel, P. M., and van der Wal, A., Energy consumption and constant current operation in membrane capacitive deionization, *Energy & Environmental Science*, 5 (2012) 9520.
- [88] Zhao, R., Satpradit, O., Rijnaarts, H. H., Biesheuvel, P. M., and van der Wal, A., Optimization of salt adsorption rate in membrane capacitive deionization, *Water Res*, 47 (2013) 1941-1952.
- [89] Biesheuvel, P. M. and van der Wal, A., Membrane capacitive deionization, *Journal of Membrane Science*, 346 (2010) 256-262.
- [90] Strathmann, H., Ion-exchange membrane separation processes, Elsevier, Amsterdam, 2004.
- [91] Kim, Y. J. and Choi, J. H., Enhanced desalination efficiency in capacitive deionization with an ion-selective membrane, *Separation and Purification Technology*, 71 (2010) 70-75.
- [92] Kim, Y. J., Hur, J., Bae, W., and Choi, J. H., Desalination of brackish water containing oil compound by capacitive deionization process, *Desalination*, 253 (2010) 119-123.
- [93] Lee, J. Y., Seo, S. J., Yun, S. H., and Moon, S. H., Preparation of ion exchanger layered electrodes for advanced membrane capacitive deionization (MCDI), *Water Research*, 45 (2011) 5375-5380.
- [94] ASTOM Corporation, Neosepta, <http://www.astom-corp.jp/en/product/02.html#03>, 2013.
- [95] Higa, M., Nishimura, M., Kinoshita, K., and Jikihara, A., Characterization of cation-exchange membranes prepared from poly(vinyl alcohol) and poly(vinyl alcohol-b-styrene sulfonic acid), *International Journal of Hydrogen Energy*, 37 (2012) 6161-6168.
- [96] Yee, R. S. L., Rozendal, R. A., Zhang, K., and Ladewig, B. P., Cost effective cation exchange membranes: A review, *Chemical Engineering Research and Design*, 90 (2011) 950-959.
- [97] FuMA-Tech, Fumasep Technical Data Sheet, Germany, 2005.
- [98] MEGA a.s., Cation-exchange membranes Ralex® product data sheets, Czech Republic, 2012.
- [99] AGC ENGINEERING, Selemion Ion Exchange Membranes, 2013.
- [100] Kwak, N.-S., Koo, J. S., Hwang, T. S., and Choi, E. M., Synthesis and electrical properties of NaSS–MAA–MMA cation exchange membranes for membrane capacitive deionization (MCDI), *Desalination*, (2011)
- [101] Rhim, J., Park, H., Lee, C., Jun, J., Kim, D., and Lee, Y., Crosslinked poly(vinyl alcohol) membranes containing sulfonic acid group: proton and methanol transport through membranes, *Journal of Membrane Science*, 238 (2004) 143-151.
- [102] Nagarale, R. K., Gohil, G. S., and Shahi, V. K., Recent developments on ion-exchange membranes and electro-membrane processes, *Advances in Colloid and Interface Science*, 119 (2006) 97-130.
- [103] Kim, J. S. and Choi, J. H., Fabrication and characterization of a carbon electrode coated with cation-exchange polymer for the membrane capacitive deionization applications, *Journal of Membrane Science*, 355 (2010) 85-90.

- [104] Harrison, W. L., Hickner, M. A., Kim, Y. S., and McGrath, J. E., Poly(Arylene Ether Sulfone) Copolymers and Related Systems from Disulfonated Monomer Building Blocks: Synthesis, Characterization, and Performance—A Topical Review, *Fuel Cells*, 5 (2005) 201-212.
- [105] Taeger, A., Vogel, C., Lehmann, D., Jehnichen, D., Komber, H., Meier-Haack, J., Ochoa, N. A., Nunes, S. P., and Peinemann, K. V., Ion exchange membranes derived from sulfonated polyaramides, *Reactive and Functional Polymers*, 57 (2003) 77-92.
- [106] Meier-Haack, J., Taeger, A., Vogel, C., Schlenstedt, K., Lenk, W., and Lehmann, D., Membranes from sulfonated block copolymers for use in fuel cells, *Separation and Purification Technology*, 41 (2005) 207-220.
- [107] Allegrezza Jr, A. E., Parekh, B. S., Parise, P. L., Swiniarski, E. J., and White, J. L., Chlorine resistant polysulfone reverse osmosis modules, *Desalination*, 64 (1987) 285-304.
- [108] Iojoiu, C., Maréchal, M., Chabert, F., and Sanchez, J.-Y., Mastering Sulfonation of Aromatic Polysulfones: Crucial for Membranes for Fuel Cell Application, *Fuel Cells*, 5 (2005) 344-354.
- [109] Geise, G. M., Paul, D. R., and Freeman, B. D., Fundamental Water and Salt Transport Properties of Polymeric Materials, *Progress in Polymer Science*,
- [110] Kang, M., Choi, Y.-J., Choi, I.-J., Yoon, T.-H., and Moon, S.-H., Electrochemical characterization of sulfonated poly(arylene ether sulfone) (S-PES) cation-exchange membranes, *Journal of Membrane Science*, 216 (2003) 39-53.
- [111] Quentin, J. P., Sulfonated Polyaryleneethersulfones, *US Patent 3,709,841*, January 9 1973.
- [112] Chao, H. S. and Kelsey, D. R., Process for preparing sulfonated poly(aryl ether resins), *US Patent 4,625,000*, November 25 1986.
- [113] Genova-Dimitrova, P., Baradie, B., Foscallo, D., Poinsignon, C., and Sanchez, J. Y., Ionomeric membranes for proton exchange membrane fuel cell (PEMFC): sulfonated polysulfone associated with phosphatoantimonic acid, *Journal of Membrane Science*, 185 (2001) 59-71.
- [114] Lufano, F., Gatto, I., Staiti, P., Antonucci, V., and Passalacqua, E., Sulfonated polysulfone ionomer membranes for fuel cells, *Solid State Ionics*, 145 (2001) 47-51.
- [115] Nolte, R., Ledjeff, K., Bauer, M., and Mülhaupt, R., Partially sulfonated poly(arylene ether sulfone) - A versatile proton conducting membrane material for modern energy conversion technologies, *Journal of Membrane Science*, 83 (1993) 211-220.
- [116] Klaysom, C., Ladewig, B. P., Lu, G. Q. M., and Wang, L., Recent Advances in Ion Exchange Membranes for Desalination Applications, in *Functional Nanostructured Materials and Membranes for Water Treatment*, Wiley-VCH Verlag GmbH & Co. KGaA, 2013, pp. 125-161.
- [117] Xie, W., Park, H. B., Cook, J., Lee, C. H., Byun, G., Freeman, B. D., and McGrath, J. E., Advances in membrane materials: desalination membranes based on directly copolymerized disulfonated poly(arylene ether sulfone) random copolymers, *Water Science and Technology*, 61 (2010) 619-624.
- [118] Rozière, J. and Jones, D. J., Non-Fluorinated Polymer Materials For Proton Exchange Membrane Fuel Cells, *Annual Review of Materials Research*, 33 (2003) 503-555.
- [119] Dai, H., Guan, R., Li, C., and Liu, J., Development and characterization of sulfonated poly(ether sulfone) for proton exchange membrane materials, *Solid State Ionics*, 178 (2007) 339-345.
- [120] Kopitzke, R. W., Linkous, C. A., Anderson, H. R., and Nelson, G. L., Conductivity and Water Uptake of Aromatic-Based Proton Exchange Membrane Electrolytes, *Journal of the Electrochemical Society*, 147 (2000) 1677-1681.
- [121] Kimura, S. G., Reverse Osmosis Performance of Sulfonated Poly(2,6-dimethylphenylene Ether) Ion Exchange Membranes, *Industrial & Engineering Chemistry Product Research and Development*, 10 (1971) 335-339.

- [122] Hamza, A., Chowdhury, G., Matsuura, T., and Sourirajan, S., Sulphonated poly(2,6-dimethyl-1,4-phenylene oxide)-polyethersulphone composite membranes. Effects of composition of solvent system, used for preparing casting solution, on membrane-surface structure and reverse-osmosis performance, *Journal of Membrane Science*, 129 (1997) 55-64.
- [123] Friedrich, C., Driancourt, A., Noel, C., and Monnerie, L., Asymmetric reverse osmosis and ultrafiltration membranes prepared from sulfonated polysulfone, *Desalination*, 36 (1981) 39-62.
- [124] Klaysom, C., Moon, S.-H., Ladewig, B. P., Lu, G. Q. M., and Wang, L., Preparation of porous ion-exchange membranes (IEMs) and their characterizations, *Journal of Membrane Science*, 371 (2011) 37-44.
- [125] Klaysom, C., Marschall, R., Moon, S.-H., Ladewig, B. P., Lu, G. Q. M., and Wang, L., Preparation of porous composite ion-exchange membranes for desalination application, *Journal of Materials Chemistry*, 21 (2011) 7401.
- [126] Klaysom, C., Ladewig, B. P., Lu, G. Q. M., and Wang, L., Preparation and characterization of sulfonated polyethersulfone for cation-exchange membranes, *Journal of Membrane Science*, 368 (2011) 48-53.
- [127] Klaysom, C., Moon, S. H., Ladewig, B. P., Lu, G. Q., and Wang, L., The effects of aspect ratio of inorganic fillers on the structure and property of composite ion-exchange membranes, *Journal of Colloid and Interface Science*, 363 (2011) 431-439.
- [128] Klaysom, C., Marschall, R., Wang, L., Ladewig, B. P., and Lu, G. Q. M., Synthesis of composite ion-exchange membranes and their electrochemical properties for desalination applications, *Journal of Materials Chemistry*, 20 (2010) 4669.
- [129] Kreuer, K. D., On the development of proton conducting polymer membranes for hydrogen and methanol fuel cells, *Journal of Membrane Science*, 185 (2001) 29-39.
- [130] Lafitte, B. and Jannasch, P., Proton-Conducting Aromatic Polymers Carrying Hypersulfonated Side Chains for Fuel Cell Applications, *Advanced Functional Materials*, 17 (2007) 2823-2834.
- [131] Kerres, J. A., Development of ionomer membranes for fuel cells, *Journal of Membrane Science*, 185 (2001) 3-27.
- [132] Lafitte, B., Karlsson, L. E., and Jannasch, P., Sulfophenylation of Polysulfones for Proton-Conducting Fuel Cell Membranes, *Macromolecular Rapid Communications*, 23 (2002) 896-900.
- [133] Karlsson, L. E. and Jannasch, P., Polysulfone ionomers for proton-conducting fuel cell membranes, *Electrochimica Acta*, 50 (2005) 1939-1946.
- [134] Liu, B., Robertson, G. P., Kim, D.-S., Guiver, M. D., Hu, W., and Jiang, Z., Aromatic Poly(ether ketone)s with Pendant Sulfonic Acid Phenyl Groups Prepared by a Mild Sulfonation Method for Proton Exchange Membranes, *Macromolecules*, 40 (2007) 1934-1944.
- [135] Meier-Haack, J., Komber, H., Vogel, C., Butwilowski, W., Schlenstedt, K., and Lehmann, D., Side-Chain Sulfonated Poly(arylene ether)s for Fuel Cell Applications, *Macromolecular Symposia*, 254 (2007) 322-328.
- [136] Kim, D.-S., Robertson, G. P., Kim, Y. S., and Guiver, M. D., Copoly(arylene ether)s Containing Pendant Sulfonic Acid Groups as Proton Exchange Membranes, *Macromolecules*, 42 (2009) 957-963.
- [137] Liu, B., Robertson, G. P., Kim, D.-S., Sun, X., Jiang, Z., and Guiver, M. D., Enhanced thermo-oxidative stability of sulfophenylated poly(ether sulfone)s, *Polymer*, 51 (2010) 403-413.
- [138] Vogel, C., Komber, H., Quetschke, A., Butwilowski, W., Pötschke, A., Schlenstedt, K., and Meier-Haack, J., Side-chain sulfonated random and multiblock poly(ether sulfone)s for PEM applications, *Reactive and Functional Polymers*, 71 (2011) 828-842.

- [139] Feng, S., Shang, Y., Xie, X., Wang, Y., and Xu, J., Synthesis and characterization of crosslinked sulfonated poly(arylene ether sulfone) membranes for DMFC applications, *Journal of Membrane Science*, 335 (2009) 13-20.
- [140] Lee, H., Roy, A., Lane, O., Dunn, S., and McGrath, J. E., Hydrophilic-hydrophobic multiblock copolymers based on poly(arylene ether sulfone) via low-temperature coupling reactions for proton exchange membrane fuel cells, *Polymer*, 49 (2008) 715-723.
- [141] Lee, H., Roy, A., Lane, O., Lee, M., and McGrath, J. E., Synthesis and characterization of multiblock copolymers based on hydrophilic disulfonated poly(arylene ether sulfone) and hydrophobic partially fluorinated poly(arylene ether ketone) for fuel cell applications, *Journal of Polymer Science Part A: Polymer Chemistry*, 48 (2010) 214-222.
- [142] Roy, A., Hickner, M. A., Yu, X., Li, Y., Glass, T. E., and McGrath, J. E., Influence of chemical composition and sequence length on the transport properties of proton exchange membranes, *Journal of Polymer Science Part B: Polymer Physics*, 44 (2006) 2226-2239.
- [143] Wang, F., Hickner, M. A., Kim, Y. S., Zawodzinski, T. A., and McGrath, J. E., Direct polymerization of sulfonated poly(arylene ether sulfone) random (statistical) copolymers: candidates for new proton exchange membranes, *Journal of Membrane Science*, 197 (2002) 231-242.
- [144] Harrison, W. L., Wang, F., Mechem, J. B., Bhanu, V. A., Hill, M., Kim, Y. S., and McGrath, J. E., Influence of the Bisphenol Structure on the Direct Synthesis of Sulfonated Poly(arylene ether) Copolymers. I, *Journal of Polymer Science Part A: Polymer Chemistry*, 41 (2003) 2264-2276.
- [145] Ueda, M., Toyota, H., Ouchi, T., Sugiyama, J.-I., Yonetake, K., Masuko, T., and Teramoto, T., Synthesis and characterization of aromatic poly(ether sulfone)s containing pendant sodium sulfonate groups, *Journal of Polymer Science Part A: Polymer Chemistry*, 31 (1993) 853-858.
- [146] Kim, Y. S., Dong, L., Hickner, M. A., Pivovar, B. S., and McGrath, J. E., Processing induced morphological development in hydrated sulfonated poly(arylene ether sulfone) copolymer membranes, *Polymer*, 44 (2003) 5729-5736.
- [147] Paul, M., Park, H. B., Freeman, B. D., Roy, A., McGrath, J. E., and Riffle, J. S., Synthesis and crosslinking of partially disulfonated poly(arylene ether sulfone) random copolymers as candidates for chlorine resistant reverse osmosis membranes, *Polymer*, 49 (2008) 2243-2252.
- [148] Xie, W., Cook, J., Park, H. B., Freeman, B. D., Lee, C. H., and McGrath, J. E., Fundamental salt and water transport properties in directly copolymerized disulfonated poly(arylene ether sulfone) random copolymers, *Polymer*, 52 (2011) 2032-2043.
- [149] Xie, W., Geise, G. M., Freeman, B. D., Lee, C. H., and McGrath, J. E., Influence of processing history on water and salt transport properties of disulfonated polysulfone random copolymers, *Polymer*, 53 (2012) 1581-1592.
- [150] Park, H. B., Freeman, B. D., Zhang, Z. B., Sankir, M., and McGrath, J. E., Highly chlorine-tolerant polymers for desalination, *Angewandte Chemie*, 47 (2008) 6019-6024.
- [151] Harrison, W. L., Synthesis and characterization of sulfonated poly(arylene ether sulfone) copolymers via direct copolymerization: Candidates for proton exchange membrane fuel cells, Virginia Polytechnic Institute and State University, 2002.

Chapter Three

Side-chain Sulfonated Random and Multiblock Copolymer Cation Exchange Membranes for Membrane Capacitive Deionisation

3.1 Overview

This chapter discusses the synthesis and characterisation of three random copolymers and one multiblock copolymer and their suitability as cation exchange membranes for CDI. The copolymers investigated are poly(arylene ether sulfone)s and were all synthesised from the same precursor monomers. Fundamental polymer and membrane characterisation techniques were used, including ^1H NMR, Fourier transform infrared spectroscopy (FTIR), and measurements for contact angle, IEC, water uptake, resistance and transport number.

The effects of side-chain sulfonation, precursor monomer composition and the structure of the copolymer on the membranes' IEC, water uptake, conductivity and transport number are presented. All membranes were found to have relatively low water uptake and good mechanical stability, while yielding values for IEC, conductivity and transport number comparable to those of commercial membranes and similar cation exchange membranes in the literature. The results indicated that the hydrophilic domains in the polymers enhanced IEC and conductivity, with the membranes potentially suitable for use in membrane CDI systems.

Note that with the exception of FTIR, transport number and contact angle experiments, all work in this chapter was conducted at the Leibniz-Institut für Polymerforschung Dresden in Germany.

3.2 Relevant Theory

This section provides some theory on the key membrane properties discussed in this chapter used to characterise the membranes for MCDI applications, namely IEC, water uptake, conductivity, selectivity and transport number.

3.2.1 Ion-Exchange Capacity

A membrane's IEC is a measure of the number of fixed charges per mass of dry membrane material. It is expressed in either milliequivalents or mmol per gram of dry membrane, and the two are typically interchangeable when the fixed charges are monovalent (as is the case in this study). As the fixed charges impart ion-exchange membranes with the ability to selectively transport counterions, this parameter greatly affects the properties of the membrane.

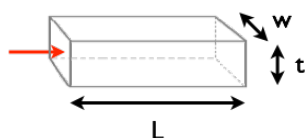
3.2.2 Water Uptake

The water uptake or membrane swelling describes the maximum amount of water that can be held by a membrane, and largely determines a membrane's mechanical stability, conductivity (or resistance) and ion permselectivity. It is affected by the constituent monomers and their arrangement within the polymer (i.e. block, graft or random copolymer), the homogeneity of the membrane, the number of fixed charges (i.e. the IEC), and the type of fixed charges. Strongly acidic or basic fixed charges tend to increase the water uptake compared to weakly acidic or basic fixed charges. The sulfonic acid group used in this study is strongly acid and is therefore expected to yield a greater water uptake compared to weaker acid groups.

3.2.3 Conductivity

Ion exchange membranes require good ionic conductivity to facilitate the transport of counterions when an electrical potential is applied. Similar to the water uptake, the number and type of fixed charges influences the conductivity, where homogeneous membranes with an even distribution of fixed charges promote good conductivity.

In-Plane Conductivity



Through-Plane Conductivity

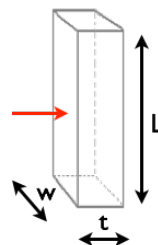


Figure 3.1 - In-plane and through-plane conductivity, with the direction of measurement shown by the red arrow.

Conductivity can be measured in either the through-plane or in-plane direction, as shown in Figure 3.1. These values are often found to be greater in the in-plane direction due to the direction of polymer extrusion and the alignment of the polymer chains [1]. For MCDI applications (and indeed most ion-exchange membrane processes), ion transport occurs in the through-plane direction and so through-plane conductivity is often reported in literature for commercial membranes. However, through-plane measurements are often delicate and it can be difficult to achieve results that are both consistent and accurate. Consequently in-plane conductivity is often measured using a standard four-point probe, which

still yields accurate and meaningful results. Furthermore, as measurements with a four-point probe are not made with the membranes submersed in solution, the measured resistance is not influenced by boundary layer effects.

3.2.4 Selectivity and Transport Number

For MCDI applications, the mass transport of ions through the membrane is a large factor in determining the overall process efficiency. To help measure the mass transfer of the membranes, both the selectivity and transport number can be determined. Selectivity is a function of conductivity, water uptake and IEC, and can be used to quantify the relationship between mechanical stability and conductivity. It is calculated from the hydration number, λ , a measure of the water molecules absorbed per fixed charge, which is calculated using the following equation:

$$\lambda = \frac{WU}{IEC \times 18.02}$$

Equation 3.1

where WU is the water uptake, IEC is the ion-exchange capacity (mol/g) and 18.02 is the molecular weight of water (g/mol). The selectivity, ψ , can then be calculated using the following equation:

$$\psi = \frac{\sigma}{\lambda}$$

Equation 3.2

where σ is the membrane conductivity (mS/cm). Ion exchange membranes with a high selectivity and low hydration number are more suited to practical applications.

When a potential difference is applied across an ion-exchange membrane, the transport number describes the fraction of the total current that is carried by a specific ionic species. Considering a cation exchange membrane in an aqueous solution, both anions and cations are able to carry current applied by an external source. However, due to the incorporation of fixed negative charges and hence the selective transportation of cations, the majority of the current will be carried by the cations. This is expressed as the transport number (t_i), defined as [2]:

$$t_i = \frac{z_i J_i}{\sum_i z_i J_i}$$

Equation 3.3

where t_i is the transport number of component i , z_i is its valence, and J_i its molar flux. The sum of all transport numbers for all ions in solution is equal to one. If the sum of the individual transport numbers for

all cations is equal to one, this indicates an ideal cation-exchange membrane that is completely permselective, i.e. one that completely blocks the passage of anions. Note that the fixed charges within the membrane are not able to carry current through the membrane, and thus have a transport number of zero. For the application of MCDI, a transport number close to one is desirable as the reduced movement of co-ions (anions) improves energy efficiency. The simplest method to determine membrane transport number is based on measuring the potential difference between two electrolyte solutions of different concentration separated by the membrane. The transport number, t_i , can then be calculated using the following modified Nernst equation [3]:

$$E_m = \frac{RT}{F} (2t_i - 1) \ln \frac{a_1}{a_2}$$

Equation 3.4

where E_m is the measured potential (V), R is the gas constant (J/mol.K), T is the temperature (K), F is the Faraday constant, and a_1 and a_2 are the activities of the two electrolyte solutions (mol/L).

The permselectivity differs to the transport number in that it describes the degree to which a membrane passes ions of a certain charge and blocks ions of the opposite charge. A membrane with a permselectivity of one exclusively transmits counterions, while a permselectivity of zero indicates that the transport number of the counterion in the membrane is the same as its transport number in the electrolyte. For membrane separation processes, membranes typically should have a permselectivity greater than 0.97 [4].

3.3 Experimental

3.3.1 Materials

4,4'-difluorodiphenyl sulfone (DFDPhS) was purchased from FuMA-Tech GmbH (Germany) and was purified by vacuum distillation. 4,4'-dihydroxydiphenyl sulfone (98%) (DHDPhS) was obtained from Aldrich (Germany). 2,5-diphenylhydroquinone (DPhHQ) had been prepared as per the procedure described by Vogel et al. [5]. NMP and calcium carbonate were purchased from Merck (Germany) and NMP was distilled twice under reduced pressure from CaH_2 . Potassium carbonate was purchased from Fluka (Germany), and concentrated sulfuric acid (min. 96%) was obtained from Acros (Belgium).

3.3.2 Random Copolymer Synthesis

Random copolymers were synthesised from DFDPHS, 4,4'-dihydroxydiphenyl sulfone bis-trimethylsilylether (bis-TMS-DHDPHS) and 2,5-diphenylhydroquinone bis-trimethylsilylether (bis-TMS-DPhHQ). The synthesis scheme is shown in Figure 3.2. 10 mmol of DFDPHS, x mmol of bis-TMS-DPhHQ and $10 - x$ mmol of bis-TMS-DHDPHS were weighed into a 50 mL three-necked round-bottomed flask with 30 mL of anhydrous NMP, where $x = 6$ for RCP 1, $x = 5$ for RCP 2 and $x = 4$ for RCP 3. The monomers were stirred under argon purging until complete dissolution was achieved. To facilitate the condensation polymerisation reaction, 3.33 mmol of anhydrous potassium carbonate and 16.65 mmol of anhydrous calcium carbonate were added to the solution. The reaction mixture was then heated to 175 °C for 24 h under stirring and argon purging, followed by a further 2 h at 190 °C. The cooled reaction mixture was diluted with NMP to reduce its viscosity. The polymer was precipitated dropwise in methanol, then filtered and thoroughly washed with water (and subsequently methanol) to remove residual NMP, potassium carbonate and calcium carbonate. The polymers were finally dried under vacuum at 100 °C to constant weight.

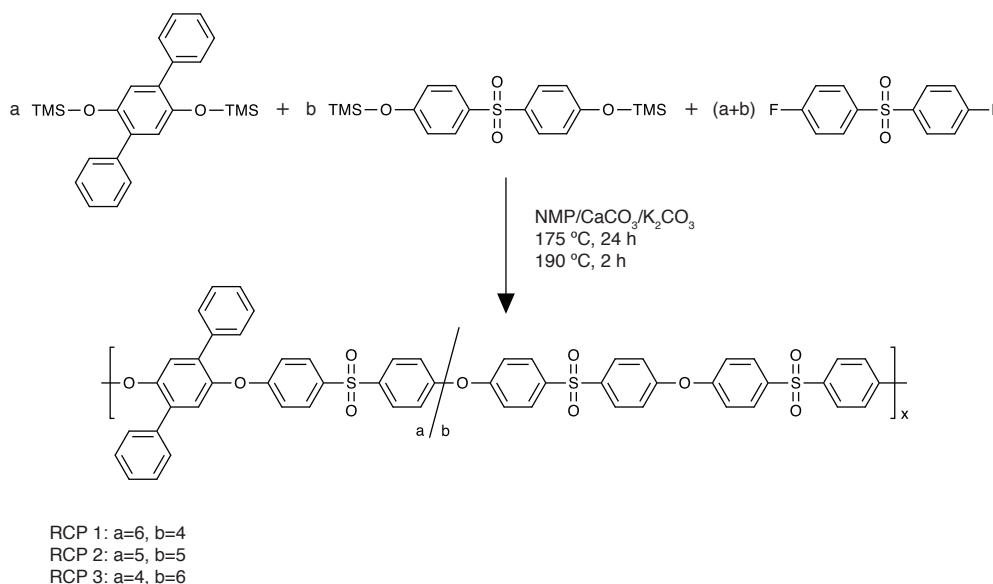


Figure 3.2 - Random copolymer synthesis with a mmol of bis-TMS-DPhHQ, b mmol of bis-TMS-DHDPHS and $(a+b)$ mmol DFDPHS. The trimethylsilyl ether groups are hydrolysed during the nucleophilic displacement polycondensation reaction (not shown).

3.3.3 Multiblock Copolymer Synthesis

The multiblock copolymer (MB) was synthesised from oligomers prepared from 2,5-diphenylhydroquinone bis-trimethylsilylether and 4,4'-difluorodiphenyl sulfone (oligo-DP-PES), and 4,4'-dihydroxydiphenyl

sulfone bis-trimethylsilylether and 4,4'-difluorodiphenyl sulfone (oligo-PES). Both oligomers had been prepared as per the procedure described by Vogel et al. [5]. To polymerise the oligomers, 0.3 mmol of the end-capped oligo-PES and 0.3 mmol of oligo-DP-PES were weighed into a three-necked round-bottomed flask with 50 mL of anhydrous NMP. After complete dissolution of the precursor oligomers, 2 mmol of anhydrous potassium carbonate was added to the reaction mixture and the temperature was raised to 100 °C under stirring and argon purging for 24 h. The cooled reaction mixture was precipitated in methanol, filtered to isolate the product from any insoluble material, and then washed with water and methanol. Finally the polymer was dried in vacuum at 100 °C to constant weight. The synthesis scheme for the multiblock copolymer can be seen in Figure 3.3.

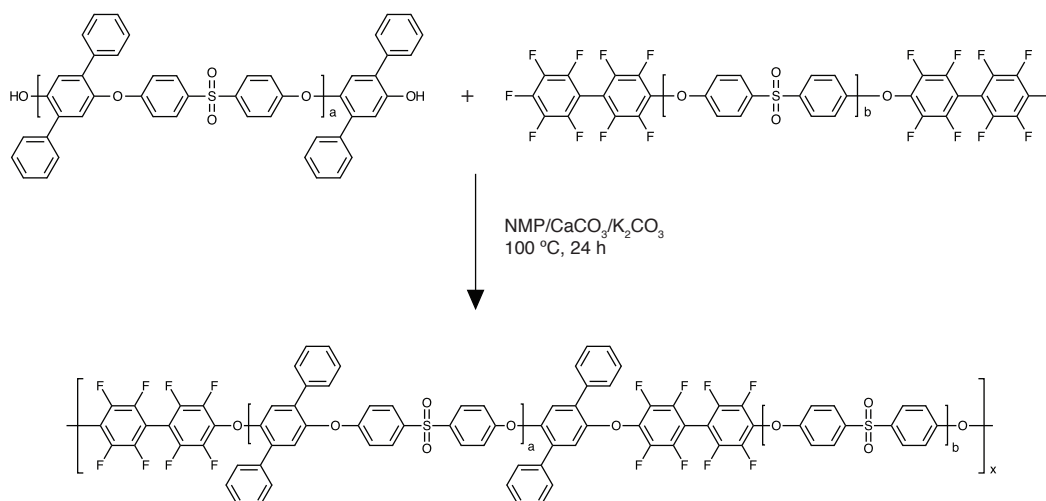


Figure 3.3 - Multiblock copolymer synthesis scheme, where a = 39 and b = 25.

3.3.4 Copolymer Sulfonation

All polymers were sulfonated using concentrated sulfuric acid (min. 96%). 30 ml of concentrated sulfuric acid was added to 3 g of polymer in a small flask under stirring for 24 h. The sulfonated polymers were then precipitated in water and thoroughly washed with water until the solution obtained a neutral pH. The final products were dried under vacuum at 110 °C to constant weight.

3.3.5 Polymer Characterisation

¹H NMR spectra of polymers prior to and post sulfonation were recorded on a Bruker DRX500 spectrometer operating at 500.13 MHz. Using 5 mm o.d. sample tubes, polymer samples were dissolved in dimethyl sulfoxide-*d*₆, which was also used as an internal chemical shift reference (2.50 ppm). ATR-

FTIR was performed using a PerkinElmer Spectra 100 to confirm the chemical structure of the cation exchange membranes.

3.3.6 Membrane Preparation

Membranes were prepared by dissolving 0.4 g of sulfonated polymer in 5 mL NMP such that the concentration of the polymer solution was 7.2 wt.%. The solutions were cast into 80 mm glass petri dishes and dried under vacuum for 2 h at 60 °C to remove the bulk of the NMP, then for a further 24 h at 80 °C. Membrane samples were removed from the dishes using deionised water and thoroughly rinsed with deionised water to remove residual NMP before soaking for 24 h in 1 M NaCl to convert them to the Na⁺ form. The membranes were finally rinsed and stored in deionised water at room temperature.

3.3.7 Membrane Characterisation

3.3.7.1 Contact Angle

Contact angle measurements were made using a PGX+ Goniometer. 3.5 µl of water was dropped onto a dry, flat membrane sample. The static contact angle was measured with the PocketGoniometer software, taking ten measurements over a period of 54 seconds. Each sample was measured several times at different points on the surface to ensure repeatability.

3.3.7.2 Ion-Exchange Capacity

The IEC of the membranes was calculated using the titration method. Titration was carried out on a Metrohm Titrando using potentiometric titration. Membrane pieces were first dried at 80 °C under vacuum until constant weight was reached. They were then soaked in 1 M HCl for 24 h to ensure full protonation, thoroughly rinsed with deionised water to remove excess protons from the polymer matrix, then soaked in 2 M NaCl for 24 h to fully exchange the protons with Na⁺ ions. This NaCl solution, containing displaced protons, was titrated with 0.01 M NaOH to measure the number of protons, and hence the number of ion exchange sites within the polymer. The final IEC values were calculated using the following equation:

$$IEC = \frac{n(H^+)}{m_{dry}}$$

Equation 3.5

where $n(H^+)$ is the number of protons in the titration solution, and m_{dry} is the mass of the dry membrane piece. $n(H^+)$ was calculated based on the titration of both the sample solution and of a blank 2M NaCl solution of the same volume as the test solution as shown in Appendix A1.

3.3.7.3 Water Uptake

Water uptake was measured by first drying membrane pieces at 80 °C under vacuum until constant weight was reached. After soaking the pieces in water at room temperature for 24 h, they were removed and excess water was gently wiped with a tissue before immediate weighing. The water uptake (WU) was calculated using the following equation:

$$WU = \frac{m_{wet} - m_{dry}}{m_{dry}}$$

Equation 3.6

where m_{wet} is the weight of the swollen membrane and m_{dry} is the weight of the dry membrane.

3.3.7.4 Conductivity

In-plane conductivity was determined using electrochemical impedance spectroscopy (EIS) with a four-point probe. Using a Gamry Reference 600 potentiostat in a frequency range from 1 Hz to 1 MHz, the membrane resistance was taken at the frequency where the phase angle was closest to zero. Membranes were measured in the Na^+ form at 30 °C and a relative humidity of 99% to prevent them from drying out. As the samples were tested in a humid environment and not submersed in solution, the measured resistance is not influenced by boundary layer effects. Conductivity was calculated based on the measured membrane resistance, R_m (Ω), distance between electrodes, L (cm), and the effective membrane cross section (thickness multiplied by width), A (cm^2), such that:

$$\sigma = \frac{L}{R_m A}$$

Equation 3.7

3.3.7.5 Transport Number

Membrane transport number was determined by measuring membrane potential. The experimental setup is shown in Figure 3.4. Using a two-chamber cell, a vertically positioned membrane separated solutions of 0.5 M NaCl and 1 M NaCl. The potential difference across the cell was measured by a potentiostat connected to Ag/AgCl reference electrodes, which were positioned such that the tips of the electrodes

were adjacent to the membrane surface. The transport number was then calculated using Equation 3.4 described in section 3.2.4.

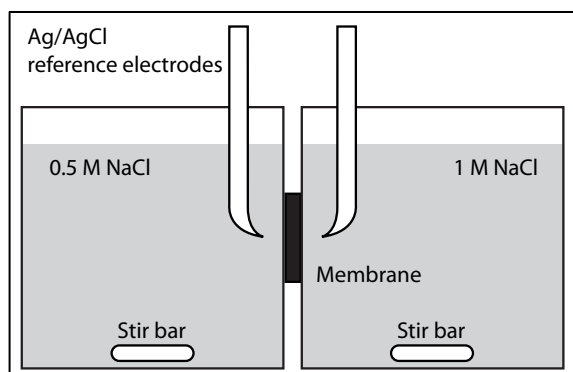


Figure 3.4 - Schematic of the cell used to measure transport number.

3.4 Results and Discussion

3.4.1 ^1H NMR Analysis

The copolymers in this study have been previously characterised by ^1H NMR by Vogel et al. [5]. This section provides some additional information to this characterisation and confirms the chemical structure of the copolymers.

3.4.1.1 ^1H NMR of Random Copolymers Prior to Sulfonation

Figure 3.5 shows the ^1H NMR spectrum of RCP 3 prior to sulfonation. The peaks seen in the region 8.02 – 7.74 ppm were assigned to signals of proton a, which is in the *ortho*-position to the sulfone group. This proton was represented by four different peaks due to the influence of the diphenylhydroquinone and dihydroxydiphenyl sulfone monomers. As previously postulated by Vogel et al. [5], a triad of diphenylsulfone-centred substructures is produced via the polycondensation reaction of the silylated monomers with the difluorodiphenyl sulfone fluoroaromatic. These substructures are shown in Figure 3.6.

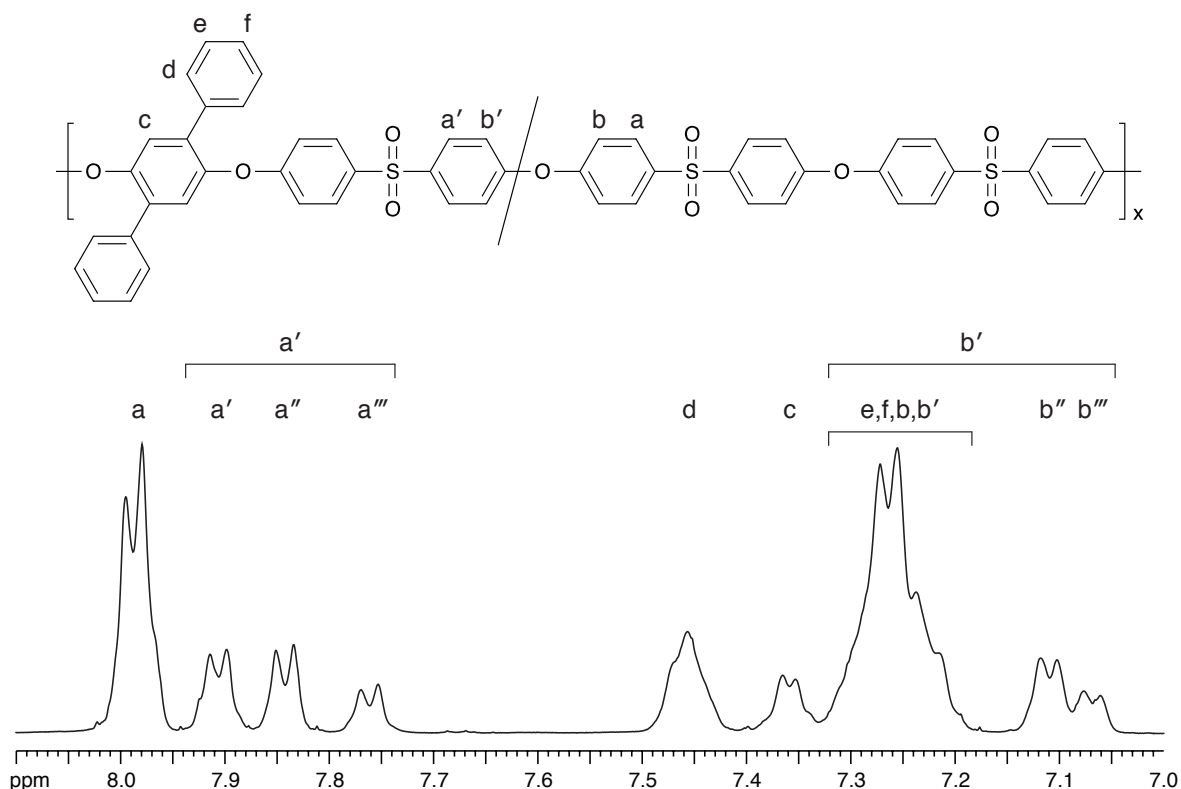


Figure 3.5 - ¹H NMR spectrum of RCP 3 prior to sulfonation.

When the centred diphenylsulfone unit is bound to two diphenylsulfone units (substructure I), only one signal is produced, represented by the doublet at 7.99 ppm. This signal was assigned to proton a. Substructure II represents both a diphenylsulfone unit and a diphenylhydroquinone unit bound to the centred diphenylsulfone. The two side-chain benzene rings on the diphenylhydroquinone unit are weakly activating substituents, and as such donate electrons into the main-chain benzene ring. This increased electron density caused a shielding effect on proton a in the *ortho*-position to the sulfone group, resulting in an upfield chemical shift. Thus, the peaks at 7.91 ppm and 7.84 ppm were assigned to protons a' and a'', respectively. With two diphenylhydroquinone units bound to the centred diphenylsulfone unit, the shielding effects are even greater, and a greater upfield chemical shift was observed. The peak at 7.76 ppm was therefore assigned to proton a'''.

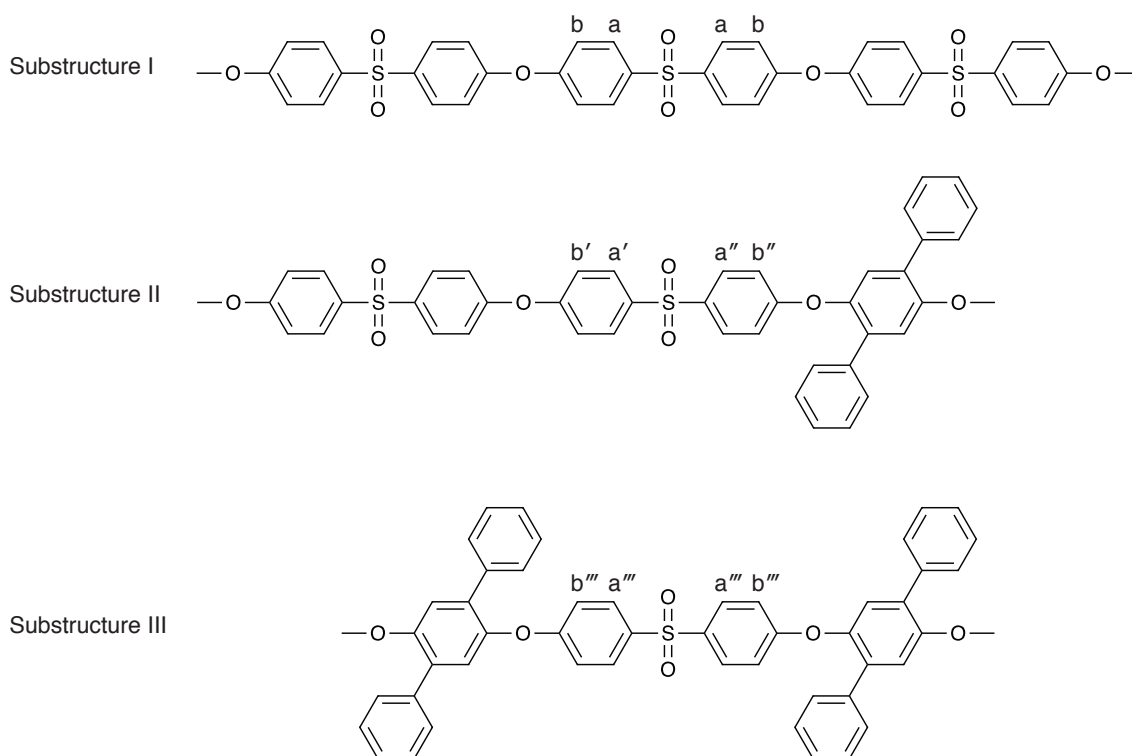


Figure 3.6 - Random copolymer substructures as postulated by Vogel et al. [5], which describes protons a and b.

Similar to proton a there were four peaks that represented proton b due to the triad of diphenylsulfone-centred substructures. The broad peak in the region 7.19 – 7.32 ppm was assigned protons b and b' (substructures I and II), as well as protons e and f in the *meta*- and *para*-positions on the pendant phenyl rings, respectively. The upfield chemical shift of proton b relative to proton a was due to its proximity to the strongly activating ether link along the polymer backbone, which increases the shielding effect on proton b. The two doublets in the region 7.05 – 7.14 ppm were assigned to protons b'' and b''' . Similar to protons a'' and a''' , the shielding effects from the benzene side chains on the adjacent diphenylhydroquinone units caused an upfield shift. As expected, the area under the peaks assigned to protons b'' and b''' was found to be the same as the area under the peaks assigned to protons a'' and a''' . The peak at 7.36 ppm was assigned to proton c, which in the *ortho*-position to the ether link on the diphenylhydroquinone unit. The peak at 7.46 ppm was assigned to proton d, which is in the *ortho* position of the pendant phenyl ring.

The product ratio of the precursor monomers for the random copolymers was calculated based on the sum of the area under the peaks assigned to proton a (i.e., $a-a'''$), which represents the relative combined moles of the dihydroxydiphenyl sulfone and difluorodiphenyl sulfone monomers, and the area under the

peak assigned to proton d, which represents the relative moles of the diphenylhydroquinone monomer. The calculated product ratios for each copolymer are shown in Table 3.1. It can be seen that for each copolymer, the product ratio was close to the original feed ratio.

Table 3.1 - Calculated product ratios for random copolymers.

Polymer	Feed ratio		Product ratio	
	DHDPHS	DPhHQ	DHDPHS	DPhHQ
RCP 1	4	6	4	6.1
RCP 2	5	5	5	5.0
RCP 3	6	4	6	4.2

3.4.1.2 Sulfonated Random Copolymers ^1H NMR

The spectrum of sulfonated RCP 3 is shown in Figure 3.7, and can be used to confirm side-chain sulfonation in the *para*-position on the pendant phenyl rings. Specifically, no peak could be assigned to proton f (previously in the region 7.19 – 7.32 ppm and superimposed in Figure 3.7), indicating that sulfonation occurs in the *para*-position on the side-chain phenyl ring. Further evidence of this sulfonation was the downfield shift of the peak assigned to proton e in the *meta*-position, from the region 7.19 – 7.32 ppm to a single peak at 7.57 ppm. The sulfonic acid group adjacent to proton e is an activating substituent and as such had an electron withdrawing effect on the phenyl ring, reducing the electron density of the ring as well as the shielding effect these electrons exert on the hydrogen atoms. No other loss of proton signals in the spectrum was observed, indicating that sulfonation only occurred on the side-chains.

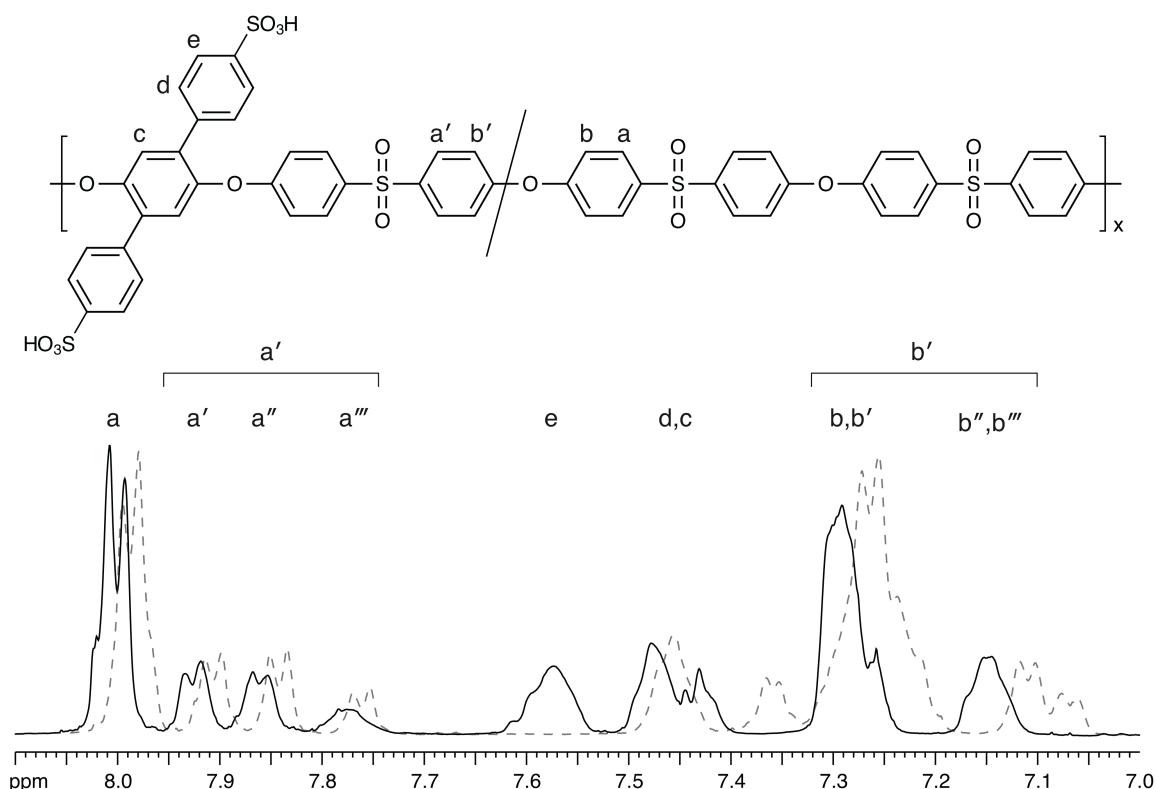


Figure 3.7 - Chemical structure and ^1H NMR spectrum of RCP 3 post-sulfonation (solid line), with the spectrum prior to sulfonation also shown (dashed line).

A downfield shift was in fact observed for all peaks of the sulfonated polymers, which could be attributed to this deshielding, although this is less prominent for the peaks assigned to protons a and b. The signals for proton b and b' are significantly easier to distinguish due to the downfield shift of signal d and the disappearance of signal f. The peak in the region 7.11-7.19 ppm was assigned to the merged peaks of proton b'' and b'''. The signals for protons c and d were seen to shift downfield and form a single peak of the same intensity in the region 7.40 - 7.50 ppm.

Spectra of all three sulfonated random copolymers are shown in Figure 3.8. As described above, the four peaks assigned to proton a are based on a triad of diphenylsulfone centred substructures. The peak at 8.0 ppm, which was assigned to proton a, increases in intensity from RCP 1 to RCP 3, indicating an increased presence of substructure I and hence the dihydroxydiphenyl sulfone precursor monomer in RCP 3. The peaks at 7.93 ppm and 7.87, assigned to protons a' and a'' respectively, were found to have the same intensity as each other for each of the polymers, although these peaks have a greater intensity for RCP 1. The peak at 7.77 ppm was assigned to proton a''' and has the greatest intensity for RCP 1. The greater intensity of the a', a'' and a''' proton signals for RCP 1 are a result of a greater presence of substructures II and III, arising from a higher diphenylhydroquinone precursor monomer content.

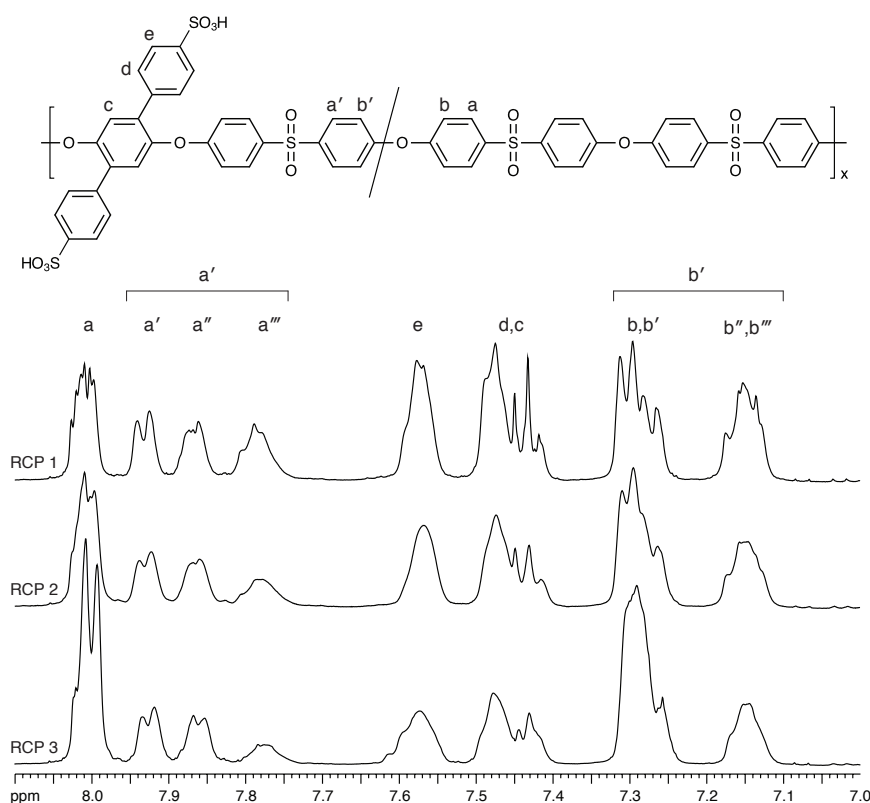


Figure 3.8 - ^1H NMR spectra of sulfonated RCP 1, RCP 2 and RCP 3.

3.4.1.3 Multiblock Copolymer ^1H NMR

The spectrum and chemical structure of the sulfonated multiblock copolymer are shown in Figure 3.9. As the precursor monomers for the multiblock copolymer are the same as those used for the random copolymers, the peaks are analogous to those in the random copolymer spectra. Nonetheless, the ordered nature of the polymer backbone means the substructures found in the random copolymers do not exist, and so fewer signals are observed. The doublet in the region 7.60 ppm is consistent with proton e in the *meta*-position on the pendant phenyl ring. As with the random copolymers, the absence of a signal for a proton in the *para*-position of the pendant phenyl ring indicates side chain sulfonation in this position.

Similar to the random copolymers, the doublet 7.99 ppm was assigned to proton a in the *ortho*-position to the sulfone group in the diphenylsulfone repeating unit, while the doublet at 7.80 ppm was assigned to proton a''' in the *ortho*-position to the sulfone group in the sulfonated repeating unit. This peak is analogous to proton a''' in the random copolymers, as each dihydroxydiphenyl sulfone unit in this block is bound to two diphenylhydroquinone units. Similarly, the doublets at 7.27 and 7.14 ppm are assigned to protons b and b''', analogous to the protons b and b''' in the random copolymers. The ratio of the area

under the peaks a:a''' and b:b''' was found to be 1:0.65, yielding a block ratio of 39:25.4. This is consistent with the chain length of the precursor oligomers shown in Table 3.2, which was calculated to be 38.7 for the oligo-PES oligomer (synthesised with the dihydroxydiphenyl monomer), and 25.6 for the oligo-DP-PES block (synthesised with the diphenylhydroquinone monomer).

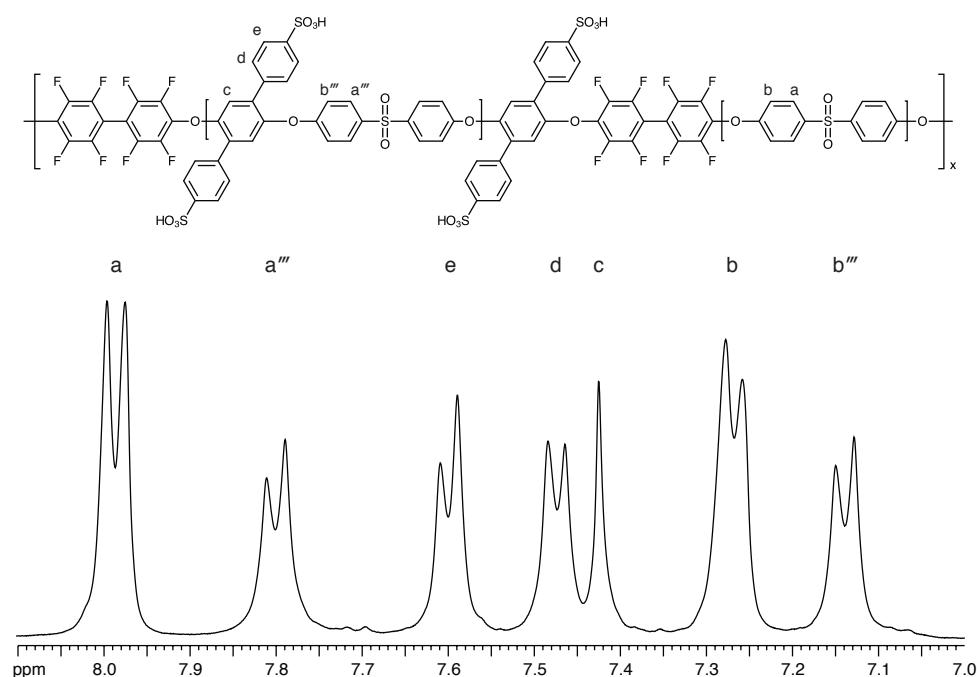


Figure 3.9 - ^1H NMR spectrum of the sulfonated multiblock copolymer.

Table 3.2 – Multiblock precursor oligomer properties used to determine block length.

Oligomer	Repeating unit	M_n repeating unit (g/mol)	M_n oligomer ^a (g/mol)	Block Length
oligo-DP-PES	$\text{C}_{30}\text{H}_{20}\text{O}_4\text{S}$	476	12,175	25.6
oligo-PES	$\text{C}_{12}\text{H}_8\text{O}_4\text{S}$	248	9,600	38.7

^a Obtained from GPC measurements on a Knauer GPC. A mixture of DMAc with 2 vol.% water and 3 g/L LiCl was used as eluent.

3.4.2 FTIR Analysis

FTIR is a useful tool to further examine the chemical structure of the polymer membranes. The FTIR spectra of membranes cast from each polymer are shown in Figure 3.10. Although the random copolymers have different monomer ratios, the constituent monomers are the same for each polymer. Similarly, the multiblock copolymer was synthesised from oligomers using the same monomers. Consequently, each polymer yields a similar spectrum.

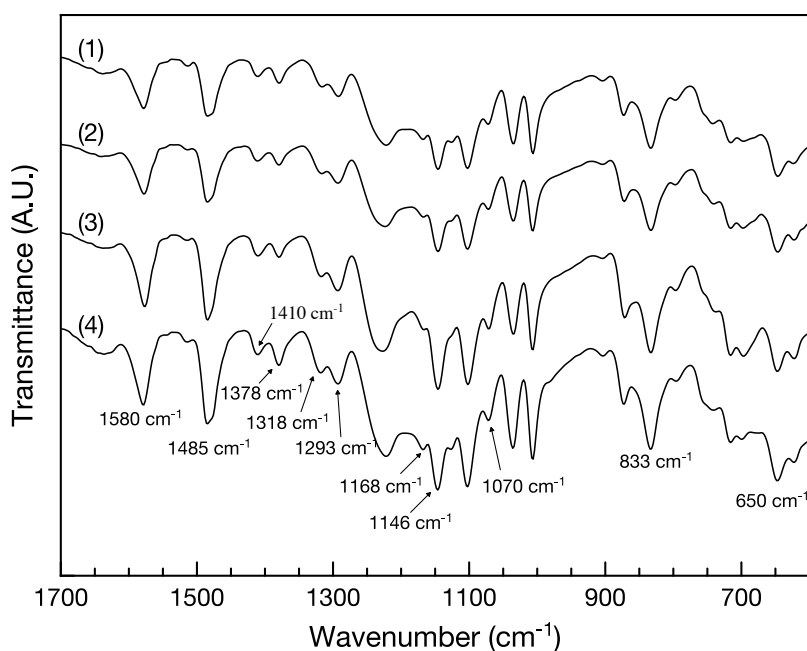
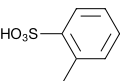
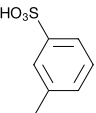
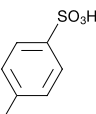


Figure 3.10 - FTIR spectra of copolymer membranes: (1) RCP 1, (2) RCP 2, (3) RCP 3 and (4) Multiblock copolymer.

The aromatic rings are characterised by carbon-carbon stretching vibrations at both 1580 cm^{-1} and 1485 cm^{-1} . The sulfone groups in the polymer backbone exhibit S=O asymmetric stretching vibrations in the region $1318 - 1293\text{ cm}^{-1}$, as well as symmetrical stretching vibrations at 1146 cm^{-1} [6]. The S=O bond of the sulfonated group on the side chain was characterised by the peak at 1168 cm^{-1} (symmetrical stretching) and the peak at either 1410 cm^{-1} or 1378 cm^{-1} (asymmetrical stretching). The peak at 1070 cm^{-1} was attributed to the symmetrical stretching of the SO_3 group and the sharp band at 650 cm^{-1} is attributed to the S-O stretch [6]. Other strong peaks in the region $1300 - 1000\text{ cm}^{-1}$ were attributed to stretching vibrations from the ether links between aromatic rings and C-S stretching vibrations [6, 7].

Table 3.3 - IR absorptions for C-H bends on substituted benzene rings. Data from [6, 7].

Substitution position	Peak Location
Ortho 	$770\text{-}735\text{ cm}^{-1}$ (strong)
Meta 	$810\text{-}750\text{ cm}^{-1}$ (strong), $900\text{-}860\text{ cm}^{-1}$ (medium)
Para 	$860\text{-}800$ (strong)

Evidence from the FTIR analysis can be used to confirm the sulfonation position on the pendant phenyl rings. Table 3.3 outlines the typical absorption characteristics of di-substituted benzene rings for C-H out-of-plane bending. Based on the peak locations in Table 3.3, the peak at 833 cm^{-1} can be attributed to out-of-plane C-H bends on both the sulfonated pendant phenyl ring and the diphenylsulfone aromatic rings in the polymer backbone. The absence of a strong band in the region $770 - 735\text{ cm}^{-1}$ eliminates the possibility of *ortho*-substitution, while the absence of dual bands in the region $900 - 860\text{ cm}^{-1}$ and $810 - 750\text{ cm}^{-1}$ eliminates the possibility of *meta*-substitution.

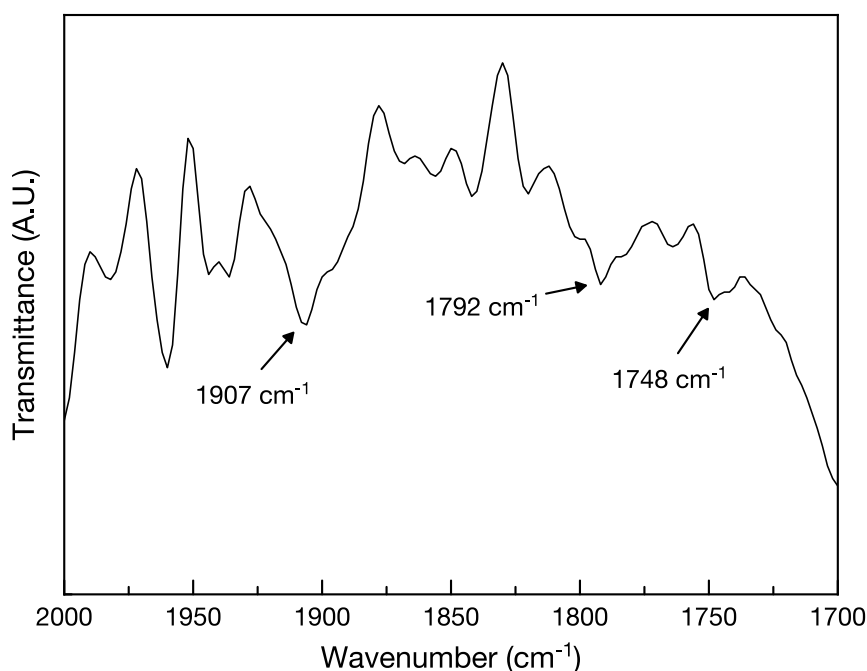


Figure 3.11 - FTIR of RCP 1 in the region $2000\text{-}1700\text{ cm}^{-1}$ showing weak overtones from benzene ring substitution.

Benzene ring substitution also produces weak absorption bands in the form of overtones. These overtones are observed in the region $1700 - 2000\text{ cm}^{-1}$ and are shown in Figure 3.11, however as seen in the full spectrum in Figure 3.12, these bands are very weak. Evidence of *para*-substituted aromatic rings in both the random and multiblock copolymers are observed with bands at 1907 cm^{-1} and 1792 cm^{-1} [6]. The band at 1748 cm^{-1} is a result of the 1,2,4,5-tetra substitution along the main chain from the diphenylhydroquinone monomer [6].

Figure 3.12 shows the copolymer spectra from $4000 - 600\text{ cm}^{-1}$. Weak C-H aromatic stretching links can be observed at approximately 3096 cm^{-1} . Furthermore, the broad peak in the region $3700 - 3150\text{ cm}^{-1}$ is attributed to stretching of O-H groups in the SO_3H [8], as well as any water within the polymers (note that

although membranes were measured in the dry state and had been stored in a desiccator, moisture in the air may have been absorbed by the membranes prior to testing). This broad peak is seen to be greatest for the multiblock copolymer, and less pronounced for the random copolymers with RPC 1 and RPC 2 yielding greater intensities than RPC 3. These intensities can be approximately correlated to each membrane's IEC and water uptake (as described in section 3.4.3).

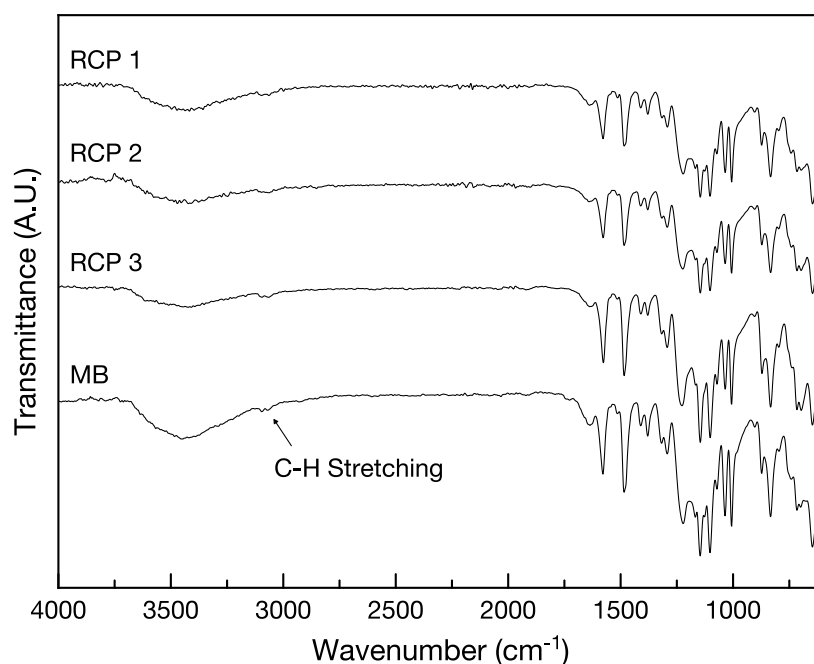


Figure 3.12 - FTIR spectra of random and multiblock copolymers in the region 4000 - 600 cm^{-1} .

3.4.3 Ion Exchange Capacity and Water Uptake

Table 3.4 gives the IEC for all four copolymers. For the random copolymers, the IEC is seen to increase with increasing diphenylhydroquinone monomer content, ranging from 1.44 mmol/g for RCP 3 up to 2.05 mmol/g for RCP 1. This increase is due to the greater number of pendant phenyl rings for side-chain sulfonation to occur. In comparison, the multiblock copolymer possesses an IEC of 1.91 mmol/g, placing it in the higher end of the copolymer IEC range. The high IEC values for all copolymers are due to the high degree sulfonation of the side chains achieved with concentrated sulfuric acid, which allowed for sulfonation on two pendant phenyl rings per diphenylhydroquinone monomer. The degree of sulfonation for each copolymer, as shown in Table 3.4, was calculated by comparing the theoretical IEC (calculated based on a 100% degree of sulfonation) with the measured IEC. All polymers were found to have a high degree of sulfonation of at least 95%.

Table 3.4 - IEC, degree of sulfonation (DS) and water uptake of random and multiblock copolymer membranes

Polymer	IEC (mmol/g)	DS (%)	Water Uptake (%)			
			H ⁺	Na ⁺	0.017 M NaCl	0.5 M NaCl
RCP 1	2.05	97	66.4	49.9	49.1	40.2
RCP 2	1.73	95	46.8	35.7	35.0	31.4
RCP 3	1.44	96	30.0	26.4	25.9	21.8
MB	1.91	>99	68.2	54.0	53.5	46.9

Membrane water uptake values are presented in Table 3.4. While a greater water uptake is known to improve membrane conductivity, it also serves to reduce mechanical stability. Nonetheless, in the swollen state all copolymer membranes were easily handled and showed good dimensional stability due to their hydrophobic properties imparted by the diphenylsulfone units.

Similar to the IEC, for the random copolymers there is a clear correlation between the water uptake and the monomer ratio, where a greater presence of the hydrophilic diphenylhydroquinone monomer allows for greater swelling. Despite having a lower IEC than RCP 1, the multiblock copolymer was found to have a water uptake exceeding all random copolymers. This greater rate of swelling is due to the multiblock copolymer's microheterogeneity, in which hydrophilic clusters of fixed counterions increase the water uptake. In contrast, the homogeneous random copolymers do not have micro hydrophobic or hydrophilic domains to allow a greater water uptake.

Membranes were tested for water uptake in both the H⁺ and Na⁺ forms in distilled water, and with various concentrations of NaCl solution in the Na⁺ form. The difference in membrane swelling under the influence of different ions is an important consideration for membranes that may be used to desalinate water of various salinities and different ionic compositions. For all copolymers, protonated membranes exhibited greater swelling than those in the sodium form. This difference can be attributed to the affinity between the sodium ions and the sulfonate group. In general, a greater affinity between the counter ion and the sulfonate group is accompanied by a decrease in water uptake [9-11]. The interaction between the charged sulfonate groups and the sodium ions in the copolymer membrane matrices suppresses the ability of the polar water molecules to interact with the sulfonate groups, hence reducing water uptake.

Water uptake in the Na^+ form was measured for 0.017 M (1000 mg/L) and 0.5 M (29220 mg/L) NaCl, approximately simulating brackish water and seawater. The change in water uptake between deionised water and 0.017M NaCl was found to be negligible, while a more obvious decrease was observed for membranes soaked in 0.5 M NaCl. Lower swelling at higher concentrations is expected as a result of a reduced osmotic pressure between the external solution and the solution in the interstitial phase of the polymer matrix. Water uptake at different concentrations is also known to vary depending on the chemical structure of the polymer; for instance, Neosepta CMX water uptake has been shown to be independent of concentration, a result of its high degree of crosslinking [12]. The decrease in swelling of the copolymer membranes with concentration is more pronounced for the more hydrophilic copolymers, indicating that this property largely influences water uptake in solutions with different concentrations.

Any potential loss in membrane conductivity in solutions of high concentration due to lower swelling may be partially offset by the increased conductivity of the solution. Unfortunately testing membrane resistance in solution was not feasible for this study, although swelling and conductivity measurements in solutions with different concentrations and ionic compositions would provide useful information regarding the expected performance of the membranes for MCDI applications (see section 3.4.5 for a discussion on membrane conductivity)

The properties of common commercial membranes for electrodialysis and MCDI are shown in Table 3.5, in addition to lab synthesised membranes prepared by Kwak et al. [13] and Rhim et al. [14]. The copolymers in this study were found to have IECs in the typical range for commercial copolymers, with RCP 1 and the multiblock copolymer firmly towards the upper end of this range. Compared with non-commercial membranes used for CDI testing, the random and multiblock copolymers outperform the styrenesulfonic acid/methacrylic acid/methyl methacrylate copolymers synthesised by Kwak et al. [13], with superior IEC at significantly lower swelling rates, indicating greater mechanical stability. Furthermore, the IEC and swelling rates were found to be similar to the PVA polymers crosslinked with sulfosuccinic acid prepared by Rhim et al. [14] (and subsequently used for MCDI by Kim and Choi [15]). The high number of ion exchange sites for these copolymers compared with commercial and lab synthesised polymers indicates they are good candidates for use in MCDI applications.

Table 3.6 - Properties of commercial and lab membranes for electrodialysis and MCDI. Data from [13, 14, 16-19].

Membrane	IEC (mmol/g)	Transport Number ^a	Permselectivity ^a (%)	Resistance ^b ($\Omega \cdot \text{cm}^2$)	Water Uptake (%)	Thickness (μm)	Uses	Properties
<i>Fumasep</i> [®]								
FKS	> 1	-	> 96	< 8	-	110 - 130 (wet)	Electrodialysis	High chemical stability
FKE	> 1	-	> 98	< 3	15	50 - 70 (dry)	Electrolysis	Excellent chemical and mechanical stability
<i>Neosepta</i> [®]								
CM-1	2.0 - 2.5	-	> 96	1.2 - 2.0	35 - 40	120 - 170	Electrodialysis	Low electrical resistance
CMX	1.5 - 1.8	-	> 96	3.0	25 - 30	140 - 200	General concentration and desalination	High mechanical strength
<i>Ralex</i> [®]								
CMH-PES	2.2	> 0.95	> 90	< 8	< 65	< 700 (wet)	Electrodialysis,	Resistance against aggressive chemicals and fouling components
CMH-PES HD	-	> 0.95	> 90	< 18	< 65	< 850 (wet)	Electrodialysis, electrodeionization	High mechanical strength
CMH-PP	-	> 0.95	> 90	< 8	< 70	< 700 (wet)	Electrodialysis, electrodeionization	Long-term stability in pH range 0–14
<i>Selemion</i> [®]								
CMV	2.01*	> 0.96	> 92	3.0	20*	130	Electrodialysis	Standard CEM
CMD	-	> 0.94	-	17	-	380	Electrodialysis	High mechanical strength
<i>Non-commercial</i>								
Kwak et al. [14]	0.51 - 0.99	-	-	0.7 - 2.6	75 - 120	90 - 140	Capacitive deionisation	
Rhim et al. [15]	0.65 - 2.24	-	-	-	13 - 78	100 - 150	Capacitive deionisation ^c	

^a Transport number and permselectivity measured using 0.5 and 0.1 M KCl solutions^b Resistance measured in 0.5 M NaCl^c Initially synthesised for fuel cell applications [14], but later applied as polymer electrode coatings for CDI [15]

3.4.4 Contact Angle

The initial contact angle and the contact angle after 54 seconds for each membrane is shown in Table 3.6 and Figure 3.13. Despite the multiblock copolymer yielding a greater water uptake it was seen to have a much greater contact angle compared to the three random copolymers, with only minor changes in contact angle over time. Furthermore, the drops on the multiblock copolymer were largely able to retain their volume with minimal absorption. In comparison, due to the hydrophilic nature of the random copolymers each water drop was observed to immediately disperse over the membrane surface and penetrate into the polymer. After the initial reduction in contact angle over the first 12 seconds, a relatively stable contact angle was observed.

Table 3.6 – Membrane contact angle measured at $t = 0$ s and at $t = 54$ s

Membrane	Contact Angle	
	$t = 0$ s	$t = 54$ s
RCP 1	51.8	30.3
RCP 2	52.1	38.2
RCP 3	62.3	46.1
MB	70.2	68.5

Considering only water uptake, the multiblock copolymer would be expected to have the lowest contact angle due to its hydrophilicity and greater swelling rate. However, its greater contact angle demonstrates the phase separation between hydrophilic and hydrophobic domains, and its low wettability is a strong indicator of the formation of large hydrophobic domains within the polymer matrix. These are significant enough to reduce the rate of swelling despite the presence of similarly large hydrophilic domains that have been shown to increase the overall water uptake. On the other hand, the statistical distribution of the hydrophobic and hydrophilic monomers within the random copolymers does little to enhance either of these properties. The influence of the precursor monomers in forming these hydrophilic and hydrophobic domains is shown in Figure 3.14. While the balance of hydrophilic and hydrophobic domains becomes important in determining the properties of a membrane, it can be concluded that the wettability of the copolymers is strongly linked to the structure of the block and random copolymers.

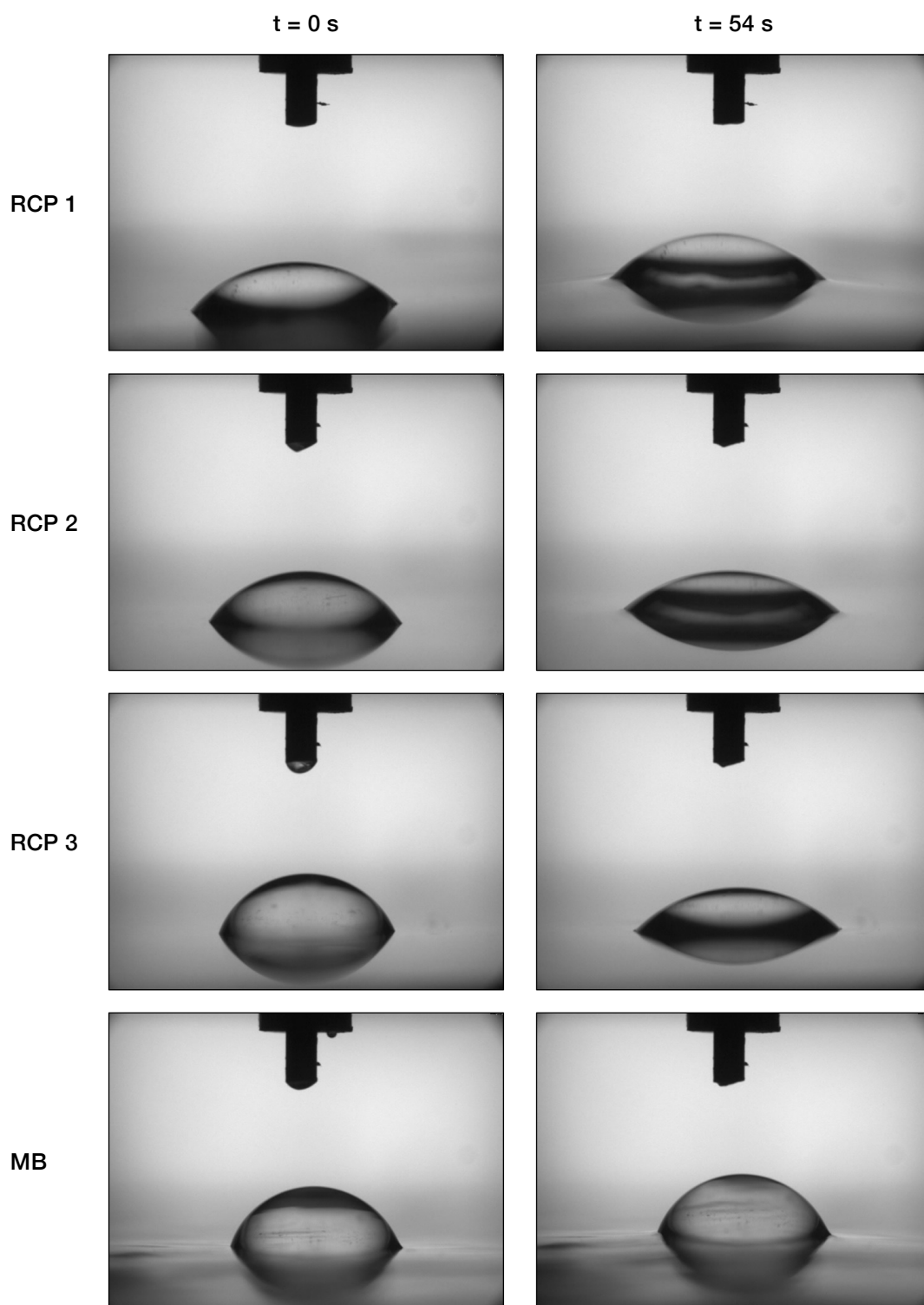
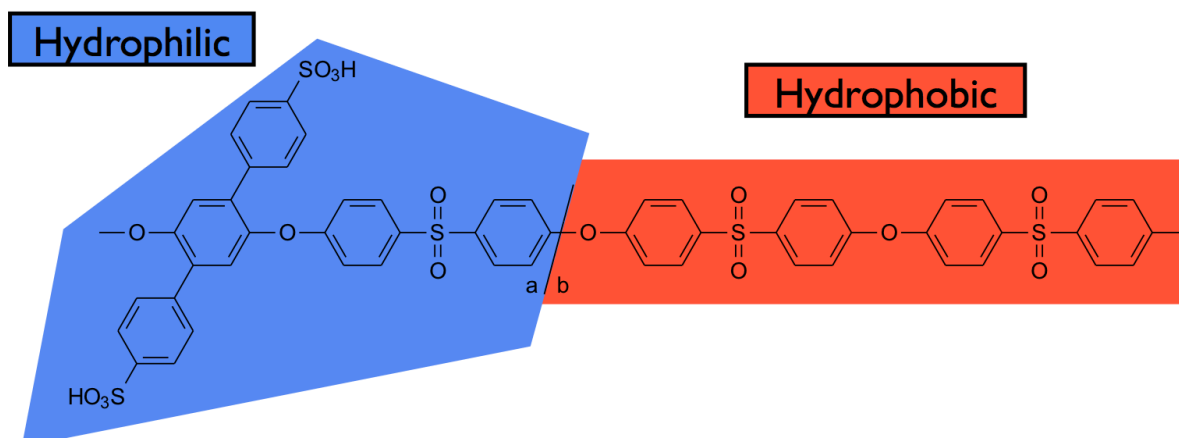


Figure 3.13 - Random and multiblock copolymer contact angle images taken at initial contact with the membrane ($t = 0$) and after 54 seconds.

a)



b)

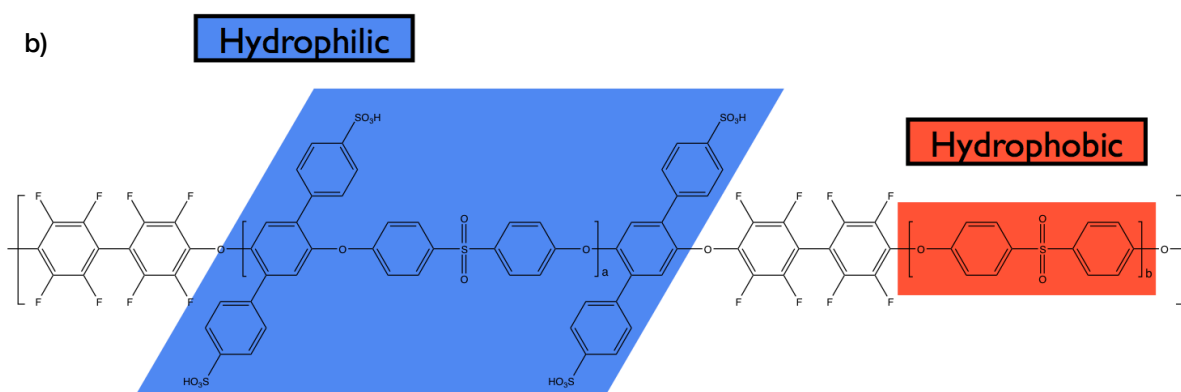


Figure 3.14 - Influence of the precursor monomers on the hydrophilic and hydrophobic regions of a) random copolymers and b) the multiblock copolymer.

3.4.5 Conductivity

The in-plane conductivity for the three random copolymers and the multiblock copolymer are shown in Table 3.7. Similar to the water uptake, the conductivity increased for each of the random copolymers with IEC. The multiblock copolymer was measured as having the highest conductivity of all membranes in spite of RCP 1 having the greatest IEC. The conductivity of RCP 1, RCP 2 and the multiblock copolymer exceeded the estimated conductivity of Neosepta CMX, a commercial membrane commonly used for MCDI studies, while RCP 3 had a somewhat lower conductivity. Due to the distinct hydrophobic and hydrophilic domains formed by its precursor oligomers, the block copolymer membrane can be classified as microheterogeneous. On the other hand, the random copolymers have a more even distribution of fixed charges and are homogeneous in nature, which typically yields higher conductivities than heterogeneous membranes. However, in this instance it is thought that the microheterogeneity of the block copolymer does not influence the distribution of charges enough to reduce conductivity.

Conversely, interconnectivity between large hydrophilic domains created by the sulfonated side-chains is thought to allow for a greater passage of current through the polymer matrix, increasing conductivity.

Table 3.7 - Electrochemical and transport properties of random and multiblock copolymer membranes.

Polymer	IEC (mmol/g)	Conductivity (mS/cm)	Transport Number	Permselectivity	Hydration Number	Selectivity
RCP 1	2.05 ± 0.01	15.13 ± 0.19	0.94	0.88	13.54	1.12
RCP 2	1.73 ± 0.01	8.36 ± 0.15	0.99	0.99	11.67	0.72
RCP 3	1.44 ± 0.01	3.79 ± 0.56	0.98	0.96	10.20	0.37
MB	1.91 ± 0.01	16.74 ± 0.05	0.86	0.72	15.70	1.07
Neosepta CMX	1.62 ^a	5.64 ^{a,b}	> 0.98 ^c	> 0.96 ^a	6.17	0.91

^a Data from [20].

^b Based on resistance measured in 0.5M NaCl solution at 25 °C.

^c Data from [21].

3.4.6 Transport Number and Selectivity

The transport numbers and permselectivities for the copolymers are shown in Table 3.7. All membranes exhibited relatively high transport numbers, a result of their high level of sulfonation that minimises the transport of negatively charged chloride ions. RCP 2 and RCP 3 had transport numbers comparable to the commercial membranes presented in Table 3.5, with values close to one indicating a high exclusion of counterions. Unlike the IEC, conductivity and water uptake of the random copolymers, which were all found to increase with increasing diphenylhydroquinone monomer content, the transport number of RCP 1 was found to be lower than both RCP 2 and RCP 3 in spite of its greater fixed charge content. Similarly, the multiblock copolymer was seen to have the lowest transport number of all membranes tested. This reduced transport number at high IEC values is due the accompanying high water uptake that swells the hydrophilic channels in the polymer matrix. The swollen channels dilute the sulfonated regions of the polymer and reduce their effectiveness as cation exchange membranes, an effect which is exacerbated in the microheterogeneous multiblock copolymer membrane. This effect highlights the delicate balance required to produce a polymer that is both highly conductive and highly selective towards counter ions. The high transport number of RCP 2 makes it an attractive option for MCDI applications, even with a lower conductivity than RCP 1; it has a greater ability to reduce the simultaneous desorption of anions during the adsorption phase, potentially improving the energy efficiency of the process.

Values for hydration number and selectivity calculated from Equation 3.1 and Equation 3.2 are presented in Table 3.7, and are graphically represented in Figure 3.15. The random copolymers are seen to have an increasing selectivity with conductivity and hydration number. Recalling that a high selectivity and low hydration number is most desirable for both conductive and mechanically stable membranes, the linear trend of the random copolymers shows the increasing trade-off between conductivity and mechanical strength. The greater hydration number of the multiblock copolymer compared with the random copolymers indicates that its larger hydrophilic domains are able to hold more water per sulfonated group. This is due to its microheterogeneous structure and the large hydrophilic domains that promote greater membrane swelling. Further to this, even with a greater conductivity than the random copolymers this swelling reduced its selectivity. In spite of this, its hydrophobic domains still allowed for the membrane to remain stable in water, with the membrane easily handled when hydrated.

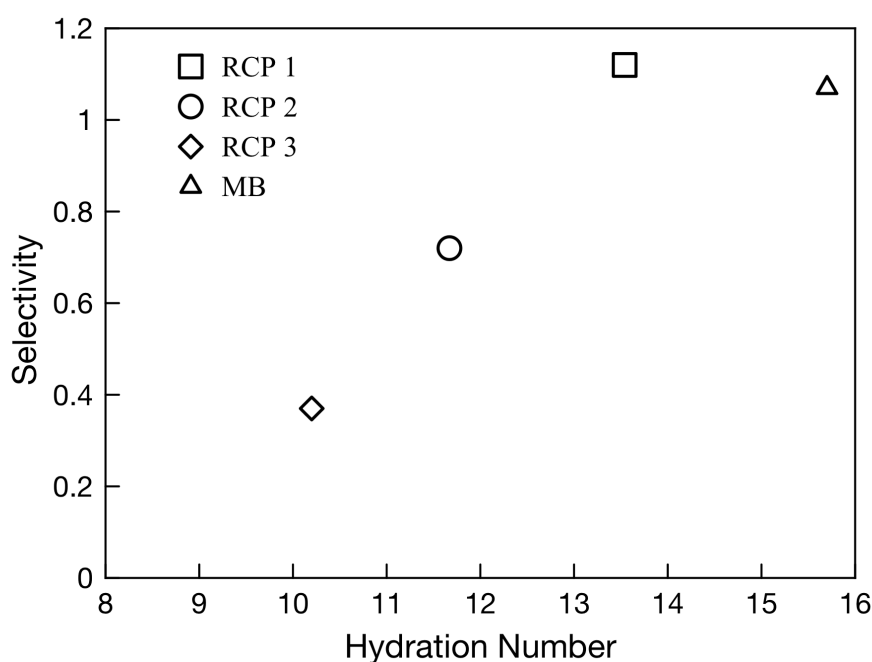


Figure 3.15 - Selectivity as a function of hydration number for the three random copolymers (RPC 1, RCP 2 and RCP 3) and the multiblock copolymer (MB).

3.5 Conclusions

In this chapter, random and multiblock side-chain sulfonated poly(arylene ether sulfone)s have been characterised for electrodialysis and MCDI applications. The chemical structure of the polymers, including the product ratio of the constituent monomers and the successful sulfonation of the side chains was confirmed using ^1H NMR and FTIR analysis.

The wettability of the membranes was strongly linked to the structure of the copolymers. The microheterogeneous structure of the multiblock copolymer reduced its wettability compared to the homogeneous random copolymers, while simultaneously increasing its water uptake and conductivity. Due to the high degree of sulfonation and the two potential sulfonation sites per diphenylhydroquinone monomer the membranes were found to have ion exchange capacities in the range 1.44 – 2.05 mmol/g, which is comparable to commercially available cation exchange membranes. The high degree of sulfonation also increased swelling, however all membranes were able to retain good mechanical stability due to the incorporation of the diphenylsulfone units along the main polymer chain.

Membrane conductivity in the Na⁺ form was found to be as high as 15.13 mS/cm for the RCP 1 and 16.74 mS/cm for the multiblock copolymer. While the multiblock copolymer was found to be highly conductive as a result of its microheterogeneous structure, this simultaneously reduced its transport number. Coupled with its additional processing steps, this multiblock copolymer is less desirable for commercial applications. For the random copolymers, with its balance of hydrophobic and hydrophilic monomers RCP 2 was found to have the highest transport number of 0.99. With good conductivities and favourable transport properties, these random copolymers are attractive materials for MCDI applications, particularly RCP 1 and RCP 2.

3.6 Publications

The following publications are based on the results from this chapter (see Appendix A5 for 'Side-chain sulfonated copolymer cation exchange membranes for electro-driven desalination applications'):

Journal Article

Asquith, B.M., Meier-Haack, J., Vogel, C., Butwilowski, W. and Ladewig, B.P., Side-chain sulfonated copolymer cation exchange membranes for electro-driven desalination applications, *Desalination*, 324 (2013) 93-98.

Conference Presentations

Asquith, B.M., Ladewig, B.P. and Meier-Haack, J., Preparation and Characterisation of Side-Chain Sulfonated Copolymer Cation Exchange Membranes, in: *3rd Early Career Researchers Membrane Symposium*, University of Queensland, St. Lucia Campus, Brisbane, 2012.

Asquith, B.M., Ladewig, B.P. and Meier-Haack, J., Preparation and Characterisation of Side-Chain Sulfonated Random Copolymer Cation Exchange Membranes, in: *2nd Annual Monash University Chemical Engineering Conference*, Monash University, Clayton Campus, 2012.

3.7 References

- [1] Cooper, K., Characterizing Through-Plane and In-Plane Ionic Conductivity of Polymer Electrolyte Membranes, *ECS Transactions*, 41 (2011) 1371 - 1380.
- [2] Strathmann, H., Ion-exchange membrane separation processes, Elsevier, Amsterdam, 2004.
- [3] Klaysom, C., Moon, S.-H., Ladewig, B. P., Lu, G. Q. M., and Wang, L., Preparation of porous ion-exchange membranes (IEMs) and their characterizations, *Journal of Membrane Science*, 371 (2011) 37-44.
- [4] Strathmann, H., Electrodialysis, a mature technology with a multitude of new applications, *Desalination*, 264 (2010) 268-288.
- [5] Vogel, C., Komber, H., Quetschke, A., Butwilowski, W., Pötschke, A., Schlenstedt, K., and Meier-Haack, J., Side-chain sulfonated random and multiblock poly(ether sulfone)s for PEM applications, *Reactive and Functional Polymers*, 71 (2011) 828-842.
- [6] Dyer, J. R., Applications of Absorption Spectroscopy of Organic Compounds, Prentice Hall, Englewood Cliffs, N.J., 1965.
- [7] Coates, J., Interpretation of Infrared Spectra, A Practical Approach, in R. A. Meyers (Ed.) *Encyclopedia of Analytical Chemistry*, John Wiley & Sons Ltd, Chichester, 2000, pp. 10815-10837.
- [8] Hasanzadeh, M., Pournaghi-Azar, M. H., Shadjou, N., and Jouyban, A., A new mechanistic approach to elucidate furosemide electrooxidation on magnetic nanoparticles loaded on graphene oxide modified glassy carbon electrode, *RSC Advances*, 4 (2014) 6580.
- [9] Bonner, O. D. and Payne, W. H., Equilibrium Studies of Some Monovalent Ions on Dowex 50, *The Journal of Physical Chemistry*, 58 (1954) 183-185.
- [10] Bonner, O. D. and Smith, L. L., A Selectivity Scale for Some Divalent Cations on Dowex 50, *The Journal of Physical Chemistry*, 61 (1957) 326-329.
- [11] Geise, G. M., Paul, D. R., and Freeman, B. D., Fundamental Water and Salt Transport Properties of Polymeric Materials, *Progress in Polymer Science*,
- [12] Długolecki, P., Anet, B., Metz, S. J., Nijmeijer, K., and Wessling, M., Transport limitations in ion exchange membranes at low salt concentrations, *Journal of Membrane Science*, 346 (2010) 163-171.
- [13] Kwak, N.-S., Koo, J. S., Hwang, T. S., and Choi, E. M., Synthesis and electrical properties of NaSS–MAA–MMA cation exchange membranes for membrane capacitive deionization (MCDI), *Desalination*, (2011)
- [14] Rhim, J., Park, H., Lee, C., Jun, J., Kim, D., and Lee, Y., Crosslinked poly(vinyl alcohol) membranes containing sulfonic acid group: proton and methanol transport through membranes, *Journal of Membrane Science*, 238 (2004) 143-151.
- [15] Kim, J. S. and Choi, J. H., Fabrication and characterization of a carbon electrode coated with cation-exchange polymer for the membrane capacitive deionization applications, *Journal of Membrane Science*, 355 (2010) 85-90.
- [16] FuMA-Tech, Fumasep Technical Data Sheet, Germany, 2005.
- [17] ASTOM Corporation, Neosepta, <http://www.astom-corp.jp/en/product/02.html#03>, 2013.
- [18] MEGA a.s., Cation-exchange membranes Ralex® product data sheets, Czech Republic, 2012.
- [19] AGC ENGINEERING, Selemion Ion Exchange Membranes, 2013.
- [20] Długolecki, P., Nijmeijer, K., Metz, S., and Wessling, M., Current status of ion exchange membranes for power generation from salinity gradients, *Journal of Membrane Science*, 319 (2008) 214-222.

- [21] Choi, J. H., Lee, H. J., and Moon, S. H., Effects of Electrolytes on the Transport Phenomena in a Cation-Exchange Membrane, *J Colloid Interface Sci*, 238 (2001) 188-195.

Chapter Four

Double Layer Formation in Activated Carbon Electrodes

4.1 Overview

Activated carbon is a widely used material for CDI due to its low cost and ease of fabrication. However, its use is hindered by its relatively poor electrosorption performance when compared with other materials such as carbon aerogels and graphene [1]. This chapter examines the characterisation of carbon electrodes fabricated from activated carbon, and the effects of conductive graphite filler on its performance for CDI applications. In particular, the effect of conductive graphite filler on the formation of the EDL in the mesopores and micropores is elucidated.

A parametric study was conducted to determine the optimal graphite content for electrodes with activated carbon and PVDF binder. Samples were found to be highly hydrophobic regardless of the graphite or binder content, however the electrochemical performance varied greatly between the different samples, with a higher graphite content yielding better adsorption performance. The poor performance was found to be a result of negligible micropore double layer formation. The phenomenon of slow double layer formation was examined using EIS, with poor wettability of the samples and resistance to diffusion through the pores found to be the primary causes. The continual cycling of the potential using CV was seen to improve capacitance and reduce resistance by increasing the penetration depth of the electrolyte into the pores.

The results from this study have highlighted the need for both an appropriately conductive filler material, and the requirement for an adsorbent with a suitable pore size distribution to maximise both mesopore and micropore double layer formation.

4.2 Relevant Theory

4.2.1 Specific Surface Area and Pore Size Distribution

Specific surface area and pore size distribution are calculated from isotherms obtained from physical adsorption experiments. For CDI applications, N_2 is commonly used as the adsorbate. The BET method is used for determining the specific surface area of a sample. Unlike the well-known and commonly used Langmuir method, the BET method accounts for multilayer adsorption in pores during physical adsorption experiments. There are several assumptions made when using the BET method that have implications for its usefulness on microporous materials, such as the activated charcoal used in this study. In particular [2, 3]:

- The adsorption energies of all molecules in the first layer are considered identical
- Interactions between molecules adsorbed in the same layer are neglected
- The reduction of adsorption forces as layers build is neglected
- There is no steric limit to the multilayer thickness

Furthermore, due to the overlapping of potential of the micropore walls, a high adsorption potential is obtained, creating a situation where multilayer adsorption and micropore filling are difficult to differentiate [4]. Thus, for a microporous material, the surface area calculated by the BET method does not accurately reflect the surface area of the material, and is better considered as a characteristic BET surface area.

To calculate a reliable, repeatable characteristic BET surface area, the Roquerol transform must be applied, whereby only linear data on the BET plot is considered. Convention is to use data in the relative pressure range 0.05 - 0.35, although this is not suitable for microporous materials. Instead, a relative pressure range is chosen so that the value $Q(P_0 - P)$ increases with relative pressure P/P_0 (where Q is the volume of gas adsorbed, P is the measured pressure and P_0 is the saturation pressure) [3]. Figure 4.1 shows an example of a typical BET plot for a microporous material (a) and $Q(P_0 - P)$ plotted against relative pressure (b).

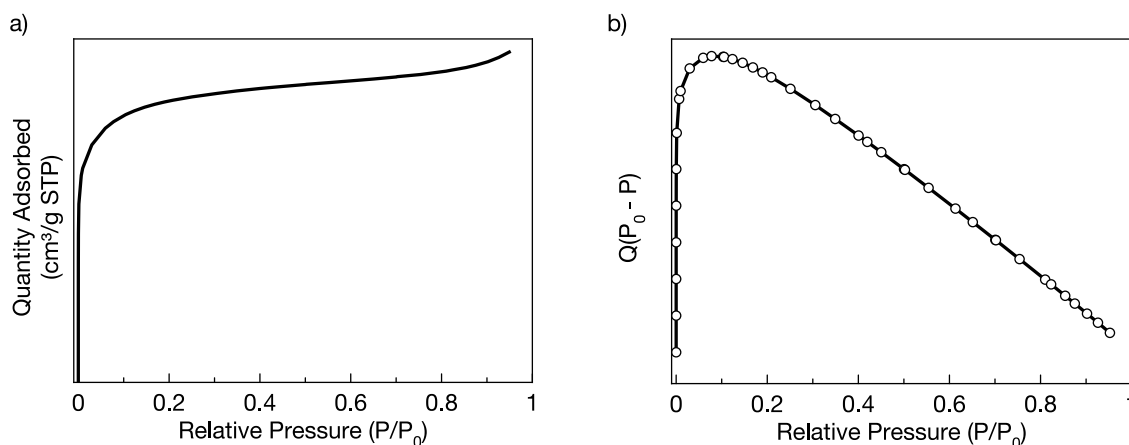


Figure 4.1 - a) BET plot for a microporous material and b) $Q(P_0 - P)$ plotted against relative pressure for a microporous material.

Pore size distribution can be calculated using density functional theory (DFT). This is a purely mathematical method that is calculated based on the minimum free energy of the adsorbate at equilibrium. A set of model isotherms is calculated for a range of pore sizes (from several angstroms up to free surface) over the appropriate pressure range, assuming a fixed pore geometry for graphitised carbon

black (typically slit or cylindrical shaped). This set of isotherms is then scaled to fit the experimental data, and the pore size, volume and area distribution can be calculated based on the scaling factor.

4.2.2 The Electrical Double Layer

The formation of an EDL is fundamental in the electrosorption process. An EDL forms when a potential is applied to a polarisable surface immersed in an aqueous electrolyte solution; when no charge transfer occurs across the electrode-solution interface, the build up of charge in the electrode creates a similar build up of oppositely charged ions in the solution at the interface. Graphical representations of an EDL are shown in Figure 4.2 and Figure 4.3.

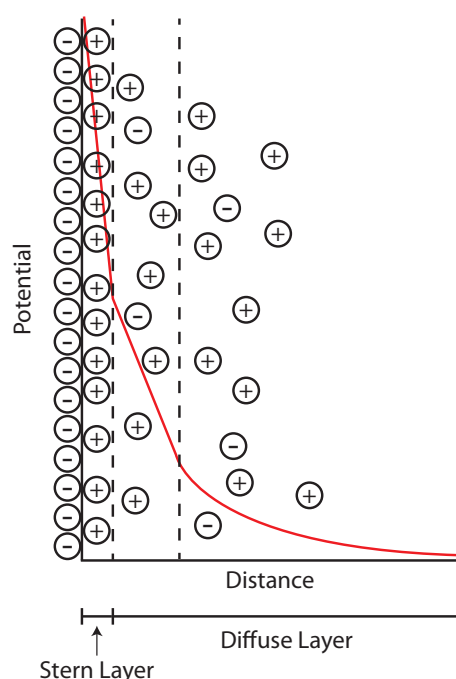


Figure 4.2 - Graphical representation of an EDL with a negatively charged electrode surface and the build up of cations in the Stern layer. The decay in potential through the solution as the distance from the electrode-solution interface increases is shown in red.

The EDL acts in a similar manner to a capacitor, whose capacitance C (farads) is defined as:

$$C = \frac{q}{E}$$

Equation 4.1

where q is the charge stored on the capacitor (coulombs) and E is the potential across the capacitor (volts). For an electrode immersed in solution, the charge on the electrode can be defined as q^M , and the charge in solution as q^S , which represents excess cations or anions in solution at the interface. It follows that for an EDL $q^M = -q^S$, as so for CDI the amount of salt that can be adsorbed is directly proportional to the capacitance of the electrode.

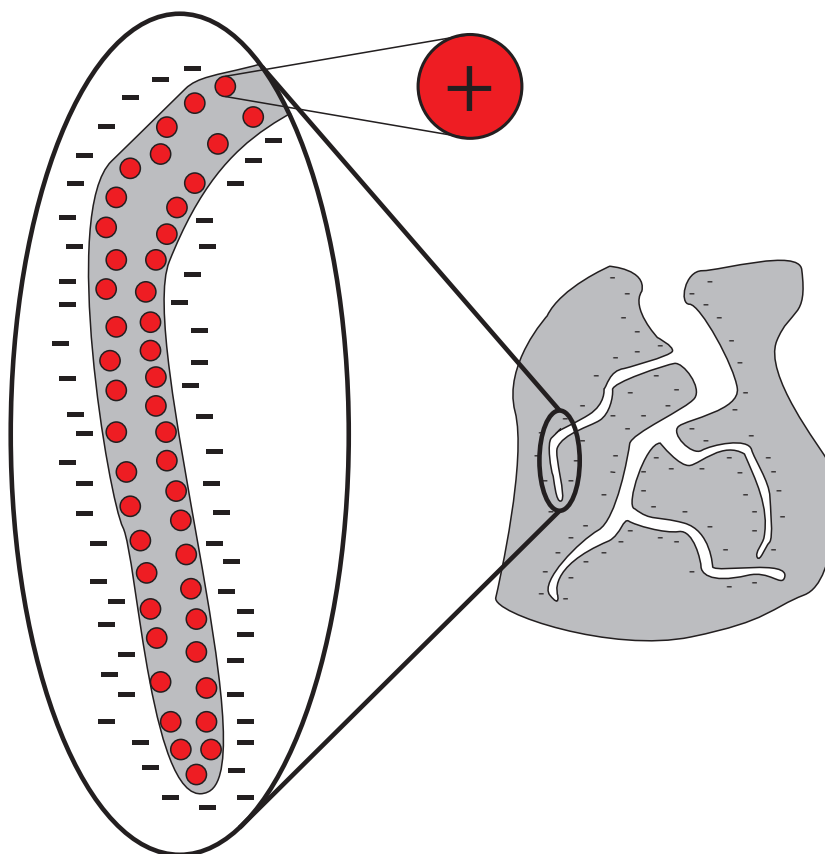


Figure 4.3 - Graphical representation of EDL formation in the pores of a negatively charged activated carbon particle.

4.2.3 Cyclic Voltammetry to Measure the Electrical Double Layer

If the electrode behaves as an ideal polarised electrode (i.e. an electrode where no charge transfer occurs across the electrode-solution interface), CV can be used to measure its capacitance [5]. Considering an ideal polarised electrode immersed in an electrolyte, the system can be represented by the equivalent circuit in Figure 4.4, where C_D is the capacitance of the electrode and R_s is the solution resistance.

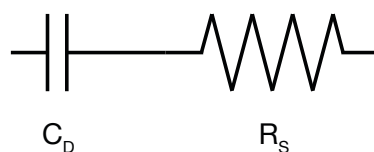


Figure 4.4 - Equivalent circuit for an ideal polarised electrode immersed in an electrolyte.

For this circuit, the applied voltage is equal to the sum of the voltage across the capacitor and resistor, E_C and E_R , such that:

$$E = E_C + E_R$$

Equation 4.2

CV operates with a linearly increasing potential at a sweep rate of v (V/s), and the potential at any time t (s) can be described as $E = vt$. By substituting the voltage across the capacitor from Equation 4.2 with

Equation 4.1, describing the voltage across the resistor by $V = iR$, and noting that $i = dq/dt$, the following equations is derived:

$$E = vt = iR_s + \frac{q}{C_d} = R_s \frac{dq}{dt} + \frac{q}{C_d}$$

Equation 4.3

Re-arranging:

$$\frac{dq}{dt} = \frac{-q}{R_s C_d} + \frac{vt}{R_s}$$

Equation 4.4

Solving with the initial condition of an uncharged capacitor, $q = 0$ at $t = 0$, the current can be expressed as:

$$i = vC_d \left[1 - e^{\left(\frac{-t}{R_s C_d}\right)} \right]$$

Equation 4.5

For the ideal polarisable electrode, steady state is reached when t becomes large and the exponential term approaches zero so that $i = vC_d$. Furthermore, if the time constant ($R_s C_d$) is small compared to the sweep rate (v), then C_d can simply be measured as a function of potential. The activated carbon electrodes in this study can be considered as ideal polarisable electrodes if the CV experiments occur within a potential window where no charge-transfer reactions (as is also desirable in CDI systems). The specific capacitance of the activated carbon electrodes, C (F/g), can therefore be calculated from the current using the following equation [5]:

$$C = \frac{i}{mv}$$

Equation 4.6

where i is the current (A), m is the mass of sample (g) and v is the scan rate (V/s).

4.2.4 Electrochemical Impedance Spectroscopy and Equivalent Circuits

4.2.4.1 Transmission Line Model

The transmission line model by de Levie is often used to describe the formation of an EDL within the pores of a porous electrode [6]. This model, shown in Figure 4.5, assumes the pores of the electrodes to be circular cylinders with a uniform diameter and semi-infinite length. Although the model is a simplified version of an actual electrode and assumes uniform pore structure, it enables simplifications that would otherwise be too complicated for the random pore networks of activated carbons. Importantly, it has been shown that when applying a sinusoidal potential, the phase angle between the potential at the pore

orifice and the charging current is 45° . Thus, the charging current behaves like the Warburg diffusion impedance of a flat electrode [6].

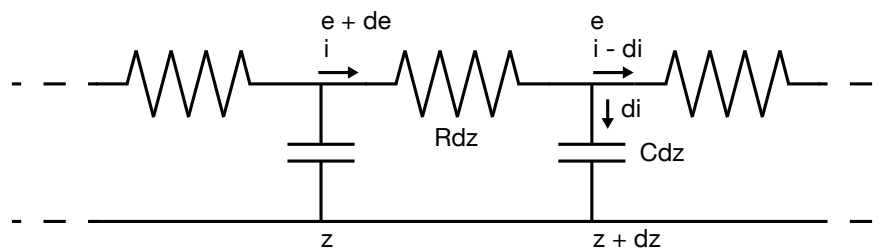


Figure 4.5 - Transmission line model proposed by de Levie [6], which describes the resistance and capacitance along the length of a pore of an ideal polarisable electrode, where the pore opening is located at $z = 0$.

Additionally, as shown in Figure 4.6, while the frequency of the signal remains constant throughout the pore, the amplitude decreases with pore depth [6]. Lower frequencies are therefore required to achieve suitable penetration and double layer formation within the electrode, allowing the measurement of capacitance [6]. Assuming ideal capacitive behaviour, at low frequencies the capacitance can be calculated from the imaginary impedance measured during EIS (EIS), based on the following relationship:

$$C = \left| \frac{1}{Z''\omega} \right|$$

Equation 4.7

where C is the capacitance (F/g), Z'' is the imaginary impedance and ω is the angular frequency.

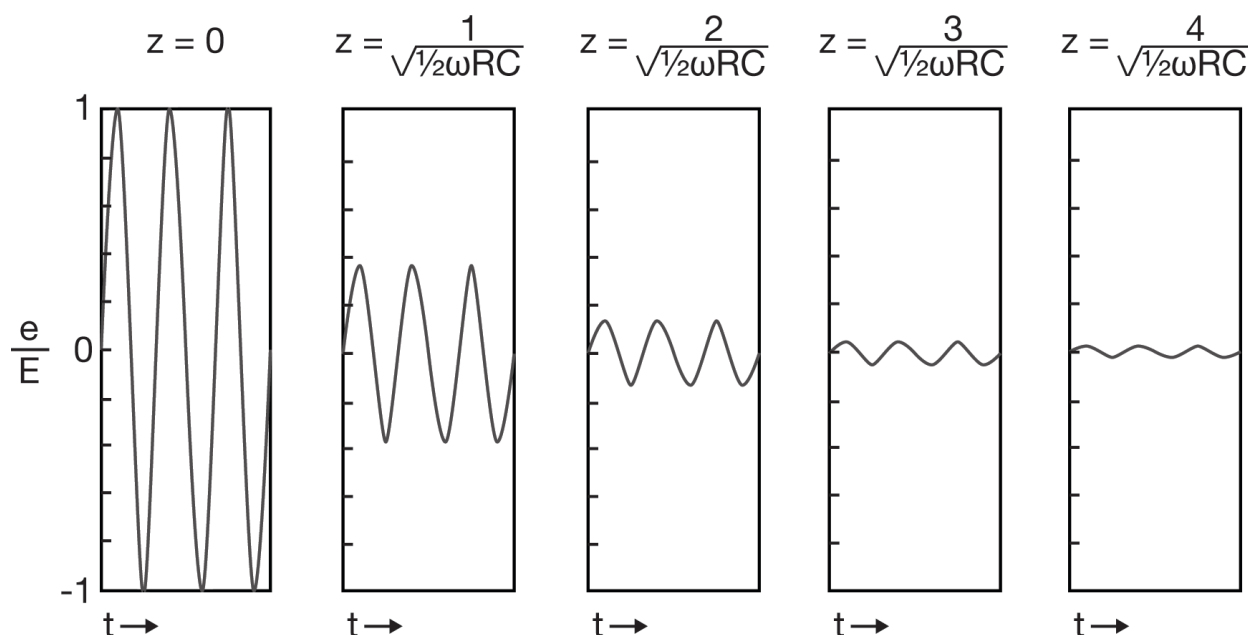


Figure 4.6 - Potential response at different distances z from the orifice of a pore as a function of time, when a sinusoidal potential with constant amplitude and frequency is applied at $z = 0$. Adapted from [6].

4.2.4.2 Equivalent Circuits

For the carbon electrodes in this study, the equivalent circuit in Figure 4.7 was found to fit the Nyquist plots obtained from EIS well.

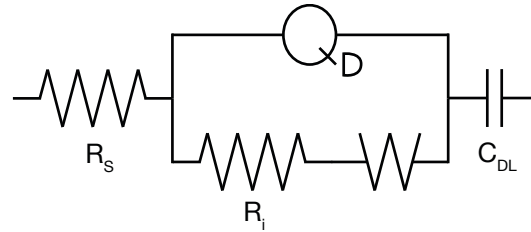


Figure 4.7 - Equivalent circuit model for the carbon electrodes, where R_s is the solution resistance, Q_D is a constant phase element, R_i is the interface resistance, W is the Warburg impedance, and C_{DL} is the double layer capacitance.

When considering the Nyquist plot from an EIS experiment, the ohmic resistance of the electrolyte solution, carbon electrode and testing cell is given by the intercept of the curve with the real axis. This is represented by the single resistor R_s in Figure 4.7, and its impedance, which is independent of frequency, is given by:

$$Z_s = R_s$$

Equation 4.8

The diffusion of ions through the electrolyte and into the pores is represented by a constant phase element (CPE) in parallel with a resistor and Warburg element. The CPE Q_D is a measure of the porosity or roughness of the electrode surface at high frequencies [7], and its impedance is given by:

$$Z_D = \frac{1}{Y_0(j\omega)^\alpha}$$

Equation 4.9

where Y_0 is capacitance, ω is the frequency and α is a dimensionless parameter between zero and one. When $\alpha = 1$, the CPE behaves as an ideal capacitor and when $\alpha = 0$, the CPE behaves as a resistor. At high frequencies there is no penetration of ions into the pores, and both Q_D and R_i are associated with the impedance at the interface between the carbon particles and the current collector, and between the carbon particles themselves [7]. The Warburg element W describes the charging current as the ions diffuse into the pores, and is a CPE where $\alpha = 0.5$. The Warburg impedance increases as frequency lowers and the ions must diffuse further. Its impedance is given by:

$$Z_W = \frac{1}{Y_0\sqrt{j\omega}}$$

Equation 4.10

Double layer formation at the electrode-solution interface is represented by the element C_{DL} , and its impedance is given by:

$$Z_{DL} = \frac{1}{j\omega C_{DL}}$$

Equation 4.11

4.3 Experimental

4.3.1 Materials

Anhydrous NMP, PVDF ($M_w \sim 530,000$ g/mol), activated carbon and graphite powder were purchased from Sigma Aldrich (Australia). Prior to use, the activated charcoal was sieved to ensure a nominal particle size of $<38 \mu\text{m}$. Both the activated charcoal and graphite powder were dried for 24 h at 150°C to remove any moisture or other volatiles.

4.3.2 Fabrication of Carbon Electrodes

Carbon electrodes were fabricated from activated charcoal, graphite and PVDF. The activated carbon was used as an adsorbent, the graphite as a non-porous conductive medium, and the PVDF as a hydrophobic binder to hold the carbon and graphite particles together.

Electrodes were prepared by first dissolving PVDF powder in NMP, with the concentration being approximately 5 wt.%. Once fully dissolved, graphite powder was added and the solution was mixed for several hours. Activated charcoal was then added to form a thick slurry, which was stirred for 12-16 h to ensure an even distribution of graphite and carbon particles in the PVDF solution. The carbon slurry was coated onto graphite sheet substrates using a doctor blade to a thickness of $350 \mu\text{m}$, then dried in a vacuum oven for 16 h at 120°C to completely remove the solvent. Each sample had a final mass of 2 - 5 mg.

4.3.3 Carbon & Graphite Specific Surface Area and Pore Size Distribution

Adsorption isotherms were obtained using a Micrometrics ASAP 2020 Physisorption Analyser using N_2 as the adsorbate at 77 K. Specific surface area was calculated using the BET method using the Roquerol transform described in section 4.2.1 with relative pressures in the range 0 - 0.08. The pore size distribution was calculated using DFT assuming a slit pore orientation using Micrometrics ASAP 2020 software. The assumption of slit shaped pore is considered to be most appropriate in this study, as

carbon pores have an approximate slit shape, and previous studies have shown this orientation to fit well with microporous activated carbons [8-10].

4.3.4 Electrode Characterisation

4.3.4.1 SEM and Contact Angle

SEM images were obtained using a Nova NanoSEM 450 with an acceleration voltage of 5 kV using the secondary imaging mode. The samples were coated with iridium prior to imaging. Contact angle measurements were made with a Dataphysics OCA 15EC measuring instrument using the sessile drop method.

4.3.4.2 Electrochemical Characterisation

CV and EIS experiments were performed using a Biologic VSP potentiostat connected to a three-electrode electrochemical cell. The working electrode was the carbon material to be tested with an exposed surface area of 0.785 cm^2 . The reference electrode was a saturated KCl Ag/AgCl electrode inserted into a bridge tube with the working electrolyte used as the filling solution. The bridge tube was used to slow the rate of contamination between the reference electrode and the working solution, and to allow the tip of the electrode to be placed close to the surface of the working electrode. The counter electrode was a mesh platinum electrode, with a surface area of 3.5 cm^2 . The potential window for CV experiments was varied to avoid faradaic reactions. EIS was performed over the frequency range 10 mHz to 1 MHz, with an applied voltage amplitude of 10 mV.

The electrolyte for all tests was 0.5 M NaCl (29,220 mg/l). This concentration is unrealistically high compared with the brackish water concentration typically used for CDI, with estimates suggesting that only concentrations below 5000 mg/L are economically viable [11]. Nonetheless, solutions with higher concentrations are more conductive and more reliable results are achieved. Furthermore, the conversion from high concentration NaCl capacitance to salt storage capacity for brackish water CDI applications has previously been studied [12].

4.4 Results and Discussion

4.4.1 Activated Carbon and Graphite Specific Surface Area and Pore Size Distribution

The isotherm obtained for the activated charcoal is shown in Figure 4.8. The large increase in adsorbed gas at low relative pressure is typical for that of Brunauer Type 1 isotherm, which describes a microporous solid [13]. At very low relative pressures there is a great increase in adsorbed gas due to the filling of micropores, which levels off once the micropores have filled. The gradual increase in the quantity of adsorbed gas from a relative pressure of around 0.2 combined with the hysteresis loop indicates the presence of mesopores. This gradual increase combined with the closure of the hysteresis loop at a relative pressure of approximately 0.4 is indicative of small mesopores. The BET specific surface area of the activated carbon was calculated to be 1039 m²/g, which is in the expected range for an activated carbon, which typically have surface areas of 1000 - 2000 m²/g. The BET specific surface area calculations can be seen in Appendix A2.

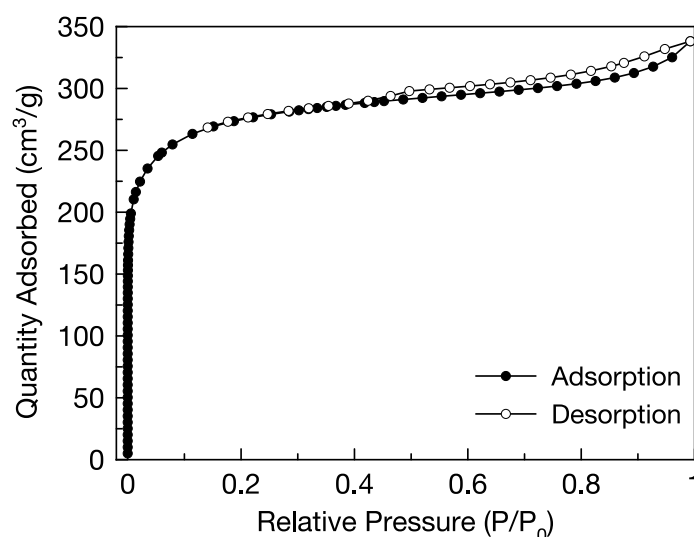


Figure 4.8 - Activated carbon adsorption isotherm measured by physical adsorption.

The pore size distribution, shown in Figure 4.9, confirms the largely microporous nature of the carbon, with a large spike in specific surface area observed at 0.59 nm, and smaller peaks in the regions 0.80-0.86 nm and 1.18-1.27 nm. Pores greater than 2 nm (mesopores) were found to contribute only small amounts of surface area. The actual microporous and mesoporous contributions to the total surface area can be seen in Table 4.1, with the mesopores contributing only 81.3 m²/g while the micropores contribute 777 m²/g. It should be noted that a significant difference between the BET surface area and

the DFT surface area was observed, largely due to the assumptions of the BET method described in section 4.2.1. Regardless of the inaccuracy of this method, the characteristic BET surface area is important, as it allows for comparison with other materials. Conversely, the DFT model isotherm was seen to fit well with the measured isotherm, perhaps providing a more accurate estimation of microporous and mesoporous surface area.

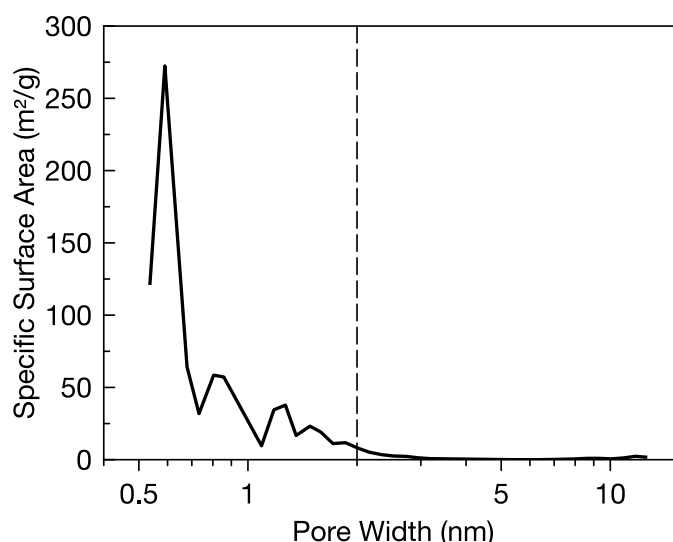


Figure 4.9 - Pore size distribution of the activated carbon measured by physical adsorption. The dashed line at 2 nm indicates the boundary between micropores and mesopores.

Table 4.1 - Cumulative surface area of activated carbon with decreasing pore size, calculated using DFT.

Pore size (nm)	Cumulative Surface Area (m ² /g)
12.7	57.0
5.03	65.7
2.00	81.3
1.00	253.3
0.73	368.6
0.50	858.3

The adsorption isotherm of the graphite powder is shown in Figure 4.10, and is a typical Brunauer Type 2 isotherm for a non-porous material [13]. A relatively large amount of gas is adsorbed at low pressure, with more than a quarter of the maximum adsorption volume occurring at relative pressures less than 0.1. This is a result of gas molecules initially adsorbing to the most energetic regions of the graphite. In the relative pressure range 0.2 – 0.7, a steady increase in the adsorbed gas volume is observed as molecules continue to adsorb to less energetic regions of the graphite, then form additional layers. The sharp rise at

the end of the curve is a result of bulk condensation. The BET surface area of the graphite was calculated to be 21.12 m²/g. This value is very low compared with the surface area of the activated charcoal described. As CDI relies on highly porous materials to adsorb salt ions, the conductive graphite filler can be considered as having a negligible impact on the total salt adsorption capacity of the electrodes.

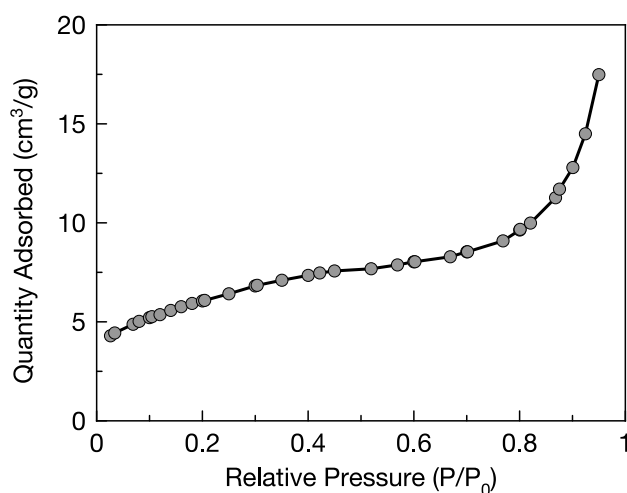


Figure 4.10 - Adsorption isotherm of graphite measured by physical adsorption.

4.4.2 Electrode Preparation Optimisation

Several electrode preparation methods and compositions were tested to optimise the preparation of the carbon electrodes. The iterations of this process are described in Table A3, found in Appendix A3. The key processes that needed to be optimised were the mixing of the components to form a consistent carbon slurry, casting thickness, and the evaporation of solvent. This needed to be done in such a way as to produce homogenous films free from defects, and to ensure the binder would hold the carbon particles together.

As the graphite is used as conductive filler, proper dispersion throughout the film is required to allow the build up of charge in the carbon particles and hence double layer formation. Good mixing of the graphite and carbon is also required to prevent the agglomeration of particles, and to ensure adequate binding from the PVDF. To achieve this, a PVDF solution was initially prepared, then graphite particles were added and allowed to mix for several hours with a high shear rate. This ensured the graphite particles were completely dispersed. Activated carbon particles were then added to polymer-graphite slurry and left to stir for several hours, effectively coating the carbon particles with the PVDF/graphite solution.

The electrode thickness is important in terms of both electrode preparation and pore access for the electrolyte during electrosorption. Due to the tortuous path created by the voids in the carbon composite, a thicker layer can both hinder full solvent evaporation and slow electrolyte access to the pores during electrosorption. Although initial electrodes were cast at 650 μm and formed consistent carbon films without cracks, this was reduced to 350 μm to ensure complete solvent evaporation and better pore access in future electrochemical tests. The evaporation of the solvent must be carefully done, as rapid evaporation can lead to the formation of cracks. It was found the best method to produce the films was to leave freshly cast samples in the fume cupboard until the surface appeared dry. Following this, the samples were slowly heated in an oven from room temperature to 120 $^{\circ}\text{C}$ without vacuum. After two hours, the samples were placed under vacuum at 120 $^{\circ}\text{C}$ and allowed to dry for 12-16 hours. Samples that were dried at lower temperature or shorter amounts of time were prone to forming cracks.

4.4.3 Electrode Morphology and Contact Angle

Samples with 5, 10 and 15 wt.% graphite were prepared (5G, 10G and 15G, respectively), as outlined in Table 4.2. A PVDF content of 5 wt.% was unable to bind the carbon particles together, so a minimum of 10 wt.% was used. To test the hydro- and thermal stability of the electrodes, they were placed in water at 80 $^{\circ}\text{C}$ for 6 h. No degradation was observed and no carbon was removed from the surface. All electrodes were stored in water at room temperature before use, with no loss of carbon observed.

Table 4.2 - Electrode compositions and contact angle.

#	Composition (wt. %)			Contact Angle ($^{\circ}$)
	Activated carbon	Graphite	PVDF	
5G	85	5	10	135.2
10G	80	10	10	132.6
15G	70	15	15	138.8

SEM images of the three electrodes at low magnification can be seen in Figure 4.11. The electrode surfaces are shown to be similar in appearance and although it is not easy to distinguish between the graphite and carbon particles, no obvious agglomerations of carbon or graphite particles were observed. This indicates that the solutions were well mixed and a homogeneous carbon layer was achieved. In Figure 4.11 c) the higher PVDF content is more obvious than in the 5G and 10G samples, particularly with the long fibrous strand of polymer on the surface.

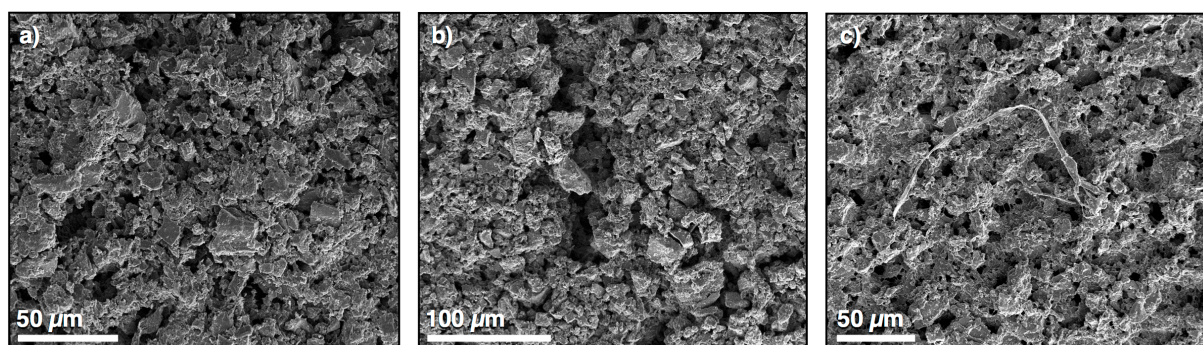


Figure 4.11 - SEM images of a) 5G b) 10G and c) 15G samples.

Figure 4.12 presents SEM images of 10G and 15G samples at higher magnifications. The difference in PVDF binder is again visible, with fibrils that bind the carbon together observed for the 15G sample (Figure 4.12 c & d). For all images while no pore openings on the carbon particles were observed due to magnification limitations, the extensive coating of the PVDF indicates that pore blockages by the hydrophobic binder are likely to occur.

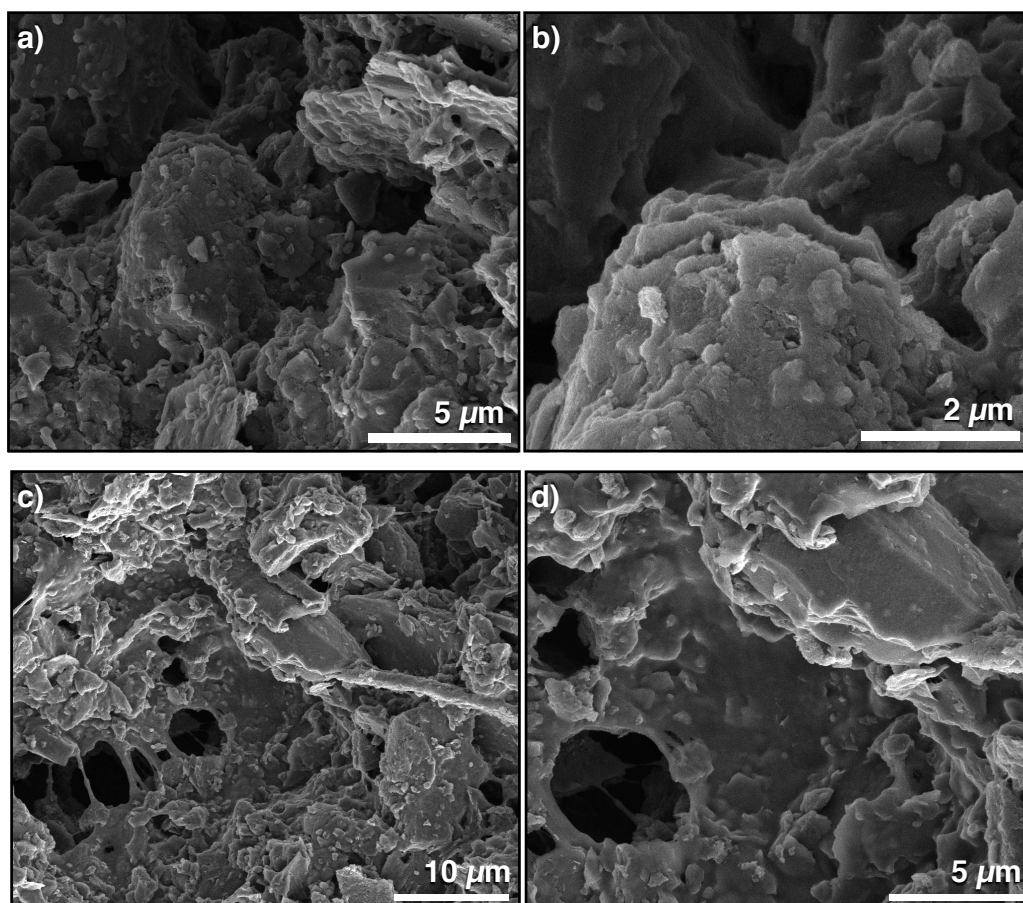


Figure 4.12 - SEM images showing the PVDF binding activated carbon and graphite particles of a & b) 10G and c & d) 15G electrodes.

The contact angle of each electrode is shown in Table 4.2, and images taken during measurements are shown in Figure 4.13, in addition to the contact angle of a pure PVDF membrane. The electrode surfaces were found to be highly hydrophobic, with contact angles in the range of 132° - 139° . In comparison, the PVDF membrane was observed to have a contact angle of 81.3° . This highlights that although the hydrophobic PVDF binder plays a large role in causing the hydrophobicity of the carbon electrodes, the surface roughness and carbon particles also significantly contribute to the large contact angle, resulting in electrodes with poor wettability. Due to surface roughness, the observed contact angle is not equivalent to Young's contact angle (which defines the contact angle in terms of liquid-vapour, solid-vapour and solid-liquid interfacial tensions). All contact angles were found to be stable, with variations less than 0.5° when measured over a period of 60 seconds. The importance of the low wettability of the electrodes will be discussed further when considering the resistance to double layer formation in section 4.4.6.

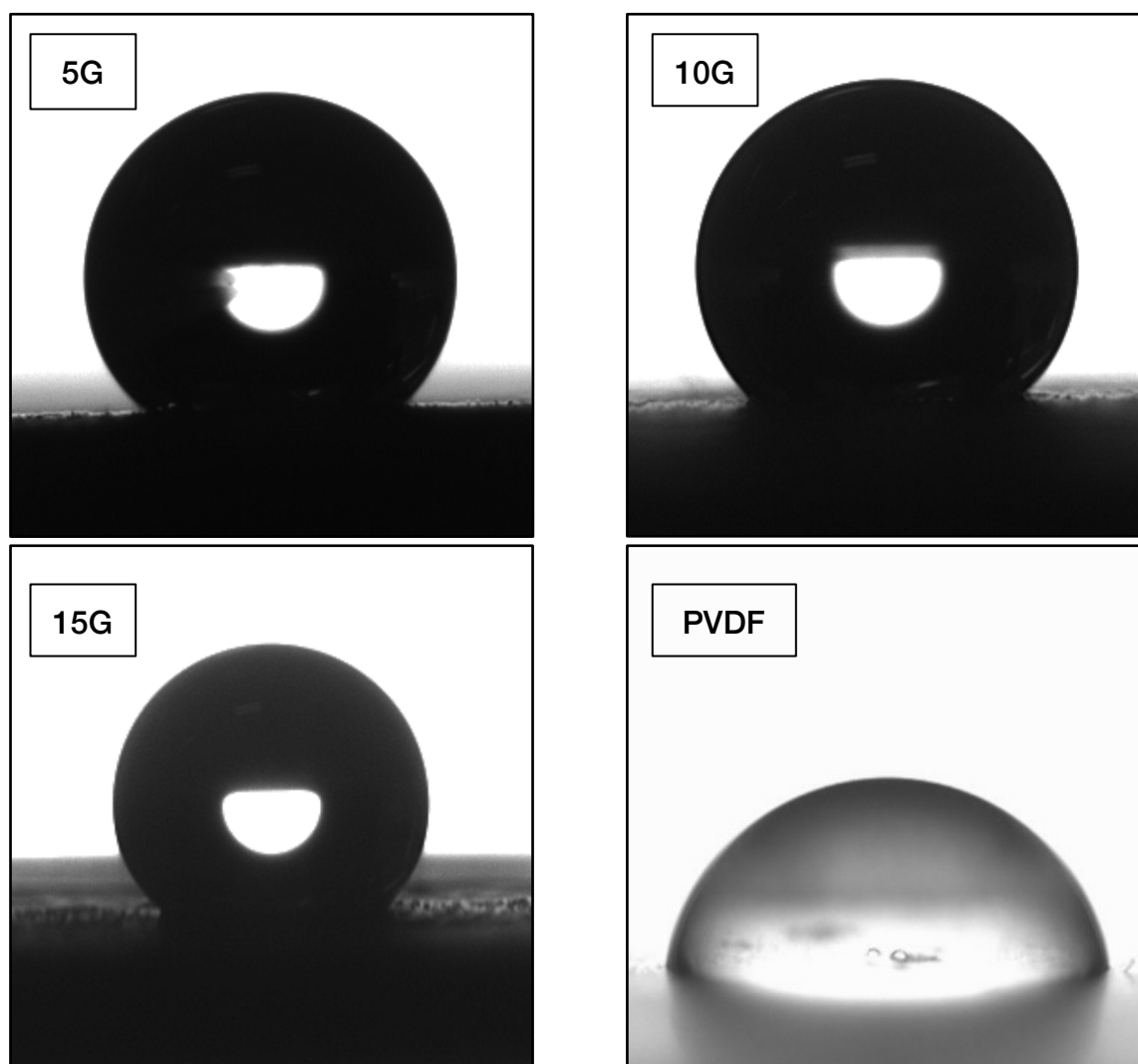


Figure 4.13 - Contact angles of 5G, 10G and 15G electrodes, as well as a PVDF membrane.

4.4.4 Cyclic Voltammetry

Typical cyclic voltammograms showing the specific capacitance of the electrodes at scan rates of 1, 5 and 20 mV/s are presented in Figure 4.14, Figure 4.15 and Figure 4.16. Note that different potential windows were chosen for each sample to avoid faradaic reactions.

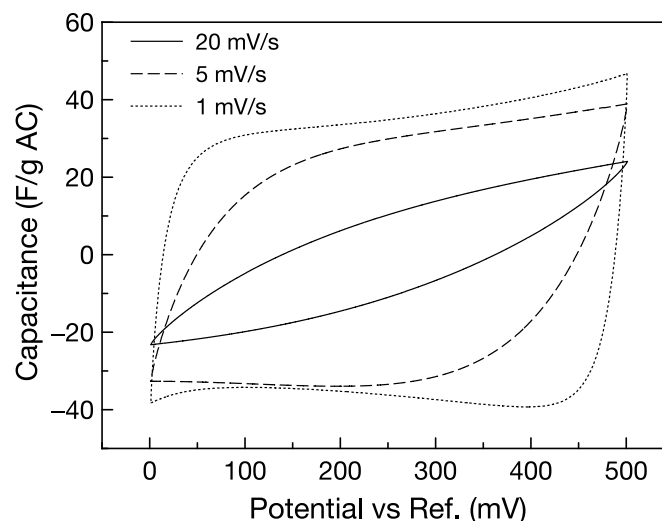


Figure 4.14 - Specific capacitance of a 15G electrode in 0.5M NaCl, obtained at scan rates of 20 mV/s (solid line), 5 mV/s (dashed line) and 1 mV/s (dotted line).

Sample 15G, shown in Figure 4.14, yielded typical behaviour for a microporous carbon sample, with symmetrical curves indicating a reversible process and no faradaic reactions. At the fastest scan rate of 20 mV/s no constant capacitance was observed, as the scan rate was too fast to fully allow the transport of ions into the pores. The larger, rectangular curves at slower scan rates of 5 and 1 mV/s indicated the ions had greater time to penetrate into the pores and form an EDL. Considering the reverse scan (from 500 to 0 mV), at a scan rate of 5 mV/s a stable capacitance of approximately 34 F/g was reached at around 250 mV versus the reference potential, with little variation at potentials lower than this. Conversely, the 1 mV/s scan rate was seen to have a greater capacitance before a shallow minimum that approached the 5 mV/s curve was observed at approximately 100 mV. This minimum yielded the point of zero charge (PZC), the point at which the surface potential of the carbon is zero, and is an outcome of the microporous nature of the carbon causing overlapping EDLs, pores being too small for ion penetration, and ion hydration effects [10, 14, 15]. It is thought that at a scan rate of 5 mV/s the capacitance predominantly arose from mesopores, indicating this scan rate is too slow to allow significant micropore penetration in the samples with 15 wt.% graphite, while at 1 mV/s both micropores and mesopores contributed to capacitance.

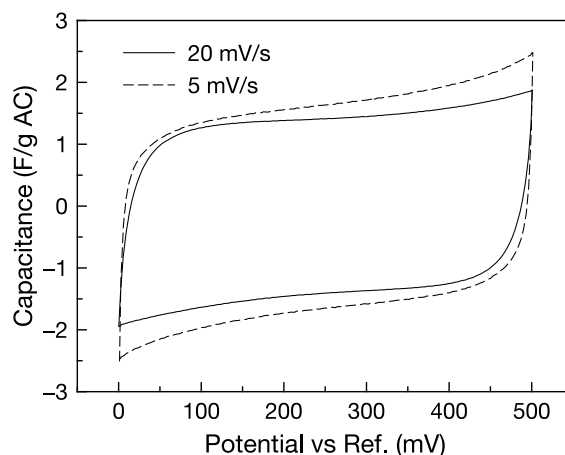


Figure 4.15 - Specific capacitance of a 5G electrode in 0.5M NaCl, obtained at scan rates of 20 mV/s (solid line) and 5 mV/s (dashed line).

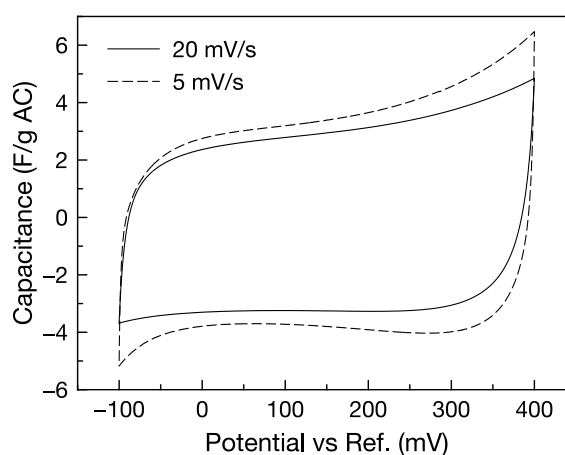


Figure 4.16 - Specific capacitance of a 10G electrode in 0.5M NaCl, obtained at scan rates of 20 mV/s (solid line) and 5 mV/s (dashed line).

The 5G and 10G samples, presented in Figure 4.15 and Figure 4.16, were observed to have rectangular curves at the fastest scan rate of 20 mV/s rather than more distorted curves. Both capacitances are also considerably lower than the 15G sample. As seen in Equation 4.6, the specific capacitance is directly proportional to the current, and so the low capacitance and rectangular curves at a fast scan rate are likely to be due to either poor electrode conductivity or poor ionic conductivity (i.e. the mobility of ions inside the pores). This poor conductivity has resulted in minimal electrolyte penetration into the micropores. The 10G sample was found to have a PZC at 80 mV versus the reference potential, while no PZC was found for the 5G sample. This showed that with insufficient graphite content, minimal micropore double layer formation occurs.

Based on the pore size distribution described in section 4.4.1, the mesoporous and microporous capacitances of samples 10G and 15G were calculated for the reverse scan. This was done assuming

only mesopore penetration at 5 mV/s, and the additional capacitance at 1 mV/s due to micropore penetration. Capacitance was measured at both the PZC and a point with a surface potential 100 mV less than the PZC (-20 mV for 10G samples, 0 mV for 15G samples) are shown in Table 4.3. The mesopores capacitance is known to remain approximately constant with voltage and be similar to a clean graphite sheet, which is approximately 20 $\mu\text{F}/\text{cm}^2$.

Only small variations in mesopores capacitance with changing potential were observed, although the 10G capacitance was much lower than the expected 20 $\mu\text{F}/\text{cm}^2$, while the 15G sample was approximately double the expected value. It is likely that poor conductivity in samples with 5 and 10 wt.% graphite contributed to poor double layer formation in not only the micropores, but also the mesopores. The larger than expected 15G mesoporous capacitance may be due to an underestimation of the mesopores specific surface area from the DFT model, which helps to explain the discrepancy between BET and DFT specific surface areas described in section 4.4.1. Considering a mesopore capacitance of approximately 20 $\mu\text{F}/\text{cm}^2$ [10], it is reasonable to assume that the actual mesoporous surface area may be up to double that of the surface area calculated from DFT. Furthermore, an amount of the calculated ‘mesoporous capacitance’ may actually be due to considerably more micropore penetration at 5 mV/s than expected. This result shows that at even at fast scan rates of 5 mV/s, with suitable graphite content micropore penetration in activated carbon is achievable, unlike previously tested carbon aerogels where negligible micropore double layer formation was observed at slow scan rates [10].

Table 4.3 - Mesoporous and microporous capacitances of 10G and 15G electrodes based on CV experiments and DFT surface area.

Point of Measurement	Specific Capacitance (F/g)		Capacitance ($\mu\text{F}/\text{cm}^2$)	
	10G	15G	10G	15G
<i>Mesopores</i>				
PZC	3.15	34.46	3.87	42.41
-20/0 mV ^a	3.33	34.08	4.09	41.94
<i>Micropores</i>				
PZC	0.48	1.85	0.06	0.24
-20/0 mV ^a	0.89	6.89	0.11	0.89

^a Capacitance was taken at 100 mV below the PZC. For 10G samples this was -20 mV versus the reference potential, while for 15G samples the point was 0 mV versus the reference potential

As the surface potential decreased, both samples were seen to have only modest increases in micropore capacitance, with the largest increase observed for the 15G sample. From the pore size distribution in Figure 4.9, it is known that up to 45% of the total surface area is held within micropores with openings of less than 5.9 Å. Although the hydrated radius of a sodium ion is 3.58 Å [16], it is in these pores that overlapping of the EDL is likely to be occurring, wasting surface area of the highly microporous carbon. Compounding the low micropore capacitance is the 15 wt. % PVDF, which may be blocking pores and reducing the number of accessible micropores, shown in Figure 4.17. Poor access to the pores, even in suitably conductive electrodes, has been shown to restrict double layer formation and capacitance.

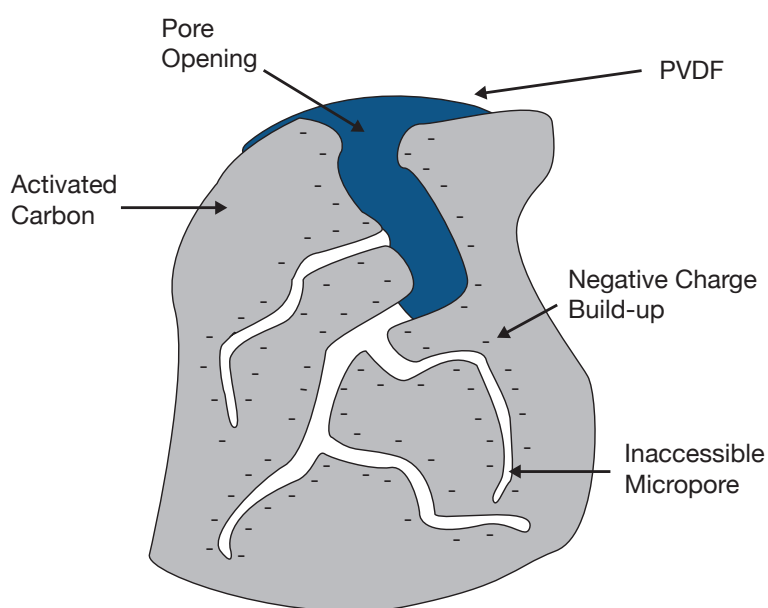


Figure 4.17 - Graphical representation of PVDF blocking an activated carbon pore.

The low capacitance of samples with 5 and 10 wt.% graphite and the lack of significant microporous capacitance are linked to the conductivity of the electrode, which depends on intra-particle resistance, contact resistance between particles and the current carrying path. The conductive graphite filler is therefore important for effectively distributing electrical current through the electrode and to the activated carbon pores. As seen in Figure 4.18 a, the graphite particles are flat with a small thickness relative to their length and width. This shape directly affects the contact resistance between particles and the current carrying path, especially as graphite is known to have a two-dimensional conductivity that requires the edges of the graphite particles to be in contact with other particles to allow the flow of electrons. This can be difficult to achieve with the relatively large activated carbon particles, shown in Figure 4.18 b).

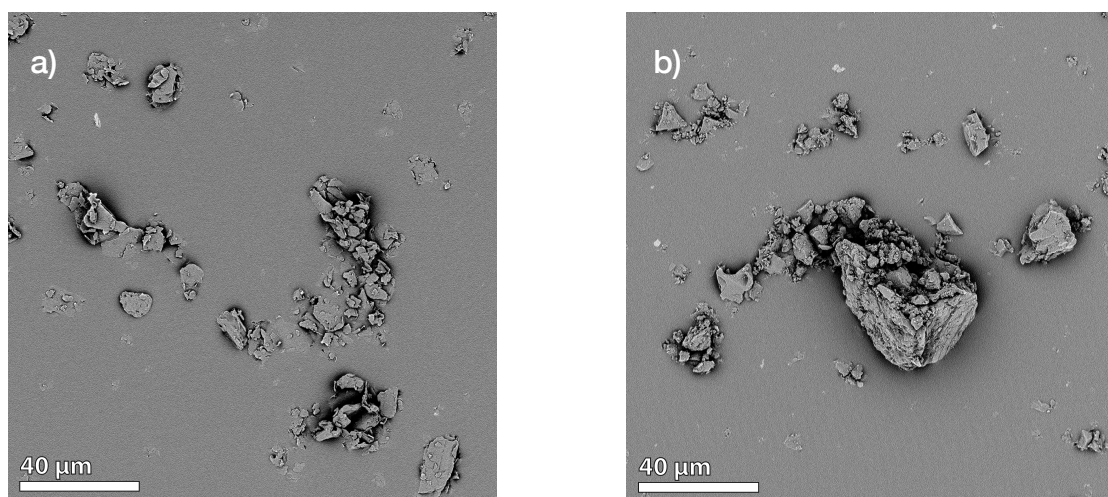


Figure 4.18 - SEM images of a) graphite particles and b) activated carbon particles.

The percolation threshold for the carbon electrode describes the minimum amount of graphite required to yield a homogeneous carbon film electrode with evenly distributed properties, including conductivity. Based on the difference in capacitance between the 10G and 15G samples, the percolation threshold for graphite content is between 10-15 wt.%. Below this threshold there is too little graphite to make effective contact with the activated carbon particles, outweighing the expected loss of capacitance due to the low surface area of the graphite.

The CV results highlight the importance of using a suitable conductive filler. When the concentration of graphite was too low, poor conductivity was observed, and the mesopores capacitance was reduced. Above the percolation threshold, modest double layer formation in the micropores was achieved, highlighting the need for both conductive filler and materials with a good balance of mesopores and micropores with large enough pore openings to minimise wasted surface area in the micropores.

4.4.5 Electrochemical Impedance Spectroscopy

EIS was employed to further elicit the behaviour of the electrodes and to examine the ionic conductivity in the electrodes. Typical Nyquist plots for each of the three samples are shown in Figure 4.19. 15G samples behaved in a manner typically expected for porous carbon electrodes. The intercept with the real axis measured at high frequencies corresponds to the ohmic resistance of the electrode, electrolyte and cell connections. In the middle frequency range ions were observed to diffuse into the pores, represented by a small half semi-circle that transforms into an approximate straight line at an angle of close to 33° , similar to that of typical Warburg diffusion. At frequencies lower than 100 mHz a near vertical spike was

observed, indicating typical capacitive behaviour and the build-up of charge at the electrode-electrolyte interface as ions have sufficient time to migrate into the pores and form an EDL. For 5G and 10G samples similar behaviour was observed at high frequencies, however at lower frequencies strong capacitive behaviour was not observed. Particularly, large increases in both real and imaginary impedances were observed which is atypical of a double layer capacitor.

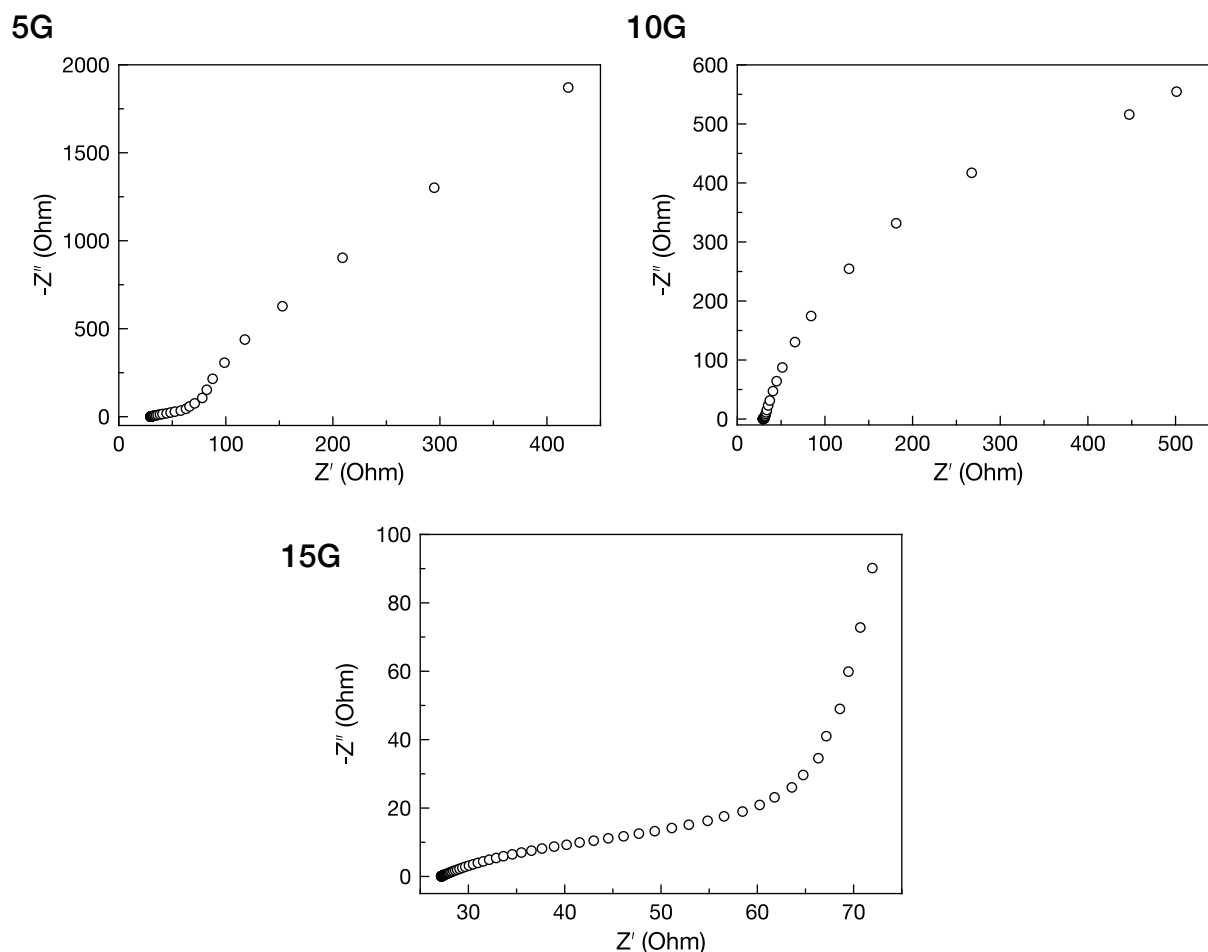


Figure 4.19 - Nyquist plots of typical responses for 5G, 10G and 15G electrodes.

From the Nyquist plot three key parameters can be determined: ohmic resistance, capacitance and diffusion (or charging) resistance. The ohmic resistance of the carbon electrodes was calculated by subtracting the ohmic resistance of blank graphite sheets from that of the samples. A general trend was observed with the ohmic resistance increasing with decreasing graphite content, however the ohmic resistance data was found to be too inconsistent to draw firm conclusions.

4.4.5.1 Capacitance from Electrochemical Impedance Spectroscopy

From Equation 4.7 the capacitance for each electrode was calculated as a function of frequency, with typical results shown in Figure 4.20. Double layer build-up for 15G samples began at approximately 1 Hz

and started to plateau as the frequency approached 10 mHz, as seen in Figure 4.20 a). Similar increases in capacitance were observed for 5G and 10G samples at lower frequencies, observed in Figure 4.20 b). The low capacitance increases for 5G samples at frequencies lower than 100 mHz confirms that negligible micropore penetration and double layer formation was achieved. 10G samples exhibited a sharp rise in capacitance at frequencies below 100 mHz. Such a delayed onset of capacitance increase compared with 15G samples may be due to delayed pore penetration following the overcoming of an additional resistive force that causes the large arc in 10G samples (see Figure 4.19). As discussed in section 4.4.4, 10G samples displayed minimal micropore penetration, and the rise may be associated with better mesopore filling as the AC wavelength increases. The poor capacitance measured for 5G and 10G samples confirmed the lack of micropore penetration below the percolation threshold.

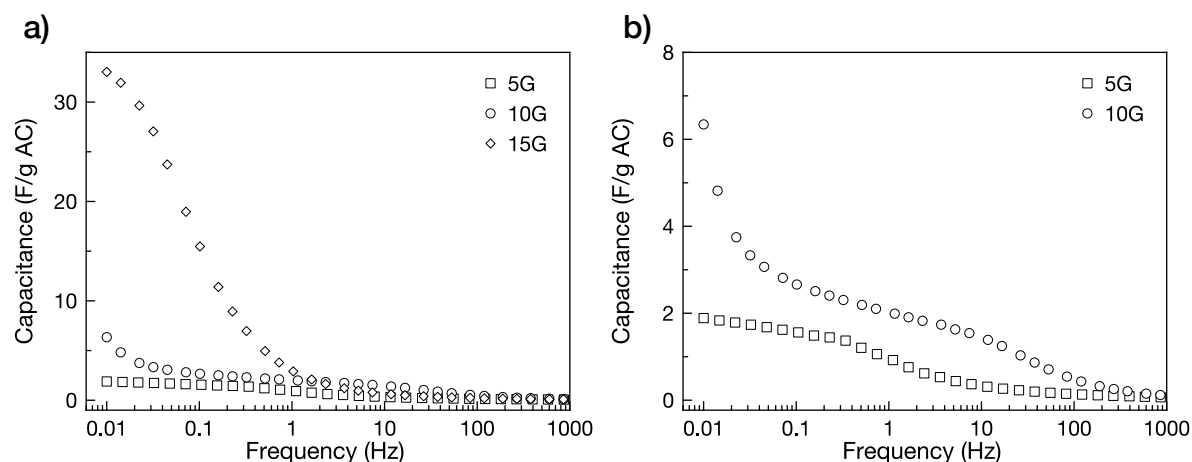


Figure 4.20 - Capacitance as a function of frequency for a) all three electrodes and b) 5G and 10G electrodes.

4.4.5.2 Diffusive Resistance

The diffusive resistance describes the electrolyte resistance within the pores. This arises from de Levie's transmission line model of a porous electrode, as described in section 4.2.4.1 above. It was calculated based on the following equation:

$$R_D = Z' - R_S$$

Equation 4.12

where R_D is the diffusive resistance (Ohm), Z' is the real impedance (Ohm) and R_S is the ohmic resistance (Ohm). The diffusive resistance describes the real impedance from the initial ohmic resistance to the low frequency point at which the curve spikes vertically and capacitive behaviour begins to dominate. For a porous carbon electrode, beyond this point the diffusive resistance should plateau and only experience minor increases. Both the capacitance and diffusive resistance are plotted against frequency in Figure

4.21, which reveals the extent of the resistance to ion mobility within the pores of 5G and 10G samples. The atypical behaviour of these samples saw large increases in resistance at low frequencies, in contrast with 15G samples where the resistance plateaued. The low frequency increase in capacitance for 5G and 10G samples is accompanied by large spikes in resistance, particularly for the 10G sample.

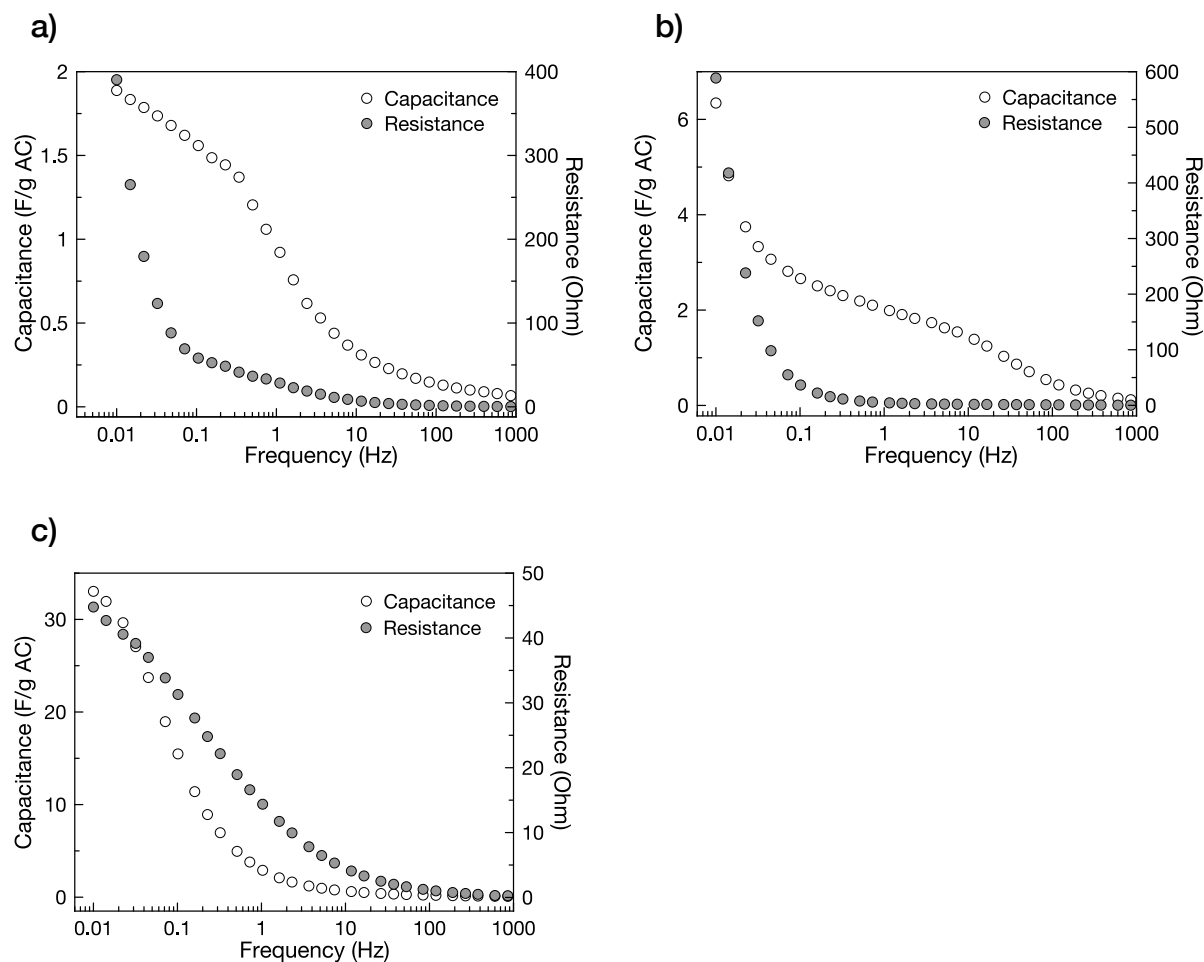


Figure 4.21 - Capacitance and resistance as a function of frequency for a) 15G, b) 10G and c) 5G electrodes.

From Figure 4.6 the AC penetration depth, z , can be expressed as:

$$z \propto \frac{1}{\sqrt{\frac{1}{2}\omega RC}}$$

Equation 4.13

where R is the solution resistance per unit pore length and C is double layer capacitance per unit pore length. As the frequency decreases, greater pore penetration is achieved. However, when there is high solution resistance, lower frequencies are required to achieve the same penetration depth. The poor conductivity and large resistance of the samples below the percolation threshold caused a lack of penetration into both the mesopores and micropores. In contrast, above the percolation threshold the

bulk of the resistance increase occurs in midrange frequencies, and begins to level off at low frequencies as capacitive behaviour dominates. This highlights the resistance caused by the small micropores ($<5.9 \text{ \AA}$) and the 15 wt.% PVDF binder in the 15G samples.

4.4.5.3 Equivalent Circuits

Using the equivalent circuit described in section 4.2.4.2 and presented again in Figure 4.22 a), only the 15 G samples could be accurately modelled. Modifications were required to model both 5G and 10G samples, which help to explain their non-ideal behaviour. To account for the non-ideal capacitive behaviour of 5G samples, the double layer capacitor C_{DL} was replaced with a CPE, Q_{DL} , shown in Figure 4.22 b. For 10G samples the circuit was modified further by placing Q_{DL} in parallel with a resistor, R_{DL} , to describe the low-frequency resistance, shown in Figure 4.22 c. Table 4.4 gives the values for the equivalent circuits derived from a typical sample of each electrode, and the simulated curves are presented in Figure 4.22. The model is seen to fit well for the 15G samples, and at high frequencies for the 10G and 15G samples. However, at low frequencies the model is less robust, a result of the large resistance and non-ideal capacitive behaviour. The validity of the model and the derived capacitance values is discussed below

Q_D and the R_i are associated with high frequency interfacial impedance, with these elements contributing less to the overall impedance with decreasing frequency as the electrolyte penetrates further into the electrodes and Warburg impedance takes over [7]. The results from the simulated data for 5G and 15G samples suggest that the interfacial resistance R_i is significantly larger than the diffusive resistance described by the Warburg impedance. This indicates that the poor wettability of the electrodes rather than diffusive resistance contributed to the drawn out resistance. For 10G samples, although low interfacial resistance was measured, the excessively large R_{DL} value suggests that resistance to micropore penetration and double layer formation in the micropores is the dominant term, even in midrange frequencies.

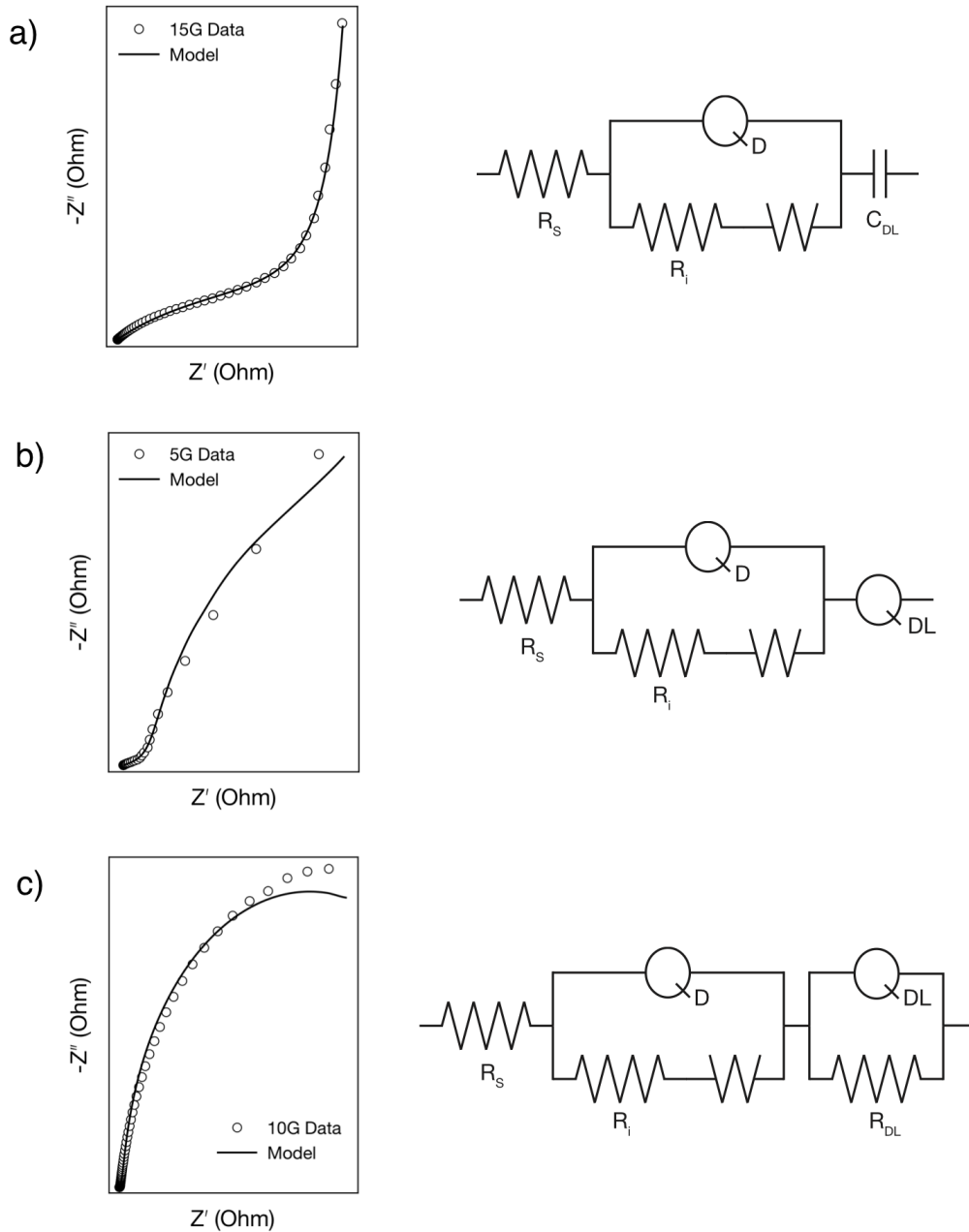


Figure 4.22 - Equivalent circuits for a) 15G, b) 5G and c) 10G electrodes.

Table 4.4 - Equivalent circuit values for each electrode type.

Sample	Q_D ($F.s^{(\alpha-1)}$)	α_s	R_i (Ω)	W ($\Omega/s^{0.5}$)	C_{DL} (F)	Q_{DL} ($F.s^{(\alpha-1)}$)	α_{DL}	R_{DL} (Ω)
15G	1.544×10^{-2}	0.54	46.81	1.449	0.1985	-	-	-
10G	3.846×10^{-3}	1	1.015	4.902	-	1.145×10^{-2}	0.93	1202
5G	4.712×10^{-3}	0.67	38.24	1.000	-	6.005×10^{-3}	0.88	-

Capacitance measured from EIS and CV scans were compared with those from the model and presented in Table 4.5. The non-ideal capacitive behaviour of the CPE Q_{DL} for 5G and 10G samples is described by α_{DL} , with more capacitive behaviour occurring as the value approaches one. This non-ideal

behaviour and the additional resistance term for 10G samples (described by R_{DL}) gives a smaller capacitance compared with those calculated from CV results or imaginary impedance from EIS. In spite of the inaccuracies of the modelled data at low frequencies (see Figure 4.22), the model may be a more accurate measure of capacitance than the capacitance calculated from CV or imaginary impedance due to the necessary ideal behaviour assumptions (see sections 4.2.3 and 4.2.4.1). When considering samples with 15 wt.% graphite, there is much better alignment between the modelled capacitance and the EIS and CV values. This strongly suggests that even considering the large interfacial resistance (which is not often observed), the ideal behaviour assumptions in the EIS and CV calculations are valid.

Table 4.5 - Comparison of capacitance based on different methods of measurement.

Sample	Capacitance (F/g)		
	EIS at 10 mHz	Equivalent Circuit ^a	CV ^b
15G	33.03	37.16	38.31
10G	6.34	2.53	5.18
5G	1.89	1.33	2.52

^a Taken from C_{DL} or Q_{DL} . Capacitive behaviour is assumed for 5G and 10G samples due to the large α_{DL} value

^b Maximum capacitance values measured from reverse CV scans.

4.4.6 Resistance to Electrical Double Layer Formation

During CV experiments, low currents were measured over the first cycle for all samples, which slowly increased until a steady current for both the forward and reverse scans was observed. At a scan rate of 20 mV/s, the current was observed to increase for up to 1200 cycles. Similar behaviour has previously been observed for similar activated carbon electrodes with PVDF binder due to the poor wettability of the carbon samples and physical adsorption of ions onto the electrode, however only to the extent of 25 cycles at 10 mV/s [17].

This phenomenon is shown in Figure 4.23 for a typical 15G sample. The rate of current increase slowed with each cycle, so that the greatest increases were observed in the first 200 cycles. The same phenomenon was also observed at 5 mV/s, with a lower number of cycles needed to attain consistent results. 5G and 15G samples tested at 20 mV/s were seen to have smaller changes in current, and only over the first 100 cycles. This is consistent with the previously described low capacitance of these samples due to poor micropore double layer formation.

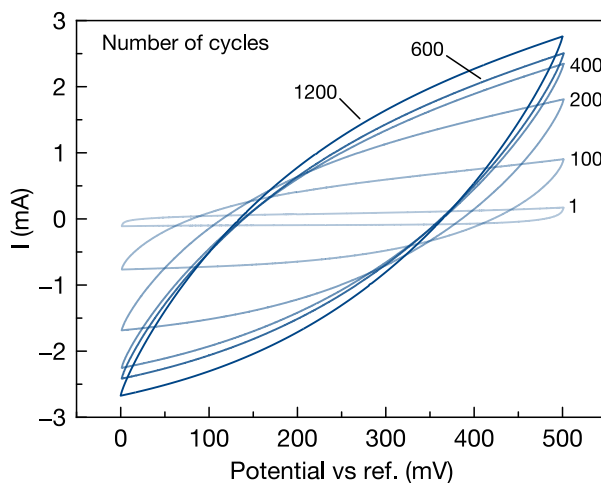


Figure 4.23 - Cyclic voltammogram of a 15G electrode at a scan rate of 20 mV/s in 0.5 M NaCl.

The initial low current indicates either very little electrical charge build-up in the activated carbon, or poor electrolyte penetration into the carbon pores. The fact that a large current is eventually achieved indicates that electrolyte penetration and double layer formation is achievable once some resistance is overcome. Note that no changes were observed in electrodes left in solution without CV testing, so this resistance must be overcome through electro-driven adsorption.

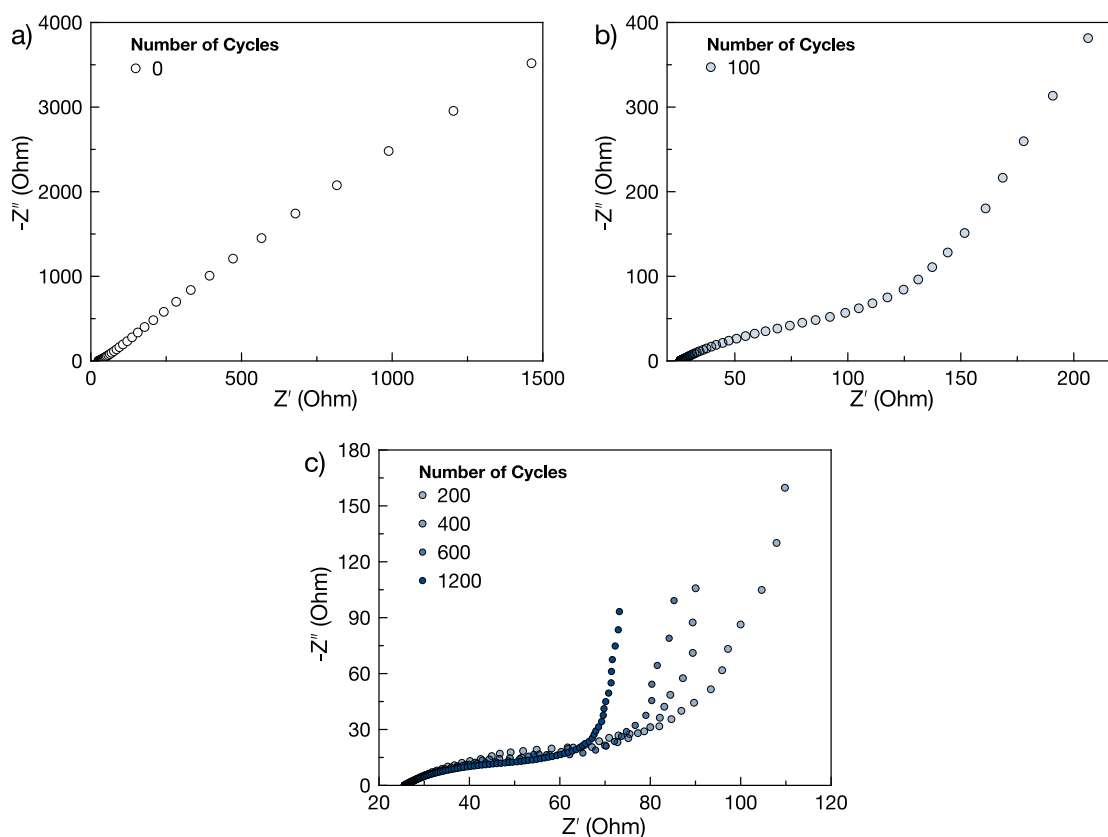


Figure 4.24 - Nyquist plot of a 15G electrode a) prior to CV, b) after 100 cycles and c) from 200-1200 cycles.

To examine the changing behaviour of the electrodes, EIS was employed, with measurements taken prior to testing, then after 100, 200, 400, 600, and 1200 cycles. The Nyquist plots can be seen in Figure 4.24. Prior to CV experiments no capacitive behaviour was observed, seen in Figure 4.24 a. After 100 cycles a low-frequency spike indicated capacitive behaviour of the electrode, seen in Figure 4.24 b. The real component of the impedance had also decreased, indicating less resistance to electrolyte penetration. As the number of cycles increased the capacitive region of the plot became more pronounced, decreasing in size as the samples yielded a greater capacitance, while the real impedance continued to decrease. This decrease in resistance over time is shown in Figure 4.25.

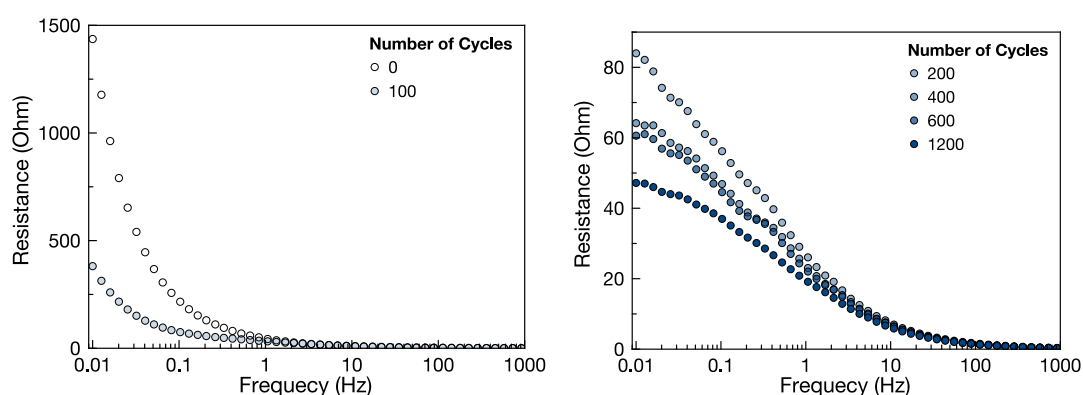


Figure 4.25 - Charging resistance of a 15G electrode.

The equivalent circuit in Figure 4.22 a) was used to quantify the increase in capacitive behaviour and reduction in real impedance, with the equivalent circuit fitting the experimental data well. The results from the fitted curves are given in Table 4.6. A noticeable decrease in both interfacial resistance (R_i) and Warburg diffusion (W) was observed as the number of cycles increased. Thus, the continual cycling is seen to improve the wettability at the surface and reduce resistance to diffusion through the pores. This resulted in a greater capacitance as evidenced by the increases in C_{DL} . As the interface resistance is a measure of the resistance between the carbon particles and the current collector, as well as between the carbon particles themselves, the slow double layer formation may be partially caused by a gradual build up of electrical charge within the carbon, caused by ineffective contact between the graphite particles and the activated carbon or the current collector.

Table 4.6 - Equivalent circuit values for a 15G electrode.

Cycles	Q_D ($F \cdot s^{(\alpha-1)}$)	α	R_i (Ω)	W ($\Omega/s^{0.5}$)	C_{DL} (F)	R_{DL} (Ω)
0	3.042×10^{-3}	0.684	995	96.92	5.075×10^{-3}	14,874
100	4.975×10^{-3}	0.648	117	23.75	5.633×10^{-2}	-
200	6.494×10^{-3}	0.611	67.7	6.385	0.1218	-
300	7.090×10^{-3}	0.604	60.1	4.881	0.1655	-
400	7.893×10^{-3}	0.587	60.1	2.817	0.1753	-
500	8.24×10^{-3}	0.585	57.9	2.432	0.1801	-
600	8.578×10^{-3}	0.578	57.5	1.872	0.1812	-
1200	9.449×10^{-3}	0.576	46.0	1.522	0.1890	-

Note: R_s was found to be approximately 25.85 Ω

The poor wettability and the extent of the slow double layer formation, which is excessively large when compared with previous examples [17], is likely a result of polar surface charges, the hydrophobic PVDF binder and the highly microporous carbon. The random pore network of microporous activated carbon means ions must diffuse through a tortuous path to the micropores. Furthermore, smaller pore openings are known to reduce the penetration depth of an AC signal during EIS testing. The extent of small pore openings due to the microporosity of the carbon may be exacerbated by PVDF restricting the size of some larger pore openings, demonstrated in Figure 4.26. This hypothesis could not be proven with SEM images, however the extent of PVDF coverage shown in Figure 4.11 and Figure 4.12 shows that there is potential for this to occur. Nonetheless, the overall improvement in capacitance and reduction in resistance indicates that the continual cycling can partially overcome the lack of penetration depth in the micropores for suitably conductive samples.

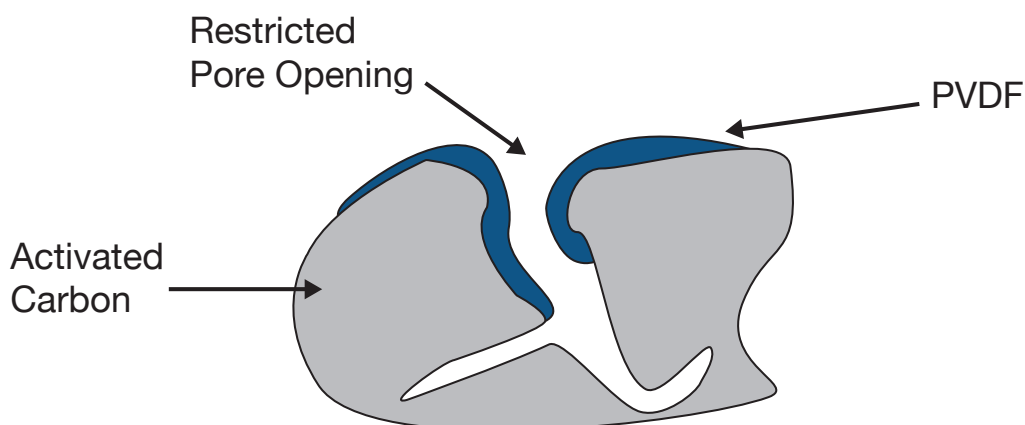


Figure 4.26 - Illustration of PVDF binder restricting a pore opening.

4.5 Conclusions

Preparation of activated carbon electrodes with graphite as a conductive filler and PVDF as a binder was achieved, with an optimal binder content found to be 10-15% to adequately hold the carbon particles together and form thin, uniform carbon layers. Contact angle measurements revealed the electrode surfaces to be highly hydrophobic and have poor wettability, with contact angles in the range of 132° - 139°.

Electrochemical testing revealed that when the graphite content was varied, vastly different electrochemical responses were recorded, highlighting the importance of the conductive filler. Below the percolation threshold of 10-15 wt.% graphite, poor conductivity was observed and both the mesoporous and microporous capacitance were severely reduced. While the capacitance of samples above the percolation threshold increased considerably, only modest micropore double layer formation was achieved, highlighting the need for appropriate conductive filler and a suitable adsorption material with a sufficiently large mesoporous surface area to minimise wasted surface area in the micropores

EIS was used to confirm the lack of micropore penetration for the 5G and 10G samples below the percolation threshold, caused by the large resistance of the samples to electrolyte diffusion. In the case of these samples, modelled EIS data using equivalent circuits was found to be a more robust measure of capacitance than the ideal behaviour assumed for capacitance measured using CV or EIS. However, when considering ideal capacitive behaviour at low frequency for the 15G sample, comparisons with the modelled data showed that both CV and EIS results could be considered accurate, even with large interfacial resistance.

Using EIS, the phenomenon of slow double layer formation observed for the 15G sample was found to be a result of poor wettability and resistance to diffusion through the pores. Continual cycling was seen to improve electrode capacitance and reduce resistance, possibly through overcoming the lack of penetration depth caused by both the microporous nature of the carbon and PVDF restricting pore openings. Thus, the capacitance of the electrodes is directly affected by its wettability, although this can be partially overcome via electrochemical charging of the electrode. To counter the resistance for all samples, modification with polymers as thin coatings or used as hydrophilic binders is suggested. This is studied in detail in chapters five and six.

The results from this study have highlighted the need for a significantly mesoporous activated carbon, as the bulk of the double layer formation occurs in the mesopores, and micropore adsorption is restricted due to double layer overlapping and poor conductivity. Practically, the results indicate that without modification, the highly microporous carbon with a high PVDF content is not an ideal material for CDI. The relatively low capacitance compared with other carbon materials increases the size of the electrodes required to remove salt ions from the feed stream. Moreover, the slow double layer formation indicates poor kinetics and a loss of efficiency, reducing the benefits of CDI based on the cost per unit volume of desalinated water when compared with other desalination techniques.

4.6 References

- [1] Wang, X. Z., Li, M. G., Chen, Y. W., Cheng, R. M., Huang, S. M., Pan, L. K., and Sun, Z., Electrosorption of ions from aqueous solutions with carbon nanotubes and nanofibers composite film electrodes, *Applied Physics Letters*, 89 (2006) 053127.
- [2] Webb, P. A. and Orr, C., Analytical Methods in Fine Particle Technology, Micromeritics Instrument Corporation, 1997.
- [3] Rouquerol, J., Llewellyn, P., and Rouquerol, F., Is the BET equation applicable to microporous adsorbents?, in P. Llewellyn, F. Rodriguez-Reinoso, J. Rouquerol, and N. Seaton (Eds.) *Studies in Surface Science and Catalysis*, Elsevier, 2007, pp. 49-56.
- [4] Lowell, S., Characterization of porous solids and powders : surface area, pore size and density, Dordrecht, London, 2004.
- [5] Bard, A. J. and Faulkner, L. R., Electrochemical Methods: Fundamentals and Applications, John Wiley, New York, 2001.
- [6] de Levie, R., On porous electrodes in electrolyte solutions: I. Capacitance effects, *Electrochimica Acta*, 8 (1963) 751-780.
- [7] Liu, X., Juan, L., Zhan, L., Tang, L., Wang, Y., Qiao, W., Liang, X., and Ling, L., Effect of conductive filler on the impedance behaviors of activated carbon based electric double layer capacitors, *Journal of Electroanalytical Chemistry*, 642 (2010) 75-81.
- [8] Landers, J., Gor, G. Y., and Neimark, A. V., Density functional theory methods for characterization of porous materials, *Colloids and Surfaces A: Physicochemical and Engineering Aspects*, 437 (2013) 3-32.
- [9] Seaton, N., Walton, J. P. R. B., and Quirke, N., A new analysis method for the determination of the pore size distribution of porous carbons from nitrogen adsorption measurements, *Carbon*, 27 (1989) 853-861.
- [10] Yang, K. L., Yiacoumi, S., and Tsouris, C., Electrosorption capacitance of nanostructured carbon aerogel obtained by cyclic voltammetry, *Journal of Electroanalytical Chemistry*, 540 (2003) 159-167.
- [11] Anderson, M. A., Cudero, A. L., and Palma, J., Capacitive deionization as an electrochemical means of saving energy and delivering clean water. Comparison to present desalination practices: Will it compete?, *Electrochimica Acta*, 55 (2010) 3845-3856.

- [12] Kim, T. and Yoon, J., Relationship between capacitance of activated carbon composite electrodes measured at a low electrolyte concentration and their desalination performance in capacitive deionization, *Journal of Electroanalytical Chemistry*, 704 (2013) 169-174.
- [13] Brunauer, S., The Adsorption of Gases and Vapors. Vol. I, Physical Adsorption, Princeton University Press, Princeton, NJ, 1943.
- [14] Ying, T. Y., Yang, K. L., Yiacoumi, S., and Tsouris, C., Electrosorption of ions from aqueous solutions by nanostructured carbon aerogel, *Journal of Colloid and Interface Science*, 250 (2002) 18-27.
- [15] Qu, D. and Shi, H., Studies of activated carbons used in double-layer capacitors, *Journal of Power Sources*, 74 (1998) 99-107.
- [16] Nightingale, E. R., Phenomenological Theory of Ion Solvation. Effective Radii of Hydrated Ions, *The Journal of Physical Chemistry*, 63 (1959) 1381-1387.
- [17] Hou, C.-H., Huang, J.-F., Lin, H.-R., and Wang, B.-Y., Preparation of activated carbon sheet electrode assisted electrosorption process, *Journal of the Taiwan Institute of Chemical Engineers*, 43 (2012) 473-479.

Chapter Five

Activated Carbon Electrodes with Poly(arylene ether sulfone) Copolymer Coatings

5.1 Overview

In this chapter the effects of cation exchange polymer coatings on activated carbon electrodes for CDI were investigated, with the goal of investigating their effect on electrode resistance and capacitance, and improving the kinetics of activated carbon electrodes. Electrodes were fabricated from activated carbon, graphite and PVDF, then coated with sulfonated poly(arylene ether sulfone) random copolymers. As described in chapter 3, the poly(arylene ether sulfone) copolymers are characterised by high conductivity and good mechanical stability. Similar ion-exchange copolymers have been developed for pressure-driven desalination membranes and for fuel cell applications [1-8], but few studies have focused on their application for CDI [9].

The coating layers were found to create additional resistance, however compared with uncoated electrodes the coatings did not significantly affect the rate of charge build up. EIS results indicated that both capacitance and charging resistance were influenced by polymer conductivity, water uptake and the thickness of the coating layer. Energy-dispersive X-ray spectroscopy (EDX) results also indicated that in addition to functioning as a superficial charge barrier, copolymer that penetrates into the carbon substrate might offset the loss in capacitance caused by PVDF binder pore blockage. The results indicated that these random copolymers can be used to improve ion transport into the pores of the electrodes and are applicable as membranes or coatings in MCDI applications, with RCP 1 found to significantly enhance activated carbon electrode electrosorption performance.

5.2 Experimental

5.2.1 Materials

The materials used for this chapter are the same as those described in chapters three and four.

5.2.2 Electrode Preparation

Carbon electrodes were prepared using the method described in chapter four. Briefly, using NMP as a solvent, a slurry consisting of activated charcoal, graphite powder as conductive material and PVDF as a binder was prepared, such that the final (dry) content of the electrode was 75 wt.% activated charcoal, 15 wt.% graphite and 10 wt.% PVDF. The slurry was coated onto graphite sheets to a thickness of 350

μm using a doctor blade and dried in a vacuum oven for 24 h at 120 °C to completely remove the solvent.

Three random copolymers were synthesised using the silyl-method as per the procedure previously described in chapter three. The ratio of the monomers in the random copolymers was varied such that the monomer ratio of hydrophilic diphenylhydroquinone to hydrophobic dihydroxydiphenyl sulfone was 6:4 for RCP 1, 5:5 for RCP 2 and 4:6 for RCP 3. All polymers were sulfonated using concentrated sulfuric acid (min. 96%). The molecular structure of the random copolymers can be seen in Figure 5.1, and the properties measured in chapter three are reproduced in Table 5.1.

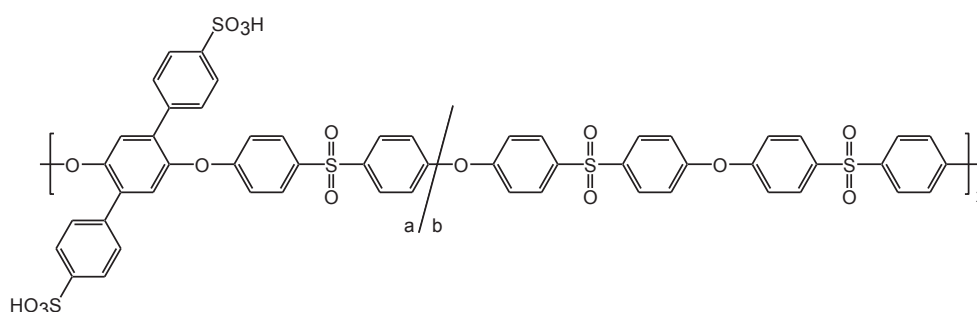


Figure 5.1 - Repeating unit of the random copolymer. RCP 1: a = 6, b = 4; RCP 2: a = 5, b = 5; RCP 3: a = 4, b = 6.

Table 5.1 – Random copolymer properties.

Polymer coating	IEC (mmol/g)	Water uptake* (%)	Conductivity** (mS/cm)	Contact Angle (°)	Transport number
RCP 1	2.05	49.9	15.13	51.8	.94
RCP 2	1.73	35.7	8.36	52.1	.99
RCP 3	1.44	26.4	3.79	62.3	.98

*Measured in the Na⁺ form

**In-plane conductivity

Polymer coated electrodes were prepared by first dissolving the sulfonated polymers in NMP such that the concentration of the solution was 15 wt.%. The polymer solutions were degassed for two hours then added dropwise to each electrode until complete coverage was achieved, with an approximate surface coverage of 0.16 mL/cm². The coated electrodes were then dried under vacuum for 2 h at 60°C, before a further 24 h at 80 °C. Once dried, the samples were rinsed with distilled water to removed any residual NMP, soaked in 0.5M NaCl to convert the cation exchange polymer to the Na⁺ form, then rinsed again

with distilled water to remove excess NaCl from the polymer matrix. The coated electrodes were stored in deionised water at room temperature before use.

5.2.3 Electrode Characterisation

5.2.3.1 Physical Electrode Characterisation

SEM images were obtained using a Nova NanoSEM 450 with an acceleration voltage of 5 kV using the secondary imaging mode. Prior to imaging, all samples were coated with iridium. EDX was obtained using the same instrument, with the samples coated with carbon prior to imaging. Cross sections were prepared by fracturing the samples after freezing in liquid nitrogen. ATR-FTIR was performed using a PerkinElmer Spectra 100 to confirm the chemical structure of the cation exchange polymer coatings.

5.2.3.2 Electrochemical Characterisation

CV and EIS experiments were performed using a Biologic VSP potentiostat connected to a three-electrode cell, as described in chapter four. The working electrode was the carbon material to be tested with an exposed surface area of 0.785 cm², the reference electrode was a saturated KCl Ag/AgCl electrode inserted into a bridge tube with the working electrolyte used as the filling solution, and the counter electrode was a mesh platinum electrode. As described in chapter four, the specific capacitance of the activated carbon, C (F/g activated carbon), was calculated using the following equation [10]:

$$C = \frac{i}{mv} \quad \text{Equation 5.1}$$

where i is the current (A), m is the mass of carbon (g) and v is the scan rate (V/s). EIS was performed using the same three-electrode cell over the frequency range 1 MHz to 10 mHz, with an applied voltage amplitude of 10 mV. Assuming ideal capacitor behaviour the capacitance of the electrode was derived from the imaginary part of the impedance spectrum based on the formula [11]:

$$C = \left| \frac{1}{\omega Z''} \right| \quad \text{Equation 5.2}$$

where ω is the frequency and Z'' is the imaginary impedance.

5.3 Results and Discussion

5.3.1 Electrode Morphology

5.3.1.1 Polymer Coatings

SEM images of both uncoated electrodes and electrodes coated with polymer using a doctor blade are shown in Figure 5.2. There is little difference seen between the uncoated sample (Figure 5.2 a & b) and the sample coated with a 10 wt.% polymer at a thickness of 200 μm (Figure 5.2 c & d). However, with a 15 wt.% polymer solution cast at a thickness of 300 μm (Figure 5.2 e & f), a more distinct polymer layer that adhered to the carbon was observed. In both instances, the solution was not able to form a continuous coating layer, rather seeping into the voids of the carbon substrate. Thus, in spite of the copolymer penetration into the electrodes consistent coverage across each electrode could not be achieved with a doctor blade. This is seen in Figure 5.2 f, which shows the surface of the electrode coated with the 15 wt.% polymer solution and the transition between a region of dense coating and the thin coating observed in the cross-section of Figure 5.2 e.

Figure 5.3 shows an SEM image of an electrode coated using a dropwise method. The polymer coating in Figure 5.3 a is clearly distinct from the carbon substrate, while Figure 5.3 b shows complete coverage of the substrate with no carbon visible. Due to the more consistent coverage of the dropwise method, this was selected as the most appropriate method to prepare samples. Note that all subsequent samples in this thesis describe samples prepared with the dropwise method.

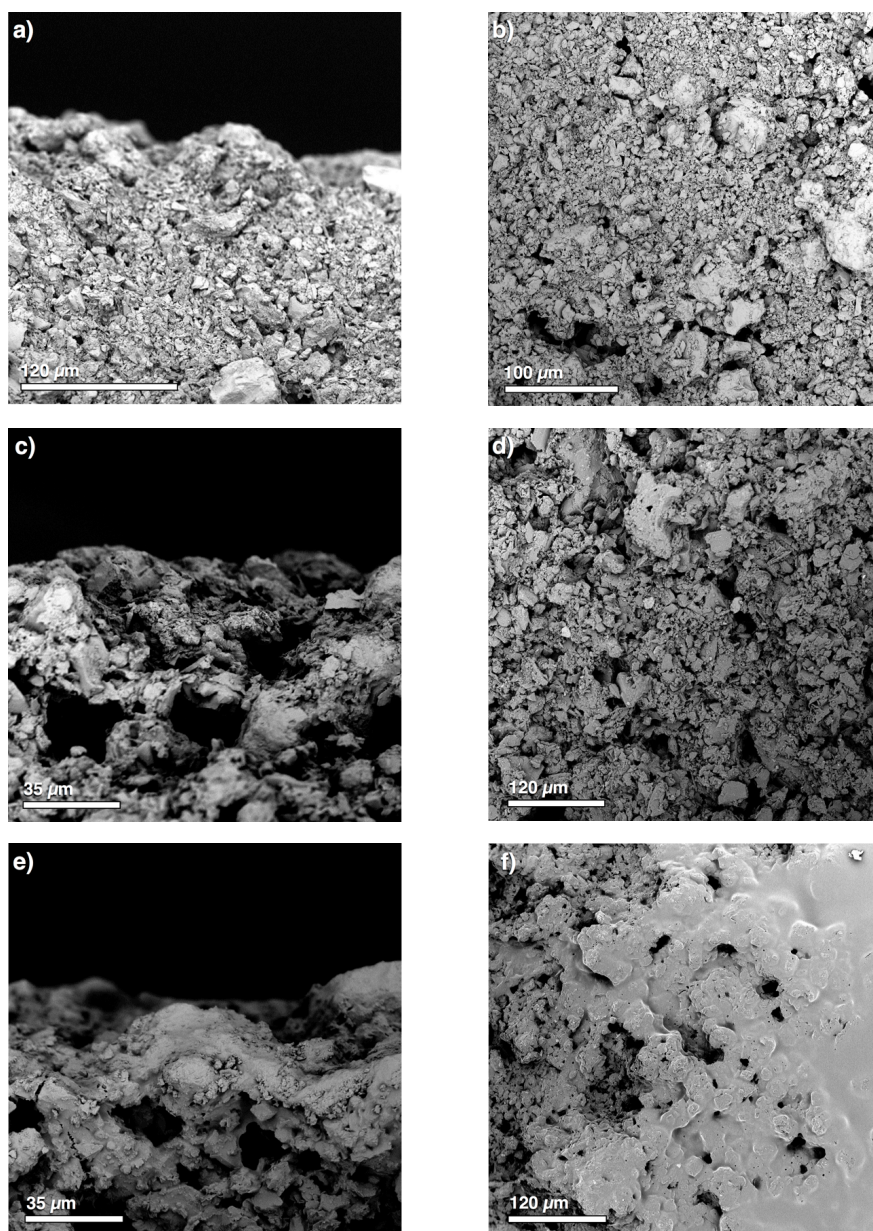


Figure 5.2 - Cross-section and surface SEM images of a) & b) uncoated carbon electrodes, c) & d) coated electrodes cast at 200 μm and e) & f) coated electrodes cast at 300 μm .

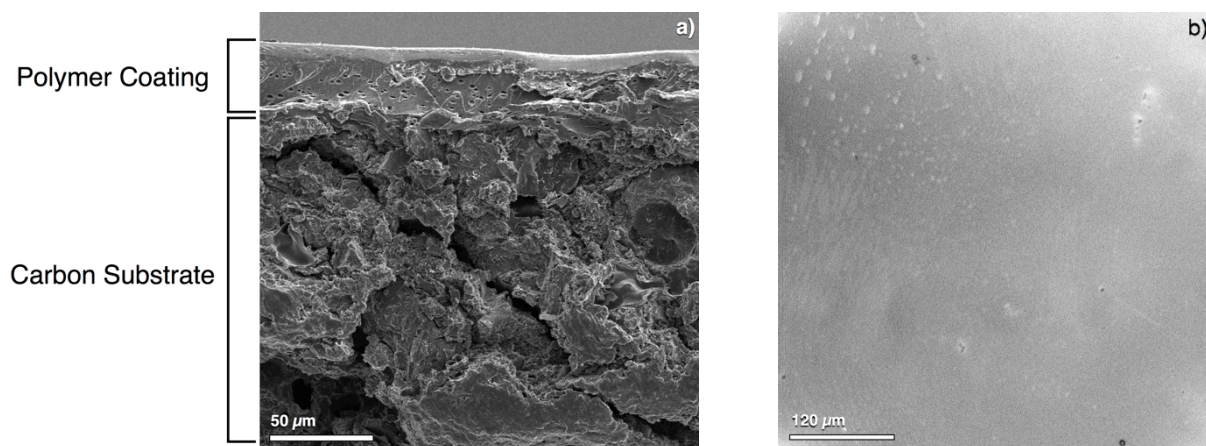


Figure 5.3 - a) Cross section and b) surface SEM images of a carbon electrode coated with 15 wt.% random copolymer solution, cast using a dropwise method.

5.3.1.2 Hydro and Thermal Stability

All coated electrodes were tested for hydro- and thermal stability by placing them in water at 80 °C for 6 h. No degradation was observed, and all polymers adhered strongly to the carbon such that they were not removed after hydrothermal treatment. Furthermore, all electrodes were stored in water at room temperature before use, with no loss of carbon or polymer observed. Due to the adhesion of the coating layer to the carbon electrode, the polymer acts as a pseudo-binder providing additional binding strength for the carbon particles.

5.3.1.3 FTIR Analysis

Due to the similarities of the copolymer spectra observed in chapter three, FTIR is not a useful tool when attempting to distinguish between unknown samples of the random copolymers in this study. Nonetheless, for the scope of this thesis, i.e., polymeric coatings on carbon substrates, FTIR can be used as a quick and effective technique to confirm a successful electrode coating.

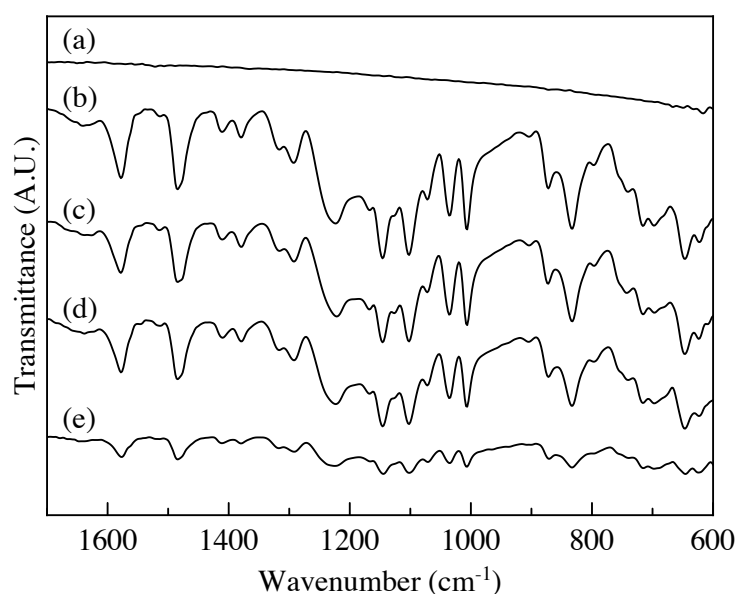


Figure 5.4 - ATR-FTIR spectra of (a) an uncoated carbon electrode, (b) a stand-alone membrane, (c) an RCP 1 coated electrode, (d) an RCP 2 coated electrode and (e) an RCP 3 coated electrode.

Figure 5.4 shows a comparison of the FTIR spectra of uncoated electrodes (a), coated electrodes (c-e) and a flat sheet membrane cast from RCP 1 (b). Only the signal from one membrane is shown due to the identical spectra yielded from the membranes, arising from the use of the same precursor monomers as discussed in chapter three. The uncoated spectrum was found to have no characteristic peaks, largely due to poor contact between the rough carbon surface and the ATR crystal. The spectra of the coated

electrodes for all three random copolymers were seen to match the spectrum of the flat sheet membrane, confirming the successful application of the polymers onto the carbon substrates. The difference in signal strength for sample e) is thought to be due to poor contact between the sample and the ATR-FTIR crystal, however importantly all characteristic peaks were still observed.

5.3.2 Cyclic Voltammetry

5.3.2.1 Uncoated Electrodes

The capacitance of uncoated electrodes as a function of potential measured at scan rates of 5 mV/s and 20 mV/s can be seen in Figure 5.5. At both the fast and slow scan rates, a rectangular shape is observed, indicating the formation of an EDL at the carbon-solution interface and the successful adsorption/desorption of ions. The shape of the curve at 20 mV/s is similar to those recorded at 5 mV/s in chapter four, but with a greater capacitance than those results (the difference is attributed to the lower PVDF content of 10 wt.%, which blocks fewer pores compared with electrodes consisting of 15 wt.% PVDF). The relatively constant capacitance at 20 mV/s as the potential increases or decreases indicates full mesopore adsorption. At a scan rate of 5 mV/s, relatively constant capacitance was observed between 0 and 600 mV (both scan directions), although no local minimum or PZC could be seen.

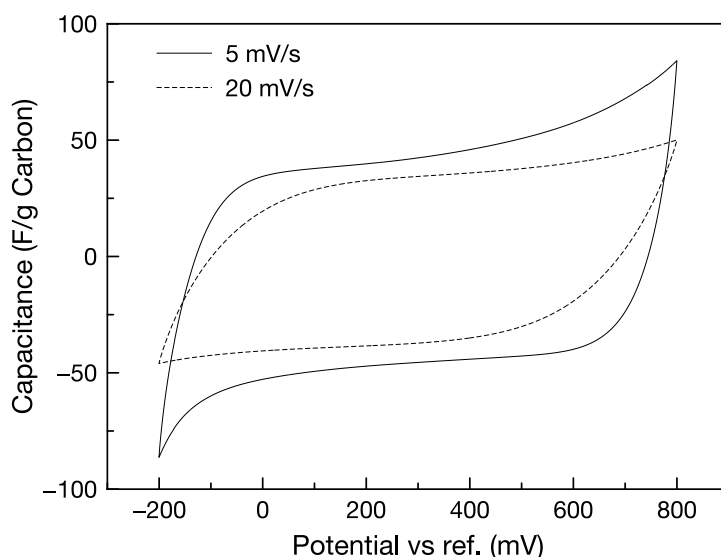


Figure 5.5 - Specific capacitance of uncoated electrodes measured in 0.5 M NaCl at scan rates of 5 mV/s (solid line) and 20 mV/s (dotted line).

Assuming that at 20 mV/s the scan rate is too fast to allow micropore adsorption, the mesopore capacitance was calculated at this scan rate for a number of potentials in both scan directions, with the

results presented in Table 5.2. The micropore capacitance shown is the difference in capacitance between the 5 mV/s and 20 mV/s scan rates.

Table 5.2 - Mesoporous and microporous capacitance of uncoated electrodes based on CV at scan rates of 20 and 5 mV/s.

Applied Potential	Specific Capacitance (F/g carbon)		Capacitance ($\mu\text{F}/\text{cm}^2$ carbon)	
	Mesopores	Micropores	Mesopores	Micropores
Forward Scan				
200 mV	32.57	7.25	40.09	0.93
400 mV	35.89	10.03	44.16	1.29
600 mV	40.33	17.13	49.63	2.20
800 mV	50.08	34.05	61.63	4.38
Reverse Scan				
400 mV	35.02	9.13	43.10	1.17
200 mV	38.43	8.71	47.29	1.12
0 mV	40.58	12.23	49.93	1.57
-200 mV	46.01	40.24	56.62	5.18

The most stable mesopore capacitance was observed between the applied potentials of 200 - 600 mV (forward scan) and 400 - 0 mV (reverse scan), where the capacitance does not vary by more than $10 \mu\text{F}/\text{cm}^2$. The values are slightly larger than those of the 15G samples measured in chapter four of $42.41 \mu\text{F}/\text{cm}^2$ at the PZC. Similar to the results in chapter four, it is likely that the mesopore capacitance has been overestimated, a combination of an underestimated mesopore surface area of $81.3 \text{ m}^2/\text{g}$ and appreciable micropore penetration occurring at a scan rate of 20 mV/s. The relatively large increase in the assumed mesopore capacitance at the end of each scan (at applied potentials of 800 mV and -200 mV) suggests that micropore penetration is indeed occurring at 20 mV/s, as the mesopore capacitance was expected to remain relatively constant. Considering this, the actual micropore capacitance could be almost double that shown in Table 5.2.

5.3.2.2 Coated Electrodes

Cyclic voltammograms of electrodes coated with three random copolymers at scan rates of 5 mV/s and 20 mV/s are presented in Figure 5.6. At 20 mV/s, electrodes coated with RCP 1 (Figure 5.6 a) were seen to have a greater calculated capacitance for both the forward and reverse scans over a wider potential range. At this scan rate, electrodes coated with RCP 2 and RCP 3 (Figure 5.6 c & e) were seen to

generally have poorer responses for most of the potential window. At a slower scan rate of 5 mV/s, for both the forward and reverse scans (Figure 5.6 b, d and f), the build-up of charge on all coated samples was seen to be better than the uncoated samples over a wider range of potentials, as the electrolyte has greater time to penetrate the pores of the electrode.

Assuming that the changes in capacitance at 5 mV/s between the coated and uncoated electrodes are due to micropore adsorption only (as the mesopores have fully formed double layers), the micropore capacitance of the coated electrodes was calculated as the difference between the coated electrodes and the mesopore capacitance of the uncoated electrodes (calculated at 20 mV/s). These changes in micropore capacitance are shown in Table 5.3. At the end of each scan (800 and -200 mV) it can be seen that there is a drop off in the capacitance compared with the uncoated electrodes. This suggests that for fully charged electrodes, capacitance in the coated electrodes is not achievable, although no plausible reason for this can currently be determined.

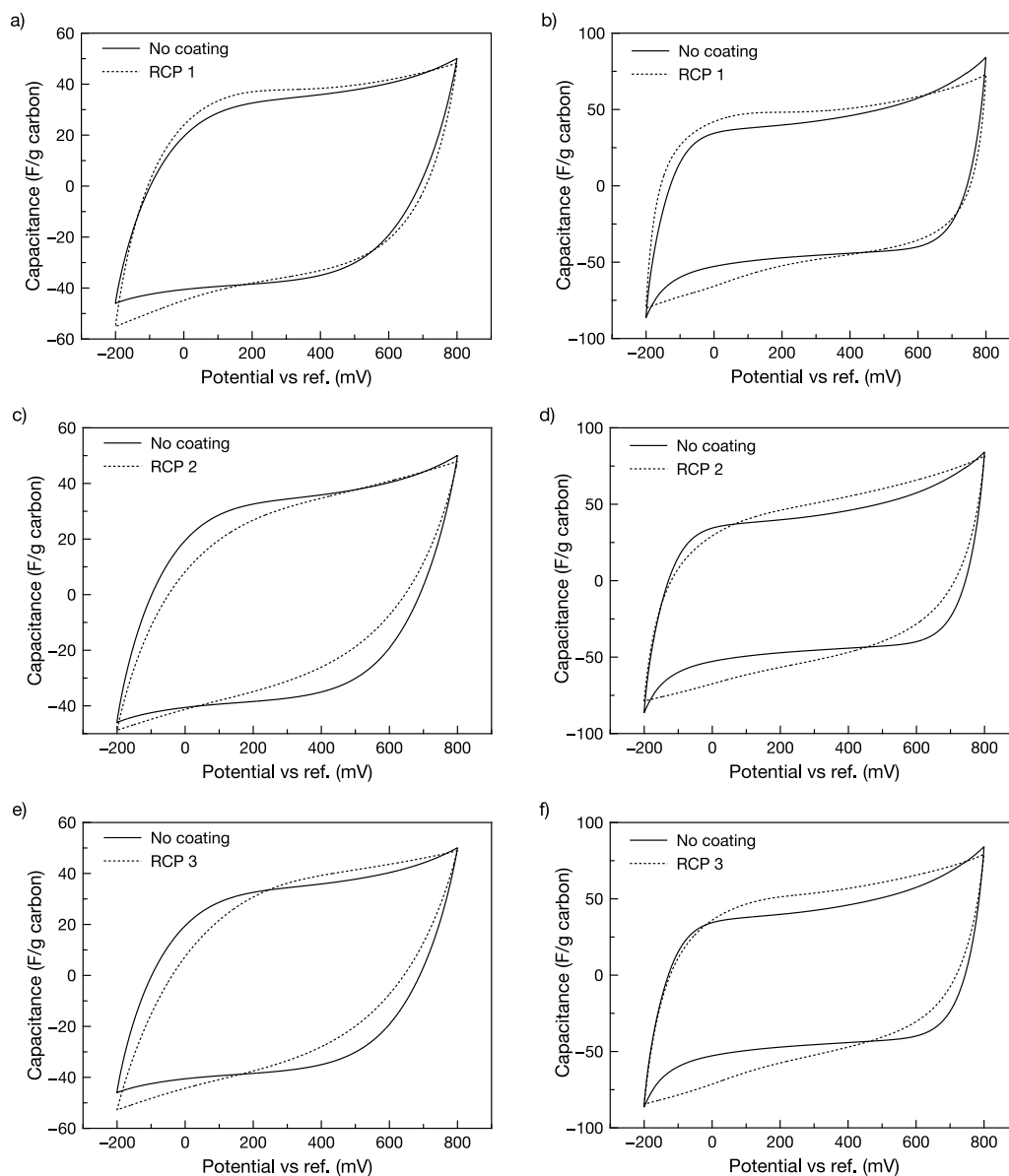


Figure 5.6 - Specific capacitance of coated electrodes measured in 0.5 M NaCl: a) RCP 1 coating, scan rate = 20 mV/s; b) RCP 1 coating, scan rate = 5 mV/s; c) RCP 2 coating, scan rate = 20 mV/s; d) RCP 2 coating, scan rate = 5 mV/s; e) RCP 3 coating, scan rate = 20 mV/s; f) RCP 3 coating, scan rate = 5 mV/s.

At 5 mV/s the capacitance of the coated samples is greater across a wider potential window. Regardless of scan direction, after an initial potential increase or decrease of 400 mV, a greater capacitance was observed for all coated electrodes, almost until the scan direction changes. This greater micropore capacitance over a wider potential range, and a continuous build up of charge and micropore filling rather than a plateau in capacitance is attributed to two factors:

1. The cation exchange coatings improved both the transport of cations towards the electrodes during the reverse scan as the electrode becomes more negatively charged, as well as the expulsion of cations during the forward scan as the electrode becomes more positively charged.

2. The polymer matrix of the coating layer provided a location for electrolyte to build up directly adjacent to the carbon surface. As capacitance is known to increase with electrolyte concentration, this additional electrolyte storage may have contributed to the improved performance.

Table 5.3 - Micropore capacitance of coated and uncoated electrodes at various applied potentials for both forward and reverse scans.

Applied Potential	Micropore Capacitance ($\mu\text{F}/\text{cm}^2$ carbon)			
	Uncoated	RCP 1	RCP 2	RCP 3
Forward Scan				
200 mV	0.93	2.01	1.74	2.40
400 mV	1.29	1.91	2.48	2.69
600 mV	2.20	2.33	3.28	3.24
800 mV	4.38	2.96	4.06	3.75
Reverse Scan				
400 mV	1.17	1.29	1.53	1.56
200 mV	1.12	1.80	2.35	2.46
0 mV	1.57	3.24	3.46	3.96
-200 mV	5.18	4.39	4.22	4.96

No strong correlation was observed between the changes in micropore capacitance and the key polymer properties (IEC, water uptake, conductivity and transport number). In particular, the most hydrophobic and least conductive polymer (RCP 3) was expected to yield the smallest increase in specific capacitance by hindering electrolyte access to the pores more so than the other polymers. To the contrary, for the reverse scan it was observed to yield the greatest increase at all applied potentials. It is the combined effects of the polymer properties that make it difficult to find a strong correlation; for instance, the lower transport number of RCP 1 reduces the polymer's ability to selectively transport cations to and from the electrode, while its greater water uptake increases concentration directly adjacent to the carbon promoting greater capacitance.

In addition to overall capacitance, the rate of charge build up can be examined. The greatest rate of change for the uncoated electrodes was seen to occur during the first 200 mV for both the forward and reverse scans. The average rate of change of capacitance in this region for both the uncoated and coated electrodes was calculated at both scan rates, and the results are presented in Table 5.4 (note that

this table presents units of F/g.s, which is equivalent to the change in current with changing potential. This therefore describes the current per volt, or electrical conductance). At both scan rates the transient responses of the coated electrodes are generally slower during the reverse scan than the forward scan. This is a result of the resistance to the expulsion of anions from the pores caused by the cation exchange polymer, causing additional hindrance to the desorption process.

Table 5.4 - Transient responses of coated and uncoated electrodes at scan rates of 20 mV/s and 5 mV/s, calculated for the first 200 mV of each scan direction.

Sample	Forward Scan		Reverse Scan	
	20 mV/s (F/g.s)	5 mV/s (F/g.s)	20 mV/s (F/g.s)	5 mV/s (F/g.s)
RCP 1	7.90	3.05	6.91	2.72
RCP 2	5.70	2.70	5.53	2.75
RCP 3	6.01	3.01	5.63	2.74
No Coating	6.55	3.02	6.93	3.10

Considering the start of the forward scan (during which cations are expelled from the carbon pores as the electrode becomes positively charged), the response of electrodes coated with RCP 2 and RCP 3 at both scan rates was slower than the uncoated samples. Due to the increased resistance provided by the coating layer, this effect is more pronounced at 20 mV/s when there is less time for the ions to diffuse through the polymer matrix. Although at 5 mV/s the rate of charge build up is in fact slower, the ions have more time to diffuse through the polymer and into the pores of the activated carbon, thus reducing the effect of the additional coating resistance.

The response of electrodes coated with RCP 1 to a change in scan direction was seen to be faster when compared with electrodes coated with polymers RCP 2 and RCP 3. This is attributed to the greater water uptake and conductivity of RCP 1 compared with the other copolymers. Surprisingly, in spite of the additional resistance caused by the coating layer (see section 5.3.3.2), this response is also faster than that of the uncoated sample. This result may have been caused by the penetration of the RCP 1 copolymer into the carbon substrate, which could reduce resistance to adsorption due to its hydrophilic properties.

Elemental mapping via EDX was employed to investigate the actual penetration of copolymer into the carbon substrate. The SEM image in Figure 5.7 a shows a clear separation of the carbon substrate and

an RCP 1 polymer coating, where the polymer acts similarly to a dense phase membrane that increases resistance to electrolyte penetration during adsorption (see also Figure 5.3 a). EDX imaging shows the location of sulfur atoms (Figure 5.7 b) as well as that of carbon, sulfur and oxygen atoms (Figure 5.7 c). A high concentration of sulfur atoms was expected to be observed in the polymer coating, a direct result of the sulfonic acid groups in the polymer. However the presence of sulfur atoms is also indicated throughout the carbon layer, even through to the underside of the electrode, albeit in a lower concentration. The presence of sulfur atoms in the carbon substrate suggests that the polymer has indeed penetrated into the voids.

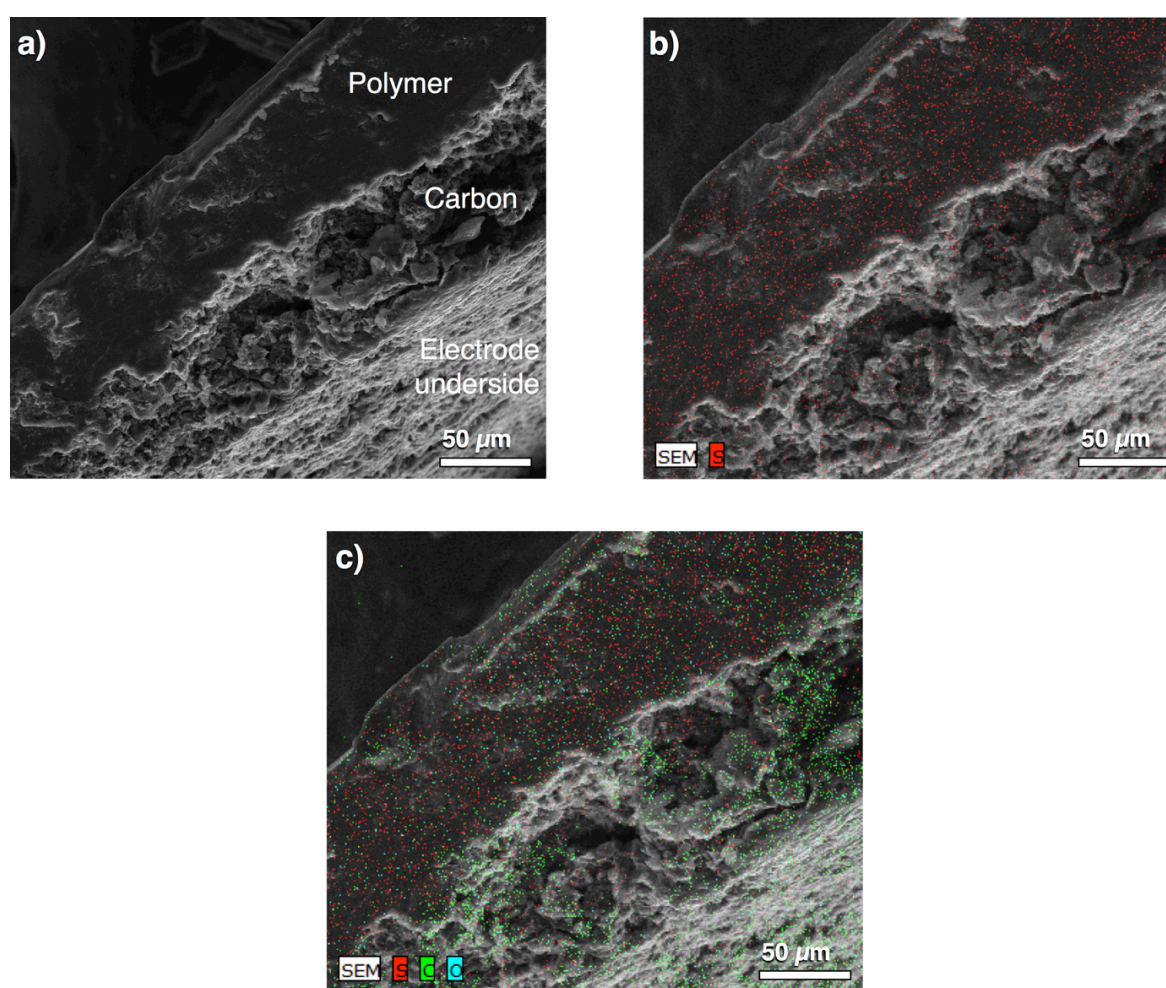


Figure 5.7 - EDX images of a carbon electrode coated with RCP 1: a) SEM image, b) EDX showing sulfur atoms and c) EDX showing sulfur, carbon and oxygen atoms.

For the uncoated sample, the PVDF binder in the carbon substrate behaves like a partial, hydrophobic membrane layer that blocks pores and creates hindrance to the adsorption/desorption process. In contrast, penetration of the RCP 1 copolymer into the voids of the carbon substrate may reduce this hindrance by providing better access to the pores due to its hydrophilic properties. Based on elemental

mapping and the solubility of PVDF in NMP (which is used as a solvent for both the polymer coatings and the carbon substrate), it is hypothesised that in addition to simply filling voids in the substrate, the PVDF has been partially dissolved and re-cast during the polymer coating process. This process would effectively re-cast some of the carbon substrate with both PVDF and random copolymer as a binder, thereby reducing the influence of the hydrophobic PVDF binder. Although this penetration occurred for all samples, the effect is more pronounced with the most hydrophilic polymer (RCP 1) and is enough to create a faster CV response than the uncoated electrodes.

5.3.3 Electrochemical Impedance Spectroscopy

EIS was used to further examine the performance of the electrodes and to measure the charging resistance. Specifically, the specific capacitance, polymer resistance and conductivity, and diffusive resistance were measured.

5.3.3.1 Capacitance from Electrochemical Impedance Spectroscopy

The capacitance (calculated using Equation 5.2) versus frequency is plotted Figure 5.8. The capacitance of the coated samples is seen to increase with polymer IEC. The increased capacitance as a function of IEC is likely a result of greater water uptake, which reduces resistance to ion transport through the swollen hydrophilic channels of the polymer, encouraging greater pore access for the electrolyte. This result confirms the influence of the region of concentrated electrolyte storage in the polymer layer directly adjacent to the carbon layer, as discussed in section 5.3.2.2. Note that the influence of the coating layer resistance, where the resistance (area resistance, measured in $\Omega\cdot\text{cm}^2$) of the layers was found to be $\text{RCP } 2 < \text{RCP } 1 < \text{RCP } 3$, seems to be less significant than the water uptake (the measurement of coating resistance and its influence on the adsorption/desorption process is discussed in section 5.3.3.2).

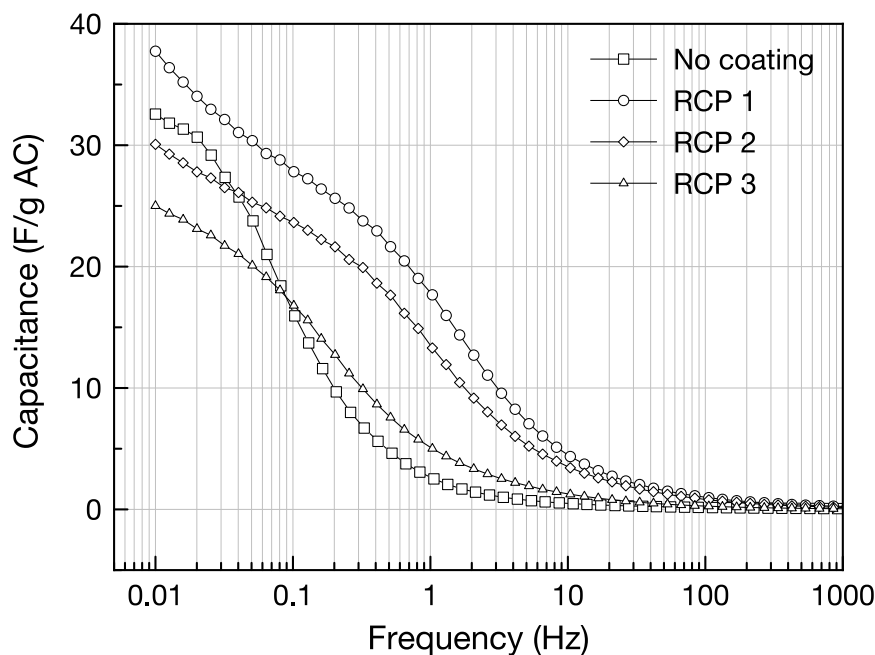


Figure 5.8 - Capacitance versus frequency for uncoated and coated electrodes.

The capacitance of the coated electrodes in Figure 5.8 is seen to increase at higher frequencies compared to the uncoated electrodes. There is a correlation between this increase and the wettability of the electrode coating (measured by the contact angle in chapter three and shown in Table 5.5), with the capacitance of the more wettable samples rising at higher frequencies. As discussed in chapter four, the penetration depth of the ac signal increases with decreasing frequency, but greater solution resistance hinders this depth. The coatings improve the penetration depth of the sinusoidal signal in the pores by improving wettability and by creating a higher electrolyte concentration at the electrode/polymer/solution interface. This result also sheds further light on the faster transient responses of electrodes coated with RCP 1. Note that the increase in capacitance at low frequencies for the coated samples does not reduce at the same rate as the uncoated samples, suggesting that the capacitance may plateau at frequencies lower than 10 mHz.

Table 5.5 - Contact angle of polymer coatings and uncoated electrodes at $t = 0$ s and $t = 54$ s, as well as electrode capacitance calculated at 10 mHz.

Sample	Contact Angle (°)		Capacitance (F/g)
	$t = 0$	$t = 54$	
RCP 1	51.8	30.3	37.7
RCP 2	52.1	38.2	30.1
RCP 3	62.3	46.1	25.0
Uncoated electrode	135.31	-	32.6

The final capacitance of the electrodes measured at 10 mHz is presented in Table 5.5. Note that these values are similar to the mesopore capacitance values for the 15G sample measured from CV experiments in chapter four - thus, these values largely consider mesopore adsorption. Despite the disparity between these results and the capacitance measured from CV, the values are consistently lower, and there is a clear trend between the capacitance and the polymer properties of IEC, water uptake and conductivity. Although the surface area of the activated carbon cannot be increased by the addition of a polymer coating (and hence sorption capacity cannot increase unless the electrolyte concentration increases), the increase of this apparent capacitance of RCP 1 confirms that the polymer facilitates better access to the carbon pores and may even provide access to pores otherwise blocked by PVDF binder. Conversely, the greater resistance and lower water uptake of polymers RCP 2 and RCP 3 appeared to hinder the adsorption/desorption process.

5.3.3.2 Polymer Resistance and Conductivity

The resistance and conductivity of the coating layers were calculated based on the real impedance at the high-frequency intercept of the Nyquist plot. Although ohmic resistance values were unattainable for the uncoated electrodes in chapter four, this was due to inconsistencies between a range of samples and blank samples. However, the resistance of the coatings was easily measured by directly comparing the resistance of each sample with and without a polymer coating. The values from typical samples are shown in Table 5.6. The area resistances presented are not normalised to account for the variable thickness of the coatings, and as such the resistances do not decrease with increasing IEC. Importantly, the resistances of the RCP 1 and RCP 2 coatings are comparable to Neosepta CMX, which has a resistance of $3.0 \Omega \cdot \text{cm}^2$ and is commonly used for MCDI testing [12].

Table 5.6 - Electrochemical properties of the coating layers.

Coating	IEC (mmol/g)	Thickness (μm)	Resistance ($\Omega\cdot\text{cm}^2$)	Conductivity (mS/cm)
RCP 1	2.05	82	3.31	2.48
RCP 2	1.73	46	2.37	1.94
RCP 3	1.44	59	9.86	0.60

As expected, the conductivity of the coatings is seen to increase with IEC. These values differ to those reported in chapter three (and presented again in Table 5.1) due to the methods of testing. Here coating conductivity is measured normal to its exposed surface (through-plane conductivity) while immersed in 0.5M NaCl, while membrane conductivity in chapter three was measured parallel to the surface (in-plane conductivity) using a four-point probe with the electrodes in direct contact with the membrane. It was expected that the influence of the 0.5 M NaCl would increase the conductivity compared to the humidity chamber with relative humidity of 99% due to the ability of the sodium and chloride ions to carry current. The loss of conductivity therefore highlights the disparity between the two methods of measurement, recalling that as discussed in chapter three, conductivity measurements have often been found to be greater in the in-plane direction than the through-plane direction. Nonetheless, crucially the same trend for both measurements was observed, i.e., the conductivity increases with polymer IEC. This confirms that while changing the direction of measurement affects conductivity, it does so consistently and either method of measurement can be deemed as useful when determining the relative conductivity of polymers tested under the same conditions.

5.3.3.3 Charging Resistance

Electrode charging (or diffusive) resistance versus frequency is shown in Figure 5.9. This is the resistance to ion transport through the polymer coating and into the carbon pores, and is calculated as the real impedance minus the ohmic resistance at each frequency. For the coated samples, it was observed that the greater the coating area resistance, the higher frequency at which the increase in charging resistance occurs. Although RCP 1 coated samples had a greater area resistance than RCP 2 coated samples, the charging resistances were found to be similar. This result further suggests that the higher conductivity and greater water uptake of RCP 1 reduces hindrance to ion transport.

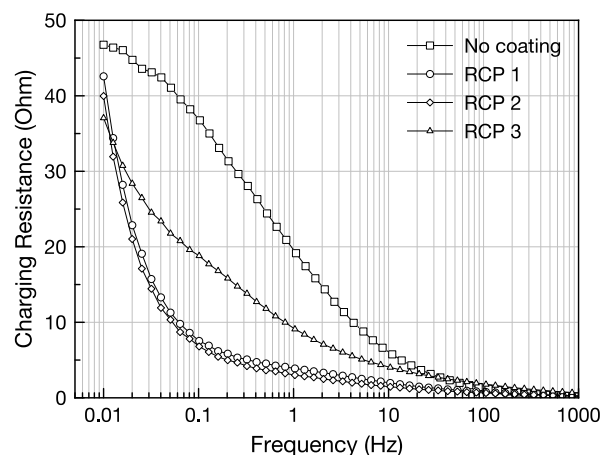


Figure 5.9 - Charging resistance versus frequency for uncoated and coated electrodes.

For uncoated samples, the rise in charging resistance occurred at much higher frequencies than the coated samples. However, as the frequency approaches 10 mHz, the resistance reaches a plateau as the sample yields more typical capacitive behaviour. Conversely, the real impedance of the coated samples was observed to increase sharply at low frequencies. Here, the impedance response is dominated by the resistance of the coating rather than the capacitive behaviour of the carbon substrate. In light of this, while coating area resistances are comparable to those of commercial membranes, the polymer layer thickness must be optimised to minimise this charging resistance while still adequately enhancing electrosorption performance.

5.4 Conclusions

In this chapter, activated carbon electrodes coated with cation exchange random copolymers were successfully fabricated, with the coating layer strongly adhering to the carbon. Confirmation of successful coating was observed through SEM images and FTIR analysis. CV revealed that at a scan rate of 5 mV/s, a greater micropore capacitance was observed for all coated electrodes over a wide range of potentials. This was attributed to the selective transport properties of the cation exchange polymers, and the increased electrolyte concentration in the polymer coating directly adjacent to the carbon electrodes.

CV results have shown that in the case of the most conductive coating (RCP 1), charge was seen to build up at a faster rate than uncoated samples, despite the additional resistance of the coating. A high PVDF binder content may increase charging resistance, slowing the build up of ions at the electrode-solution interface. However, the coating of electrodes with an ion exchange polymer may partially offset this

phenomenon through copolymer penetration into the carbon substrate, despite adding additional resistance as a charge barrier layer. These results indicated that the random copolymer coatings, although increasing overall resistance, can be used to improve the ion transport into the pores of the electrodes, and are applicable as membranes or coatings in MCDI applications. However, the polymer coatings are seen to influence the resistance of the carbon electrodes, causing a sharp rise in charging resistance at low frequencies during EIS testing. The optimisation of coating thickness therefore becomes important in reducing the additional resistance created by the coating layer.

EIS results indicate that the charging resistance and capacitance of the coated electrodes are influenced by both conductivity and water uptake. Since the conductivity and water uptake are strong functions of IEC, suitable polymer design to maximise IEC while retaining mechanical stability is a crucial parameter in enhancing the performance of activated carbon electrodes. In light of this, RCP 1 is seen to appreciably enhance the electrosorption performance of the activated carbon electrodes. Overall, based on the CV and EIS results it can be concluded that polymers with a high IEC are important in reducing resistance to the adsorption/desorption process and improving the kinetics of electrodes for CDI.

5.5 Publications

The following publication is based on the results from this chapter (see Appendix A5):

Journal Article

Asquith, B.M., Meier-Haack, J. and Ladewig, B.P., Cation exchange copolymer enhanced electrosorption, *Desalination*, 345 (2014) 94-100.

5.6 References

- [1] Park, H. B., Freeman, B. D., Zhang, Z. B., Sankir, M., and McGrath, J. E., Highly chlorine-tolerant polymers for desalination, *Angew Chem Int Ed Engl*, 47 (2008) 6019-6024.
- [2] Paul, M., Park, H. B., Freeman, B. D., Roy, A., McGrath, J. E., and Riffle, J. S., Synthesis and crosslinking of partially disulfonated poly(arylene ether sulfone) random copolymers as candidates for chlorine resistant reverse osmosis membranes, *Polymer*, 49 (2008) 2243-2252.
- [3] Xie, W., Park, H. B., Cook, J., Lee, C. H., Byun, G., Freeman, B. D., and McGrath, J. E., Advances in membrane materials: desalination membranes based on directly copolymerized disulfonated poly(arylene ether sulfone) random copolymers, *Water Science and Technology*, 61 (2010) 619-624.
- [4] Xie, W., Cook, J., Park, H. B., Freeman, B. D., Lee, C. H., and McGrath, J. E., Fundamental salt and water transport properties in directly copolymerized disulfonated poly(arylene ether sulfone) random copolymers, *Polymer*, 52 (2011) 2032-2043.

-
- [5] Xie, W., Geise, G. M., Freeman, B. D., Lee, C. H., and McGrath, J. E., Influence of processing history on water and salt transport properties of disulfonated polysulfone random copolymers, *Polymer*, 53 (2012) 1581-1592.
 - [6] Harrison, W. L., Synthesis and characterization of sulfonated poly(arylene ether sulfone) copolymers via direct copolymerization: Candidates for proton exchange membrane fuel cells, Virginia Polytechnic Institute and State University, 2002.
 - [7] Vogel, C., Komber, H., Quetschke, A., Butwilowski, W., Pötschke, A., Schlenstedt, K., and Meier-Haack, J., Side-chain sulfonated random and multiblock poly(ether sulfone)s for PEM applications, *Reactive and Functional Polymers*, 71 (2011) 828-842.
 - [8] Vogel, C. and Meier-Haack, J., Preparation of ion-exchange materials and membranes, *Desalination*, 342 (2014) 156-174.
 - [9] Asquith, B. M., Meier-Haack, J., Vogel, C., Butwilowski, W., and Ladewig, B. P., Side-chain sulfonated copolymer cation exchange membranes for electro-driven desalination applications, *Desalination*, 324 (2013) 93-98.
 - [10] Bard, A. J. and Faulkner, L. R., *Electrochemical Methods: Fundamentals and Applications*, John Wiley, New York, 2001.
 - [11] Monk, P. M. S., *Fundamentals of Electroanalytical Chemistry*, Wiley, Chichester, 2001.
 - [12] ASTOM Corporation, Neosepta, <http://www.astom-corp.jp/en/product/02.html#03>, 2013.

Chapter Six

Poly(arylene ether sulfone) Copolymers as Binders for Activated Carbon Electrodes

6.1 Overview

This chapter focuses on the use of novel random cation exchange copolymers as a binder material for activated carbon electrodes. Typically PTFE or PVDF are used to bind activated carbon powder and conductive filler to form thin carbon electrodes. However, their use is associated with numerous problems, namely the blockage of pores, reduced electrode wettability and reduced electrode conductivity. While a greater binder content increases the strength of the electrode, this simultaneously reduces capacitance and adsorption efficiency [1-3]. An optimal amount of binder is therefore required to allow adequate binding strength while limiting the drop off in capacitance and efficiency, with typical binder content in the range 5 - 15 wt.%.

The three key areas of study in this chapter are the mechanical properties of the three previously studied random copolymers, the mechanical properties of carbon electrodes prepared with these polymers, and the electrochemical performance of the electrodes when tested using CV and EIS. Based on these three areas, the efficacy of the random copolymers as binder materials for CDI applications will be discussed, particularly with regard to the electrochemical performance.

Due to the reduced mechanical strength of the random copolymers compared with PVDF, a copolymer content of 15 wt.% was found to adequately bind particles; binder content lower than this saw carbon losses when electrodes were treated in water. The hydrophilic nature of the polymers increased the wettability of the electrodes, which were seen to have low contact angles and readily absorbed water. Finally, CV and EIS testing revealed a loss in capacitance compared with electrodes prepared with PVDF. This is thought to have been a result of the swollen polymers which reduced particle contact and hence charge transfer pathways within the carbon electrodes. As a result, poor micropore double layer formation was observed. Promisingly, EIS testing showed low charging resistance compared with binders prepared with PVDF, indicating the potential for hydrophilic polymers to be used as binders in CDI electrodes if charge transfer pathways between carbon particles can be maintained.

6.2 Experimental

6.2.1 Materials

The materials used for this chapter are the same as those described in chapters three and four.

6.2.2 Carbon Electrode preparation

Carbon electrodes were prepared using the method described in chapter four, with carbon black used as a conductive filler instead of graphite powder, and either PVDF or one of the sulfonated random copolymers synthesised in chapter three used as a binder. Carbon black was used instead of graphite, as it is able to improve electrode conductivity through its three-dimensional conductivity and effectiveness in filling voids between activated carbon particles (as discussed in Section 2.2.4.2). The slurry was coated onto graphite sheets to a thickness of 200 μm using a doctor blade and dried under vacuum to completely remove the solvent (see section 6.3.2.1).

6.2.3 Binder Properties

Molecular weights of the sulfonated polymers were obtained from GPC measurements on a Knauer GPC equipped with Zorbax PSM Trimodal S columns and a RI detector. A mixture of DMAc with 2 vol.% water and 3 g/L LiCl was used as eluent. Thermogravimetric Analysis (TGA) was performed using an EXSTAR TG/DTA 6300 (Seiko Instruments Inc.) under an argon purge at a flow rate of 120 mL/min. The temperature range was 50 - 700 $^{\circ}\text{C}$ with a heating rate of 10 $^{\circ}\text{C}/\text{min}$. Tensile testing was performed using an Instron Model 5848 MicroTester with a 100 N load cell.

6.2.4 Electrode Properties

Contact angle measurements of electrodes were made with a Dataphysics OCA 15EC Measuring Instrument using the sessile drop method. SEM images were obtained using a Nova NanoSEM 450 with an acceleration voltage of 5 kV using the secondary imaging mode. All samples were coated with iridium prior to imaging. CV and EIS experiments were performed using a Biologic VSP potentiostat connected to a three-electrode electrochemical cell, as described in chapter four. The working electrode was the carbon material to be tested with an exposed surface area of 0.785 cm^2 , the reference electrode was a saturated KCl Ag/AgCl electrode, and the counter electrode was a mesh platinum electrode. EIS was

performed using the same cell over the frequency range 10 mHz to 1 MHz, with an applied voltage amplitude of 10 mV. The electrolyte for all electrochemical tests was 0.5 M NaCl.

6.3 Results and Discussion

6.3.1 Mechanical Properties of Binder Materials

6.3.1.1 Water Uptake and Contact Angle

The water uptake and contact angle of all random copolymers (as presented in chapter three) and PVDF can be seen in Table 6.1, where the initial and final contact angles were measured at $t = 0$ s and $t = 54$ s.

The contact angle of these polymers is also presented in Figure 6.1.

Table 6.1 - Contact angle and water uptake of random copolymers and PVDF.

Polymer	Contact Angle (°)		Water Uptake*
	Initial	Final	
RCP 1	51.8	30.3	49.9
RCP 2	52.1	38.2	35.7
RCP 3	62.3	46.1	25.9
PVDF	81.8	81.3	0.95

* Water uptake measured in the Na⁺ form

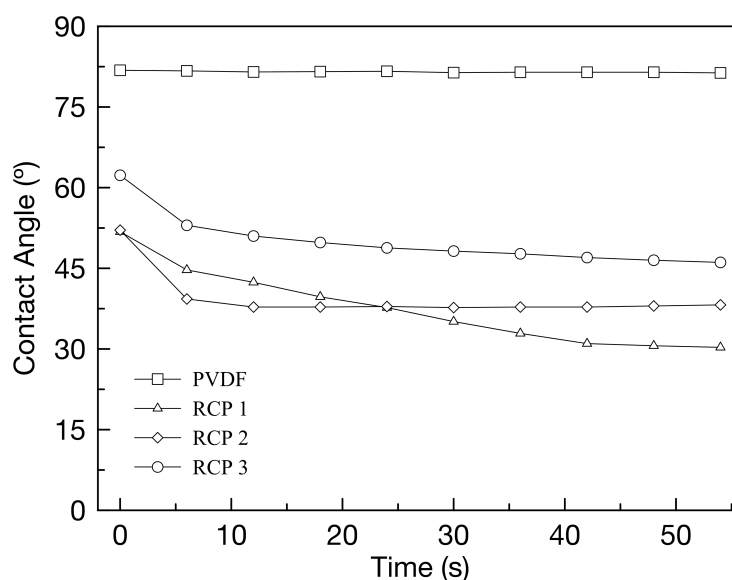


Figure 6.1 - Contact angle of random copolymers and PVDF as a function of time.

The hydrophobicity of PVDF compared with the random copolymers is clearly seen in both Table 6.1 and Figure 6.1, with a contact angle of 81.8° and a water uptake of 0.95%. By way of comparison, the cation exchange copolymers have much greater swelling properties, ranging from 26.4 – 49.9% in the Na⁺ form.

Unlike the dynamic contact angles of the copolymers seen in Figure 6.1, the contact angle of the PVDF remained relatively constant over a period of one minute. In terms of usefulness as a binder material, the increased hydrophilicity of the random copolymers is a double-edged sword; the greater swelling softens the polymers and reduces their strength and ability to effectively bind together carbon particles. However, it is this property that can allow a greater transport of cations to the electrode pores and allow electrolyte access to pores previously blocked by the hydrophobic PVDF.

6.3.1.2 Molecular Weight and Thermogravimetric Analysis

The molecular weight of the random copolymers and PVDF is given in Table 6.2. The greater molecular weight of RCP 1 compared to RCP 2 and RCP 3 is a result of the greater number of sulfonic acid groups, which promotes the formation of aggregates due to hydrogen bonds between sulfonic acid groups on different polymer chains [4-7]. These intermolecular forces are not thought to be as strong in the PVDF due to the presence of only hydrogen and fluorine atoms along the polymer chain. However, its greater molecular weight compared to the random copolymers is an indication of longer polymer chains and greater mechanical strength. The similarity of the molecular weights of RCP 2 and RCP 3 is a reflection of the nature of polymer synthesis, where not only monomer content but also slight differences in synthesis conditions can affect the final polymer properties, including molecular weight.

Table 6.2 - Molecular weights of random copolymers and PVDF.

Polymer	M_n (g/mol)	M_w (g/mol)
RCP 1	50,000	155,000
RCP 2	26,500	82,500
RCP 3	25,000	84,000
PVDF	-	~534,000*

***Material specification from Sigma-Aldrich, measured by GPC**

The TGA results of the three copolymers and PVDF are shown in Figure 6.2. Due to the similar compositions of all the copolymers, the family of the curves of the random copolymers exhibited similar characteristics. A small loss of absorbed ambient moisture was observed for all three copolymers, with the most obvious loss for that of the most hydrophilic copolymer RCP 1 (approximately 5% total mass loss). Three larger distinct regions of decomposition were observed for each copolymer, 250 - 400 °C, 400 - 540 °C and 540 - 700 °C. The two copolymers with similar molecular weights (RCP 2 and RCP 3) were seen to degrade at almost the same rate, with the greater content of the more thermally stable

dihydroxydiphenyl sulfone in RCP 3 thought to have reduced the rate of degradation compared with RCP 2 in the temperature range 250 - 400 °C. On the other hand, despite a larger content of the less thermally stable diphenylhydroquinone monomer, the degradation of RCP 1 is seen to be less than both other copolymers. Here the monomer content appears to be less important, with the greater molecular weight of the polymer (and therefore greater intermolecular forces between the polymer chains) reducing its thermal degradation. The behaviour of PVDF was vastly different to that of the random copolymers. No ambient moisture loss was observed, and the polymer underwent rapid thermal degradation beginning at 415 °C and continuing until 470 °C, with a total mass loss of 60 wt.%. At temperatures beyond 470 °C a steady rate of mass loss was observed.

While CDI electrodes do not operate at elevated temperatures, these results reinforce the importance of chain length and molecular weight on polymer properties and in maintaining the integrity of the polymer chain. Note also that while outside the scope of this thesis, the thermal stability of the cation exchange copolymers may prove useful for fuel cell applications operating at elevated temperatures.

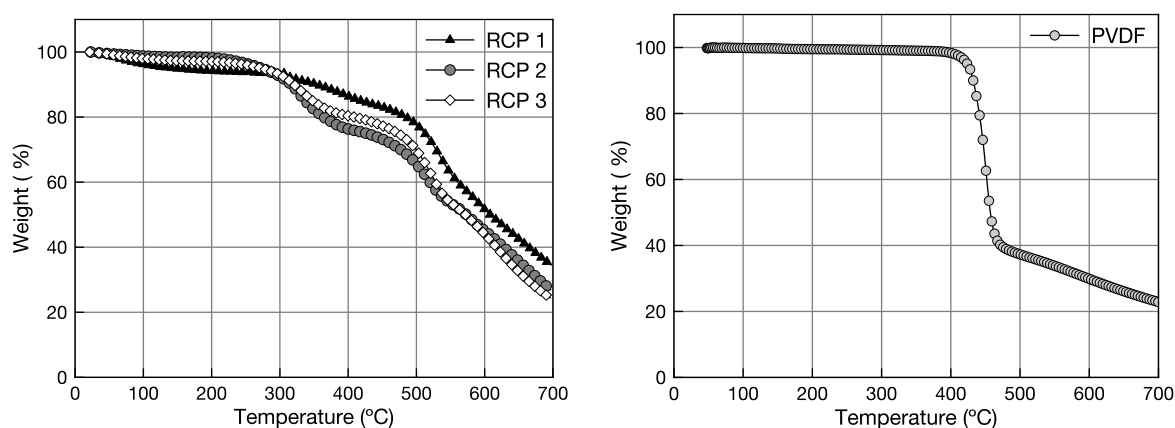


Figure 6.2 - TGA results of RCP 1, RCP 2, RCP 3 and PVDF.

6.3.1.3 Polymer Tensile Strength

Stress versus strain curves for membranes in the dry state are shown in Figure 6.3. The tensile strengths of RCP 1 and RCP 3 were found to be 40.1 MPa and 42.5 MPa, respectively, placing both samples in the expected range for thermoplastic polymers such as PVDF, PTFE and polystyrene. The increased molecular weight of RCP 1 is not enough to yield a greater tensile strength than RCP 3, so the dominant factor is the monomer composition. Although RCP 2 was not able to be tested due to defects caused during sample preparation, with a monomer ratio of dihydroxydiphenyl sulfone to diphenylhydroquinone between

that of RCP 1 and RCP 3, it is reasonable to expect the tensile strength would lie somewhere between 40.1 and 42.5 MPa.

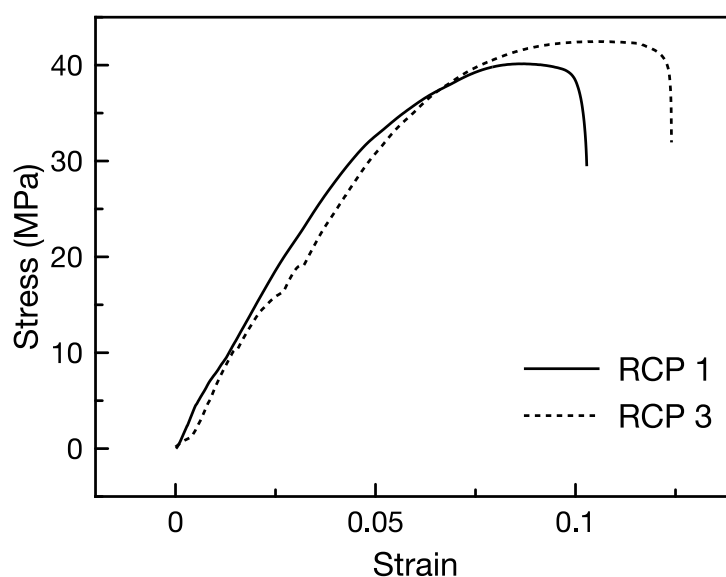


Figure 6.3 - Stress versus strain curves for RCP 1 and RCP 3.

The testing of membranes in the wet state yielded inconclusive results. The wet samples began to dry rapidly when exposed to air (particularly RCP 1 with its heightened swelling properties), causing them to shrink. This led to variable sample dimensions throughout testing, which must be constant to accurately calculate both stress and strain. The shrinking samples also placed additional tension on the load cell creating further inconsistencies in the results. Notwithstanding the inconclusive results, the samples that were tested were seen to remain partially wet and underwent much greater plastic deformation than the dry samples, indicating greater ductility. These measurements are perhaps of greater importance than those in the dry state as they reflect the nature of the polymer when used as a binder, i.e. swollen. The stress versus strain curves for unsuccessful tests can be found in Appendix A4.

6.3.2 Physical Properties of Carbon Electrodes with Copolymer Binders

6.3.2.1 Electrode Thickness

The successful formation of defect free electrodes was achieved by gentle solvent evaporation, as cracking and peeling of thin carbon films during drying can be caused by rapid solvent evaporation. Although the solvent NMP has a boiling point of 202°C, rapid evaporation may still occur when dried under vacuum. To prevent this, the solvent was initially allowed to evaporate from the samples in a fume

cupboard for several hours without heating. Samples were then transferred to a vacuum oven at room temperature, and under vacuum the temperature was slowly increased, initially for 2 h at 40 °C, followed by 12 h at 60 °C and finally 24 h at 100 °C.

Figure 6.4 presents the severity of cracking that can occur due to thickness, even with gentle drying conditions. Carbon electrodes composed of 75 wt.% activated carbon, 15 wt.% carbon black and 10 wt.% RCP 1 as binder were cast using a doctor blade at 200 μm , 250 μm and 300 μm . The electrode cast at 200 μm showed no defects, however at 250 μm small cracks towards the top of the sample were visible, and at 300 μm significant cracking and peeling was observed. The thicker carbon coatings were more susceptible to cracking, as there existed both a greater quantity of solvent to evaporate and a longer tortuous path through which the solvent must pass.

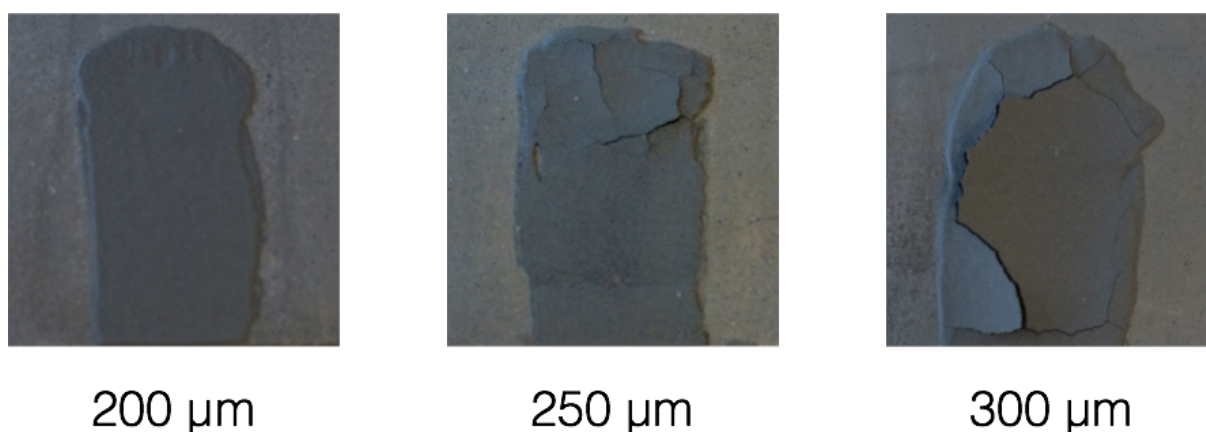


Figure 6.4 - Carbon electrodes cast at 200, 250 and 300 μm , with cracks visible at thicknesses of 250 and 300 μm .

Under the gentle drying conditions described above, all copolymers were repeatedly able to form defect free films cast at a thickness of 200 μm , regardless of the electrode composition or polymer used. This thickness is considered acceptable for thin film carbon electrodes [8]. It should be noted that electrodes with similar compositions of PVDF binder and graphite filler were successfully cast using a doctor blade at thicknesses of 650 μm . The greater thickness of defect-free electrodes cast using PVDF highlights the additional strength of the polymer and its superior ability to bind the carbon particles together.

6.3.2.2 Electrode Contact Angle

The data in Table 6.3 presents the contact angle of the electrode fabricated from 75 wt.% activated carbon, 10 wt.% carbon black and 15 wt.% binder. All electrodes prepared with a random copolymer binder were found to have hydrophilic surfaces and contact angles much lower than electrodes prepared

with a PVDF binder (note that the contact angle of electrodes prepared with activated carbon, PVDF and *carbon black* (142.4°) was similar to that of electrodes prepared with activated carbon, PVDF and *graphite* (138.8°) seen in chapter four). RCP 1 and RCP 2 binders were observed to have similarly low contact angles, indicating very high hydrophilicity and wettability of the electrodes. In contrast, the RCP 3 electrodes were seen to have a contact angle nearly double that of the RCP 1 and RCP 2 electrodes. Such an increase between RCP 2 and RCP 3 was not expected, especially considering the similar contact angle of electrodes prepared with RCP 1 and RCP 2. This result highlights the hydrophobic effect of the dihydroxydiphenyl sulfone monomer on both the polymer and composite electrode properties, and the ability of the hydrophilic diphenylhydroquinone to increase the wettability of the electrode surface once a certain threshold has been met. In this instance, the threshold lies between a hydrophilic to hydrophobic monomer ratio of 4:6 (RCP 3) and 5:5 (RCP 2) (i.e. the ratio of diphenylhydroquinone dihydroxydiphenyl sulfone). This result also underscores the importance of polymer design when preparing polymers for specific applications such as MCDI, and the attainable improvements in wettability when using a hydrophilic binder.

Table 6.3 - Contact angle of electrodes prepared with random copolymer or PVDF binder.

Binder	Contact Angle (°)	Error
RCP 1	37.44	± 7.38
RCP 2	36.35	± 4.68
RCP 3	65.51	± 1.81
PVDF	142.39	± 0.05

Despite the variable contact angle and degree of hydrophilicity of the electrodes shown in Table 6.3, all those fabricated with random copolymer were found to readily absorb water, as shown in Figure 6.5. Over a period of 30 seconds, a 4 µL drop of water fully absorbed into the electrode, regardless of binder type. In contrast, the PVDF electrode's highly hydrophobic surface resulted in a very stable contact angle over the same duration.

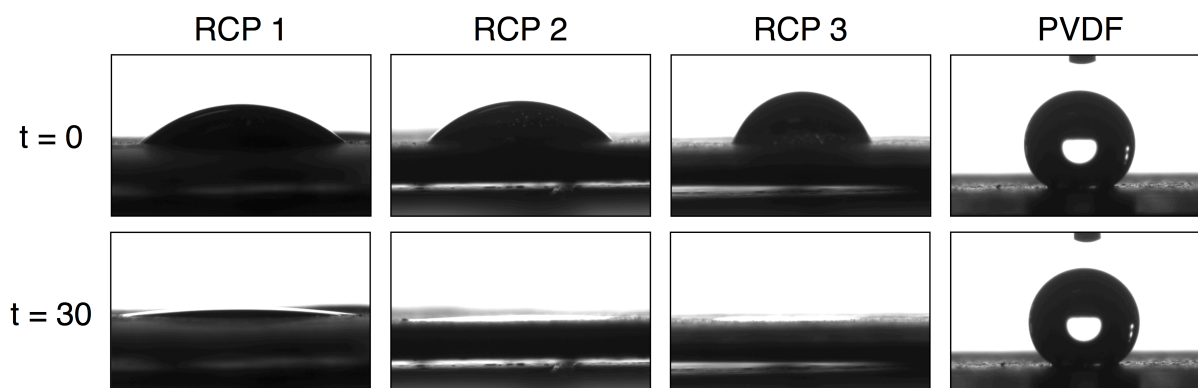


Figure 6.5 - Contact angle of electrodes fabricated from 75 wt.% activated carbon, 10 wt.% carbon black and 15 wt.% binder at $t = 0$ s and $t = 30$ s

6.3.2.3 Effect of Binder Type and Electrode Composition on Physical Structure

Using carbon black as a conductive filler, the amount of binder was adjusted to determine the most suitable composition. Electrodes with 5 wt.%, 10 wt.% and 15 wt.% RCP 3 were cast, each with 5 wt.% carbon black and variable activated carbon content. Electrodes with only 5 wt.% RCP 3 did not sufficiently bind and rather than forming a thin film electrode, the consistency of the samples was similar to that of the constituent powders. Although some adhesion was observed and the film was somewhat able to retain its form, when gently rinsed with water carbon was easily removed from the surface. Despite ample stirring for 12-16 h to evenly disperse the polymer throughout the carbon slurry prior to casting, 5 wt.% is considered to be too low a concentration to provide adequate binding.

Electrodes prepared with 10 and 15 wt.% binder were seen to produce thin films when cast onto graphite. The 10 wt.% electrodes were found to lose a small amount of carbon during rinsing and washing, although overall the electrodes retained their form. Electrodes with 15% binder were able to retain their form and held together very well, even when soaked in water. SEM images of these electrodes can be seen in Figure 6.6, with 15 wt.% binder shown in Figure 6.6 a & b, and 10 wt.% binder shown in Figure 6.6 c & d.

Samples with 15 wt.% binder were seen to form a homogeneous carbon layer free of defects, held together well by the copolymer binder. The close up SEM image in Figure 6.6 b reveals that good adhesion of the carbon black to the activated carbon particles was achieved. The cross-section of the 10 wt.% binder in Figure 6.6 c shows a large crack; although this is an artefact of the sample preparation process, it should be noted that samples with 10 wt.% binder were more difficult to handle and prepare

for SEM imaging than those with 15 wt.% binder. Although the carbon particles were still well held by the binder and the carbon black adhered to the activated carbon (seen in Figure 6.6 d), the samples were more susceptible to breaking.

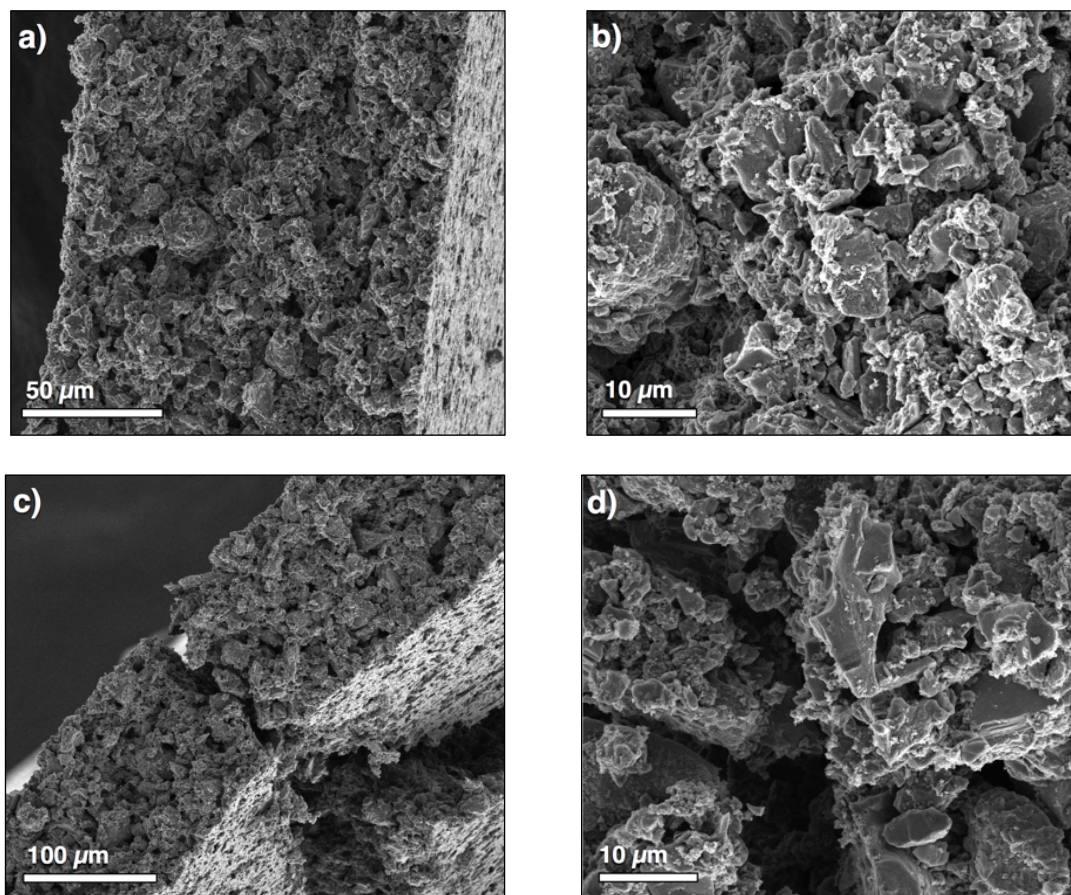


Figure 6.6 - SEM images of electrodes with varying binder content: a & b) 80 wt.% activated carbon, 5 wt.% carbon black, 15 wt.% RCP 3, c & d) 85 wt.% activated carbon, 5 wt.% carbon black, 10 wt.% RCP 3.

The images presented in Figure 6.7 show electrodes with the same composition by mass, varying only by binder type (RCP 1, a & b; RCP 2, c & d; RCP 3, e & f; PVDF, g). The cross-sections (Figure 6.7 a, c & e) reveal that regardless of binder type, thin uniform electrodes were able to be produced. From the high magnification images (Figure 6.7 b, d, f & g), strong adhesion of the carbon black particles to the activated carbon was observed, although no fibrils of binder connecting carbon particles could be seen. Based on these results and observations when handling the electrodes (i.e. no loss of carbon when gently rubbed), electrodes with 15 wt.% random copolymer binder (RCP 1, 2 or 3) are similar to those prepared with PVDF, and acceptable for further electrochemical characterisation.

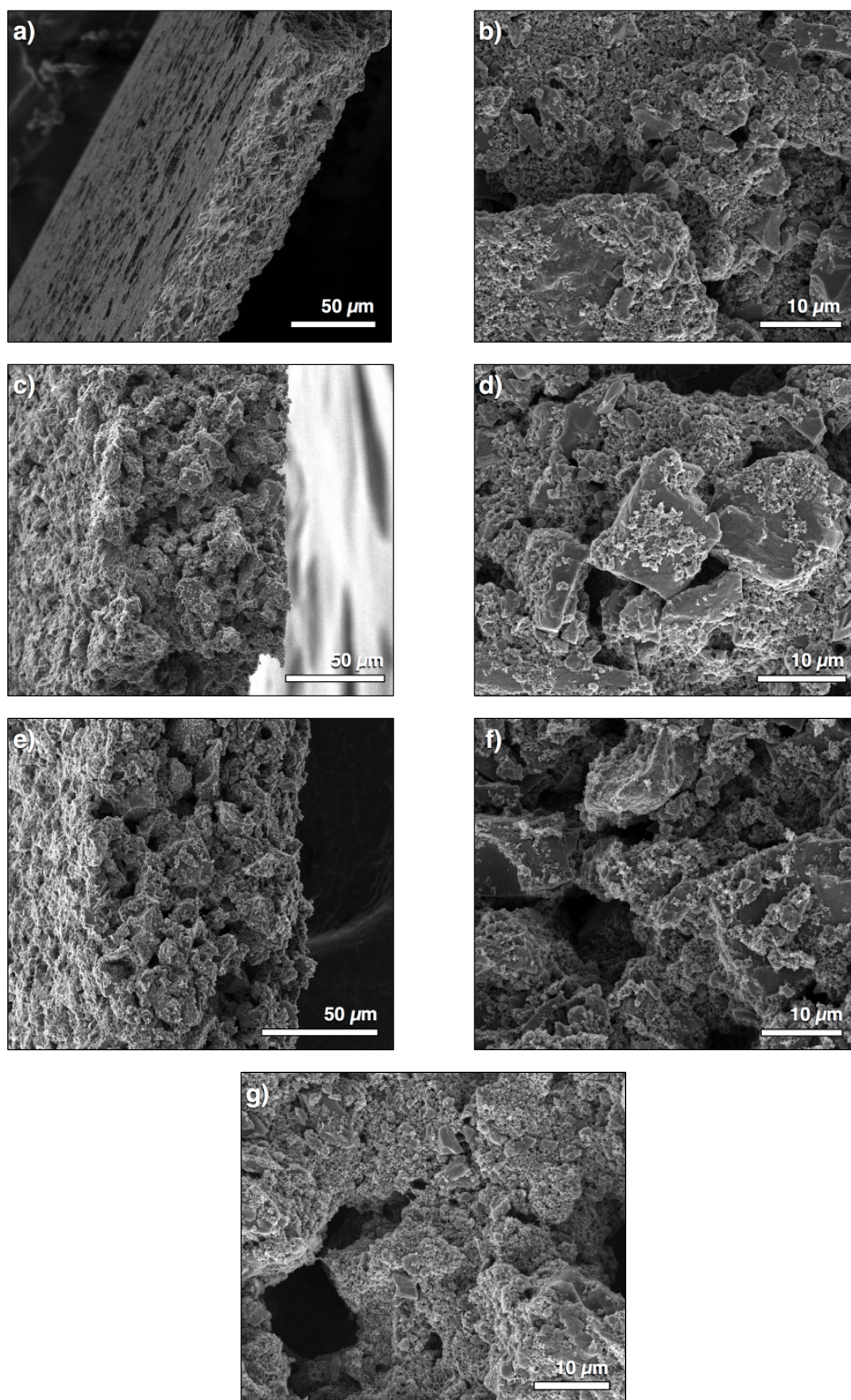


Figure 6.7 - Cross-section and surface SEM images of electrodes consisting of 75 wt.% activated carbon, 10 wt.% carbon black and 15 wt.% polymer binder, prepared with the following binders: a & b) RCP 1, c & d) RCP 2, e & f) RCP 3, g) PVDF (surface only, no cross-section available).

6.3.3 Electrode Electrochemical Characterisation

6.3.3.1 Comparison of Binder Type Using Cyclic Voltammetry

The specific capacitance as a function of potential of electrodes prepared with RCP 1-3 or PVDF as binder material, measured using CV at scan rates of 20 mV/s and 5 mV/s, is shown in Figure 6.8 and Figure 6.9. The electrodes consisted of 75 wt.% activated carbon, 10 wt.% carbon black and 15 wt.% binder.

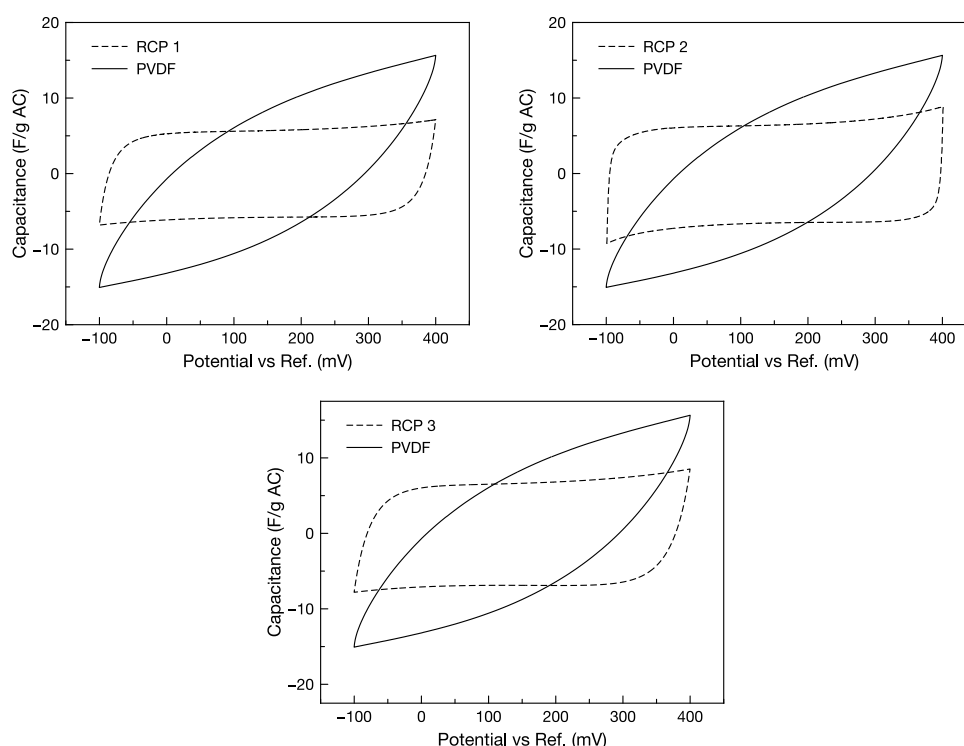


Figure 6.8 - Specific capacitance of electrodes with various binder materials measured at 20 mV/s in 0.5 M NaCl.

Samples prepared with copolymer binder were observed to form rectangular curves at 20 mV/s. In contrast, samples with PVDF binder produced larger, more distorted curves typical of electrodes at a fast scan rate with negligible micropore penetration. At a slower scan rate of 5 mV/s, the PVDF samples produced more rectangular curves with an increased capacitance over the 20 mV/s scan, indicating double layer formation within the micropores. The random copolymer samples were seen to have only slight increases in capacitance between the two scan rates, indicating the electrodes had almost reached their maximum electrosorption capacity and that negligible micropore penetration was occurring, even at a slow scan rate. Thus, the random copolymer binders appeared to facilitate double layer formation in the mesopores while restricting micropore double layer formation.

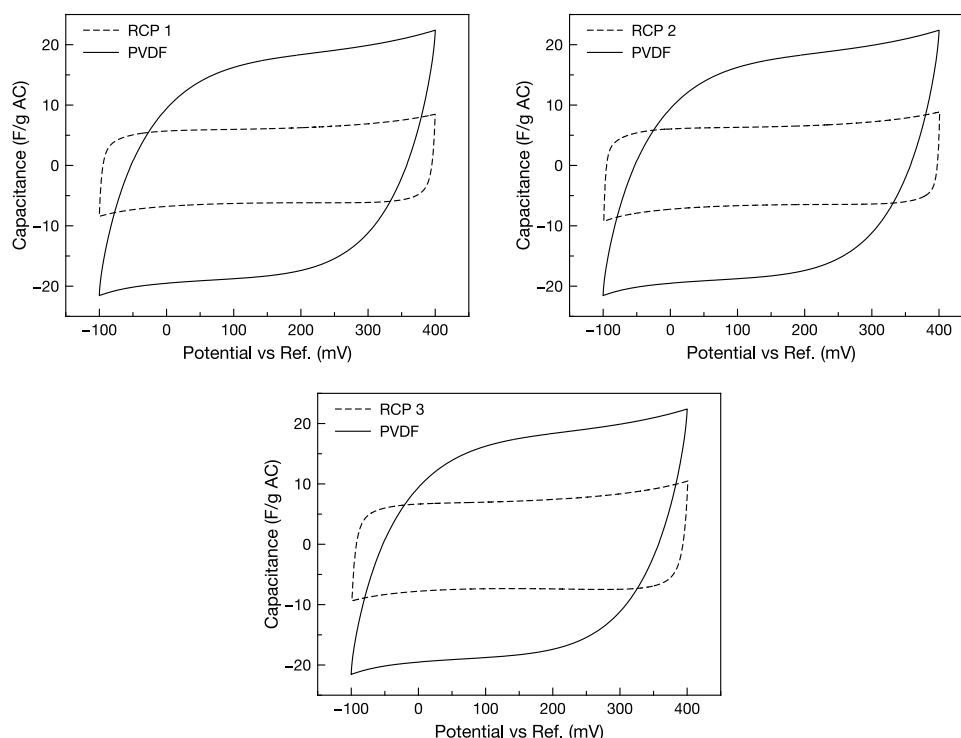


Figure 6.9 - Specific capacitance of electrodes with various binder materials measured at 5 mV/s in 0.5 M NaCl.

The behaviour of electrodes prepared with random copolymer binders is similar to that observed in chapter four for samples with a graphite content below the percolation threshold; it can be concluded that the low capacitance and rectangular curves are a result of either poor electrode conductivity or poor ionic conductivity. The hydrophilic nature of the random copolymers suggests that sufficient ion mobility can be achieved, with the potential for the random copolymers to even increase capacitance by allowing electrolyte transport to previously blocked pores. The low capacitance is therefore likely a result of poor electrode conductivity, reducing the carbon's ability to form microporous double layers. It is postulated that this is due to a loss of charge transfer pathways between the carbon particles, caused by the swollen random copolymer, as demonstrated in Figure 6.10. The hydrophobic PVDF binder does not swell in solution and allows carbon particles to remain in contact with both each other and with carbon black particles. In contrast, the hydrophilic copolymer swells to a much greater degree and causes some of this contact to be lost, meaning particles further away from the current collector are less conductive. This is represented by the shading of the particles in Figure 6.10, where a lower conductivity is represented by lighter coloured particles. Although the polymers are conductive and do allow some charge transfer, this is not as great as direct particle contact.

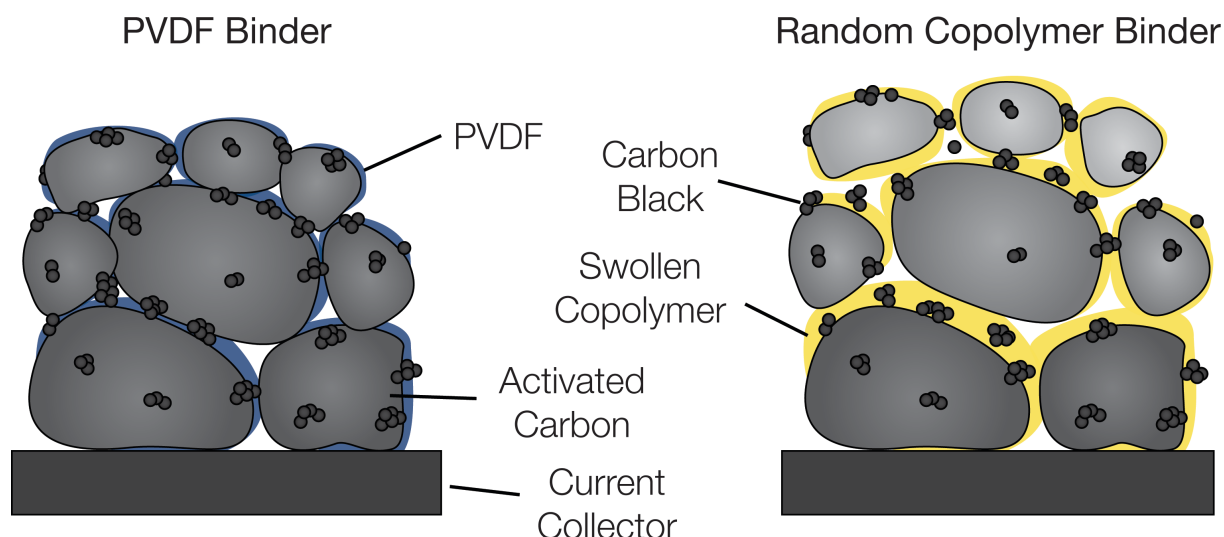


Figure 6.10 - Illustration of the potential loss of charge transfer pathways within a carbon electrode using a hydrophilic binder. Carbon electrodes prepared with PVDF (left) remain in contact with each other, while the swollen random copolymer (right) reduces particle contact and hence conductivity. Darker particles represent those that have a greater conductivity.

Note also that the tests were conducted in 0.5 M NaCl, while practical applications of CDI involve the desalination of brackish water, which is considerably less conductive. This would serve to reduce the conductivity of the electrolyte solution within the swollen polymers and decrease the charge transfer even further.

6.3.3.2 Electrochemical Impedance Spectroscopy

The Nyquist plots of the electrodes are presented in Figure 6.11. Similarly to the CV curves, different responses caused by the binder type were observed. The shape of all curves was typical for that of a double layer capacitor, notwithstanding the excessively large magnitude of the imaginary impedance for the random copolymers, nor the large real and imaginary impedances for the PVDF binder.

PVDF electrodes showed very large charging resistance at low frequencies, which is highlighted in Figure 6.12. Conversely, the copolymer binder electrodes had much lower resistance, with the real impedance only increasing notably at frequencies lower than 100 mHz. This may be a combination of minimal micropore penetration as well as the ability of the copolymers to facilitate electrolyte transport. The low resistance at high frequencies, combined with the increase in capacitance at high frequencies compared with the PVDF (shown in Figure 6.13), suggests that the random copolymers facilitate fast mesopore double layer formation, despite the swelling reducing the micropore capacitance.

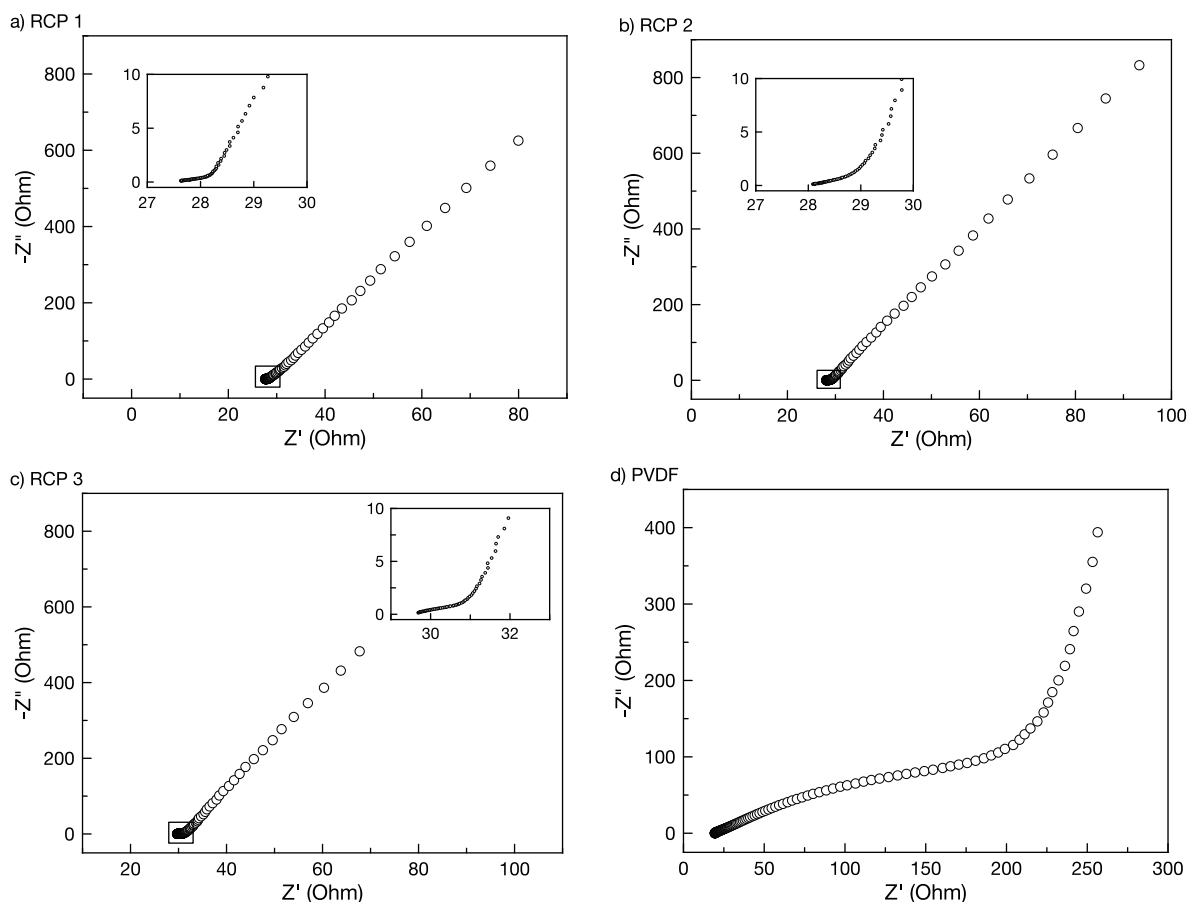


Figure 6.11 - Nyquist plots of electrodes with 15 wt.% binder: a) RCP 1, b) RCP 2, c) RCP 3 and d) PVDF.

The differences in capacitance for electrodes with different random copolymer binders (presented in both Figure 6.8 and Figure 6.13) were seen to follow the trend of lower swelling yielding greater capacitance, such that the capacitance of the electrodes with RCP 3 binder > RCP 2 binder > RCP 1 binder. The reduced swelling of RCP 3 allows better particle contact, more charge transfer pathways and greater electrode conductivity, despite the polymer itself having a lower conductivity. Considering the high proportion of inaccessible surface area within micropores with openings less than 5.9 Å (as discussed in chapter four), greater capacitance that exceeds that of PVDF binder electrodes might be observed when using the copolymers as binders in electrodes with a higher proportion of mesopores and large micropores.

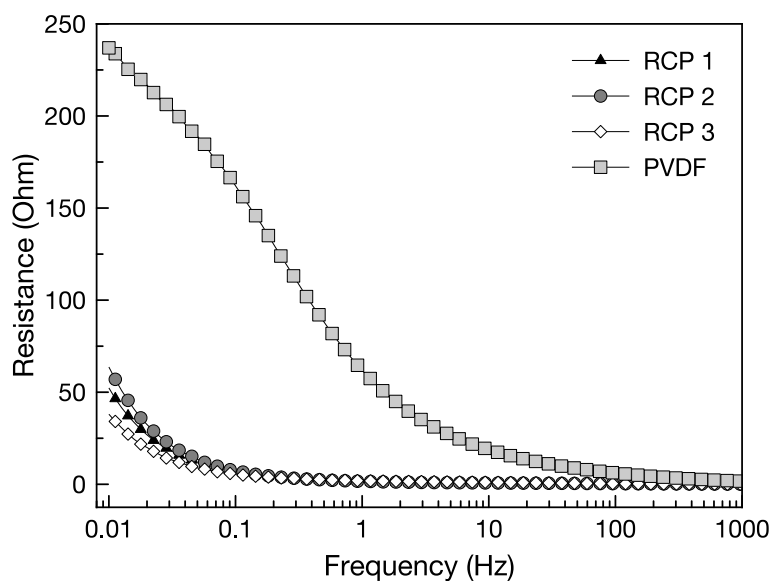


Figure 6.12 - Resistance versus frequency of electrodes with various binder materials.

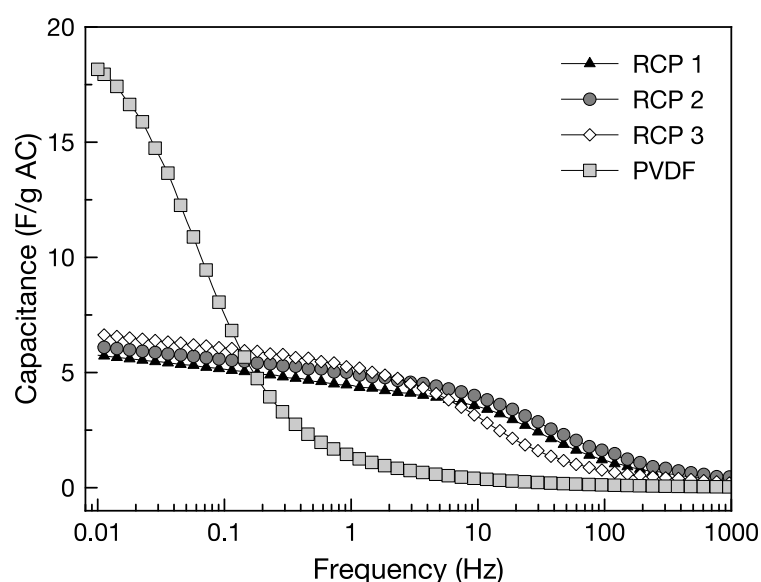


Figure 6.13 - Capacitance versus frequency of electrodes with various binder materials.

6.4 Conclusions

Carbon electrodes were prepared with random poly(arylene ether sulfone)s as binder materials and compared with those prepared with PVDF as a binder. A copolymer mass composition of 15% was found to adequately bind carbon particles, with no loss of carbon observed when treated in water. Regardless of the polymer used, good adhesion of the conductive carbon black to the activated carbon was observed. Electrodes with 10 wt.% random copolymer, while still forming thin carbon layers, were more brittle and lost some carbon when treated with water. Those with 5 wt.% random copolymer provided no effective binding. The thickness of electrodes that could be cast with the random

copolymers was lower than that previously identified with PVDF in chapter four, and although an acceptable casting thickness of 200 μm was achieved, this result highlighted the loss in stability when the copolymers were used.

As noted in chapter three, the polymers are hydrophilic with low contact angles and swelling rates in the range 26.4 – 49.9%. The effect of this hydrophilicity was directly observed when the random copolymers were incorporated into carbon electrodes. Electrode surfaces were observed to be hydrophilic with low contact angles in the range 37.44 - 65.51° and readily absorbed water. In comparison, electrodes prepared with a PVDF binder were hydrophobic with a much higher contact angle of 142.39°, and no absorption into the electrode was observed

CV and EIS testing revealed that although the binders were able to provide adequate strength at 15 wt.%, the capacitance of the electrodes was lower than electrodes prepared with PVDF. The high swelling rates of the polymers are thought to have reduced the charge transfer pathways between carbon particles, resulting in a lack of micropore double layer formation. The increases in capacitance at high EIS frequencies and lower charging resistance suggested that a more hydrophobic polymer that can still facilitate the selective transport of ions, and may indeed yield better results by maintaining charge transfer pathways. Furthermore, the use of an activated carbon material with larger micropores and a greater mesoporous surface area may improve results such that they are comparable or even exceed those achieved with a hydrophobic binder such as PVDF.

6.5 References

- [1] Park, B.-H., Kim, Y.-J., Park, J.-S., and Choi, J., Capacitive deionization using a carbon electrode prepared with water-soluble poly(vinyl alcohol) binder, *Journal of Industrial and Engineering Chemistry*, 17 (2011) 717-722.
- [2] Humplik, T., Lee, J., O'Hern, S. C., Fellman, B. A., Baig, M. A., Hassan, S. F., Atieh, M. A., Rahman, F., Laoui, T., Karnik, R., and Wang, E. N., Nanostructured materials for water desalination, *Nanotechnology*, 22 (2011) 292001.
- [3] Hou, C.-H., Huang, J.-F., Lin, H.-R., and Wang, B.-Y., Preparation of activated carbon sheet electrode assisted electrosorption process, *Journal of the Taiwan Institute of Chemical Engineers*, 43 (2012) 473-479.
- [4] Wang, F., Hickner, M., Ji, Q., Harrison, W., Mecham, J., Zawodzinski, T. A., and McGrath, J. E., Synthesis of highly sulfonated poly(arylene ether sulfone) random (statistical) copolymers via direct polymerization, *Macromolecular Symposia*, 175 (2001) 387-396.

-
- [5] Wang, F., Hickner, M. A., Kim, Y. S., Zawodzinski, T. A., and McGrath, J. E., Direct polymerization of sulfonated poly(arylene ether sulfone) random (statistical) copolymers: candidates for new proton exchange membranes, *Journal of Membrane Science*, 197 (2002) 231-242.
 - [6] Ueda, M., Toyota, H., Ouchi, T., Sugiyama, J.-I., Yonetake, K., Masuko, T., and Teramoto, T., Synthesis and characterization of aromatic poly(ether sulfone)s containing pendant sodium sulfonate groups, *Journal of Polymer Science Part A: Polymer Chemistry*, 31 (1993) 853-858.
 - [7] Vogel, C., Komber, H., Quetschke, A., Butwilowski, W., Pötschke, A., Schlenstedt, K., and Meier-Haack, J., Side-chain sulfonated random and multiblock poly(ether sulfone)s for PEM applications, *Reactive and Functional Polymers*, 71 (2011) 828-842.
 - [8] Pandolfo, A. G., Wilson, G. J., Huynh, T. D., and Hollenkamp, A. F., The Influence of Conductive Additives and Inter-Particle Voids in Carbon EDLC Electrodes, *Fuel Cells*, 10 (2010) 856-864.

Chapter Seven

Conclusions and Future Work

7.1 Thesis Conclusions

Activated carbon is widely used as a carbon material for CDI due to its economic benefits, but faces a number of drawbacks including the requirement for a polymeric binder, unfavourable pore size distribution and low conductivity. To offset these setbacks, this thesis has investigated the enhancement of activated carbon electrodes through state-of-the-art poly(arylene ether sulfone) copolymers. This class of polymers has been studied extensively for pressure-driven desalination and fuel cell applications, but never applied to electro-driven systems such as CDI.

Chapter three focused on the synthesis and characterisation of membranes prepared from random and multiblock poly(arylene ether sulfone) copolymers. The polymers incorporated the hydrophilic 2,5-diphenylhydroquinone monomer to impart conductivity and ion exchange properties, as well as hydrophobic diphenylsulfone monomers to impart mechanical stability. Pendant phenyl rings along the polymer backbone were selectively sulfonated using the simple and cost effective post-sulfonation technique, resulting in a high degree of sulfonation. Random copolymers with different monomer ratios and a multiblock copolymer with defined hydrophilic and hydrophobic block lengths were synthesised to determine the effects of side-chain sulfonation, monomer ratio and copolymer structure on fundamental membrane properties for CDI, namely: ion-exchange capacity, water uptake, conductivity and transport number.

All membranes were found to have relatively low water uptake and good mechanical stability due to the incorporation of the diphenylsulfone monomers. Ion-exchange capacities were found to be in the range 1.44 – 2.05 mmol/g, and membrane conductivity in the Na⁺ form as high as 15.13 mS/cm for the random copolymers and 16.74 mS/cm for the multiblock copolymer. These values are comparable to commercially available cation exchange membranes. The microheterogeneous structure of the multiblock copolymer increased its water uptake and conductivity, while simultaneously reducing its transport number. Conversely, random copolymer membranes with a balance of hydrophobic and hydrophilic monomers were found to have both good conductivity and high transport numbers, making them an attractive material for membranes for application in MCDI applications.

Chapter four examined the use of activated carbon as an electrode material, including a study on the effects of graphite as a conductive filler. All samples were found to be highly hydrophobic regardless of

graphite or binder content, however the electrochemical performance varied greatly between the different samples. Electrodes with a graphite content below the percolation threshold of 10-15 wt.% graphite were observed to have poor conductivity and low mesoporous and microporous capacitance. Above the percolation threshold, only modest increases in capacitance were observed. This highlighted the need for not only an appropriate conductive filler, but also a suitable carbon material with a favourable pore size distribution and adequate mesoporous surface area to minimise inaccessible surface area in the micropores.

EIS was used to examine the charging behaviour of the electrodes; a lack of micropore penetration for samples with a graphite content below the percolation threshold was caused by the large resistance of the samples to electrolyte diffusion. The phenomenon of slow double layer formation was also examined using EIS, with both poor wettability and resistance to diffusion through the pores contributing factors. Continual electrochemical charging and discharging via CV was seen to increase the penetration depth of the electrolyte, improving capacitance and reducing resistance. The slow double layer formation indicated poor electrical efficiency and kinetics of the electrodes, and highlighted the need for modification of activated carbon electrodes to perform effectively in CDI applications. This was studied in the following two chapters.

Chapter five examined the effects of random copolymer cation exchange polymer coatings on activated carbon electrodes. As expected, the coating layers were found to create additional resistance, however this did not significantly hinder the rate of double layer formation compared with uncoated electrodes. CV revealed that a greater micropore capacitance was observed for all coated electrodes over a wide range of potentials, which can be attributed to the selective transport properties of the cation exchange polymers, and the increased electrolyte concentration in the polymer coating directly adjacent to the carbon electrodes. EDX results showed copolymer penetrates into the carbon substrate during casting, which may offset the reduced capacitance and poor electrode kinetics caused by the PVDF binder.

Electrochemical impedance results identified the influence of the conductivity and water uptake on both the charging resistance and capacitance of the coated electrodes. The reliance of these properties on IEC indicated that optimal polymer design for MCDI applications will maximise IEC to improve capacitance and reduce resistance without compromising mechanical stability. The optimisation of

coating thickness is also an important factor in reducing additional resistance created by the coating layer. Overall, it was found that the cation exchange polymers, and in particular RCP 1 can be used to improve ion transport into the pores of the electrodes, and they can be considered as candidates for potential membranes or coatings in MCDI applications

Based on the penetration of random copolymer coatings into the carbon substrate in chapter five, chapter six investigated the use of random poly(arylene ether sulfone)s as binders for activated carbon electrodes. With a content of 15 wt.%, the copolymer was found to effectively bind carbon particles and provide good adhesion of the conductive carbon black filler to the activated carbon. Nonetheless, reductions in mechanical strength compared with PVDF binder were observed, with a low casting thickness required to maintain the integrity of the electrodes during drying.

The hydrophilicity of the copolymers translated into hydrophilic electrodes that readily absorbed water, compared with the hydrophobic surface of similar electrodes prepared with PVDF. CV and EIS testing revealed that although the binders improved electrode hydrophilicity, the capacitance was found to be lower than electrodes prepared with PVDF. This was a result of the high swelling rates of the polymers that eliminated or reduced charge transfer pathways between carbon particles, resulting in a loss of particle conductivity and a lack of micropore double layer formation. Promisingly, the increased capacitance at high frequencies during EIS combined with the relatively low charging resistances suggested the random copolymers could facilitate the transport of ions into mesopores. While PVDF and PTFE are commonly used as binder materials, it can be concluded that there is potential to improve the relative poor performance of activated carbon electrodes using hydrophilic binder materials.

7.2 Recommendations for Future Work

7.2.1 Improved Membrane Conductivity Testing

Numerous attempts were made to measure the through-plane conductivity of membranes in solution, although no accurate measurements could be made. Through-plane conductivity measurements in solutions with varying concentration and ionic composition would provide useful information regarding the expected performance of the membranes for MCDI applications, and should be considered for future work for both these and other classes of polymer.

7.2.2 Variation in Carbon Material

The activated carbon selected for this study was found to be highly microporous with a pore size distribution unfavourable for electrosorption. A study incorporating a range of microporous and mesoporous carbons enhanced with copolymers would supplement this work and further highlight the benefits of CDI with cation exchange materials.

7.2.3 Optimised Polymer Coating Thickness

The polymer layer thickness must be optimised to minimise charging resistance while still adequately enhancing electrosorption performance. This could be coupled with a more detailed EIS study on the optimised polymer coatings, including the development of a rigorous model, to better determine the effect of the coatings on the electrode performance.

7.2.4 Hydrophilic Polymer Optimisation

The loss of charge transfer pathways may be overcome through the optimisation of polymers designed specifically for application as a binder. For the random copolymers used in this study, a greater diphenylsulfone content will increase hydrophobicity and increase contact between particles, while retaining sufficient IEC and hydrophilicity through sulfonated side chains. Other classes of polymers that are more cost effective such as polystyrenes, poly(vinyl chloride)s and poly(arylene ether ketone)s could also be studied as either cation or anion exchange polymers for binder materials.

7.2.5 Testing of Electrodes in a CDI Cell

While this study focused on cation exchange polymers for the improvement of activated carbon CDI electrodes, the actual testing of electrodes in a CDI cell was unfeasible. Testing of the coated electrodes and optimised electrodes with copolymer binders in a CDI cell will provide a direct comparison with other studies and help assess the suitability of these materials for commercial use. In an Australian context, such a study should examine the performance of brackish water desalination from inland water sources with commonly encountered salts, including sodium, calcium, magnesium, potassium, chloride, nitrate and sulphate, and perhaps examine the selectivity of ions based on charge and size. Other contaminants such as arsenic and foulants like natural organic matter could also be studied. A comparison of coated electrodes or those prepared with hydrophilic binders to activated carbon electrodes with commercial membranes would also provide useful.

7.2.6 Anion Exchange Coatings

The focus of the study has been on cation exchange membranes, largely due to the extensive literature in the field of cation exchange membranes for fuel cells, and their ease of fabrication with relatively simple methods of sulfonation now widely practiced. Coatings fabricated from aminated polystyrenes or PVA may provide cheap and simple solutions that complement the now expanding suite of cation exchange polymers available for CDI.

Appendices

Appendix A1 - Ion Exchange Capacity Calculations

The moles of protons, $n(H^+)$, is calculated using the following equation:

$$n(H^+) = n(OH^-) = cvF = cF[v_{sample} - v_{blank}]$$

where c is the concentration of the NaOH solution (0.01 M), v_{sample} is the volume required to neutralise the sample solution, v_{blank} is the volume required to neutralise a 2M NaCl solution, and F is the NaOH correction factor used to calibrate the NaOH solution. F was calculated by titrating both water and benzoic acid solutions with 0.01M NaOH, such that:

$$F = \frac{m_{BA}}{cM_{BA}[v_{benzoic} - v_{water}]}$$

where m_{BA} is the mass of the benzoic acid being titrated, M_{BA} is the molar mass of the benzoic acid, c is the apparent concentration of the NaOH solution (0.01 M), and $v_{benzoic}$ the volume required to neutralise the benzoic acid, and v_{water} the volume required to neutralise the same amount of distilled water.

Appendix A2 - Calculation of BET Surface Area for a Microporous Material

The Roquerol transform is applied to calculate the BET surface area of a microporous material. This method is shown below, with the isotherm data for activated carbon in the relative pressure range 0.000 - 0.323 presented in Table A1, along with the calculated values for $Q \times (P_0 - P)$ and $1/[Q \times (P_0/P - 1)]$ (where Q is the quantity adsorbed ($\text{cm}^3/\text{g STP}$), P is the measured pressure (mmHg) and P_0 is the saturation pressure (mmHg)). To determine the BET surface area of a microporous material, the values of $Q \times (P_0 - P)$ are plotted against relative pressure. The pressure range from the origin to the maximum yields a linear BET plot, and is the range from which the BET surface area can accurately be calculated. This data is represented by the shaded pressure range in Table A1. Using this pressure range, the linear regression of $1/[Q \times (P_0/P - 1)]$ is plotted against relative pressure, as shown Figure A2. The intercept and slope of this regression are then used to calculate the BET surface area.

Table A1 - Isotherm data for an activated carbon sample measured using N2 at 77 K, along with calculated values of $Q \times (P_0 - P)$ and $1/[Q \times (P_0/P - 1)]$

Relative Pressure (P/P_0)	Quantity Adsorbed ($\text{cm}^3/\text{g STP}$)	$Q \times (P_0 - P)$	$\frac{1}{[Q \times (P_0/P - 1)]}$
1.39×10^{-6}	20.2	15,323	6.89×10^{-8}
2.72×10^{-6}	40.4	30,647	6.73×10^{-8}
5.70×10^{-6}	60.6	45,962	9.41×10^{-8}
1.50×10^{-5}	80.8	61,272	1.86×10^{-7}
3.57×10^{-5}	101.0	76,576	3.54×10^{-7}
8.18×10^{-5}	121.1	91,848	6.75×10^{-7}
2.03×10^{-4}	141.2	107,063	1.44×10^{-6}
5.78×10^{-4}	161.1	122,077	3.59×10^{-6}
1.92×10^{-3}	181.1	137,072	1.06×10^{-5}
6.25×10^{-3}	200.8	151,246	3.13×10^{-5}
9.60×10^{-3}	208.5	163,200	4.65×10^{-5}
1.37×10^{-2}	215.5	167,912	6.47×10^{-5}
2.15×10^{-2}	224.7	173,683	9.78×10^{-5}
3.33×10^{-2}	234.6	179,061	1.47×10^{-4}
5.11×10^{-2}	245.0	183,450	2.20×10^{-4}
5.71×10^{-2}	247.9	184,344	2.45×10^{-4}
7.53×10^{-2}	254.7	185,650	3.20×10^{-4}
0.112	264.4	184,652	4.78×10^{-4}
0.153	271.5	183,452	6.68×10^{-4}
0.189	276.0	180,361	8.44×10^{-4}
0.236	280.6	175,622	1.10×10^{-3}
0.265	283.1	170,333	1.27×10^{-3}
0.298	285.8	163,845	1.49×10^{-3}
0.323	287.6	158,963	1.66×10^{-3}

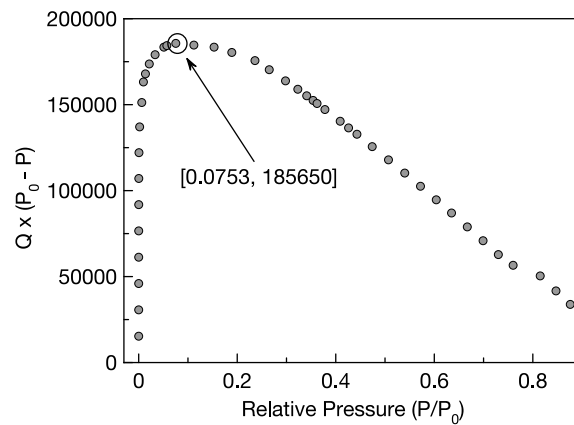


Figure A1 - $Q(P_0 - P)$ plotted against relative pressure, highlighting the maximum value from which the BET surface area can be calculated

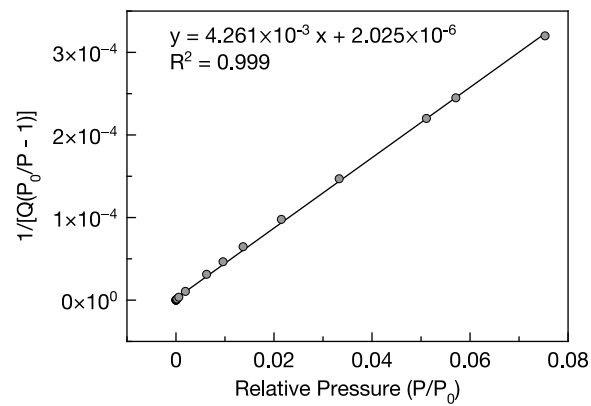


Figure A2 - Linear regression of $1/[Q(P_0/P - 1)]$ plotted against relative pressure. The intercept and slope of the line are used to calculate the BET surface area

From Figure A2:

Intercept: 2.025×10^{-6}

Slope: 4.261×10^{-3}

Note also that the area occupied by a single N_2 molecule is $16.2 \times 10^{-20} \text{ m}^2$

$$V_m = \frac{1}{\text{intercept} + \text{slope}} = \frac{1}{(2.025 \times 10^{-6}) + (4.261 \times 10^{-3})} = 234.58 \text{ cm}^3/\text{g}$$

$$C = \frac{1}{V_m \times \text{intercept}} = \frac{1}{234.58 \times (2.025 \times 10^{-6})} = 2105$$

where V_m is the volume of gas adsorbed when the entire surface is covered with a single layer of N_2 , and

C is the BET constant.

$$\text{BET surface area} = \frac{\text{Avagadro constant} \times \text{N}_2 \text{ Molecule Area} \times V_m}{\text{Molar Volume at } 0^\circ\text{C}}$$

$$= \frac{6.023 \times 10^{23} \times 16.2 \times 10^{-20} \times 234.58}{.022414 \times 10^6}$$

$$= 1021 \text{ m}^2/\text{g}$$

Table A2 - BET results from activated carbon samples

Sample	Surface Area (m²/g)	BET Constant
1	1021	2105
2	1067	2244
3	1017	2533
4	1079	2314
5	105	3791
6	1037	3163
Average	1039 ± 40	NA

Appendix A3 - Carbon Electrode Preparation

Table A3 - Carbon electrode preparation. Note that the electrodes described in this table were prepared for optimisation purposes only and were not suitable for electrochemical testing.

Composition (wt.%)	Comments
Activated carbon: 75 Graphite: 15 PVDF: 10	<p>Preparation: All components were added simultaneously and mixed until PVDF dissolved. The carbon slurry was cast onto a thin foil sheet at a thickness of 650 μm then dried at 55 $^{\circ}\text{C}$ for 17 h. Samples were not dried in a vacuum oven.</p> <p>Observations: Good carbon adhesion was achieved however the sample formed cracks</p>
Activated carbon: 75 Graphite: 15 PVDF: 10	<p>Preparation: Polymer was allowed to dissolve before the addition of activated carbon and graphite. The slurry was cast onto a solid graphite sheet (3.2 mm) at a thickness of 650 μm then left in the fume cupboard until the surface appeared dry. Dried at 120 $^{\circ}\text{C}$ for 2 h, then transferred to a vacuum oven at 80 $^{\circ}\text{C}$ for 2 h.</p> <p>Observations: Generally no cracks were observed and good adhesion was achieved</p>
Activated carbon: 80 Graphite: 15 PVDF: 5	<p>Preparation: As per #2 above.</p> <p>Observations: When lightly rubbing the electrode surface, carbon was easily removed from the sample. Due to the low PVDF content, there was insufficient binder content to adequately hold the both carbon and graphite particles together, and to adhere the slurry to the graphite sheet. Greater PVDF content is required for future electrode synthesis</p>
Activated carbon: 70 Graphite: 15 PVDF: 15	<p>Preparation: As per #2 above, with samples cast to a thickness of 350 μm. Vacuum oven drying temperature was increased to 120$^{\circ}\text{C}$ and lengthened to 16 h.</p> <p>Observations: With increased PVDF content, good adhesion was achieved and no carbon was removed when the samples were gently rubbed by hand. After the drying process, no cracks were observed</p>

Appendix A4 - Stress Versus Strain Curves for Swollen Membranes

Figure A3 shows the stress versus strain curves of inconsistent results of RCP 3 testing in the swollen state, compared with the results of RCP 1 and RCP 3. Although no definite conclusions about the tensile strength can be drawn, it is obvious that the swollen polymers exhibit greater plastic deformation with a reduced overall tensile strength.

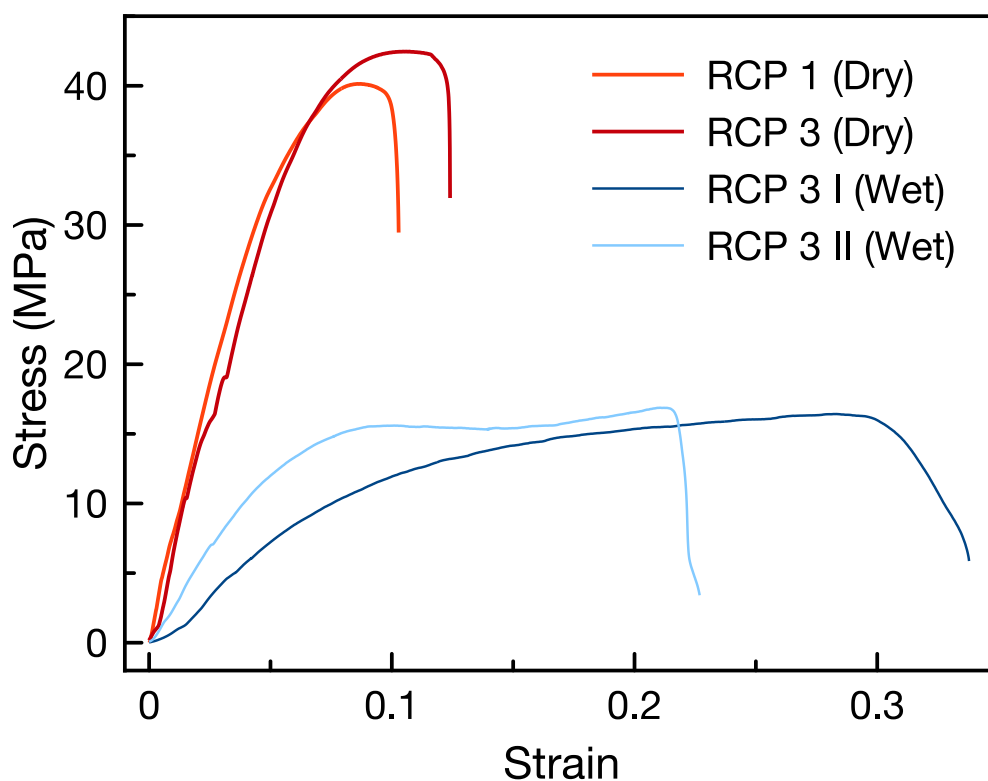


Figure A3 - Stress versus strain curves for both wet and dry membrane samples

Appendix A5 - Published Papers

Desalination 324 (2013) 93–98



Contents lists available at ScienceDirect

Desalination

journal homepage: www.elsevier.com/locate/desal

Side-chain sulfonated copolymer cation exchange membranes for electro-driven desalination applications

Benjamin M. Asquith^{a,b}, Jochen Meier-Haack^b, Claus Vogel^b, Wladimir Butwilowski^b, Bradley P. Ladewig^{a,*}^a Department of Chemical Engineering, Monash University, VIC 3800, Australia^b Leibniz Institute of Polymer Research Dresden, Hohe Strasse 6, 01069 Dresden, Germany

HIGHLIGHTS

- Random and multiblock side-chain sulfonated cation exchange membranes were prepared.
- All membranes yielded relatively low water uptake and good mechanical stability.
- Hydrophilic domains in the polymers enhanced ion exchange capacity and conductivity.
- Membrane conductivity is comparable to commercially available Neosepta CMX.
- Random copolymers exhibited high transport numbers.

ARTICLE INFO

Article history:

Received 11 March 2013

Received in revised form 19 May 2013

Accepted 29 May 2013

Available online 3 July 2013

Keywords:

Cation exchange membranes

Copolymers

Side-chain sulfonation

Electrodialysis

Membrane capacitive deionization

ABSTRACT

Cation exchange membranes prepared from random and multiblock side-chain sulfonated poly(ether sulfone)s have been characterised to evaluate their suitability for electrodialysis and membrane capacitive deionization applications. The side chain sulfonation of the copolymers resulted in membranes with a high degree of sulfonation and ion exchange capacities (IEC) in the range of 1.44–2.05 mmol/g, which is comparable to commercially available membranes. The multiblock copolymer, which can be considered as having a microheterogeneous structure, exhibited a high IEC and water uptake due to large, hydrophilic domains, while the random copolymers had lower swelling rates. Membrane conductivity in the Na⁺ form reached as high as 15.13 mS/cm for the random copolymers and 16.74 mS/cm for the block copolymer. Transport numbers were found to be as high as 0.99 for random copolymers, but as low as 0.84 for the block copolymer. Based on these results, these side-chain sulfonated random copolymers are potential candidates for use in electro-driven desalination systems.

© 2013 Elsevier B.V. All rights reserved.

1. Introduction

Given the rising global demand for water, in addition to other water conservation and reuse strategies, desalination is a key strategy to supplement water supplies. Electrodialysis and MCDI are electro-driven desalination processes that can be used for the highly efficient desalination of brackish water, the production of ultra pure water, water softening and the removal of other charged impurities from water streams [1–11]. The efficiency of these processes relies of the use of ion exchange membranes to remove unwanted charged particles from the feed stream. While many developments in ion exchange membranes have come from research for the chlor-alkali industry and fuel cells [12,13], the development of new materials and further

fundamental research into ion exchange membrane properties and functions will benefit numerous other processes, including electro-driven desalination [14].

Membranes for electrodialysis and MCDI require a high transport number and ion exchange capacity, low resistance and strong mechanical and chemical stability. There is often a trade-off between these properties; for instance, increasing polymer hydrophilicity to improve transport properties typically reduces the mechanical and chemical stability. Thus, polymer design for ion exchange membranes is a challenging task, and there is a need to balance the membrane properties for the desired application. As a way to improve the range of properties that a polymer exhibits, copolymers can be synthesised that combine hydrophobic and hydrophilic monomers. Poly(ether sulfone)s have strong mechanical, thermal and chemical stability and have been successfully used as ion exchange membranes in a wide range of applications [15–21]. State of the art random and multiblock poly(ether sulfone) copolymers have also been developed for pressure-driven desalination membranes [22–26] and for fuel cell applications

* 0011-9164/\$ – see front matter © 2013 Elsevier B.V. All rights reserved.
<http://dx.doi.org/10.1016/j.desal.2013.05.023>

[27,28], but these materials have yet to be prepared and characterised for ion exchange processes such as electrodialysis and MCDI.

For use as a cation exchange membrane, poly(ether sulfone) must be functionalised to incorporate fixed negatively charged groups. This process plays a large role in determining the properties of the polymer, in particular the electrical resistance and permselectivity [29]. Sulfonation is commonly used over other forms of functionalisation such as carboxylation or phosphonation, as the process is relatively simple and yields membranes with favourable ion transport properties [30]. Post-sulfonation, the direct functionalisation of a polymer with chlorosulfonic acid or concentrated sulfuric acid, allows for less control over the degree of sulfonation and chemical structure of the sulfonated polymer. Nonetheless it is often preferred over pre-sulfonation as it is a simpler and more cost effective process [31]. During the sulfonation process it is often the main chain that becomes sulfonated [32,33], however recent studies have shown that side chain sulfonation may enhance the chemical and mechanical properties of the polymer [28,34–36]. Results from these studies have yielded membranes with excellent properties and have shown good results when applied to fuel cells. However, side-chain sulfonated copolymers are yet to be studied for ion exchange desalination technologies.

In this work, three random and one multiblock side-chain sulfonated poly(ether sulfone)s were prepared and characterised. Correlations between the polymer structure and membrane properties are highlighted, in particular the IEC, water uptake, conductivity and transport number. Membranes are compared to the commercial membrane Neosepta CMX, which is commonly used for desalination via electrodialysis and MCDI, and the potential application of random and block copolymer membranes for these applications is discussed.

2. Experimental

2.1. Materials

4,4'-Difluorodiphenyl sulfone (DFDPhS) was purchased from FuMA-Tech GmbH (Germany) and was purified by vacuum distillation. 4,4'-dihydroxydiphenyl sulfone (DHDPhS) was obtained from Aldrich (Germany). N-methyl-2-pyrrolidone (NMP) was purchased from Merck (Germany) and distilled twice under reduced pressure from CaH_2 . Concentrated sulfuric acid (min. 96%) was obtained from Acros (Belgium). 2,5-diphenylhydroquinone (DPhHQ), hydroxy endgroup diphenylated poly(ether sulfone) oligomer (oligo-DP-PES) and decafluorobiphenyl endcapped poly(ether sulfone) oligomer (oligo-PES) were prepared as per the procedure described by Vogel et al. [28].

2.2. Polymer synthesis and sulfonation

Random and multiblock copolymers were synthesised using the silyl-method as per the procedure described by Vogel et al. [28]. For the random copolymers, 10 mmol of DFDPhS, 10–x mmol of bis-TMS-DHDPhS and x mmol of bis-TMS-DPhHQ were weighed into a three-necked flask with 30 mL of anhydrous NMP. After complete dissolution of the monomers a 1:5 mixture of anhydrous potassium carbonate and calcium carbonate was added. The reaction mixture was heated under stirring and argon purging for 24 h to 175 °C and finally for 2 h at 190 °C. The cooled reaction mixture was diluted with NMP and filtered for the removal of insoluble material. The products were precipitated in methanol, then intensively washed with water and methanol. Finally the products were dried in vacuum at 100 °C to constant weight. The molar ratios of DPhHQ and DHDPhS for the random copolymers were 6:4, 5:5 and 4:6 (RCP 1, RCP 2 and RCP 3, respectively).

For the block copolymer, 0.3 mmol of the end-capped oligo-PES and 0.3 mmol of oligo-DP-PES were weighed into a three-necked round-bottomed flask with 50 mL of anhydrous NMP. The block lengths of oligo-PES and oligo-DP-PES were 25 and 39 respectively, where the block length is related to a single diphenylsulfone unit. After complete

dissolution of the precursor oligomers, 2 mmol of anhydrous potassium carbonate was added to the reaction mixture and the temperature was raised to 100 °C under stirring and argon purging for 24 h. The cooled reaction mixture was filtered and the product was coagulated in a 10-fold excess of methanol. The product was isolated by filtration and washed intensively with water and methanol. Finally the product was dried in vacuum at 100 °C to constant weight.

All polymers were sulfonated using concentrated sulfuric acid (96–98%). 30 mL of concentrated sulfuric acid was added to 3 g of polymer in a small flask under stirring for 24 h. The sulfonated polymers were precipitated in water and thoroughly washed with water until the solution obtained a neutral pH. The final products were dried under vacuum at 110 °C to constant weight.

2.3. Membrane preparation

Membranes were prepared by dissolving the sulfonated polymers in NMP. The solutions were cast onto glass and dried under vacuum for 2 h at 60 °C, then for a further 24 h at 80 °C. Membrane samples were removed from the glass using deionised water and thoroughly rinsed with deionised water before soaking for 24 h in 1 M NaCl. The membranes were finally stored in deionised water at room temperature before use.

2.4. Polymer and membrane characterisation

^1H NMR spectra of the polymers were recorded on a Bruker DRX400 spectrometer operating at 400.17 MHz, with $\text{DMSO}-d_6$ used as a solvent and internal chemical shift reference (2.50 ppm). The molecular weights were obtained from GPC measurements on a Knauer GPC equipped with Zorbax PSM Trimodal S columns and a RI detector. A mixture of DMAc with 2 vol.% water and 3 g/L LiCl was used as eluent. Water uptake was measured by first drying membrane pieces at 80 °C under vacuum until constant weight was reached. After soaking the pieces in water at room temperature for 24 h, they were removed, excess water was gently wiped with a tissue and the pieces were immediately weighed. The water uptake (WU) was calculated using the following equation:

$$\text{WU} = \frac{m_{\text{wet}} - m_{\text{dry}}}{m_{\text{dry}}} \quad (1)$$

where m_{wet} is the weight of the swollen membrane and m_{dry} is the weight of the dry membrane. The ion exchange capacities of the membranes were measured using the titration method. Membrane pieces were first dried at 80 °C under vacuum until constant weight was reached. They were then soaked in 1 M HCl, thoroughly rinsed with deionised water, then soaked in 2 M NaCl for 24 h. The IEC was determined by titrating the NaCl solution with 0.01 M NaOH. The final IEC values were calculated by also taking into account the titration of blank 2 M NaCl solution. In-plane conductivity was determined using electrical impedance spectroscopy with a four point probe. Using a Gamry Reference 600 potentiostat in a frequency range from 1 Hz to 1 MHz, the membrane resistance was taken at the frequency where the phase angle was closest to zero. Membranes were measured in the Na^+ form at 30 °C and a relative humidity of 99% to prevent them from drying out. As the samples were tested in a humid environment and not submerged in solution, the measured resistance is not influenced by boundary layer effects. Conductivity was calculated based on the measured membrane resistance, R_m (Ω), distance between electrodes, L (cm), and the effective membrane cross section (thickness multiplied by width), A (cm^2), such that:

$$\sigma = \frac{L}{R_m A} \quad (2)$$

Membrane transport number was determined by measuring membrane potential. The experimental setup is shown in Fig. 1. Using a two-chamber cell, a vertically positioned membrane separated two solutions of 0.5 M NaCl and 1 M NaCl. The potential difference across the cell was measured by a potentiostat connected to Ag/AgCl reference electrodes. The transport number, t_+ , was then calculated using the following modified Nernst equation [20]:

$$E_m = \frac{RT}{F} (2t_+ - 1) \ln \left(\frac{a_1}{a_2} \right) \quad (3)$$

where t_+ is the transport number, E_m is the measured potential (V), R is the gas constant, T is the temperature (K), F is the Faraday constant, and a_1 and a_2 are the activities of the NaCl solutions (mol/L).

3. Results & discussion

3.1. Polymer composition

^1H NMR analysis was used to determine the chemical structure of the copolymers. The spectra and chemical structure of the random copolymers are shown in Fig. 2. Based on the set of diphenylsulfone-centred substructures previously postulated [28], the peaks in the region 8.05–7.73 ppm correspond to protons a and a' in the *ortho*-position to the sulfone group. The increase in intensity of the peak at 8.00 ppm (a) is coupled with a decrease of the peaks in the region 7.96–7.73 ppm (a') and is consistent with the decreasing monomer ratio of 2,5-diphenylhydroquinone to 4,4-dihydroxydiphenyl sulfone. The multiblock copolymer spectrum and chemical structure are shown in Fig. 3. Similar to the random copolymers, the doublet at 7.99 ppm corresponds to the protons (a) in the *ortho*-position to a sulfone group in the poly(ether sulfone) repeating unit, while the doublet at 7.80 ppm (a'') corresponds to protons in the *ortho*-position to a sulfone group in the diphenylated repeating unit. The intensity of these peaks is consistent with the chain length of the precursor ether sulfone oligomers.

For both the random and multiblock copolymers, the peak in the region 7.52–7.65 ppm is consistent with protons (e) in the *meta*-position on a sulfonated pendant phenyl ring, indicating side chain sulfonation in the *para*-position of the pendant phenyl rings. The degree of sulfonation was calculated from ^1H NMR by comparing the content of diphenylhydroquinone units in the non-sulfonated polymer with the sulfonated diphenylhydroquinone units in the sulfonated polymers. As shown in Table 1, all polymers were found to have a high degree of sulfonation of at least 95%.

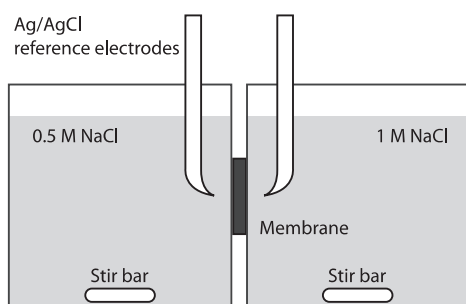


Fig. 1. Schematic of the cell used to measure transport number.

3.2. Membrane characterisation

3.2.1. Ion exchange capacity

For the random copolymers, IEC is seen to increase with increasing DPhHQ content. The DPhHQ provides sites for the side-chain sulfonation to occur and thus increases the hydrophilic properties of the copolymer. The multiblock copolymer possessed an IEC of 1.91 mmol/g, which was within the range of the random copolymers. The high IEC values for all copolymers are a result of the high degree of side-chain sulfonation, which allows for sulfonation on each of the pendant phenyl rings. All synthesised polymers were found to have comparable IEC values to Neosepta CMX, which is a standard grade Neosepta membrane characterised by a high mechanical strength in the Na^+ form [37].

3.2.2. Water uptake

Water uptake values are presented in Table 2. Similar to the IEC, water uptake of the random copolymers increased with DPhHQ content. However, the water uptake of the multiblock copolymer exceeded that of all the random copolymers. This is due to its large hydrophilic sulfonated domains, compared with the randomly distributed hydrophilic domains of the random copolymers. Water uptake in the Na^+ form was measured for 0.017 M (1000 mg/L) and 0.5 M (29220 mg/L) sodium chloride solutions, approximately simulating brackish water and seawater. The change in water uptake between deionised water and 0.017 M NaCl was found to be negligible, while a more obvious decrease was observed for membranes soaked in 0.5 M NaCl. Lower swelling at higher concentrations is expected as a result of a reduced osmotic pressure between the external solution and the solution in the interstitial phase of the polymer matrix [38]. Water uptake at different concentrations is also known to vary depending on the chemical structure of the polymer; for instance, Neosepta CMX water uptake has been shown to be independent of concentration, a result of its high degree of crosslinking [39]. The decrease in swelling of the copolymer membranes with concentration is more pronounced for those possessing larger hydrophilic domains.

While a greater water uptake is known to improve membrane conductivity, it also serves to reduce mechanical stability. Nonetheless, in the swollen state all copolymers were easily handled and showed good dimensional stability due to their hydrophobic domains. The mechanical strength of the random copolymers has previously been published [28]. In the swollen state the Young's modulus of RCP 3 is almost three times as large as that of RCP 1 due to its increased DHDPhS content and lower water uptake.

3.2.3. Membrane conductivity

Membrane conductivity can be seen in Table 3. The difference in conductivity between the different copolymers is similar to that of the water uptake, with the multiblock copolymer yielding the greatest conductivity. The conductivity of RCP 1, RCP 2 and the multiblock copolymer exceeded that of Neosepta CMX, while RCP 3 had a somewhat lower conductivity. Due to the distinct hydrophobic and hydrophilic domains formed by its precursor oligomers, the block copolymer membrane can be classified as microheterogeneous. On the other hand, the random copolymers have a more even distribution of fixed charges and are more homogeneous in nature. This causes homogeneous membranes to typically yield higher conductivities than heterogeneous membranes [30]. In this instance, the microheterogeneity of the block copolymer does not influence the distribution of charges enough to reduce conductivity, but rather increases it due to greater hydrophilicity. The greater water content assists the movement of ions through the polymer matrix and increases conductivity. The conductivity of all copolymers was found to be an order of magnitude lower in the Na^+ form than values previously reported in the protonated form [28], largely due to the high water uptake in the protonated form.

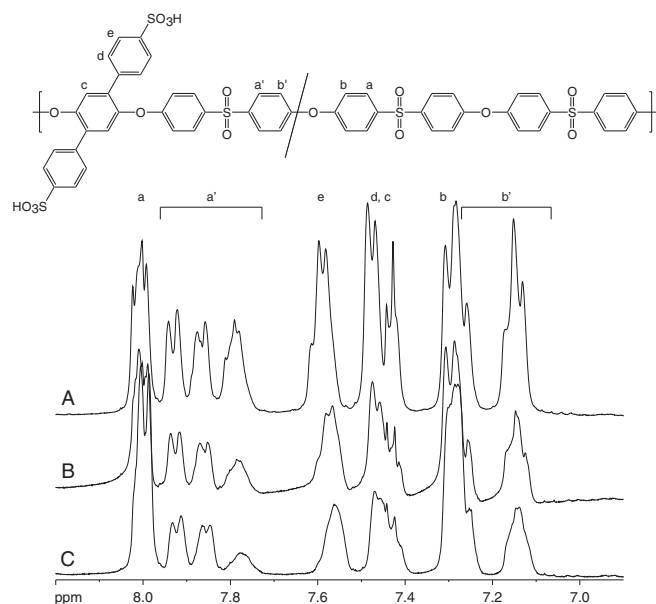


Fig. 2. ^1H NMR spectrum of sulfonated random copolymers A) RCP 1, B) RCP 2 and C) RCP 3.

3.2.4. Transport number

For electro-driven desalination processes, the transport number of a membrane describes the fraction of current that is carried by counter ions. A transport number of one therefore indicates an ideal membrane that is completely permselective, i.e. it completely blocks co-ions and only allows the passage of counter-ions. High transport numbers are desirable as the reduced movement of co-ions improves energy

efficiency. Membrane transport numbers are shown in Table 3. Due to the high level of sulfonation, all membranes exhibited high transport numbers. For RCP 2 and RCP 3, the transport number is close to one comparable with that of Neosepta CMX. Lower transport numbers were observed for RCP 1 and the multiblock copolymer in spite of their larger ion exchange capacities. The drop off in transport number at high IEC values is due these polymers' higher water uptake, which

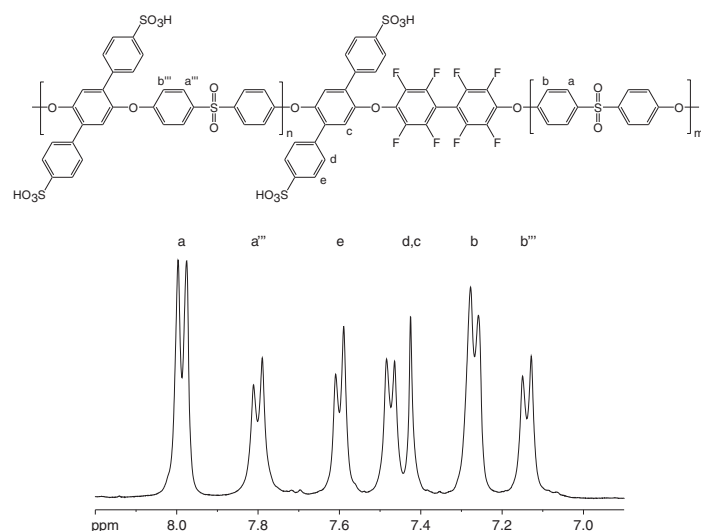


Fig. 3. ^1H NMR spectrum of the sulfonated multiblock copolymer.

M_n oligo-DP-PES (g/mol)	M_n oligo-PES (g/mol)
----------------------------	-------------------------

		H ⁺ form	Na ⁺ form	0.017 M NaCl	0.5 M NaCl
RCP 1	2.05	66.4	49.9	49.1	40.2
RCP 2	1.73	46.8	35.7	35.0	31.4
RCP 3	1.44	30.0	26.4	25.9	21.8
MB	1.91	68.2	54.0	53.5	46.9
Neosepta CMX ^a	1.62	–	18	–	–

^a Data from [40].

dilutes the sulfonated regions in the polymer matrix and allows a greater passage of co-ions. This effect highlights the delicate balance required to produce a polymer that is both highly conductive and selective towards counter ions. The high transport number makes RCP 2 more attractive even with its lower conductivity, while the high conductivity of RCP 1 also make it desirable for commercial applications.

4. Conclusions

Random and multiblock side-chain sulfonated poly(ether sulfone)s have been characterised for electrodialysis and MCDI applications. These membranes have similar ion exchange capacities to commercially available Neosepta CMX due to their high degree of sulfonation and hydrophilic domains, which increase water uptake. Random copolymers with greater DPHQ content had good conductivity and transport numbers approaching one, making them an attractive material for membranes for electro-driven desalination processes. While the multiblock copolymer was found to be highly conductive as a result of its microheterogeneous structure, its hydrophilic nature also reduced its transport number. Coupled with its additional processing steps, this multiblock copolymer is less desirable for commercial applications. Further work is aimed at the application of membranes to test their desalination performance in electro-driven systems.

RCP 1	2.05	15.13	0.94
RCP 2	1.73	8.36	0.99
RCP 3	1.44	3.79	0.98
MB 1	1.91	16.74	0.86
Neosepta CMX	1.62 ^a	5.64 ^{a,b}	0.98 ^c

^a Data from [40].

^b Based on resistance measured in 0.5 M NaCl solution at 25 °C.

^c Data from [41]. Measured by electrophoresis with seawater at a current density of 2 A/dm².

Acknowledgements

The financial support of the National Centre of Excellence in Desalination Australia (NCEDA), the German Academic Exchange Service (DAAD) and the Leibniz Institute of Polymer Research Dresden (IPF) is gratefully acknowledged. The authors would also like to thank Kornelia Schlenstedt and Ute Leuteritz for their assistance in the lab.

References

- [1] T. Sata, Studies on ion exchange membranes with permselectivity for specific ions in electrodialysis, *J. Membr. Sci.* 93 (1994) 117–135.
- [2] M.D. Andelman, G.S. Walker, Charge Barrier Flow-through Capacitor US Patent 6,709,560 82, 2004.
- [3] J. Lee, K. Park, H. Eum, C. Lee, Desalination of a thermal power plant wastewater by membrane capacitive deionization, *Desalination* 196 (2006) 125–134.
- [4] P.M. Biesheuvel, A. van der Wal, Membrane capacitive deionization, *J. Membr. Sci.* 346 (2010) 256–262.
- [5] H. Strathmann, Electrodialysis, a mature technology with a multitude of new applications, *Desalination* 264 (2010) 268–288.
- [6] M. Higa, M. Nishimura, K. Kinoshita, A. Jikihara, Characterization of cation-exchange membranes prepared from poly(vinyl alcohol) and poly(vinyl alcohol-*b*-styrene sulfonic acid), *Int. J. Hydrogen Energy* 37 (2012) 6161–6168.
- [7] N.-S. Kwak, J.S. Koo, T.S. Hwang, E.M. Choi, Synthesis and electrical properties of Na⁺-MAA-MAA cation exchange membranes for membrane capacitive deionization (MCDI), *Desalination* 285 (2012) 138–146.
- [8] M. Andelman, Flow through capacitor basics, *Sep. Purif. Technol.* 80 (2011) 262–269.
- [9] H. Li, L. Zou, Ion-exchange membrane capacitive deionization: a new strategy for brackish water desalination, *Desalination* 275 (2011) 62–66.
- [10] R. Zhao, P.M. Biesheuvel, A. van der Wal, Energy consumption and constant current operation in membrane capacitive deionization, *Energy Environ. Sci.* 5 (2012) 9520.
- [11] R. Zhao, O. Satpradit, H.H. Rijnaarts, P.M. Biesheuvel, A. van der Wal, Optimization of salt adsorption rate in membrane capacitive deionization, *Water Res.* 47 (2013) 1941–1952.
- [12] A. Taeger, C. Vogel, D. Lehmann, D. Jehnichen, H. Komber, J. Meier-Haack, N.A. Ochso, S.P. Nunes, K.V. Peinemann, Ion exchange membranes derived from sulfonated polyaramides, *React. Funct. Polym.* 57 (2003) 77–92.
- [13] J. Meier-Haack, A. Taeger, C. Vogel, K. Schlenstedt, W. Lenk, D. Lehmann, Membranes from sulfonated block copolymers for use in fuel cells, *Sep. Purif. Technol.* 41 (2005) 207–220.
- [14] M.A. Hickner, Ion-containing polymers: new energy & clean water, *Mater. Today* 13 (2010) 34–41.
- [15] J.F. Blanco, Q.T. Nguyen, P. Schaetzel, Novel hydrophilic membrane materials: sulfonated polyethersulfone Carbon, *J. Membr. Sci.* 186 (2001) 267–279.
- [16] M. Kang, Y.-J. Choi, I.-J. Choi, T.-H. Yoon, S.-H. Moon, Electrochemical characterization of sulfonated poly(arylene ether sulfone) (S-PES) cation-exchange membranes, *J. Membr. Sci.* 216 (2003) 39–53.
- [17] H. Dai, R. Guan, C. Li, J. Liu, Development and characterization of sulfonated poly(ether sulfone) for proton exchange membrane materials, *Solid State Ionics* 178 (2007) 339–345.
- [18] S. Feng, Y. Shang, X. Xie, Y. Wang, J. Xu, Synthesis and characterization of crosslinked sulfonated poly(arylene ether sulfone) membranes for DMFC applications, *J. Membr. Sci.* 335 (2009) 13–20.
- [19] C. Klayson, R. Marschall, L. Wang, B.P. Ladewig, G.Q.M. Lu, Synthesis of composite ion-exchange membranes and their electrochemical properties for desalination applications, *J. Mater. Chem.* 20 (2010) 4669.
- [20] C. Klayson, S.-H. Moon, B.P. Ladewig, G.Q.M. Lu, L. Wang, Preparation of porous ion-exchange membranes (IEMs) and their characterizations, *J. Membr. Sci.* 371 (2011) 37–44.
- [21] C. Klayson, S.H. Moon, B.P. Ladewig, G.Q. Lu, L. Wang, The effects of aspect ratio of inorganic fillers on the structure and property of composite ion-exchange membranes, *J. Colloid Interface Sci.* 363 (2011) 431–439.

- [22] H.B. Park, B.D. Freeman, Z.B. Zhang, M. Sankir, J.E. McGrath, Highly chlorine-tolerant polymers for desalination, *Angew. Chem. Int. Ed. Engl.* 47 (2008) 6019–6024.
- [23] M. Paul, H.B. Park, B.D. Freeman, A. Roy, J.E. McGrath, J.S. Riffle, Synthesis and crosslinking of partially disulfonated poly(arylene ether sulfone) random copolymers as candidates for chlorine resistant reverse osmosis membranes, *Polymer* 49 (2008) 2243–2252.
- [24] W. Xie, H.B. Park, J. Cook, C.H. Lee, G. Byun, B.D. Freeman, J.E. McGrath, Advances in membrane materials: desalination membranes based on directly copolymerized disulfonated poly(arylene ether sulfone) random copolymers, *Water Sci. Technol.* 61 (2010) 619–624.
- [25] W. Xie, J. Cook, H.B. Park, B.D. Freeman, C.H. Lee, J.E. McGrath, Fundamental salt and water transport properties in directly copolymerized disulfonated poly(arylene ether sulfone) random copolymers, *Polymer* 52 (2011) 2032–2043.
- [26] W. Xie, G.M. Geise, B.D. Freeman, C.H. Lee, J.E. McGrath, Influence of processing history on water and salt transport properties of disulfonated polysulfone random copolymers, *Polymer* 53 (2012) 1581–1592.
- [27] W.L. Harrison, Synthesis and Characterization of Sulfonated Poly(Arylene Ether Sulfone) Copolymers via Direct Copolymerization: Candidates for Proton Exchange Membrane Fuel Cells, Virginia Polytechnic Institute and State University, 2002.
- [28] C. Vogel, H. Komber, A. Quetschke, W. Butwilowski, A. Pötschke, K. Schlenstedt, J. Meier-Haack, Side-chain sulfonated random and multiblock poly(ether sulfone)s for PEM applications, *React. Funct. Polym.* 71 (2011) 828–842.
- [29] C. Iojoiu, M. Maréchal, F. Chabert, J.-Y. Sanchez, Mastering sulfonation of aromatic polysulfones: crucial for membranes for fuel cell application, *Fuel Cells* 5 (2005) 344–354.
- [30] H. Strathmann, Ion-exchange Membrane Separation Processes, Elsevier, Amsterdam, 2004.
- [31] R.S.L. Yee, R.A. Rozendal, K. Zhang, B.P. Ladewig, Cost effective cation exchange membranes: a review, *Chem. Eng. Res. Des.* 70 (2011) 950–959.
- [32] F.G. Wilhelm, I. Pünt, N.F.A. van der Vegt, H. Strathmann, M. Wessling, Cation permeable membranes from blends of sulfonated poly(ether ether ketone) and poly(ether sulfone), *J. Membr. Sci.* 199 (2002) 167–176.
- [33] C. Klayson, B.P. Ladewig, G.Q.M. Lu, L. Wang, Preparation and characterization of sulfonated polyethersulfone for cation-exchange membranes, *J. Membr. Sci.* 368 (2011) 48–53.
- [34] S. Tian, Y. Meng, A.S. Hay, Membranes from poly(aryl ether)-based ionomers containing randomly distributed nanoclusters of 6 or 12 sulfonic acid groups, *Macromolecules* 42 (2009) 1153–1160.
- [35] S. Tian, Y. Meng, A.S. Hay, Membranes from poly(aryl ether)-based ionomers containing multiblock segments of randomly distributed nanoclusters of 18 sulfonic acid groups, *J. Polymer Sci., Part A: Polymer Chem.* 47 (2009) 4762–4773.
- [36] B. Liu, G.P. Robertson, D.-S. Kim, X. Sun, Z. Jiang, M.D. Guiver, Enhanced thermo-oxidative stability of sulfophenylated poly(ether sulfone)s, *Polymer* 51 (2010) 403–413.
- [37] ASTOM Corporation, in, 2004.
- [38] L.X. Tuan, C. Buess-Herman, Study of water content and microheterogeneity of CMS cation exchange membrane, *Chem. Phys. Lett.* 434 (2007) 49–55.
- [39] P. Długołęcki, B. Anet, S.J. Metz, K. Nijmeijer, M. Wessling, Transport limitations in ion exchange membranes at low salt concentrations, *J. Membr. Sci.* 346 (2010) 163–171.
- [40] P. Długołęcki, K. Nijmeijer, S. Metz, M. Wessling, Current status of ion exchange membranes for power generation from salinity gradients, *J. Membr. Sci.* 319 (2008) 214–222.
- [41] J.H. Choi, H.J. Lee, S.H. Moon, Effects of electrolytes on the transport phenomena in a cation-exchange membrane, *J. Colloid Interface Sci.* 238 (2001) 188–195.



Contents lists available at ScienceDirect

Desalination

journal homepage: www.elsevier.com/locate/desal

Cation exchange copolymer enhanced electrosorption

Benjamin M. Asquith^a, Jochen Meier-Haack^b, Bradley P. Ladewig^{a,*}^a Department of Chemical Engineering, Monash University, VIC 3800, Australia^b Leibniz Institute of Polymer Research Dresden, Hohe Strasse 6, 01069 Dresden, Germany

HIGHLIGHTS

- Activated carbon electrodes were coated with sulfonated random copolymers.
- Coating layer resistance did not adversely affect the build up of charge.
- Electrode capacitance was enhanced by polymers with a high ion-exchange capacity.
- Coating thickness influences the resistance of the carbon electrodes.

ARTICLE INFO

Article history:

Received 18 February 2014

Received in revised form 18 April 2014

Accepted 19 April 2014

Available online 13 May 2014

Keywords:

Capacitive deionisation

Cation-exchange polymer

Activated carbon

Cyclic voltammetry

Electrochemical impedance spectroscopy

ABSTRACT

In this study the effects of cation exchange polymer coatings on activated carbon electrodes for capacitive deionization (CDI) were investigated. Electrodes were fabricated from activated carbon, graphite and PVDF, then coated with sulfonated poly(arylene ether sulfone) random copolymers. Additional resistance was created by the coating layer, however compared with the uncoated electrodes the coatings did not significantly affect the rate of charge build up. Electrochemical impedance spectroscopy (EIS) results indicated that both capacitance and charging resistance are influenced by polymer conductivity, water uptake and the thickness of the coating layer. The results also indicated that in addition to functioning as a superficial charge barrier, copolymer that penetrates into the carbon substrate might offset the loss in capacitance caused by PVDF binder pore blockage.

© 2014 Elsevier B.V. All rights reserved.

1. Introduction

Capacitive deionization (CDI) is a developing desalination technology that can be used for the highly efficient desalination of brackish water, the production of ultra pure water, water softening and the removal of other charged impurities from water streams [1–3]. It is an electrosorption process that relies on the formation of an electrical double layer on a porous, polarizable electrode. This buildup of charge creates a similar buildup of oppositely charged ions from an electrolyte solution at the electrode–solution interface, thereby removing salt ions from solution.

Activated carbon is an attractive material for electrosorption due to its relatively low cost and large specific surface area, typically in the order of 1000–2000 m²/g, and numerous studies have focused on its use for CDI [4–12]. Unfortunately the potential for activated carbon to adsorb salt ions from solution is hindered by its microporous nature, low conductivity, and high electrical and mass transfer resistances [13]. Furthermore, it typically exhibits a randomly arranged pore

network that may hinder ion movement and thus sorption [14]. As such, research efforts to improve its electrosorption capacity and efficiency are ongoing, with techniques such as surface modification and the incorporation of membranes. The modification of the activated carbon surface has been shown to improve electrosorption efficiency by neutralising polar surface charges thereby reducing unwanted physical adsorption. Studies have shown that enhanced performance can be achieved through chemical surface modification of activated carbons with titanium [15,16], titanium dioxide nanoparticles [5], potassium hydroxide and nitric acid [17,18], and zinc oxide nanorods [19].

In addition to the drawbacks of activated carbon, an inherent disadvantage of the CDI process is that during the adsorption of counter-ions, a simultaneous desorption of co-ions occurs. Thus, for each electron passing through the external circuit, less than one salt molecule is adsorbed [20–23]. To restrict this co-ion movement during adsorption, ion exchange membranes may be placed in front of each electrode. This is known as membrane capacitive deionization (MCDI), and was first introduced by Andelman and Walker in 2004 [24]. It has been shown to significantly increase salt adsorption and energy efficiency by improving the efficiency of counter-ion adsorption [25–30]. Ion exchange membranes also allow for the application of a reverse potential

* <http://dx.doi.org/10.1016/j.desal.2014.04.027>

0011-9164/© 2014 Elsevier B.V. All rights reserved.

during the desorption phase, allowing for a greater depletion of ions at the electrode and thus greater adsorption capacity in the following cycles [31].

Commercial cation exchange membranes used for MCDI include Neosepta CM-1 [25] and Neosepta CMX [32–34]. These membranes are poly(vinyl chloride) based with styrene/divinylbenzene copolymers and are designed for desalination purposes with high permselectivity, low electrical resistance, and high mechanical stability [35]. However, the use of flat sheet membranes creates additional resistance between the membrane and the electrode. One alternative approach to reduce this resistance involved the spraying of carbon cloth electrodes with bromomethylated poly(2, 6-dimethyl-1,4-phenylene oxide) (BPPO) solution, which was subsequently sulfonated with sulfuric acid to attach functional groups to the polymer [34]. Another approach by Kim et al. [36] saw the coating of carbon electrodes with poly(vinyl alcohol), which was sulfonated and crosslinked by using sulfosuccinic acid. This technique yielded ion-exchange coatings with area specific resistances lower than those of commercial membranes.

The poly(arylene ether sulfone) copolymers used in this study are characterised by having high conductivity and mechanical stability. Similar ion-exchange copolymers have been developed for pressure-driven desalination membranes and for fuel cell applications [37–44], but few studies have focused on their application for CDI [45]. In this work these cation exchange polymers have been applied as thin membrane coatings to activated carbon electrodes in order to enhance electrosorption performance. The characteristics of the coated electrodes are compared to uncoated electrodes, and correlations between the polymer properties and electrode performance are highlighted. In particular, the influence of conductivity and water uptake on resistance and capacitance is discussed.

2. Experimental

2.1. Materials

4,4'-difluorodiphenyl sulfone was purchased from FuMA-Tech GmbH (Germany) and was purified by vacuum distillation. 4,4'-dihydroxydiphenyl sulfone (DHDPhS), N-methyl-2-pyrrolidone (NMP), poly(vinylidene fluoride) (PVDF), activated carbon and graphite powder were purchased from Sigma-Aldrich (Australia). Concentrated sulfuric acid (min. 96%) was obtained from Acros (Belgium). 2,5-diphenylhydroquinone (DPhHQ) was prepared as per the procedure described by Vogel et al. [43].

2.2. Polymer synthesis and sulfonation

Three random copolymers were synthesised by using the silyl-method as per the procedure previously described [43,45]. The ratio of the monomers in the random copolymers was varied such that the monomer ratio of DPhHQ to DHDPhS was 6:4 for RCP 1, 5:5 for RCP 2 and 4:6 for RCP 3. All polymers were sulfonated by using concentrated

sulfuric acid (96–98%). The molecular structure of the random copolymers can be seen in Fig. 1.

2.3. Electrode preparation

Using NMP as a solvent, a slurry consisting of activated charcoal, graphite powder as conductive material and PVDF as a binder was prepared such that the final (dry) content of the electrode was 75 wt.% activated charcoal, 15 wt.% graphite and 10 wt.% PVDF. The slurry was coated onto graphite sheets to a thickness of 200 μm using a doctor blade and dried in a vacuum oven for 24 h at 120° to completely remove the solvent.

Polymer coated electrodes were prepared by first dissolving the sulfonated polymers in NMP such that the concentration was 15 wt.%. The solutions were cast onto the carbon electrodes and dried under vacuum for 2 h at 60 °C, then for a further 24 h at 80 °C. The samples were rinsed with distilled water to remove residual NMP, soaked in 0.5 M NaCl to convert the polymer to the Na^+ form, then rinsed again with water to remove excess NaCl from the polymer matrix.

2.4. Electrode characterisation

Specific surface area and pore size distribution were measured on a Micrometrics ASAP 2020 Physisorption Analyser using N_2 as the adsorbate at 77 K. FTIR spectra were collected by using a PerkinElmer Spectra 100 to confirm the chemical structure of the cation exchange polymer coatings. Cyclic voltammetry experiments were performed by using a Biologic VSP potentiostat connected to a three-electrode electrochemical cell. The working electrode was the carbon material to be tested with an exposed surface area of 0.785 cm^2 . The reference electrode was a saturated Ag/AgCl KCl electrode, and the counter electrode was a platinum mesh electrode. Electrochemical Impedance Spectroscopy (EIS) was performed by using the same three-electrode cell over the frequency range 10 mHz to 1 MHz, with an applied voltage amplitude of 10 mV.

3. Results & discussion

3.1. Activated carbon surface area & pore size distribution

The isotherm obtained for the activated carbon is shown in Fig. 2. The large increase in adsorbed gas at low relative pressure is a typical Type I isotherm for a microporous solid [46]. The pore size distribution for the activated carbon, also shown in Fig. 2, confirms the microporous nature of the carbon, with a single peak at 0.7–0.8 nm. The gradual uptake from a relative pressure of around 0.2 indicates some mesopores, although as seen in the pore size distribution, these do not contribute greatly to the specific surface area of the carbon.

Due to the microporous nature of the carbon, the BET specific surface area was calculated by using data from the relative pressure range 0–0.08, such that the value $Q(P_0-P)$ increased with relative pressure P/P_0 (where Q is the volume of gas adsorbed, P is the measured pressure and P_0 is the

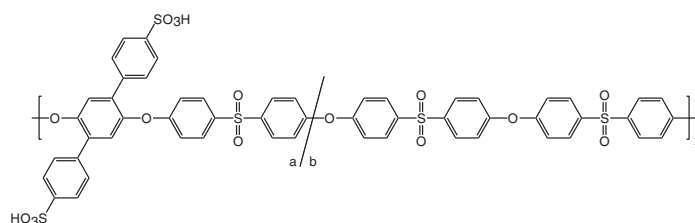


Fig. 1. Repeating unit of the random copolymer. RCP 1: a = 6, b = 4; RCP 2: a = 5, b = 5; RCP 3: a = 4, b = 6.

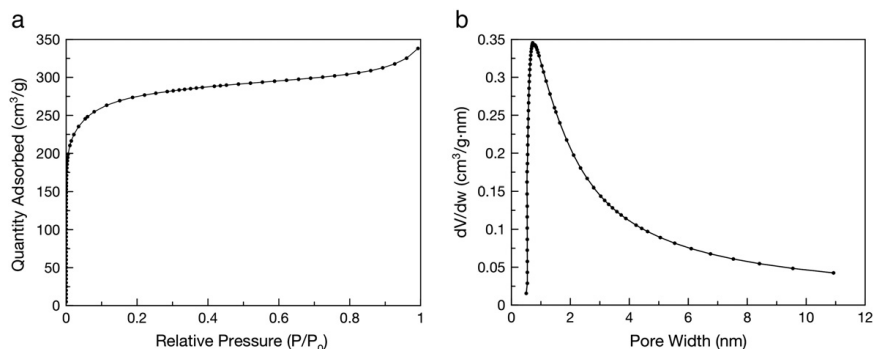


Fig. 2. a) Activated carbon adsorption isotherm and b) pore size distribution, measured by physical adsorption.

saturation pressure) [47]. The specific surface area was calculated to be 1043 m²/g. The conductive graphite filler was calculated to have a specific surface area of 21.1 m²/g, and thus is considered to have negligible impact on the adsorption of ions.

3.2. Electrode morphology

The properties of the random copolymers are presented in Table 1. All electrodes were tested for hydro- and thermal stability by placing them in water at 80 °C for 6 h. No degradation was observed, no carbon was removed from the surface of the uncoated electrodes, and all polymers adhered strongly to the carbon such that they were not removed after water treatment. Furthermore, all electrodes were stored in water at room temperature before use, with no loss of carbon or polymer observed. Due to the adhesion of the coating layer to the carbon electrode, the polymer acts as a pseudo-binder, providing additional mechanical strength.

Fig. 3 shows SEM images of both uncoated and coated carbon electrodes. Discrete carbon and graphite powder particles are observed in Fig. 3a, while in Fig. 3b the polymeric coating is seen to cover the entire electrode, analogous to placing a dense phase ion exchange membrane directly against the carbon electrode.

FTIR analysis was used to confirm successful coating of carbon electrodes by comparison with uncoated carbon electrodes and flat sheet membranes cast from the same copolymers. Fig. 4 shows the FTIR spectra of uncoated electrodes (a), coated electrodes (c–e) and a flat sheet membrane cast from RCP 1 (b). As the same precursor monomers are used for each of the random copolymers, their molecular structures differ only in the ratio of the statistically distributed monomers. Hence, each random copolymer membrane spectrum exhibited the same peaks.

C=C stretching vibrations from aromatic rings are represented by peaks at 1580 cm⁻¹ and 1485 cm⁻¹. Peaks at 1300 cm⁻¹ and 1146 cm⁻¹ are S=O stretching vibrations from the sulfone group, while the small peak at approximately 1170 cm⁻¹ indicates an S=O stretching vibration on the sulfonated side-chains. Peaks below

1000 cm⁻¹ are attributed to the S–O stretch of the sulfonate group and C–H bending on the aromatic ring. The matching spectra of the coated electrodes for all three random copolymers, in addition to the distinct difference between the coated and uncoated electrodes, confirms the successful application of the polymer onto the carbon substrate.

3.3. Electrochemical analysis – Cyclic voltammetry

Cyclic voltammetry was used to measure specific capacitance. From the measured current, the specific capacitance of the activated carbon, C (F/g activated carbon), was calculated by using the following equation [48]:

$$C = \frac{i}{mv}$$

Where *i* is the current (A), *m* is the mass of carbon (g) and *v* is the scan rate (V/s). The capacitance of uncoated electrodes as a function of potential measured at scan rates of 5 mV/s and 20 mV/s can be seen in Fig. 5. At both the fast and slow scan rates, a rectangular shape is observed, indicating the formation of an electrical double layer at the carbon-solution interface and the successful adsorption/desorption of ions. Due to the high microporosity of the carbon, a greater capacitance is observed at 5 mV/s, as the slower scan rate allows greater time for ion transport into the micropores.

A comparison of the capacitance of uncoated electrodes and electrodes coated with the random copolymers at scan rates of 5 mV/s and 20 mV/s can be seen in Fig. 6. At 20 mV/s (Fig. 6a, c and e) during the forward scan there is no enhancement in capacitance compared to the uncoated samples. However, during the reverse scan at potentials lower than approximately 200 mV an appreciable difference in capacitance between the uncoated and coated samples is observed. Similarly, for both the forward and reverse scans at 5 mV/s (Fig. 6b, d and f), the build-up of charge on the coated samples is seen to be better than the uncoated samples. This improved performance is attributed to a greater expulsion of cations during the forward scan and restricted anion movement during the reverse scan as the electrode becomes negatively charged.

For electrodes coated with RCP 2 and RCP 3 (Fig. 6c–f), slower increases in capacitance compared to the uncoated samples are observed at both scan rates when the scan direction changes. Due to the increased resistance provided by the coating layer, this effect is more pronounced at 20 mV/s when there is less time for the ions to diffuse through the polymer matrix. At 5 mV/s the ions have more time to diffuse through the polymer and into the pores of the activated carbon, thus reducing the effect of the additional coating resistance. Additionally, at 5 mV/s

Table 1
Polymer coating properties. Data from [45].

Polymer coating	IEC (mmol/g)	Water uptake (%) [*]	Conductivity (mS/cm) ^{**}	Contact angle (degrees)	Transport number
RCP 1	2.05	49.9	15.13	30.3	.94
RCP 2	1.73	35.7	8.36	38.2	.99
RCP 3	1.44	26.4	3.79	46.1	.98

^{*} Measured in the Na⁺ form.

^{**} In-plane conductivity.

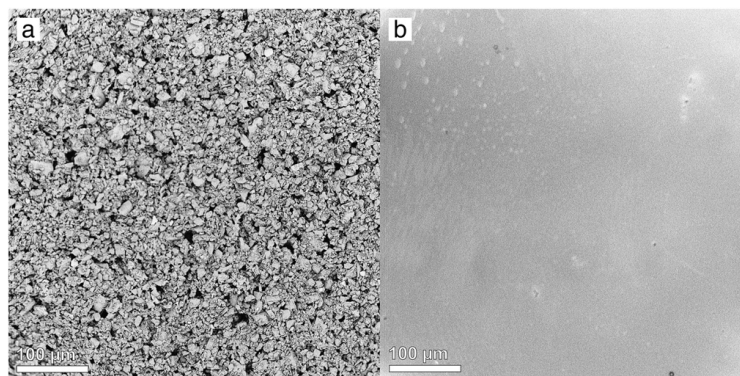


Fig. 3. SEM images of a) uncoated electrode surface and b) coated electrode surface.

the transient responses of the coated electrodes are different for the forward and reverse scans, with a slower change in capacitance at the beginning of the reverse scan. This is thought to be a result of the expulsion of anions from the pores through the cation exchange polymer matrix, which would cause additional resistance to the adsorption process.

As shown in Fig. 6a and b, the response of electrodes coated with RCP 1 to a change in scan direction is seen to be faster when compared with electrodes coated with polymers RCP 2 and RCP 3. This may be attributed to the high ion-exchange capacity and water uptake of RCP 1 compared with the other copolymers. Surprisingly, this response is also faster than that of the uncoated sample. This may be due to a high PVDF content in the substrate carbon electrode, where the PVDF behaves like a partial, hydrophobic membrane layer that blocks pores, creating additional hindrance to the adsorption/desorption process. Although the polymer coating increases resistance, copolymer penetration into the voids of the carbon substrate may simultaneously reduce the charging resistance by providing better access to the pores due to its hydrophilic properties. The solubility of the PVDF binder in NMP, which is used as a solvent for the polymer coatings, may have also resulted in a partial dissolution and re-drying of the PVDF binder during the polymer coating process, effectively re-casting some of the carbon substrate with both PVDF and random copolymer as a binder.

3.4. Electrochemical analysis – Electrochemical impedance spectroscopy

Electrochemical impedance spectroscopy was used to further examine the performance of the electrodes and to measure the charging resistance. The resistance and conductivity of the coating layers were calculated based on the real impedance at the high-frequency intercept of the Nyquist plot. The resistances of the coatings can be seen in Table 2. They have not been normalised to account for the variable thickness of the coatings and as such they do not decrease with increasing IEC. Importantly, the resistances of the RCP 1 and RCP 2 coatings are comparable to Neosepta CMX, which has a resistance of $3.0 \Omega \cdot \text{cm}^2$ [35]. The conductivity of the coatings shown in Table 2 has been calculated based on thickness, and thus is seen to increase with increasing IEC. These values differ to those reported in Table 1 due to the methods of testing; the polymer coating conductivity was measured normal to its exposed surface (through-plane conductivity), while previous measurements with a four-point probe [45] were parallel to the surface (in-plane conductivity), which is known to yield different values.

Electrode charging resistance versus frequency is shown in Fig. 7. This is the resistance to ion transport through the polymer matrix and into the carbon pores, and is calculated as the real impedance minus the ohmic resistance at each frequency. For the uncoated sample, the

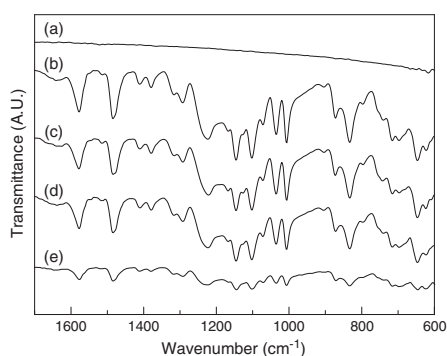


Fig. 4. ATR-FTIR spectra of (a) uncoated carbon electrode, (b) stand-alone membrane, (c) RCP 1 coated electrode, (d) RCP 2 coated electrode and (e) RCP 3 coated electrode.

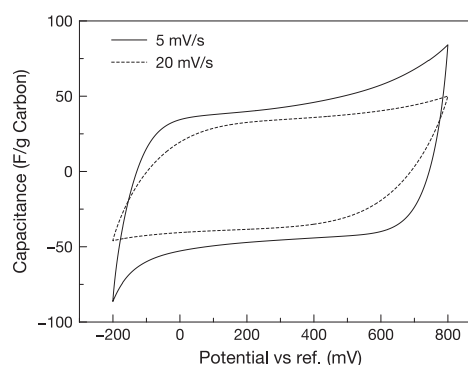


Fig. 5. Specific capacitance of uncoated electrodes measured in 0.5 M NaCl at scan rates of 5 mV/s (solid line) and 20 mV/s (dotted line).

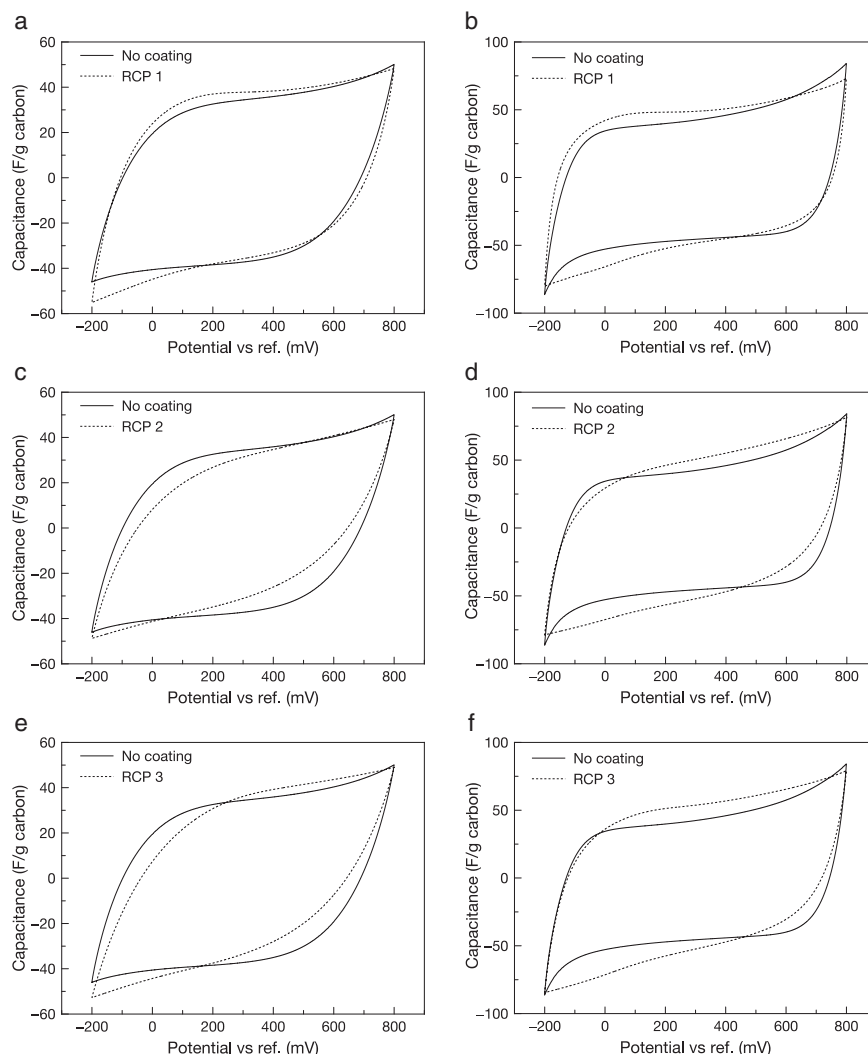


Fig. 6. Specific capacitance of coated electrodes measured in 0.5 M NaCl: a) RCP 1 coating, scan rate = 20 mV/s; b) RCP 1 coating, scan rate = 5 mV/s; c) RCP 2 coating, scan rate = 20 mV/s; d) RCP 2 coating, scan rate = 5 mV/s; e) RCP 3 coating, scan rate = 20 mV/s; f) RCP 3 coating, scan rate = 5 mV/s.

rise in charging resistance at higher frequency compared to the coated samples is likely due to the high PVDF content, which as described above blocks pores and creates additional hindrance to ion adsorption.

Table 2
Electrochemical properties of the coating layers and capacitance of coated and uncoated electrodes, measured using EIS.

Coating	IEC (mmol/g)	Thickness (μm)	Resistance (Ωcm^2)	Conductivity (mS/cm)	Capacitance (F/g carbon)
RCP 1	2.05	82	3.31	2.48	37.74
RCP 2	1.73	46	2.37	1.94	30.07
RCP 3	1.44	59	9.86	0.60	25.00
No coating	–	–	–	–	32.56

For the coated samples, the onset of charging resistance occurs at higher frequencies for polymer coatings with greater resistance. Although the RCP 1 coated sample has a higher measured resistance and greater thickness than the RCP 2 coated sample, the charging resistance is similar. This result suggests that the higher conductivity and greater water uptake of RCP 1 reduces hindrance to ion transport.

As the frequency approaches 10 mHz, the charging resistance climbs sharply for all coated samples. Here, the impedance response is dominated by the resistance of the coating rather than the capacitive behaviour of the carbon substrate. In light of this, while coating area resistances are comparable to those of commercial membranes, polymer layer thickness must still be optimised to minimise charging resistance while still adequately enhancing electrosorption capacitance.

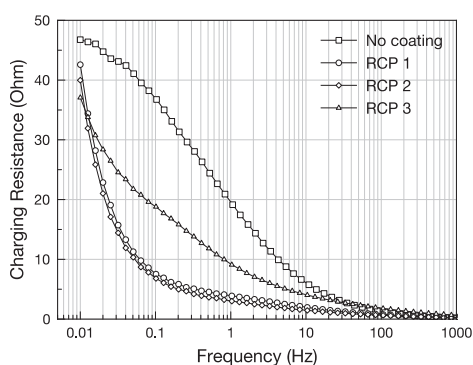


Fig. 7. Charging resistance versus frequency for uncoated and coated electrodes.

Assuming ideal capacitor behaviour, the capacitance of the electrode, C (F) can be derived from the imaginary part of the impedance spectra based on the formula [49]:

$$C = \frac{1}{\omega Z''}$$

Where ω is the frequency and Z'' is the imaginary impedance. The calculated capacitance versus frequency is plotted in Fig. 8, and the capacitance calculated at 10 mHz can be seen in Table 2. The capacitance of the coated samples is seen to increase with IEC, while the influence of the coating layer resistance seems to be less significant. The increased capacitance as a function of IEC is likely a result of greater water uptake, which reduces resistance to ion transport through the swollen hydrophilic channels of the polymer, encouraging greater pore access. Furthermore, the higher water uptake promotes a region of concentrated electrolyte storage in the polymer layer. As the charge buildup that results from electrical double layer formation is known to increase with concentration, increased electrolyte concentration directly adjacent to the carbon electrode in the polymer can increase its capacitance.

4. Conclusions

Activated carbon electrodes coated with cation exchange random copolymers were successfully fabricated, with the coating layer strongly adhering to the carbon. Cyclic voltammetry results have shown that in

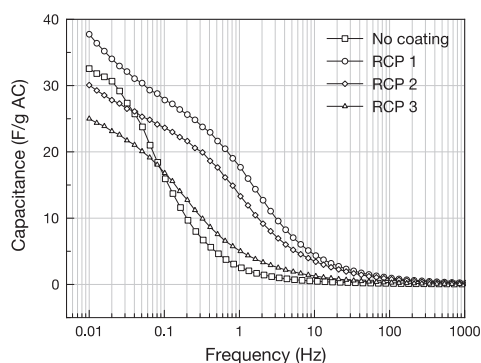


Fig. 8. Capacitance versus frequency for uncoated and coated electrodes.

the case of the most conductive coating, charge is seen to build up at a faster rate than uncoated samples, despite the additional resistance of the coating. EIS results indicate that the charging resistance and capacitance of the coated electrodes are influenced by both conductivity and water uptake. Since the conductivity and water uptake are strong functions of IEC, suitable polymer design to maximise IEC while retaining mechanical stability is a crucial parameter in enhancing the performance of activated carbon electrodes. In light of this, RCP 1 is seen to appreciably enhance the electrosorption performance of the activated carbon electrodes.

The polymer coatings are seen to influence the resistance of the carbon electrodes, causing a sharp rise in charging resistance at low frequencies during EIS testing. The optimisation of coating thickness therefore becomes important in reducing the additional resistance created by the coating layer. Further work will require a detailed EIS investigation into these systems, in particular systematically varying the polymer coating thickness, so that an EIS model can be developed and fitted to the data with a high degree of confidence. This will enable the elucidation of the relative contributions of the resistance and capacitive elements of the EIS spectra.

A high PVDF binder content can also reduce capacitance and increase charging resistance, slowing the build up of ions at the electrode-solution interface. However, the coating of electrodes with an ion exchange polymer may offset this phenomenon, possibly through copolymer penetration into the carbon substrate in addition to acting as a charge barrier layer.

These results indicate that the random copolymer coatings, although increasing overall resistance, can be used to improve the ion transport into the pores of the electrodes.

Acknowledgements

The authors acknowledge the financial support of the National Centre of Excellence in Desalination Australia, which is funded by the Australian Government through the Water for the Future Initiative.

References

- [1] J.C. Farmer, Method and Apparatus for Capacitive Deionization, Electrochemical Purification, and Regeneration of Electrodes, 1995.
- [2] M.A. Anderson, A.L. Cudero, J. Palma, Capacitive deionization as an electrochemical means of saving energy and delivering clean water. Comparison to present desalination practices: will it compete? *Electrochim. Acta* 55 (2010) 3845–3856.
- [3] Australian Desalination Research Roadmap, National Centre of Excellence in Desalination Australia, 2012.
- [4] K.-K. Park, J.-B. Lee, P.-Y. Park, S.-W. Yoon, J.-S. Moon, H.-M. Eum, C.-W. Lee, Development of a carbon sheet electrode for electrosorption desalination, *Desalination* 206 (2007) 86–91.
- [5] L. Zou, G. Morris, D. Qi, Using activated carbon electrode in electrosorptive deionisation of brackish water, *Desalination* 225 (2008) 329–340.
- [6] J. Lee, K. Park, S. Yoon, P. Park, K. Park, C. Lee, Desalination performance of a carbon-based composite electrode, *Desalination* 237 (2009) 155–161.
- [7] J.H. Choi, Fabrication of a carbon electrode using activated carbon powder and application to the capacitive deionization process, *Sep. Purif. Technol.* 70 (2010) 362–366.
- [8] C.-H. Hou, J.-F. Huang, H.-R. Lin, B.-Y. Wang, Preparation of activated carbon sheet electrode assisted electrosorption process, *J. Taiwan Inst. Chem. Eng.* 43 (2012) 473–479.
- [9] G. Wang, C. Pan, L. Wang, Q. Dong, C. Yu, Z. Zhao, J. Qiu, Activated carbon nanofiber webs made by electrospinning for capacitive deionization, *Electrochim. Acta* 69 (2012) 65–70.
- [10] B.-H. Park, Y.-J. Kim, J.-S. Park, J. Choi, Capacitive deionization using a carbon electrode prepared with water-soluble poly(vinyl alcohol) binder, *J. Ind. Eng. Chem.* 17 (2011) 717–722.
- [11] I. Villar, S. Roldan, V. Ruiz, M. Granda, C. Blanco, R. Menéndez, R. Santamaría, Capacitive deionization of NaCl solutions with modified activated carbon electrodes†, *Energy Fuels* 24 (2010) 3329–3333.
- [12] S. Nadakatti, M. Tendulkar, M. Kadam, Use of mesoporous conductive carbon black to enhance performance of activated carbon electrodes in capacitive deionization technology, *Desalination* 268 (2011) 182–188.
- [13] X.Z. Wang, M.G. Li, Y.W. Chen, R.M. Cheng, S.M. Huang, L.K. Pan, Z. Sun, Electrosorption of ions from aqueous solutions with carbon nanotubes and nanofibers composite film electrodes, *Appl. Phys. Lett.* 89 (2006) 053127.
- [14] L. Zou, Developing nano-structured carbon electrodes for capacitive brackish water desalination, in: R.Y. Ning (Ed.), *Expanding Issues in Desalination*, InTech, 2011.

- [15] M.-W. Ryoo, J.-H. Kim, G. Seo, Role of titania incorporated on activated carbon cloth for capacitive deionization of NaCl solution, *J. Colloid Interface Sci.* 264 (2003) 414–419.
- [16] M.-W. Ryoo, G. Seo, Improvement in capacitive deionization function of activated carbon cloth by titania modification, *Water Res.* 37 (2003) 1527–1534.
- [17] H.-J. Ahn, J.-H. Lee, Y. Jeong, J.-H. Lee, C.-S. Chi, H.-J. Oh, Nanostructured carbon cloth electrode for desalination from aqueous solutions, *Mater. Sci. Eng. A* 449–451 (2007) 841–845.
- [18] H. Oh, J. Lee, H. Ahn, Y. Jeong, Y. Kim, C. Chi, Nanoporous activated carbon cloth for capacitive deionization of aqueous solution, *Thin Solid Films* 515 (2006) 220–225.
- [19] M.T.Z. Myint, J. Dutta, Fabrication of zinc oxide nanorods modified activated carbon cloth electrode for desalination of brackish water using capacitive deionization approach, *Desalination* 305 (2012) 24–30.
- [20] M.Z. Bazant, K. Thornton, A. Ajdari, Diffuse-charge dynamics in electrochemical systems, *Phys. Rev. E* 70 (2004) 021506.
- [21] P.M. Biesheuvel, Thermodynamic cycle analysis for capacitive deionization, *J. Colloid Interface Sci.* 332 (2009) 258–264.
- [22] A.M. Johnson, J. Newman, Desalting by means of porous carbon electrodes, *J. Electrochem. Soc.* 118 (1971) 510–517.
- [23] Y. Oren, A. Soffer, Water desalting by means of electrochemical parametric pumping. I. The equilibrium properties of a batch unit cell, *J. Appl. Electrochem.* 13 (1983) 473–487.
- [24] M.D. Andelman, G.S. Walker, Charge Barrier Flow-through Capacitor, in, United States, 2004.
- [25] J. Lee, K. Park, H. Eum, C. Lee, Desalination of a thermal power plant wastewater by membrane capacitive deionization, *Desalination* 196 (2006) 125–134.
- [26] N.-S. Kwak, J.S. Koo, T.S. Hwang, E.M. Choi, Synthesis and electrical properties of NaSS-MAA-MMA cation exchange membranes for membrane capacitive deionization (MCDI), *Desalination* 285 (2012) 138–146.
- [27] M. Andelman, Flow through capacitor basics, *Sep. Purif. Technol.* 80 (2011) 262–269.
- [28] H. Li, L. Zou, Ion-exchange membrane capacitive deionization: a new strategy for brackish water desalination, *Desalination* 275 (2011) 62–66.
- [29] R. Zhao, P.M. Biesheuvel, A. van der Wal, Energy consumption and constant current operation in membrane capacitive deionization, *Energy Environ. Sci.* 5 (2012) 9520.
- [30] R. Zhao, O. Satpradit, H.H. Rijnaarts, P.M. Biesheuvel, A. van der Wal, Optimization of salt adsorption rate in membrane capacitive deionization, *Water Res.* 47 (2013) 1941–1952.
- [31] P.M. Biesheuvel, A. van der Wal, Membrane capacitive deionization, *J. Membr. Sci.* 346 (2010) 256–262.
- [32] Y.J. Kim, J.H. Choi, Enhanced desalination efficiency in capacitive deionization with an ion-selective membrane, *Sep. Purif. Technol.* 71 (2010) 70–75.
- [33] Y.J. Kim, J. Hur, W. Bae, J.H. Choi, Desalination of brackish water containing oil compound by capacitive deionization process, *Desalination* 253 (2010) 119–123.
- [34] J.Y. Lee, S.J. Seo, S.H. Yun, S.H. Moon, Preparation of ion exchanger layered electrodes for advanced membrane capacitive deionization (MCDI), *Water Res.* 45 (2011) 5375–5380.
- [35] ASTOM Corporation, Neosepta, <http://www.astom-corp.jp/en/en-main2-neosepta.html> 2004.
- [36] J.S. Kim, J.H. Choi, Fabrication and characterization of a carbon electrode coated with cation-exchange polymer for the membrane capacitive deionization applications, *J. Membr. Sci.* 355 (2010) 85–90.
- [37] H.B. Park, B.D. Freeman, Z.B. Zhang, M. Sankir, J.E. McGrath, Highly chlorine-tolerant polymers for desalination, *Angew. Chem. Int. Ed. Engl.* 47 (2008) 6019–6024.
- [38] M. Paul, H.B. Park, B.D. Freeman, A. Roy, J.E. McGrath, J.S. Riffle, Synthesis and crosslinking of partially disulfonated poly(arylene ether sulfone) random copolymers as candidates for chlorine resistant reverse osmosis membranes, *Polymer* 49 (2008) 2243–2252.
- [39] W. Xie, H.B. Park, J. Cook, C.H. Lee, G. Byun, B.D. Freeman, J.E. McGrath, Advances in membrane materials: desalination membranes based on directly copolymerized disulfonated poly(arylene ether sulfone) random copolymers, *Water Sci. Technol.* 61 (2010) 619–624.
- [40] W. Xie, J. Cook, H.B. Park, B.D. Freeman, C.H. Lee, J.E. McGrath, Fundamental salt and water transport properties in directly copolymerized disulfonated poly(arylene ether sulfone) random copolymers, *Polymer* 52 (2011) 2032–2043.
- [41] W. Xie, G.M. Geise, B.D. Freeman, C.H. Lee, J.E. McGrath, Influence of processing history on water and salt transport properties of disulfonated polysulfone random copolymers, *Polymer* 53 (2012) 1581–1592.
- [42] W.L. Harrison, Synthesis and Characterization of Sulfonated poly(arylene ether sulfone) Copolymers via Direct Copolymerization: Candidates for Proton Exchange Membrane Fuel Cells, in, Virginia Polytechnic Institute and State University, 2002.
- [43] C. Vogel, H. Komber, A. Quetschke, W. Butwilowski, A. Pötschke, K. Schlenstedt, J. Meier-Haack, Side-chain sulfonated random and multiblock poly(ether sulfone)s for PEM applications, *React. Funct. Polym.* 71 (2011) 828–842.
- [44] C. Vogel, J. Meier-Haack, Preparation of ion-exchange materials and membranes, *Desalination* 342 (2014) 156–174.
- [45] B.M. Asquith, J. Meier-Haack, C. Vogel, W. Butwilowski, B.P. Ladewig, Side-chain sulfonated copolymer cation exchange membranes for electro-driven desalination applications, *Desalination* 324 (2013) 93–98.
- [46] S. Brunauer, The adsorption of gases and vapors, *Physical Adsorption*, Vol. I, Princeton University Press, Princeton, NJ, 1943.
- [47] J. Rouquerol, P. Llewellyn, F. Rouquerol, Is the BET equation applicable to microporous adsorbents? in: P. Llewellyn, F. Rodriguez-Reinoso, J. Rouquerol, N. Seaton (Eds.), *Stud. Surf. Sci. Catal.* Elsevier, 2007, pp. 49–56.
- [48] A.J. Bard, L.R. Faulkner, *Electrochemical Methods: Fundamentals and Applications*, John Wiley, New York, 2001.
- [49] P.M.S. Monk, *Fundamentals of Electroanalytical Chemistry*, Wiley, Chichester, 2001.